MODELING OF CORROSION PRODUCT TRANSPORT IN PWR PRIMARY COOLANT

by

CHAN BOCK LEE

B. S., Seoul National University, Seoul, Korea
(1983)

M. S., Seoul National University, Seoul, Korea
(1985)

SUBMITTED IN PARTIAL FULFILLMENT
OF THE REQUIREMENTS FOR THE
DEGREE OF

DOCTOR OF PHILOSOPHY

at the

MASSACHUSETTS INSTITUTE OF TECHNOLOGY

February 1990

Signature of Author _____
Department of Nuclear Engineering
October 1989

Certified by _____
Michael J. Driscoll
Thesis Supervisor

_____
William T. Lindsay, Jr.
Thesis Supervisor

Accepted by _____
Allan F. Henry
Chairman, Departmental Graduate Committee

Modeling of Corrosion Product Transport in PWR Primary Coolant

by
Chan Bock Lee

Submitted to the Department of Nuclear Engineering on October 23, 1989 in partial fulfillment of the requirements for the Degree of Doctor of Philosophy in Nuclear Engineering

ABSTRACT

Radioactive nuclei deposited on out-of-core surfaces in PWR primary coolant systems, caused by the transport of corrosion products (crud) through the primary coolant, is a major source of radiation exposure to plant maintenance personnel and a costly impediment to prompt and effective repairs. Modeling and numerical estimation of crud and activity transport is essential to systematic approaches to their control, and in the present instance, for planning and interpretation of experiments using an in-pile PWR chemistry control loop (PCCL) in the MIT Research Reactor.

The semi-empirical CRUDSIM model, which successfully follows the effect of coolant chemistry changes, was adopted as the starting point. In the present work, an analytical transport model is derived, starting with basic transport phenomena, which has a similar form to the CRUDSIM model, and hence shows how to analytically estimate parameters which are defined empirically in the CRUDSIM model. The derivation shows that the CRUDSIM model is a compatible alternative formulation of relations used in other crud transport programs such as PACTOLE and CORA, all of which are based upon characterization of the main driving force for crud transport as the temperature change of the coolant throughout the primary circuit, and the resulting change in transition metal ion solubility in the coolant. Numerical calculations show that mass transfer across boundary layers is not the controlling step, but that the crystallization and dissolution steps must be considered in crud and activity transport : steps which can not be modeled quantatively at present.

Examination of specific aspects of the transport process show that very small crud particles (r_p < 0.01 μm) may precipitate in the coolant, but then are more likely to deposit on system surfaces than to grow or agglomerate into larger coolant borne particles. This analysis also shows that in the case of particle formation, the solubility difference between the S/G and the core surfaces is still the driving force for crud transport, and the only effect of particle formation is to decrease the rate of crud transport from the S/G to the core due to re-deposition of the particles on the S/G. Other mechanisms such as recoil release of Co^{58}, thermal diffusion, primary coolant purification and core refuelling have also been studied. Limiting case analytical solutions are derived to show that short tests (eg. a month or so) can be used to predict long term behavior if initial conditions are properly chosen - for example, a low starting inventory of crud in the core region.

Initial comparisons are made with the results of MIT PCCL operation, which was carried out according to a strategy determined using the model derived in the present work. It is shown that the CRUDSIM/MIT model can successfully replicate the crud and activity transport in the MIT PCCL when appropriate values are specified for the CRUDSIM transport parameters governing these two quantities.

Thesis Supervisor : Dr. M. J. Driscoll
Title : Professor Emeritus of Nuclear Engineering
Thesis Supervisor : Dr. W. T. Lindsay
Title : Consultant

ACKNOWLEDGEMENTS

The author would like to express, with respect, deep gratitude to Prof. M. J. Driscoll for supervision of this work and his continuous encouragement. I also sincerely thank Dr. W. T. Lindsay, Co-supervisor and the originator of the CRUDSIM model, for valuable discussions and advice. The direction and encouragement throughout this work by Prof. O. K. Harling is also deeply appreciated.

Particular acknowledgement is due Dr. G. Kohse, M. Ames, the NRL staff, and fellow students, J. Outwater, R. Sanchez, E. Cabello, A. Esteves, V. Mason and P. Borys for their friendly cooperation and discussions. Thanks are also extended to Ms. D. Eichel, Ms. M. Levine and R. Morton for their help during this work. Dr. I. S. Hwang provided welcome guidance and cordial advice during my stay at MIT.

I express gratitude to the Government of Korea and to the MIT-Electric Utility Program, EPRI and ESEERCO for their financial support for this work.

Finally, I thank my parents for their support.

Table of Contents **Page**

List of Tables

List of Figures

Chapter 1. INTRODUCTION

1.1 Foreword

At least since the startup of the Nautilus prototype reactor in 1953, the phenomenon of corrosion product radio-activation and transport has been recognized as a detrimental factor for water-cooled nuclear reactor maintenance. Earlier efforts to understand and mitigate radionuclide deposition on primary coolant loop surfaces are reviewed in Cohen's book [C-1], and more recently in the articles by Comley [C-2] and Wood [W-1]. Progress reports on specific research efforts have been compiled in a series of international meetings held at Bournemouth, England [B-1] [B-2] [B-3] [B-4], and in April, 1988, in Tokyo, Japan [J-1].

While maintenance dose rates have stabilized and are showing a steady decline in recent years, problems are not yet fully resolved, as indicated by measured differences of an order of magnitude among the many LWR units worldwide, and the fact that gas- or sodium-cooled reactors, the long-term competition for future nuclear power plant orders, have one or two orders of magnitude lower steam generator surface dose rates. Various authors estimate penalties because of the prolongation and reduced effectiveness of maintenance in LWR units amount to on the order of several million dollars per year per unit [T-1].

In view of the need for continuing work in this area, a project focused around the use of small in-pile loops has been initiated at MIT [D-1]. The work

reported here is part of this effort and is concerned with the modelling of corrosion product transport to the extent required to plan and interpret experiments concerned with the optimization of PWR coolant chemistry, primarily through pH control, to minimize out-of-core radionuclide buildup.

1.2 Background

As the wetted metal surfaces around the primary coolant loop corrode, the corrosion products of iron, nickel, chromium, and cobalt which are the principal constituents (and trace contaminant in the case of cobalt) of metals such as stainless steel and Inconel are released into the coolant. The resulting water borne corrosion products may be soluble (ions) or insoluble particulates. These corrosion products can deposit on fuel surfaces in the reactor core and capture neutrons to become radioactive. Some of the product radionuclides are then re-released into the coolant and eventually re-deposited on out-of-core surfaces. This radioactivity on out-of-core surfaces, especially steam generator (S/G) tubing and channel headers, has become the main source of plant worker exposure for PWR units (the reactor type of primary concern here, which represents more than two-thirds of all power reactors operating worldwide).

The main radioactive species of concern are Co^{58} and Co^{60}. Following startup of a new reactor, during its first year, Co^{58} is dominant, but it saturates in a year or so because of its short half-life ($T_{1/2}$ = 71 days). On the other hand, the long-lived Co^{60} ($T_{1/2}$ = 5.26 years) increases monotonically until stabilizing after about 5 years. In general, after several years of operation, the activities of both

Co^{58} and Co^{60} are comparable, even though the relative fraction of each species differs from plant to plant due in part to the high variability of Co^{59} (100% of natural Cobalt and the parent of Co^{60}) from stellite used in wear-susceptible surfaces such as valves, or from cobalt contamination of nickel alloys used in the spacer grids of some older fuel assembly designs.

There are many possible mechanisms which may be implicated in corrosion product and radioactive element transport, as summarized in Table 1.1. Each mechanism will be covered in the corresponding section shown in the table. Among them, the effects induced by irradiation of neutrons and gamma rays inside the core, such as magnetic/electrostatic field effects and direct photo-reduction will not be considered, since they are beyond the scope of this work and their effects are also considered minor. Sedimentation of the particulates in low velocity regions such as core lower and upper plena will not be considered, since the PWR primary coolant is continuously purified and, therefore, under ordinary circumstances, particles may not grow to a sufficiently large size that sedimentation need be considered.

The following general picture has emerged for corrosion product transport in PWR primary coolant, as developed by earlier and contemporary researchers, and as interpreted here:

1) The release of corrosion products from metal surfaces occurs primarily in soluble form ; the driving force is due to the variation of the solubility with temperature of the transition metal ions involved.

Table 1.1 Potential Corrosion Product Transport Mechanisms in a PWR Primary Circuit

Core and S/G surfaces	Boundary Layer in Core and S/G	Bulk Coolant
Dissolution of metal ions† into coolant (Sections 2.2 and 2.3) Erosion of surface metal oxide to release particulates†† (Section 2.5.3) Deposition of ions and particulates on surfaces by crystal growth, adsorption and ion exchange (Sections 2.2 and 2.3) And in core only : Recoil release of ionic nuclei (Section 2.5.2) Removal by refuelling (Section 2.5.4) Other radiation effects ; Magnetic/electrostatic field effects Direct photoreduction	Conventional mass transfer of ions and particulates (Sections 2.2 and 2.3) Thermal diffusion ; (Section 2.5.1) Soret effect of ions Thermophoresis of particulates Electrophoresis	Convection of ions and particulates (Section 2.2.2) Precipitation and dissolution of particulates (Section 2.4) Removal by purification in CVCS (Section 2.5.5) Sedimentation in low velocity regions

† ions - all types of soluble species in the coolant such as divalent ions and hydrated oxide ions.

†† particulates - charged or neutral particles, i.e., colloids or nickel ferrite crystals

2) Likewise, the deposition of the corrosion products on oxidized metal surfaces also occurs mainly via soluble forms.
3) The soluble species released into the coolant may also precipitate into particulates due to the coolant temperature and subsequent solubility changes around the coolant loop, and the concurrent aggregation of small particulates into larger ones.
4) The deposition of particulates on surfaces occurs by conventional mass transfer.
5) Direct erosion and re-deposition of surface particulates also occurs to an extent not yet entirely defined, although earlier workers in the field considered this to be the most important mechanism.

In recent times, erosion and re-deposition of surface oxide has been downgraded in its importance, although implicated in work on the fouling of fossil plant boiler surfaces [P-1]. It seems evident that there exists a particulate corrosion product inventory in the coolant, comparable in mass to the amount of solubles. However, the source of the particulates is not necessarily the erosion of surface corrosion films, since under normal steady state coolant flow conditions, the particulate erosion, which depends on the flow velocity, may not be significant [L-1].

In summary, it is now rather broadly agreed that the corrosion products are released and deposited dominantly in soluble form. As Figure 1.1 shows, significant temperature differences exist in core and S/G flow channels in a PWR primary system. This temperature difference can be shown to provide a driving

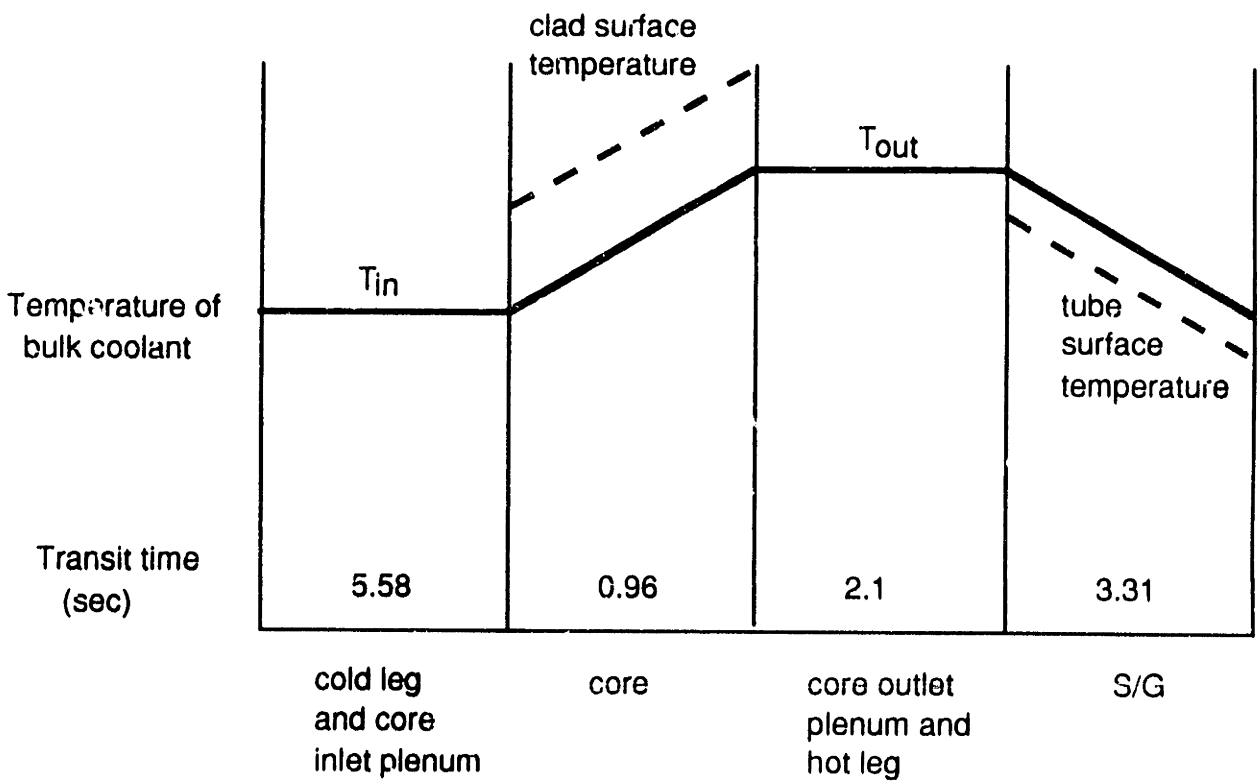

Figure 1.1 Temperature Profile in a PWR Primary Circuit

force for the transport of corrosion products which is more than adequate to fully account for the observed mass and activity of corrosion product deposits.

The state-of-art in modeling of corrosion product and activity transport is best summarized by reviewing the major computer programs now in use to predict and evaluate plant contamination levels: CORA, PACTOLE, and CRUDSIM, each of which will be examined in turn in the subsections which follow.

1.2.1 The CORA Code

The CORA computer code [K-1] developed by Westinghouse can be represented by a nodal transport diagram, as shown in Figure 1.2. The various transport mechanisms are modeled semi-empirically between the individual nodes, which represent homogeneous sources and sinks of the corrosion products in a PWR primary system. The rate processes are analyzed in terms of first order equations. For example, the transport of material between nodes 1 and 2 is given by

$$\beta_{2\text{-}1} - \beta_{1\text{-}2} = k'_m A_{12} (C_2 - C_1) \qquad (1.1)$$

where,

$\beta_{1\text{-}2}$ = amount of material passing from node 1 to 2

$\beta_{2\text{-}1}$ = amount of material passing from node 2 to 1

A_{12} = interfacing surface area between nodes 1 and 2

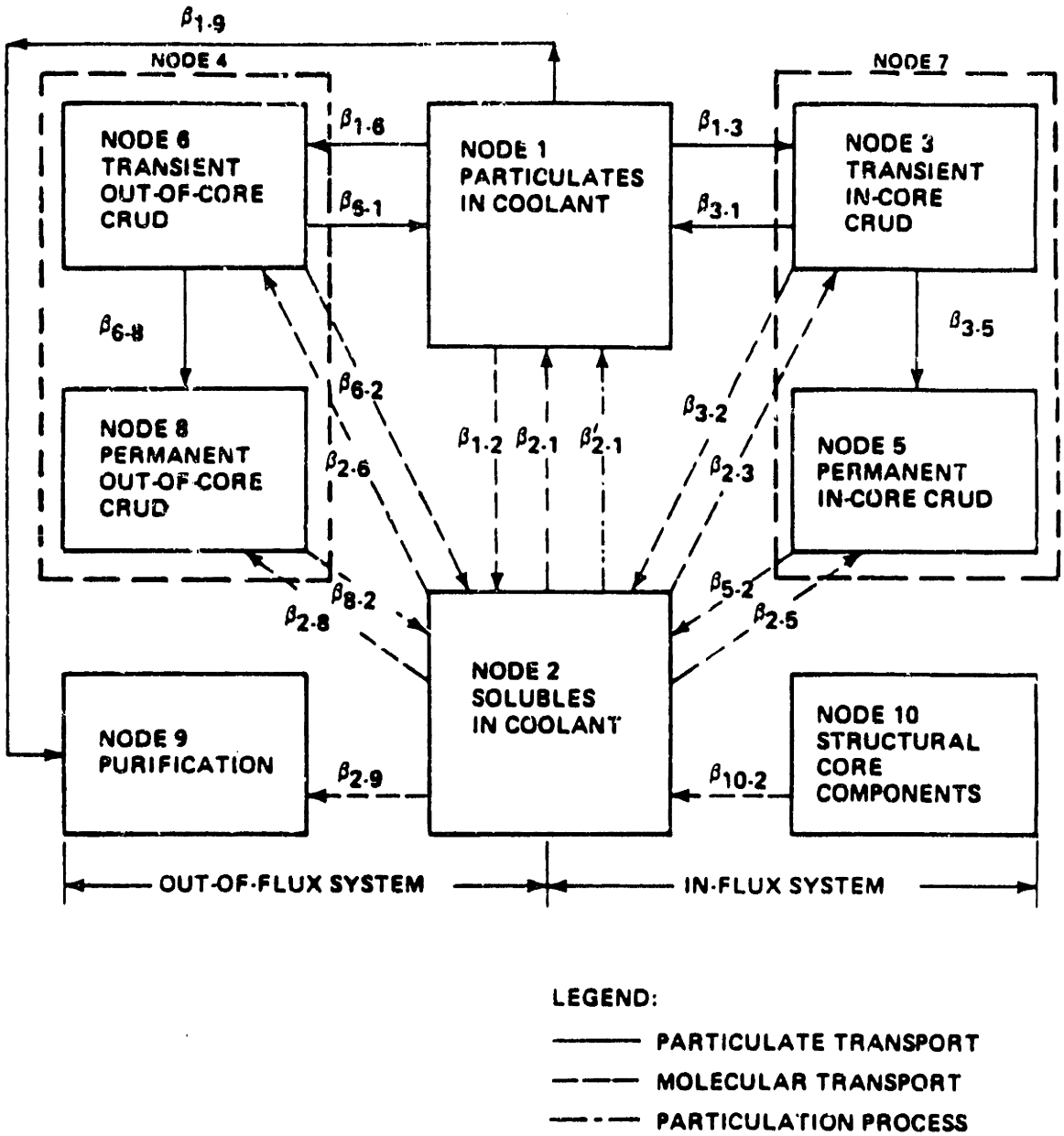

Figure 1.2 CORA Code Nodal Diagram [K-1]

C_1 and C_2 = effective concentrations in the nodes 1 and 2

k'_m = first order transfer coefficient for material,m, passing from nodes 1 and 2

The transfer coefficients have been calculated theoretically, or deduced empirically by comparisons with actual plant data.

The CORA code does not consider activity recoil processes and the effects of temperature changes on corrosion product solubility ; the latter phenomenon is currently considered one of the most important modes for the corrosion product transport in a PWR primary system. The CORA code is, nevertheless, considered one of the most comprehensive models for the PWR primary coolant system, and useful in the relative prediction of crud transport as a function of design and operating variables.

1.2.2 The PACTOLE Code

The PACTOLE program, developed in France, considers twenty different zones in the PWR coolant circuit and characterizes each by its mean temperature, flow rate, hydraulic capacity or pipe dimensions, surface material composition, neutron flux, and other physico-chemical variables. [B-5] [B-6] [B-7] [M-1] Figure 1.3 summarizes the exchange diagram used in PACTOLE.

The program takes into account plant history, e.g., power and chemistry changes, and the effect of coolant purification. The governing parameter is the

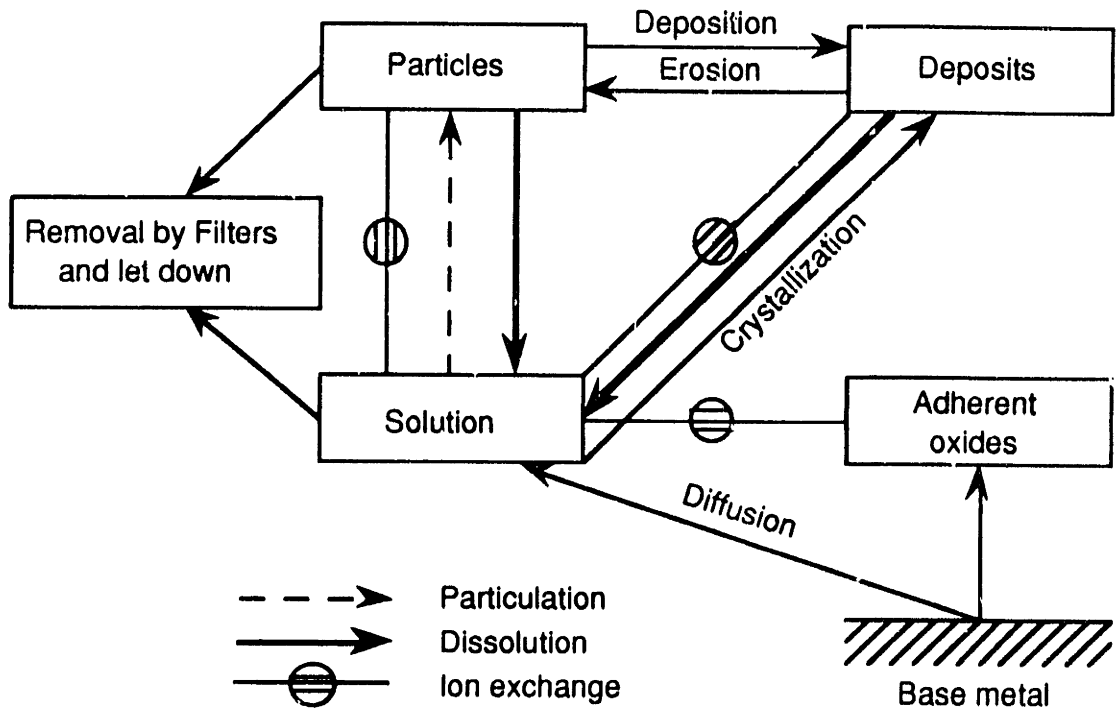

Figure 1.3 PACTOLE Code Process Diagram [B-5]

solubility of system materials. Other processes such as corrosion product release, erosion, precipitation and dissolution of particulates, and particulate transfer are included. The parent nuclides considered are Fe, Ni, Cr, Mn, and Co with their activated nuclides Fe^{59}, Co^{58}, Cr^{51}, Mn^{54}, and Co^{60}. The code solves a series of differential equations describing the variations in system parameters which include:

- the release rate of structural materials
- the mass of elements in suspension and solution in the coolant
- the mass of elements on all the surfaces
- the activities associated with soluble and insoluble species
- the activities of deposits and surface oxides in each zone and corresponding local dose rates

The PACTOLE code is also a very comprehensive model for the PWR primary coolant system and is known to predict PWR operational results rather well. Parametric studies of the MIT PCCL using the PACTOLE code are reported separately by Borys. [B-8]

1.2.3 The CRUDSIM Code

The CRUDSIM [B-9] program employs a conceptually simple model compared with the comprehensive models in CORA and PACTOLE. Only two nodes represent the PWR primary coolant circuit. The radioactive elements considered are Co^{58} and Co^{60}. Crud and activity transport is predicted only on

the basis of a solubility difference driving force. Therefore, the results of CRUDSIM calculations are generally used in relative or empirically adjusted comparisons of various coolant chemistry conditions (i.e., pH). Good comparisons with measured plant histories can be obtained using a judiciously selected transport characterization parameter.

It should be noted that the comprehensive modeling in CORA and PACTOLE may obscure the real contribution of the dominant mechanism, if any. Even though each computer code is continuously updated to match new plant data or experimental results, and in that sense is not yet "complete", it is not clear that the true significance of each mechanism has been appropriately accounted for. Furthermore, not all potential mechanisms have been included in the above-mentioned codes: e.g., thermal diffusion, electrophoresis, and adsorption, all of which were believed to be negligible: an opinion shared by the present author except perhaps for the thermal diffusion effect, which will be investigated further in Section 2.5.1 of Chapter 2.

Because of the attractive features of good results and conceptual simplicity, we selected the CRUDSIM program as the focal point for our present efforts. Earlier work at MIT by Morillon using CRUDSIM was encouraging [M-2] ; her thesis also discusses some limited comparisons with CORA.

1.3 Organization of This Work

In Chapter 2, a comprehensive model for crud and activity transport will be displayed as the basis for subsequent simplifications.

In Section 2.2, analytical models for crud and activity transport in the form of soluble species are derived and compared with the original CRUDSIM formulation.

In Section 2.3, parameters used in the modeling will be evaluated. Primary emphasis is devoted to estimation of the parameters from fundamental theory. If this is not possible, empirical estimation of the parameter in question will be attempted as the next best alternative.

In Section 2.4, the likelihood of particulate precipitation in the coolant will be estimated, and the crud and activity transport equations in the presence of particulate precipitation will be derived and compared with the versions without particulate precipitation.

In Section 2.5, other parameters and mechanisms for crud and activity transport such as thermal diffusion, recoil release, erosion of the surface oxide film, refuelling and purification will be modelled, and their effect upon net crud and activity transport will be discussed.

In Chapter 3, the computer code, CRUDSIM/MIT which employs the models developed and discussed in Chapter 2, will be analyzed and compared with measurements made on the MIT PWR Coolant Chemistry Loop (PCCL).

In Section 3.2, the MIT PCCL will be compared with a typical PWR primary coolant system in terms of operating conditions and mass transfer characteristics.

In Section 3.3, sensitivity analyses will be carried out to find the relative importance of parameters (such as the CRUDSIM transport factor, β, particulate precipitation, coolant pH, temperature and hydrogen concentration, recoil release, initial crud inventory and others) on the net transport of crud and activity. In addition, analytical solutions of crud and activity transport equations will be derived to display the short term and asymptotic long term trends for crud and activity levels.

In Section 3.4, the CRUDSIM/MIT calculation results will be compared with MIT PCCL measurements. The models employed in CRUDSIM/MIT will be tested and the uncertainty involved in the parameters will be discussed.

In Chapter 4, this work will be summarized and conclusions will be discussed. Recommendations will be also given regarding the areas where further research is needed.

Finally, in Appendix A, the FORTRAN program, CRUDSIM/MIT is documented along with sample input and output.

Chapter 2 MODELING OF CORROSION PRODUCT TRANSPORT

2.1 Introduction

In this chapter, an analytical basis for the CRUDSIM model of corrosion product and radioactivity transport will be derived, and the formulation extended to incorporate additional features. The parameters which are empirical or arbitrarily chosen in the original CRUDSIM will be clarified and redefined, and analytical estimation attempted. In particular, conventional mass transfer, dissolution and crystal growth are applied in the transport of corrosion products. The likelihood of particulate precipitation of corrosion products in the coolant will be studied and its effect on overall corrosion products behavior will be derived. And, finally, justification for neglecting several transport mechanisms of secondary importance such as thermal diffusion across the flow boundary layer in the core and S/G, erosion of the surface oxide film, and coolant purification by the chemical and volume control system(CVCS) is provided.

2.2 Derivation of Corrosion Product Transport Model

2.2.1 Analytical Basis

In this section, the analytical base for corrosion product transport in the PWR primary system will be discussed. The PWR primary coolant loop can be divided into by three major sections :

- fuel element surfaces in core: Zircaloy-4
- coolant: H_2O
- S/G tube surfaces: Inconel

The stainless steel surfaces of the cold and hot leg pipes and reactor pressure vessel internals are neglected, because their areal fractions are small compared with those of the S/G and core, as shown in Table 2.1, and the release and deposition of the soluble corrosion products for stainless steel surfaces may not be significant due to the absence of a substantial temperature difference across the fluid boundary layer.

2.2.1.1 Steam Generator (S/G)

The material used for S/G tubing is Inconel, which is a nickel-base alloy. As corrosion occurs in the steam generator through contact with the primary coolant, corrosion products form on the Inconel surface, and some of them are released into the primary coolant. The corrosion rate of Inconel depends upon the properties of the coolant and Inconel itself. The relevant coolant parameters

Table 2.1 Areal Distribution of a Typical 1000 MWe PWR primary system [C-2]

Region	Material	Area (m^2)	Fraction (%)
core	304 S. S.	3.9×10^2	1.4
	Inconel 600	6.5×10^2	2.4
	Zircaloy 4	6.1×10^3	22.6
out of core	304 S. S.	1.8×10^3	6.7
	Inconel 600	1.8×10^4	66.8

are temperature, pH, and oxygen and hydrogen concentrations. The Inconel parameters include the properties of the alloy itself, and those of its passive surface oxide film, such as porosity and oxide stoichiometry.

Under the normal operating condition of a PWR, after the initial pre-transition stage of Inconel oxidation, the corrosion rate can be regarded as a constant. On the other hand, the release into the coolant of the corrosion products formed on Inconel surfaces may occur in the form of both solubles and particles. Particulate release of corrosion products occurs by erosion, which depends upon coolant flow conditions. Soluble form of corrosion products are released by the dissolution of corrosion products, the magnitude of which depends on the coolant temperature, pH, and flow conditions, surface heat fluxes, and saturation status of soluble species in the coolant. The soluble release is driven by the solubility variation with temperature; more precisely, transition metal ion solubility decreases with temperature under conditions prevalent in PWR primary coolant.

Therefore, the change in corrosion product inventory of the S/G surfaces can be expressed as follows:

The rate of change of S/G corrosion product inventory
= corrosion rate of Inconel
- net soluble release by dissolution
+ particulate deposition
- particulate release by erosion (2.1)

2.2.1.2 Coolant

The coolant recirculates around the primary loop of the PWR in about 12 seconds. The temperature of the coolant changes along the loop, from T_{in} to T_{out}, as shown in Figure 2.1. Because the coolant temperature changes rapidly, the soluble species concentration cycles between a condition of under-saturation and one of supersaturation, repeatedly, as shown in Figure 2.2.

Therefore, in the regions of the core, core outlet plenum and hot leg , the solubles in the coolant become super-saturated and tend to deposit on the surface (e.g., on the core surface), at a rate mainly controlled by boundary layer mass transfer (driven by the temperature difference due to heat flux), and crystallization on the surface, or, instead they can precipitate to form particulates in the coolant. To the contrary, in the regions of the S/G, cold leg, and core downcomer and lower plenum, the solubles in the coolant are under-saturated, and there is a driving force tending to restore saturation. Therefore, the corrosion products on the surfaces in these regions tend to be released into the coolant at a rate controlled by the dissolution step of corrosion products and boundary layer mass transfer. The particulates in the coolant can also redissolve back into soluble (i.e., ionic) form in the under-saturated regions.

The particulate concentration in the coolant also changes around the primary loop, along with soluble species concentration. Particulates can nucleate in the super-saturated regions of the coolant and grow by the diffusion of solubles or agglomeration by the collision and flocculation of particulates in the coolant. Particles may also re-dissolve into soluble form in the under-saturated

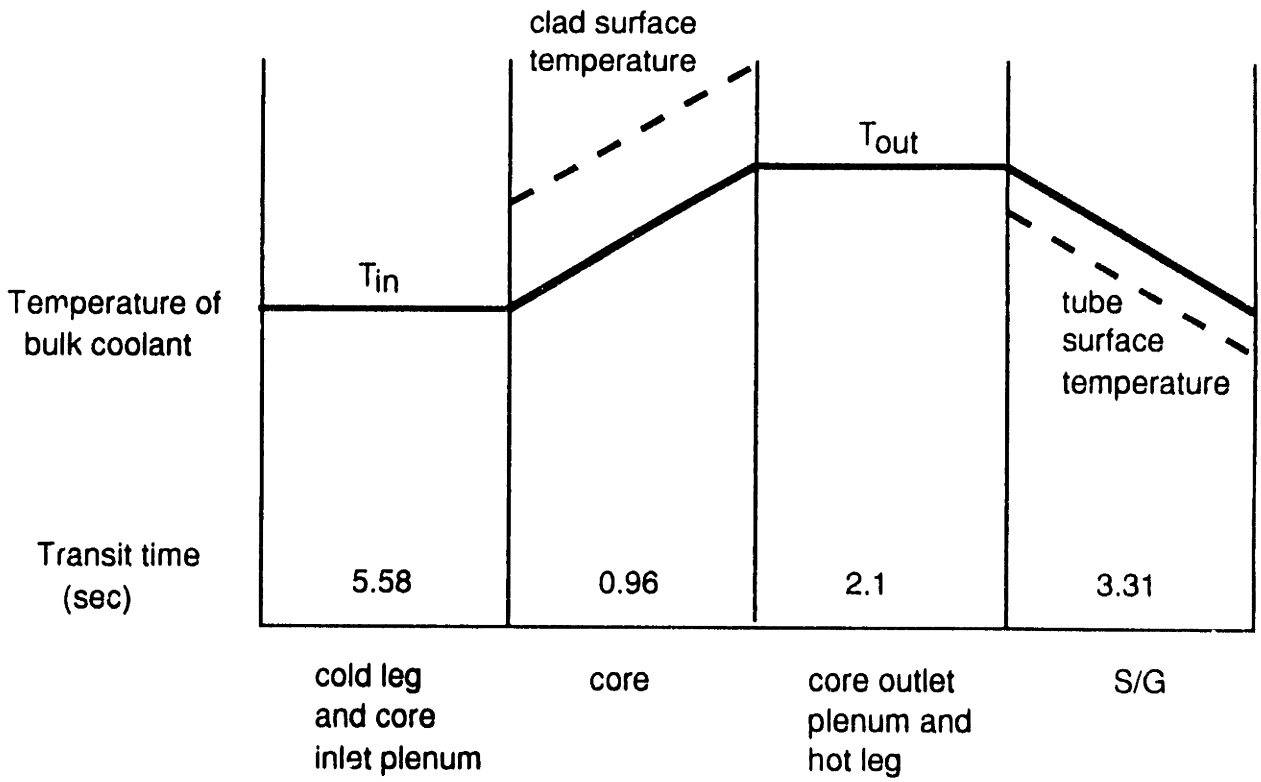

Figure 2.1 Temperature Profile in a PWR Primary Circuit

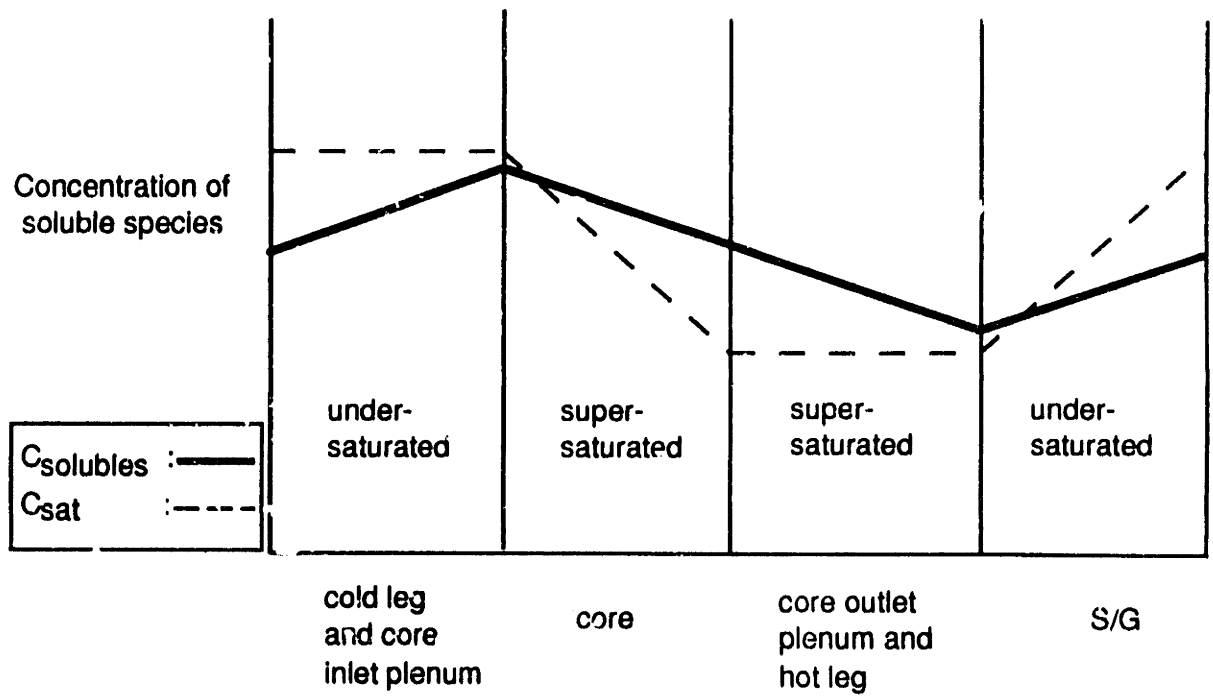

Figure 2.2 Soluble Species Concentration Profile in a PWR Primary Coolant

regions. Particulates which exist in both the super-saturated and under-saturated regions tend to deposit on metal surfaces, driven by conventional mass transfer under turbulent flow. Finally, as is the case for soluble species, a small amount are removed by the purification system. Therefore, there may exist a certain distribution of the particulates with respect to size and region : one probably similar to the exponential distribution.

By the repetition of this cycle, there is a net transport of corrosion products mainly from the S/G tubing to core fuel element surfaces, which amounts normally to about 10 kg over a three-year period of normal PWR operation (residence time of core fuel batch in core).

In the steady state, the soluble and particulate concentrations in the coolant will be constants for each region, namely:

The rate of change of solubles in the coolant
= net release rate of solubles from S/G surfaces
- net deposition rate of solubles onto core surfaces
- precipitation of solubles into particulates in the coolant
+ re-dissolution of particulates in the coolant
= 0 (2.2)

The rate of change of particulates in the coolant
= precipitation of solubles into particulates in the coolant
- re-dissolution of particulates in the coolant
- deposition of particulates onto surfaces

+ erosion of surface corrosion products as particulates

= 0 (2.3)

2.2.1.3 Core

The corrosion products released from the S/G tubing deposit on the fuel cladding in the core. Deposition from the coolant can occur in the form of both solubles and particulates. Only a small fraction (about 1 percent) of the excess solubles (the difference between the supersaturated solubles concentration and the saturation concentration) deposits on the core. The rest of the excess solubles may remain as supersaturated solubles, or they may precipitate to form particulates.

Since there is regular refuelling of the core fuel assemblies each year, at which time the oldest one-third of all fuel assemblies are replaced by new ones, the core corrosion product inventory decreases by half at every refuelling (based on the assumption of linear accumulation of crud with time).

Therefore, the change of core corrosion product inventory can be expressed as follows:

The rate of change of core corrosion product inventory

= net soluble deposition

+ particulate deposition

- particulate erosion

- removal by refuelling (2.4)

2.2.2 Original CRUDSIM Model

As noted in Chapter 1, the CRUDSIM program [B-9] is at present one of the more successful tools used to correlate and predict the transport of corrosion products and activity in PWR primary coolant systems.

The CRUDSIM code predicts corrosion product transport based on a solubility difference driving force and other empirical parameters. It successfully describes the effect of coolant chemistry changes on corrosion product transport. As shown in Figure 2.3, two nodes are used in CRUDSIM: one, called the "hot region", represents the core surfaces; and the other, called the "cold region," accounts for both the coolant and the S/G surfaces. The representative equations are as follows:

$$\frac{dI_h}{dt} = \beta F (S_c - S_h) \tag{2.5}$$

$$\frac{dI_c}{dt} = R - \beta F (S_c - S_h) \tag{2.6}$$

$$\frac{dA_h}{dt} = - \lambda A_h - \beta F (\frac{A_h}{I_h} S_h - \frac{A_c}{I_c} S_c) + \alpha P I_h \tag{2.7}$$

$$\frac{dA_c}{dt} = - \lambda A_c + \beta F (\frac{A_h}{I_h} S_h - \frac{A_c}{I_c} S_c) \tag{2.8}$$

where,

I_h = iron inventory in the hot tank (kg-Fe)

I_c = iron inventory in the cold tank (kg-Fe)

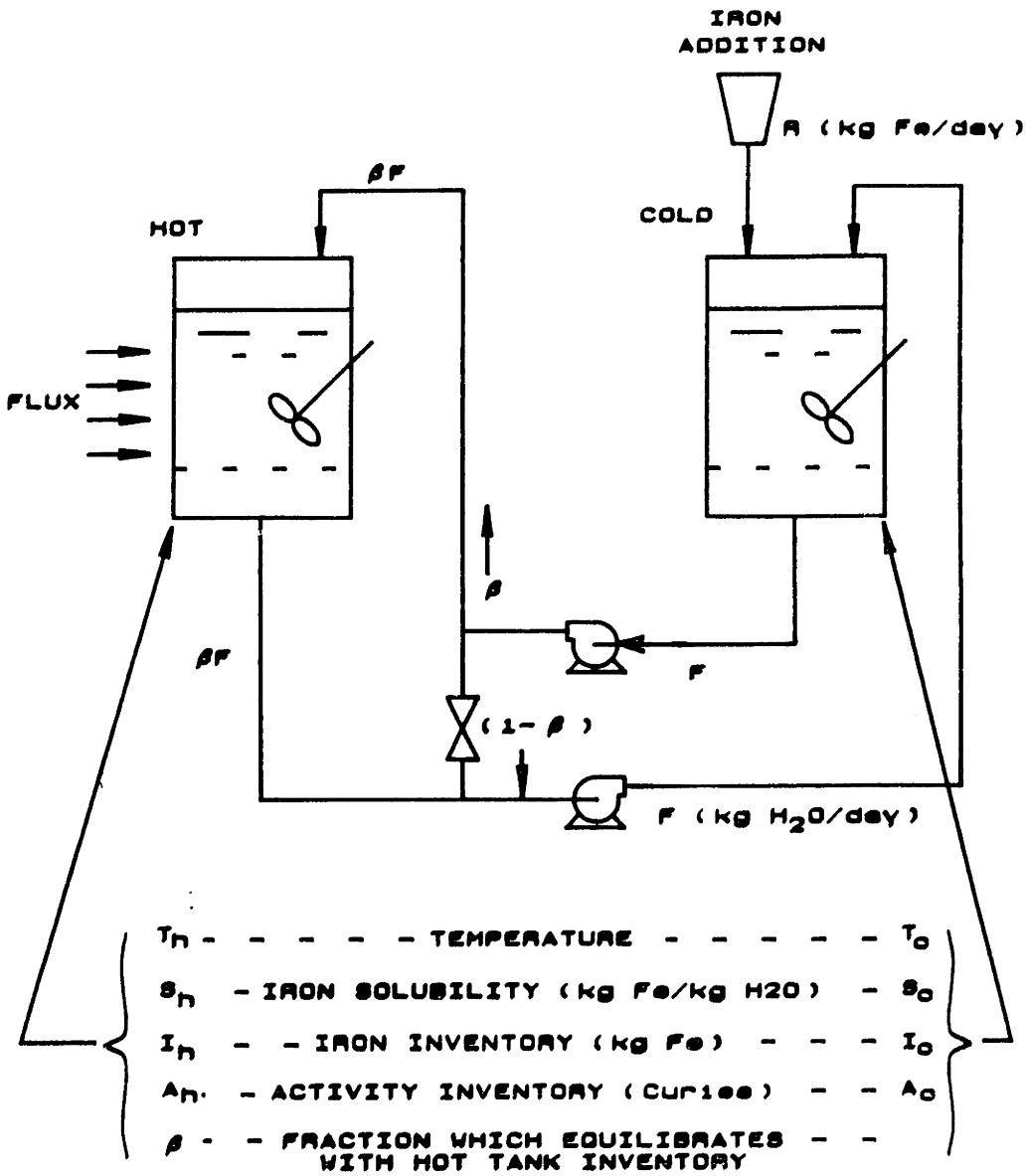

Figure 2.3 Schematic Representation of CRUDSIM "Slurry Tank" Model [B-9]

S_h = iron solubility in the hot tank (kg-Fe/kg-H_2O)

S_c = iron solubility in the cold tank (kg-Fe/kg-H_2O)

A_h = activity inventory in the hot tank, such as Co^{58} and Co^{60} (Ci)

A_c = activity inventory in the cold tank, such as Co^{58} and Co^{60} (Ci)

R = iron input into the cold tank (kg-Fe/day)

λ = decay constant (day^{-1})

α = neutron activation factor (Ci/kg-Fe. % power. day)

β = empirical transport factor for the crud and activity

F = primary system flow rate (kg-H_2O/day)

P = percent of full power (% power)

2.2.3 Three-node Model

As noted in the preceding section, the corrosion product and activity transport in PWR primary coolant can be modelled with the three nodes: core, coolant, and S/G, as shown in Figure 2.4. The balance equations are as follows.

2.2.3.1 Corrosion Product Transport

At first, only transport of soluble species of the corrosion products will be considered, postponing the discussion of corrosion product transport in particulate form until Section 2.4.1.

The corrosion product (crud) balance equation for each node can be simply expressed as follows, when only transport of soluble corrosion product is considered.

$$\frac{dI_1}{dt} = SD \qquad (2.9\ a)$$

$$\frac{dI_2}{dt} = SR - SD \qquad (2.9\ b)$$

$$\frac{dI_3}{dt} = CR - SR \qquad (2.9\ c)$$

where,

SD = deposition rate of soluble species onto core fuel surface (kg/sec)

SR = soluble species release rate from S/G tubing (kg/sec)

Figure 2.4 Three Node Model

1	2	3
Core fuel element surfaces	Coolant	S/G tubing surfaces

I_i = Iron inventory in the i-th node (kg-Fe)

A_i = Activity in the i-th node (Ci)

T_i = Temperature in the i-th node (^oC)

S_i = Iron solubility in the i-th node (kg-Fe/m^3)

k_1 = Mass transfer factor between nodes 1 and 2 (m^3/sec)

k_3 = Mass transfer factor between nodes 2 and 3 (m^3/sec)

CR = Corrosion rate of S/G tubing (kg-Fe/sec)

α_i = Neutron activation factor in the i-th node (Ci/kg-Fe. % power.sec)

CR = corrosion rate of S/G tubing (kg/sec)

I_i = corrosion product inventory in the i-th node (kg)

(1 = core fuel element, 2 = coolant and 3 = S/G tubing)

Each term of the above equation can be calculated as follows.

The soluble deposition rate in the core (SD) can be expressed by integration along the core, that is

$$SD = \int_{H_{in}^1}^{H_{out}^1} h_{dp} P_{w1} (C_2(x) - C_1(x)) dx \qquad (2.10)$$

where,

$C_i(x)$ = soluble species concentration at position, x, in the i-th node (kg/m^3)

h_{dp} = deposition coefficient of soluble species of crud (m/sec)

P_{w1} = wetted perimeter of the core fuel element (m)

H_{in}^1 and H_{out}^1 = inlet and outlet of core fuel element flow channel respectively

The soluble release rate in the S/G (SR) can also be integrated along the S/G,

$$SR = \int_{H_{in}^3}^{H_{out}^3} h_{rl} P_{w3} (C_2(x) - C_1(x)) dx \qquad (2.11)$$

where,

$C_i(x)$ = soluble species concentration at position, x, in the i-th node (kg/m^3)

h_{rl} = release coefficient of soluble species of crud (m/sec)

P_{w3} = wetted perimeter of the S/G tubing (m)

H^3_{in} and H^3_{out} = inlet and outlet of S/G tubing flow channel, respectively

The temperature profiles for the core fuel element surface, the coolant and the S/G tube surface can be approximated to increase linearly, that is,

$$T_1(x) = T_2(x) + \Delta T_1(x) \approx T_2(x) + 20 \qquad (2.12\ a)$$

$$T_2(x) = T_{in} + \frac{x}{L_i}(T_{out} - T_{in}) \qquad (2.12\ b)$$

$$T_3(x) = T_2(x) + \Delta T_3(x) \approx T_2(x) - 6.8 \qquad (2.12\ c)$$

where,

T_{in} = inlet and outlet temperatures of the coolant (^oC)

T_{out} = inlet and outlet temperatures of the coolant (^oC)

$T_i(x)$ = temperature at the position, x, in the i-th node (^oC)

ΔT_1 = temperature difference across the boundary layer of the core (^oC)

ΔT_3 = temperature difference across the boundary layers of S/G (^oC)

L_i = the length of flow channel in the i-th region (m)

(1 = core and 3 = S/G)

It can be assumed that the soluble species of the crud are always saturated at the corresponding local coolant temperature, since the available crud inventory in the S/G and the core is much larger than the amount needed for saturation of the crud in the coolant. Then Eqs. (2.10) and (2.11) can be transformed as follows:

$$SD = h_{dp}\, P_{w1} \left[\int_{T_{in}^2}^{T_{out}^2} C_2(T) \left(\frac{dT_2}{dx}\right)^{-1} dT - \int_{T_{in}^1}^{T_{out}^1} C_1(T) \left(\frac{dT_1}{dx}\right)^{-1} dT \right]$$

$$= h_{dp}\, P_{w1}\, \frac{L_1}{(T_o - T_i)} \left[\int_{T_i}^{T_o} S\, dT - \int_{T_i + \Delta T_1}^{T_o + \Delta T_1} S\, dT \right] \qquad (2.13)$$

and

$$SR = h_{rl}\, P_{w3} \left[\int_{T_{in}^3}^{T_{out}^3} C_3(T) \left(\frac{dT_3}{dx}\right)^{-1} dT - \int_{T_{in}^2}^{T_{out}^2} C_2(T) \left(\frac{dT_2}{dx}\right)^{-1} dT \right]$$

$$= h_{rl}\, P_{w3}\, \frac{L_3}{(T_o - T_i)} \left[\int_{T_i + \Delta T_3}^{T_o + \Delta T_3} S\, dT - \int_{T_i}^{T_o} S\, dT \right] \qquad (2.14)$$

and

$$A_1 = P_{w1}\, L_1 \qquad (2.15)$$

$$A_3 = P_{w3}\, L_3 \qquad (2.16)$$

$$k_1 = A_1\, h_{dp} \qquad (2.17)$$

$$k_3 = A_3\, h_{rl} \qquad (2.18)$$

where,

A_i = total surface area of the the i-th region (m^2)

k_i = mass transfer factor of the soluble species of the crud in the i-th region (m^3/sec)

Then, Eqs. (2.13) and (2.14) become,

$$SD = \frac{k_1}{(T_o - T_i)}\left[\int_{T_i}^{T_o} S\,dT - \int_{T_i+\Delta T_1}^{T_o+\Delta T_1} S\,dT\right]$$

$$= k_1 (S_2 - S_1) \tag{2.19}$$

$$SR = \frac{k_3}{(T_o - T_i)}\left[\int_{T_i+\Delta T_3}^{T_o+\Delta T_3} S\,dT - \int_{T_i}^{T_o} S\,dT\right]$$

$$= k_3 (S_3 - S_2) \tag{2.20}$$

where,

$$S_1 = \frac{1}{(T_o - T_i)}\int_{T_i+\Delta T_1}^{T_o+\Delta T_1} S\,dT \tag{2.21}$$

$$S_2 = \frac{1}{(T_o - T_i)}\int_{T_i}^{T_o} S\,dT \tag{2.22}$$

$$S_3 = \frac{1}{(T_o - T_i)} \int_{T_i + \Delta T_3}^{T_o + \Delta T_3} S \, dT \qquad (2.23)$$

and S(T) is the saturated concentration of the soluble species at temperature, T (°C).

Therefore, the crud balance equations in the primary coolant loop become

$$\frac{dI_1}{dt} = k_1 (S_2 - S_1) \qquad (2.24)$$

$$\frac{dI_2}{dt} = k_3 (S_3 - S_3) - k_1 (S_2 - S_1) \qquad (2.25)$$

$$\frac{dI_3}{dt} = CR - k_3 (S_3 - S_2) \qquad (2.26)$$

2.2.3.2 Activity Transport

The activity produced in the core is released into the coolant as solubles and deposits on S/G tube surfaces. The activity balance equations are as follows:

$$\frac{dA_1}{dt} = -\lambda A_1 + \alpha P I_1 - ASR \qquad (2.27)$$

$$\frac{dA_2}{dt} = -\lambda A_2 + ASR - ASD \qquad (2.28)$$

$$\frac{dA_3}{dt} = -\lambda A_3 + ASD \qquad (2.29)$$

where,

A_i = activity in the i-th node (Ci)

λ = radioactive decay constant (sec^{-1})

α = neutron activation factor in the core (Ci/kg-Fe. % power. sec)

P = % power of the core

ARS = activity release rate as soluble species in the core (Ci/sec)

ASD = activity deposition rate as soluble species in the S/G (Ci/sec)

In the above balance equations, we can neglect the decay of the coolant activity (λA_2) because the absolute value of the coolant activity is very small compared with the core and S/G activities, and the average residence time (~ hrs) of activity in the coolant is short compared with its half life. It was assumed here that radioactive species such as Co^{58} and Co^{60} move around together with the iron

soluble species congruently, that is, at the same ratio. Then, each term of the above equation can be obtained by integration, described as follows.

The release rate of the activity in the core in soluble form (ASR) can be expressed by

$$ASR = \int_{H_{in}}^{H_{out}} h_{rl}^{a} P_{wl} \left(\frac{A_1}{I_1} S_1 - \frac{A_2}{I_2} S_2 \right) dx$$

$$= h_{rl}^{a} P_{wl} \frac{L_1}{(T_o - T_i)} \left[\frac{A_1}{I_1} \int_{T_i + \Delta T_1}^{T_o + \Delta T_1} S \, dT - \frac{A_2}{I_2} \int_{T_i}^{T_o} S \, dT \right]$$

$$= k_1^{a} \left(\frac{A_1}{I_1} S_1 - \frac{A_2}{I_2} S_2 \right) \qquad (2.30)$$

where,

$$S_1 = \frac{1}{(T_o - T_i)} \int_{T_i + \Delta T_1}^{T_o + \Delta T_1} S \, dT$$

$$S_2 = \frac{1}{(T_o - T_i)} \int_{T_i}^{T_o} S \, dT$$

h_{rl}^{a} = release coefficient of the activity as soluble species in the core (m/sec)

k_1^{a} = mass transfer factor of the activity as soluble species in the core (m^3/sec)

Similarly, the deposition rate of activity in the S/G in soluble form (ASD) is

$$ASD = \int_{H_{in}^a}^{H_{out}^a} h_{dp}^a P_{w3} \left(\frac{A_2}{I_2} S_2 - \frac{A_3}{I_3} S_3 \right) dx$$

$$= h_{dp}^a P_{w3} \frac{L_3}{(T_o - T_i)} \left[\frac{A_2}{I_2} \int_{T_i}^{T_o} S \, dT - \frac{A_3}{I_3} \int_{T_i + \Delta T_3}^{T_o + \Delta T_3} S \, dT \right]$$

$$= k_3^a \left(\frac{A_2}{I_2} S_2 - \frac{A_3}{I_3} S_3 \right) \qquad (2.31)$$

where,

$$S_3 = \frac{1}{(T_o - T_i)} \int_{T_i + \Delta T_3}^{T_o + \Delta T_3} S \, dT$$

h_{dp}^a = deposition coefficient of the activity as soluble species in the S/G (m/sec)

k_3^a = mass transfer factor of the activity as soluble species in the S/G (m^3/sec)

Therefore, the activity balance equations in PWR primary coolant become

$$\frac{dA_1}{dt} = -\lambda A_1 + \alpha P I_1 - k_1^a \left(\frac{A_1}{I_1} S_1 - \frac{A_2}{I_2} S_2 \right) \qquad (2.32)$$

$$\frac{dA_2}{dt} = -\lambda A_2 + k_1^a \left(\frac{A_1}{I_1} S_1 - \frac{A_2}{I_2} S_2 \right) - k_3^a \left(\frac{A_2}{I_2} S_2 - \frac{A_3}{I_3} S_3 \right) \qquad (2.33)$$

$$\frac{dA_3}{dt} = -\lambda A_3 + k_3^a \left(\frac{A_2}{I_2} S_2 - \frac{A_3}{I_3} S_3 \right) \qquad (2.34)$$

One more significant approximation is required to reduce this set to the usual CRUDSIM format, as discussed in the section which follows.

2.2.4 Two-node Model

A two-node set of equations can be derived from the three-node equations by removing the coolant node. Here, the two nodes retained are the core surface and the S/G surface; the coolant is not included, differing in this respect from CRUDSIM nodalization.

It is reasonable to assume that the iron inventory in the coolant rapidly reaches its steady state concentration because of the small mass involved and the large inventory available. Hence, let $\frac{dI_2}{dt} = 0$. The activity in the coolant is also very small, and the residence time of activity in the coolant (~hrs) is very short compared with its half life. Thus, we can set $\frac{dA_2}{dt} = 0$ and $\lambda A_2 = 0$.

Therefore, Eqs. (2.25) and Eqs. (2.33) can be changed as follows. Equation (2.25) becomes

$$\frac{dI_2}{dt} = 0 = k_3 (S_3 - S_3) - k_1 (S_2 - S_1)$$

so

$$S_2 = \frac{k_1}{(k_1 + k_3)} S_1 + \frac{k_3}{(k_1 + k_3)} S_3 \qquad (2.35)$$

Equation (2.33) becomes

$$\frac{dA_2}{dt} = 0 = -\lambda A_2 + k_1^a \left(\frac{A_1}{I_1} S_1 - \frac{A_2}{I_2} S_2\right) - k_3^a \left(\frac{A_2}{I_2} S_2 - \frac{A_3}{I_3} S_3\right)$$

so

$$\frac{A_2}{I_2} S_2 = \frac{k_1^a \quad A_1}{(k_1^a + k_3^a)\, I_1} S_1 + \frac{k_3^a \quad A_3}{(k_1^a + k_3^a)\, I_3} S_3 \tag{2.36}$$

Insert Eq. (2.35) into Eqs. (2.24) and (2.26):

$$\frac{dI_1}{dt} = \frac{k_1 k_3}{k_1 + k_3} (S_3 - S_1) \tag{2.37}$$

$$\frac{dI_3}{dt} = CR - \frac{k_1 k_3}{k_1 + k_3} (S_3 - S_1) \tag{2.38}$$

Inserting Eq. (2.36) into Eqs. (2.32) and (2.34) then gives

$$\frac{dA_1}{dt} = -\lambda A_1 + \alpha P I_1 - \frac{k_1^a k_3^a}{k_1^a + k_3^a} \left(\frac{A_1}{I_1} S_1 - \frac{A_3}{I_3} S_3\right) \tag{2.39}$$

$$\frac{dA_3}{dt} = -\lambda A_3 + \frac{k_1^a k_3^a}{k_1^a + k_3^a} \left(\frac{A_1}{I_1} S_1 - \frac{A_3}{I_3} S_3\right) \tag{2.40}$$

Now note that Eqs. (2.37) through (2.40) are equivalent to Eqs. (2.5) through (2.8). The correspondence between variables is as follows.

$$I_h = I_1 \tag{2.41}$$

$$I_c = I_3 \tag{2.42}$$

$$A_h = A_1 \tag{2.43}$$

$$A_c = A_3 \tag{2.44}$$

$$S_h = \frac{S_1}{\rho_{H_2O}} \tag{2.45}$$

$$S_c = \frac{S_3}{\rho_{H_2O}} \tag{2.46}$$

The density appears in these latter relations because S_h in CRUDSIM is in [kg-Fe/kg-H_2O] and S_1 is in [kg-Fe/m^3] and, in addition:

$$\beta_c = \left(\frac{k_1\, k_3}{k_1 + k_3}\right)\frac{\rho_{H_2O}}{F} \qquad \text{for crud transport} \tag{2.47}$$

$$\beta_a = \left(\frac{k_1^a\, k_3^a}{k_1^a + k_3^a}\right)\frac{\rho_{H_2O}}{F} \qquad \text{for activity transport} \tag{2.48}$$

In the original CRUDSIM, the empirical parameter, β , represents both the crud and activity transport. However, as will be discussed in Section 2.3.4, the crud transport factor is not necessarily equal to the activity transport since their transport paths are different. The other conceptual difference between the original CRUDSIM and two node model derived above exists in the definition of each node and its temperature and solubility. The cold node in CRUDSIM is both the coolant and the S/G surface, whereas node 3 is only the S/G surface in the present model. Second, S_h and S_c in CRUDSIM are arbitrarily chosen as the saturation concentration of the soluble species of iron corrosion products corresponding to core outlet and inlet temperatures, respectively. On the other

hand, S_1 and S_3 are the averages of the saturated soluble concentrations in the coolant contacting core fuel elements and S/G tubing, respectively. That is, the temperatures of the cold (T_c) and hot (T_h) nodes in CRUDSIM are core coolant inlet and outlet temperatures, while the temperatures in node 1 (T_1) and node 3 (T_3) are the mean temperatures of core fuel element and S/G tubing surfaces, respectively. In a typical PWR, these temperature differences are close in value but not the same.

$$T_c = T_{in} = 285\ ^{o}C$$
$$T_h = T_{out} = 320\ ^{o}C$$

Thus,

$$T_h - T_c = 35\ ^{o}C$$

while,

$$T_1 = T_{avg.} + \Delta T_1$$
$$= \frac{1}{2}(285 + 320) + 20$$
$$= 322.5\ ^{o}C$$

$$T_3 = T_{avg.} + \Delta T_3$$
$$= \frac{1}{2}(285 + 320) - 6.8$$
$$= 295.7\ ^{o}C$$

So,

$$T_1 - T_3 = 26.8\ ^{o}C$$

This difference in temperature definition may be significant in determining the optimum pH value; a subject which will be discussed later.

2.3 Estimation of Parameters

2.3.1 Mass Transfer Coefficient

2.3.1.1 Soluble mass transfer

There is mass transfer of solubles from a super-saturated bulk coolant to metal surfaces in the core. The driving force for this mass transfer is the super-saturation of the soluble species in bulk coolant due to the temperature rise in the core. Since the temperature rise is so fast that the solubles in bulk coolant become over-saturated, the controlling factors for soluble deposition on the core surfaces are mass transfer through the boundary layer and incorporation of the soluble species on the core surface by crystallization or growth. On the other hand, in the S/G tubes, the temperature of the bulk coolant decreases, so that the solubles in the coolant become under-saturated quickly, and there is a driving force for release of soluble species from S/G tube surfaces to under-saturated bulk coolant across the flow boundary layer. Again, the controlling factors for soluble release are the soluble mass transfer to the bulk coolant through the boundary layer and the dissolution at the S/G tube surfaces, since the coolant temperature decreases rapidly in a S/G tube. As a first step, the mass transfer coefficient between metal surfaces and bulk coolant across the boundary layer under turbulent flow conditions will be calculated.

To estimate mass transfer, the analogy between mass and heat transfer is often used since heat transfer is well understood, based on extensive experiments and computations, to the contrary of mass transfer. The analogy

between heat and mass transfer works well when the conditions listed below are met. [R-1]

(1) Species concentration is dilute

(2) Constant concentration of the species right at the surface

(3) Negligible forced diffusion such as thermophoresis, electrophoresis, and sedimentation

(4) No homogeneous chemical reaction

In the case of corrosion product (soluble and particulate) transport in the PWR, conditions (1), (2) and (4) are fairly well satisfied, but as regards condition (3), there is some argument that the large temperature gradients across the boundary layer in the core (~ 20 ^{o}C) and S/G(~6.8 ^{o}C) may cause thermophoresis or thermal diffusion. This argument will be treated separately in Section 2.5.1, which shows that at high temperature(~300 ^{o}C), thermal diffusion of the solubles may not be significant.

The mass transfer coefficient can only be calculated using empirical correlations obtained from experimental measurements. The uncertainties in the eddy diffusivity in the boundary layer under turbulent flow make it difficult to estimate the mass transfer coefficient analytically. Since explicit correlations for mass transfer are not available for soluble species transport in a PWR, the heat and mass transfer analogy will be employed. As shown in Table 3.2, the coolant in a PWR flows inside (S/G) and outside (core) tubes with very high Reynolds numbers (Re > 10^5). For fully developed turbulent flow inside tubes

under isothermal conditions, the well known Dittus-Boelter correlation for heat transfer [H-1] is,

$$Nu = 0.023\ Re^{0.8}\ Pr^{1/3}$$

or,

$$\left(\frac{D_e\, h}{k}\right) = 0.023 \left(\frac{\rho\ V\ D_e}{\mu}\right)^{0.8} \left(\frac{C_p\ \mu}{k}\right)^{1/3} \qquad (2.49)$$

where,

ρ	=	density of the fluid (kg/m^3)
μ	=	viscosity of the fluid ($N.S/m^2$)
V	=	velocity of the fluid (m/sec)
D_e	=	hydraulic diameter of the flow channel (m)
k	=	thermal conductivity of the fluid ($w/m^2.\ °K$)
C_p	=	specific heat capacity of the fluid (J/kg.°C)
Nu	=	Nusselt number
Re	=	Reynolds Number
Pr	=	Prandtl Number

In the analogous mass transfer correlation, the Prandtl number, which is the ratio of the momentum diffusivity to the thermal diffusivity, is replaced by the Schmidt number which is the ratio of the momentum diffusivity to the mass diffusivity, and the Nusselt number is replaced by the Sherwood number. Therefore the mass transfer correlation for the same flow condition is,

$$Sh = 0.023\ Re^{0.8}\ Sc^{1/3}$$

or

$$\left(\frac{D_e\, h}{D_{ab}}\right) = 0.023 \left(\frac{\rho\ V\ D_e}{\mu}\right)^{0.8} \left(\frac{\mu}{\rho\ D_{ab}}\right)^{1/3} \qquad (2.50)$$

where,

ρ	=	density of the fluid (kg/m^3)
μ	=	viscosity of the fluid ($N.sec/m^2$)
V	=	velocity of the fluid (m/sec)
D_e	=	hydraulic diameter of the flow channel (m)
D_{ab}	=	diffusion coefficient of the species (m^2/sec)
Sh	=	Sherwood number
Re	=	Reynolds Number
Sc	=	Schmidt Number

However, Berger and Hau [B-10] , who measured the mass transfer of ions in water using an electrochemical method [M-3] , where the measured current of ions depositing on the surface is converted into the mass transfer rate, developed a new correlation, which suggests that the Dittus-Boelter correlation under-estimates the mass transfer rate by about 20-30%,

$$Sh = 0.0165\ (Re)^{0.86}\ (Sc)^{1/3} \qquad (2.51)$$

over the range,

$$10^4 < Re < 10^6$$

$$0.6 < Sc < 10^4$$

It would appear that the above correlation is better suited for PWR flow conditions than the Dittus-Boelter correlation, considering the fact that one equation with a constant exponent and multiplier should not be able to cover the wide range of Re and Sc involved in mass transfer problems with precision equal to that of a relation restricted to a specific range. Moreover, the Burger and Hau correlation is for the exact system of present interest : ions in water. There are also available in the literature other slightly different forms of the mass transfer correlations for specific ranges of Re and Sc [N-1] [P-2], and the results are closer to Eq.(2.51) than Eq.(2.50).

From Eq. (2.51), the mass transfer coefficient, h, is:

$$h = 0.0165 \left(\frac{D_{ab}}{D_e}\right)\left(\frac{\rho V D_e}{\mu}\right)^{0.86} \left(\frac{\mu}{\rho D_{ab}}\right)^{1/3}$$

$$= 0.0165 \frac{\rho^{0.53} V^{0.86} D_{ab}^{0.67}}{\mu^{0.53} D_e^{0.14}} \qquad (2.52)$$

All parameters in Eq. (2.52) are readily estimated with the exception of the diffusion coefficient for soluble species, D_{ab}, which will be discussed in Section 2.3.3.

2.3.1.2 Particulate mass transfer

Deposition of particulate corrosion products from the coolant onto metal surfaces can be divided into two steps : mass transfer through the boundary layer, and attachment of the particle to the surface. Under turbulent flow conditions, transfer of the particle through the boundary layer is induced in an additive manner by the inertial momentum of the particle and Brownian diffusion [B-11].

It is generally indicated by experiment that when the size of the particle is large ($r_p > \sim 1\ \mu m$) , particle inertia is the main contribution to mass transfer. Two models are available to explain particle deposition by inertial momentum. Friedlander [F-1] proposed the stopping distance model, in which particles with a certain inertial momentum toward the surface tend to move to the surface across the boundary layer driven by that inertia; and Cleaver and Yate [C-3] proposed the " down sweep model " based on the microscopic nature of turbulent flow, where the periodic downsweep of the turbulent flow toward the surface causes the mass transfer of particles across the boundary layer. It is not clear at this point which model best explains particle deposition by inertial momentum, even though both models give similar results.

For smaller particles ($r_p < 0.1\ \mu m$), Brownian diffusion is the main contributor [B-12], since the inertia of the particle is so small as to be negligible. Hussain [H-2] demonstrated by experiment that magnetite particle ($r_{p,\ avg.} \sim 1.5\ \mu m$) deposition occurs by the Brownian diffusion and can be predicted using the same mass transfer correlation as for soluble species such as Eq. (2.51).

There also seems to be a consensus that the sticking probability of the particle onto the surface is approximately equal to one for small particles [B-11] [H-2].

It is difficult to measure the characteristics of the particulates in PWR primary coolant and it has not yet been fully confirmed to what extent particulates actually exist in hot PWR coolant. The difficulty is that the particulates in PWR primary coolant may redissolve during the temperature decrease, or deposit on sampling line surfaces, during the sampling process.

It can be assumed based upon what credible data is available that the size of the majority of particles in PWR coolant ranges from molecular radii to about ~1 μm. For this size range, it can assumed that the particle deposition is mainly controlled by Brownian diffusion. Therefore the same correlation as for soluble mass transfer, Eq.(2.51) can be used for the deposition of particles in PWR primary coolant, using appropriate values for the diffusion coefficient, D_p, as will be discussed in Section 2.3.3.

2.3.2 Crystal Growth and Dissolution

2.3.2.1 Crystal growth

Deposition of soluble corrosion products occurs in two steps.

- Conventional mass transfer of ionic corrosion products from the bulk of the solution to the vicinity of the metal surface
- Crystallization of solubles at the interface of the metal surface and the coolant

Mass transfer of corrosion products is discussed in Section 2.3.1.

Electron microscope examination shows that the oxide film formed on the fuel element surfaces under PWR operating conditions mainly consists of small nickel ferrite crystals in a porous overall aggregation having densities ranging generally between 0.1 and 0.4 of the theoretical density of the oxide crystals [S-1]. It can be assumed that the solution at the interface of the metal surface and the coolant is saturated. Therefore, when the soluble species in bulk coolant become super-saturated, the solubles in the bulk coolant are transported into the interface across the boundary layer, and subsequently the ionic corrosion product crystallizes or precipitates at the interface and deposits onto the metal surface. The crystallization rate of the soluble corrosion products can be expressed in terms of a crystallization constant and the degree of supersaturation as [J-2] [T-2],

$$J_{cr} = k_{cr} (C_i - C_{sat})^n \qquad (2.53)$$

where,

J_{cr} = crystallization rate [$kg/m^2.sec$]

k_{cr} = crystallization constant $\left[\frac{kg/m^2.sec}{(kg/m^3)^n}\right]$

C_{sat} = saturation concentration [kg/m^3]

C_i = soluble species concentration at the interface [kg/m^3]

n = order of reaction

The crystallization constant, k_{cr} depends upon such variables as temperature, the presence of impurities, surface tension and the activation barrier energy of the ions for dehydration and diffusion jump across the interface [N-2] [C-4], and can be expressed by the Arrhenius equation. [J-2]

$$k_{cr} = k_o \exp(-Q_{cr}/RT) \qquad (2.54)$$

where,

k_o = constant

Q_{cr} = activation barrier energy of the crystallization (J/mole)

R = gas constant (8.314 J/mole °K)

T = absolute temperature (°K)

The order of the crystallization reaction is empirically determined and can be one, two or an intermediate value, which depends upon the nature of the specific chemical reaction [J-2]. For simplicity, it will be assumed here that

crystallization of a soluble corrosion product is a first order reaction, that is, n=1. Then, the crystallization rate becomes,

$$J_{cr} = h_{cr}(C_i - C_{sat}) \qquad (2.55)$$

where,

h_{cr} = crystallization coefficient (which is equal to k_{cr} when n = 1.) (m/sec)

Then, the deposition rate of the ionic corrosion product can be obtained as follows. The mass transfer rate, J_{mt} is,

$$J_{mt} = h_{mt}(C_{bulk} - C_i) \qquad (2.56)$$

where,

h_{mt} = mass transfer coefficient (m/sec)

C_{bulk} = soluble species concentration in bulk coolant (kg/m^3)

The crystallization rate, J_{cr} is,

$$J_{cr} = h_{cr}(C_i - C_{sat}) \qquad (2.57)$$

In the steady state, the mass transfer rate and the crystallization rate are equal to the deposition rate, J_{dp}, that is,

$$J_{dp} = J_{mt} = J_{cr}$$

The deposition rate becomes, after removing the soluble concentration at the interface, C_i ,

$$J_{dp} = \frac{h_{cr}\, h_{mt}}{h_{cr} + h_{mt}} (C_{bulk} - C_{sat})$$

$$= h_{dp} (C_{bulk} - C_{sat}) \qquad (2.58)$$

where,

h_{dp} = deposition coefficient of soluble species (m/sec)

At the present level of understanding, the crystallization constant, h_{cr} can not be estimated from basic principles, but can only be obtained by experiments under problem specific conditions. Unfortunately, there is not much data available on the crystallization process of corrosion products under PWR operating conditions. Lister [L-3] has shown for the deposition of Co^{60} on stainless steel under PWR coolant chemistry conditions that,

$$h_{cr} = 1.13 \times 10^{-2} \sim 1.69 \times 10^{-5} \quad (m/sec)$$
$$h_{mt} = 1.94 \times 10^{-3} \quad (m/sec)$$

that is, the crystallization constant is 10^{-3} to 10 times the value of the mass transfer coefficient. Therefore, it is not yet clear that the deposition process of ionic corrosion products is controlled by the mass transfer step (when $h_{cr} >> h_{mt}$) , or by the crystallization step (when $h_{cr} << h_{mt}$). Further investigation of the crystallization process for corrosion products is still needed. Another point

at issue is whether the same kinetics constants apply to nucleation and growth of particles in solution as opposed to those situated on system surfaces.

2.3.2.2 Dissolution

Ionic corrosion products are released into bulk coolant by two steps.

- Dissolution of ionic corrosion products at the interface between the surface oxide film and the coolant
- Conventional mass transfer of ionic corrosion products across the boundary layer

The latter step is discussed in Section 2.3.1.

The dissolution of the corrosion products is the inverse process of crystallization of soluble corrosion products. It can be assumed that the soluble species at the interface between the surface oxide film and the coolant is saturated. Therefore, when the soluble species in bulk coolant become under-saturated, the soluble species at the interface are transported into bulk coolant across the boundary layer, and the corrosion products in the oxide film dissolve to restore the coolant at the interface to the saturated condition.

The dissolution of corrosion products is a type of chemical reaction. Since the corrosion product can exist at the surface oxide film interface in many forms, such as Fe, FeO, Fe_2O_3, Fe_3O_4, and $Fe_{3-x}Ni_xO_4$, it is necessary to consider a

variety of possible chemical reactions to evaluate the overall dissolution kinetics of the corrosion products.

The dissolution rate at the interface of metal and coolant can be simply expressed by [J-2]

$$J_{ds} = k_{ds}(C_{sat} - C_i)^n \qquad (2.59)$$

where,

J_{ds} = dissolution rate [$kg/m^2.sec$]

C_{sat} = saturation concentration [kg/m^3]

C_i = soluble species concentration at interface [kg/m^3]

k_{ds} = dissolution constant $\left[\frac{kg/m^2.sec}{(kg/m^3)^n}\right]$

n = order of reaction

The dissolution constant depends upon the temperature, activation barrier energy of dissolution and physical and chemical conditions at the interface, and can be expressed by the Arrhenius relation, just as for the crystallization constant.

$$k_{ds} = k_o \exp(-Q_{ds}/RT) \qquad (2.60)$$

where,

k_o = constant

Q_{ds} = activation barrier energy of dissolution (J/mole)

R = gas constant (8.314 J/mole. °K)

T = absolute temperature (°K)

The order of the dissolution reaction is empirically determined and can be generally one, two or an intermediate value, which depends upon the specific chemical reaction [J-2]. For simplicity, it will be assumed here that dissolution of soluble corrosion products is a first order reaction, that is, n=1. Then, the dissolution rate becomes,

$$J_{ds} = h_{ds}(C_{sat} - C_i) \tag{2.61}$$

where,

h_{ds} = dissolution coefficient (which is equal to k_{ds} when n = 1.) (m/sec)

Then, the release rate of the ionic corrosion products, J_{rl} can be obtained as follows. The mass transfer rate across the boundary layer is

$$J_{mt} = h_{mt}(C_i - C_{bulk}) \tag{2.62}$$

where,

h_{mt} = mass transfer coefficient (m/sec)

C_{bulk} = soluble species concentration in bulk coolant (kg/m^3)

And the dissolution rate is

$$J_{ds} = h_{ds}(C_{sat} - C_i) \tag{2.63}$$

In the steady state, the mass transfer rate and the dissolution rate are equal to the release rate, that is,

$$J_{rl} = J_{mt} = J_{ds}$$

Therefore, the release rate, J_{rl} becomes, after removing the soluble concentration at the interface, C_i ,

$$J_{rl} = \frac{h_{ds}\, h_{mt}}{h_{ds} + h_{mt}} (C_{sat} - C_{bulk})$$

$$= h_{rl} (C_{sat} - C_{bulk}) \qquad (2.64)$$

where,

h_{rl} = release coefficient of soluble species (m/sec)

The dissolution constant, h_{ds} can only be obtained for a specific reaction by experiments under applicable conditions. Lister [L-4] has carried out experiments on the release of iron corrosion products from activated 304 stainless steel coupons. He measured a release rate of 1.15×10^{-10} (gm-Fe/cm^2.sec), corresponding to a mass transfer coefficient of 8.2×10^{-2} (cm/sec), for a saturation concentration of soluble Fe of 1.4×10^{-9} (gm-Fe/cm^3) and an Fe concentration in bulk coolant of essentially zero. From this release rate, we can deduce the dissolution constant, h_{rl} for soluble Fe as 8.2×10^{-2} (cm/sec), which happens to be equal to the mass transfer coefficient, h_{mt}. This means that the dissolution constant approaches infinity and is far greater than the mass transfer coefficient.

Hence, mass transfer across the boundary is the rate controlling step in corrosion product release, and the resistance of the dissolution step is negligible. We again caution that data is very scarce on this point, which makes it difficult to assert that this is universally true under all PWR primary coolant system conditions.

2.3.3 Diffusion Coefficient

To calculate the mass transfer of corrosion products (soluble and particulate) in PWR primary coolant, their diffusion coefficients are necessary. The primary interest is both the soluble ions of the transition metals such as iron, cobalt and nickel, and the particulate forms of these species as transition metal oxides in high temperature water.

As will be shown in Figure 2.7, soluble iron corrosion products exist in diverse forms of ions such as Fe^{++}, $Fe(OH)^{+}$, $Fe(OH)_2$ and $Fe(OH)_3^{-}$ in aqueous solution. At low temperature, Fe^{++} ion is the dominant species, and $Fe(OH)_2$ becomes dominant at high temperature. Since all the iron ions exist in the hydrated form in aqueous solution, their ionic sizes are quite similar and therefore, it can be assumed that the diffusion coefficient of each ionic form is similar, based upon the Stokes-Einstein relation, which will be discussed later. Next examined will be how the diffusion coefficient of Fe^{++} ion can be obtained. Experimentally validated values of the required diffusion coefficients are not presently available at high temperature.

The diffusion coefficient of an electrolyte in an infinitely dilute solution can be calculated using the Nernst-Einstein Equation [R-2]:

$$D_{ab} = \frac{RT}{F^2} \frac{\left(\frac{1}{n^+} + \frac{1}{n^-}\right)}{\left(\frac{1}{\lambda_+^o} + \frac{1}{\lambda_-^o}\right)} = \frac{RT}{F^2} \left(\frac{1}{n^+} + \frac{1}{n^-}\right) t_+^o \, t_-^o \, \Lambda_{ab}^o \qquad (2.65)$$

where,

D_{ab} = diffusion coefficient of the electrolyte (m^2 / sec)

R = gas constant (8.314 J/mole ^oK)

T = absolute temperature (^oK)

$\lambda^o_{+,-}$ = limiting ionic conductance $(cm^2/\Omega.equiv.)$

F = Faraday's constant (96,500 c/g-equiv.)

$n^{+,-}$ = valence of the positive or negative ion

Λ^o_{ab} = limiting electrolyte conductance, defined as

$\Lambda^o_{ab} = \lambda^o_+ + \lambda^o_-$

$t^o_{+,-}$ = transference number of positive or negative ion, which is the fraction of the current carried by an ion in solution, defined as

$$t^o_+ = \frac{\lambda^o_+}{\lambda^o_+ + \lambda^o_-} = \frac{\lambda^o_+}{\Lambda^o_{ab}}$$

$$t^o_- = \frac{\lambda^o_-}{\lambda^o_+ + \lambda^o_-} = \frac{\lambda^o_-}{\Lambda^o_{ab}}$$

The self diffusion coefficient of tracer ions in a supporting electrolyte solution is given by the simpler expression [R-2].

$$D_{A^+} = \frac{\lambda^o_{A^+} R T}{|Z_{A^+}| F^2} \qquad (2.66)$$

where,

$|Z_{A^+}|$ = absolute value of the charge of A^+ ion.

In the present application, the presence of relatively large amounts of lithium hydroxide and boric acid in PWR primary coolant should make the above limiting expression a good approximation. It has been experimentally demonstrated that the Nernst-Einstein relation is good for ideal infinitely dilute electrolyte solutions.

From Eq. (2.65), the ratio of the diffusion coefficient of the electrolyte at T ^{o}C to that at 25 ^{o}C becomes,

$$\frac{D_{ab}(T\ ^{o}C)}{D_{ab}(25\ ^{o}C)} = \frac{T\,(^{o}K)}{298}\,\frac{\Lambda^{o}_{ab}(T\ ^{o}C)}{\Lambda^{o}_{ab}(25\ ^{o}C)}\,\frac{(t^{o}_{+}\ t^{o}_{-})_{T\ ^{o}C}}{(t^{o}_{+}\ t^{o}_{-})_{25\ ^{o}C}}$$

Since the change of t^{o}_{+} and t^{o}_{-} with temperature is very slight, it can be neglected [L-5], and the diffusion coefficient of the electrolyte at T ^{o}C can be expressed in terms of that at 25 ^{o}C and the limiting electrolyte conductances of the constituent ions.

$$D_{ab}(T\ ^{o}C) = \frac{T\,(^{o}K)}{298}\,\frac{\Lambda^{o}_{ab}(T\ ^{o}C)}{\Lambda^{o}_{ab}(25\ ^{o}C)}\,D_{ab}(25\ ^{o}C) \qquad (2.67)$$

And similarly, the self diffusion coefficient of ions at T ^{o}C can be expressed by that at 25 ^{o}C and limiting ionic conductance as,

$$D_{A^{+}}(T\ ^{o}C) = \frac{T\,(^{o}K)}{298}\,\frac{\lambda_{A^{+}}(T\ ^{o}C)}{\lambda_{A^{+}}(25\ ^{o}C)}\,D_{A^{+}}(25\ ^{o}C) \qquad (2.68)$$

The diffusion coefficient of dissociated $Fe(OH)_2$ electrolyte at 25 ^oC can be estimated by application of Eq. (2.65) using data in Table 2.2.

$$D_{Fe(OH)2} = \frac{3}{2} \frac{8.3144 \times 298}{(96500)^2} \left(\frac{1}{\frac{1}{54} + \frac{1}{199.2}} \right)$$

$$= 1.7 \times 10^{-5} \, (cm^2 / sec)$$

And similarly, the diffusion coefficient of Fe^{++} ion in supporting electrolyte solution at 25 ^oC can be obtained by Eq. (2.66) as,

$$D_{Fe^{++}} = \frac{54 \times 8.3144 \times 298}{2 \times (96500)^2} = 0.72 \times 10^{-5} \quad (cm^2/sec)$$

It is shown in Table 2.3 that Eq. (2.66) estimates the self diffusion coefficients of transition metal ions such as Fe^{++}, Co^{++} and Ni^{++} with high accuracy, considering that real solutions may not be "infinitely dilute". Generally, the diffusion coefficient of ions decreases slightly with the electrolyte concentration, according to Kohlrausch's law. [R-2]

$$\Lambda (c) = \Lambda_o - A \sqrt{c} \qquad (2.69)$$

where,

$\Lambda (c)$ = electrolyte conductance of concentration c molalities $(cm^2 / \Omega \, . \, equiv)$

Λ_o = limiting conductance of infinitely dilute electrolyte $(cm^2 / \Omega \, . \, equiv)$

Table 2.2 Limiting Conductances of Ions in aqueous solution (cm^2 / Ω equiv.)

Ion	25 °C	300 °C	Ref.
H^+	350.1	894	L-6, L-7
Na^+	50.11	459	F-2, Q-1
Fe^{++}	54	-	D-2
Co^{++}	53	-	D-2
Ni^{++}	50	-	D-2
Eu^{3+}	67.9	-	D-2
OH^-	199.2	821	L-6, L-7
Cl^-	76.35	561	F-2, Q-1

Table 2.3 Comparison of diffusion coefficients estimated by Nernst-Einstein relation with literature values at 25 ^{o}C (x 10^{-5} in cm^2/sec)

Ions	Nernst-Einstein Relation	Literature values at various concentrations	Ref.
Fe^{++}	0.72	0.2-0.7	M-6
Co^{++}	0.71	0.5-1.0	M-6
Ni^{++}	0.67	0.55-0.77	M-6
Eu^{3+}	0.60	0.6	L-8

A = constant (~ 200 - ~ 400)

c = concentration of electrolyte (molality)

However, the temperature in PWR primary coolant is around 300 ^{o}C, and the limiting ionic conductances of transition metal ions are not known at that temperature. Walden's rule, which states that the product of the limiting conductance and the viscosity of the electrolyte solution is constant with temperature, can be used to estimate the limiting conductance at high temperature. There is substantial concern that Walden's rule is not correct, especially at high temperature.[N-3] Walden's rule takes into account only the hydrodynamic friction of the moving ions in terms of solution viscosity, and neglects the dielectric friction effect of the ions in the solution [H-3] [H-4], which is not negligible at high temperature when the open structure of the water is destroyed.[N-3]

Figure 2.5 compares Walden's rule to literature data for the reference ionic salts ; NaCl and $BaCl_2$ [M-5] [L-5]. As can be seen, Walden's rule overpredicts the limiting conductivity by about 25 % for both salts at 300 °C. If it is assumed that Walden's product overpredicts <u>all ions</u> in aqueous solution by the same amount, the ratio of measured reference data to Walden's prediction can be used to get the limiting conductivity of Fe^{++} at high temperature. Table 2.4 compares the diffusion coefficients of Fe^{++} ion whose limiting conductivity was obtained by the above method, those calculated from Walden's product, and the literature values calculated theoretically using thermodynamic properties [O-1]. The latter predicts a Fe^{++} diffusion coefficient larger than that from the Walden' product,

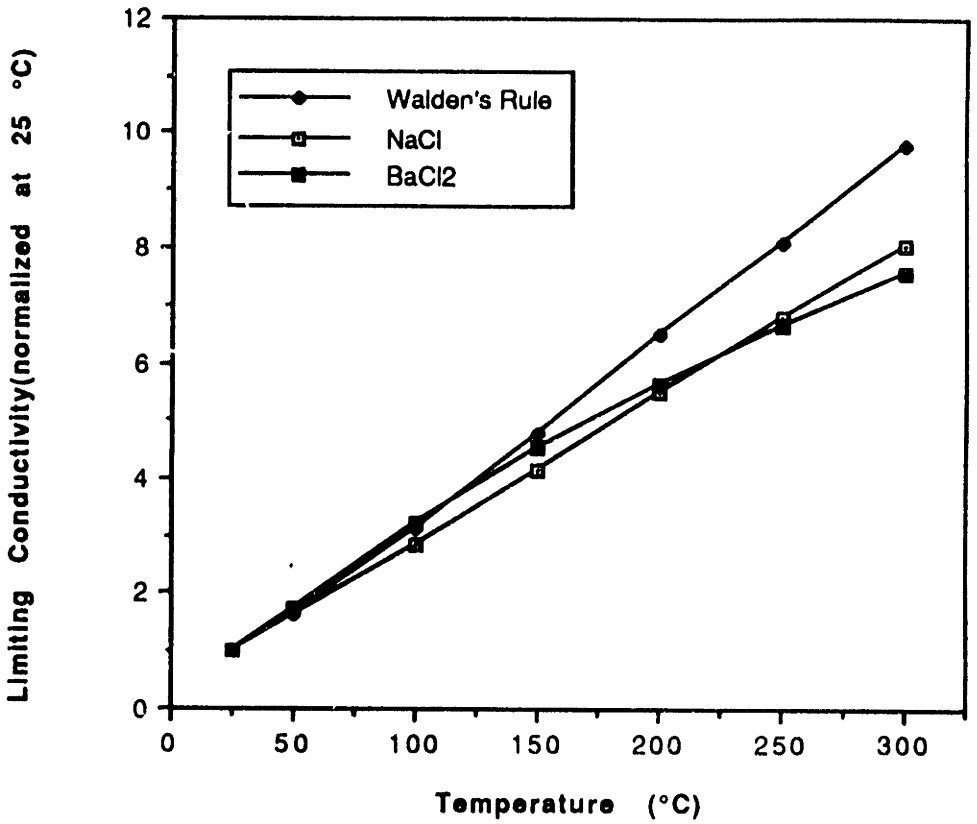

Figure 2.5 Comparison of Walden' Rule and Literature Data for the Limiting Conductivities of NaCl and $BaCl_2$

Table 2.4 Comparison of estimated Fe^{++} diffusion coefficients with those from Walden's rule and literature values ($D_{Fe^{++}} \times 10^5$ in cm^2/sec)

T (°C)	$D_{Fe^{++}}^{Estimated}$	$D_{Fe^{++}}^{Walden's\ Rule}$	$D_{Fe^{++}}^{Literature}$ [O-1]
25	0.72	0.72	0.8
100	2.74	2.84	3.2
200	6.37	7.46	8.6
300	10.8	13.5	15.4

so that it seems not to be realistic. We will choose the Fe^{++} diffusion coefficient at 300 °C to be $\underline{1.08 \times 10^{-4}}$ (cm^2/sec).

We now turn our attention to particulate species, to estimate the diffusion coefficient of a particle. The Stokes - Einstein relation can be used, in which the absolute mobility of a particle (which is assumed to be a hard sphere) is determined by hydrodynamic friction, which is related to the viscosity of the electrolyte solution and the particle radius.

$$D_p = \frac{kT}{4\pi\mu r_p} \qquad (2.70)$$

where

D_p = diffusion coefficient for a particle (m^2/sec)

k = Boltzmann constant (1.38×10^{-23} $J/^oK$)

T = absolute temperature (^oK)

r_p = radius of the particle (m)

μ = viscosity ($N.sec/m^2$)

It is known that the above equation predicts diffusion coefficients of a particle with the correct order of magnitude. [H-5]

As an example, for an 0.01 μm radius particle, the diffusion coefficient is

$$D_p = \frac{1.38 \times 10^{-23}\,(J/K) \times 573\,(^oK) \times 10^4\,(cm^2/m^2)}{4\,\pi \times 91.2 \times 10^{-6}\,(N.S/m^2) \times 0.01 \times 10^{-6}\,(m)}$$

$$= 6.9 \times 10^{-6}\ \ (cm^2/sec)$$

2.3.4 Transport Factor, β

The empirically determined transport factor, β in CRUDSIM controls the transport rate of both corrosion products and radioactivity, as shown in Eqs. (2.5) through (2.8). It was shown in Section 2.2.4 that the transport factor for crud and activity can be analytically determined as follows.

(i) Crud transport factor, β_c

The crud transport factor, β_c controls the transport rate of crud and, as derived in Section 2.2.4, can be calculated from

$$\beta_c = \left(\frac{k_1 k_3}{k_1 + k_3}\right) \frac{\rho_{H_2O}}{F} \qquad (2.47)$$

where,

k_1 = mass transfer factor of crud in core (m^3/sec)

k_3 = mass transfer factor of crud in S/G (m^3/sec)

ρ_{H_2O} = coolant density (kg/m^3)

F = coolant flow rate (kg-H_2O/sec)

Mass transfer factors in the core and S/G can be calculated using the mass transfer coefficients and dissolution or crystal growth coefficents as explained in Section 2.3.2. Release of the crud occurs in the S/G and the mass transfer factor in the S/G, k_3 , is

$$k_3 = h_{rl}\, A_3$$

$$= \frac{1}{\frac{1}{h_{ds}\, A_3} + \frac{1}{h_3\, A_3}} \qquad (2.71)$$

Deposition of the crud occurs in the core, so that the mass transfer factor in the core, k_1, is

$$k_1 = h_{dp}\, A_1$$

$$= \frac{1}{\frac{1}{h_1\, A_1} + \frac{1}{h_{dp}\, A_1}} \qquad (2.72)$$

Therefore, the crud transport factor, β_c is

$$\beta_c = \left(\frac{1}{\frac{1}{h_{ds}\, A_3} + \frac{1}{h_3\, A_3} + \frac{1}{h_1\, A_1} + \frac{1}{h_{cr}\, A_1}} \right) \frac{\rho_{H_2O}}{F} \qquad (2.73)$$

(ii) Activity transport factor, β_a

The activity transport factor, β_a controls the transport rate of activity, and can be calculated by the relation :

$$\beta_a = \left(\frac{k_1^a \, k_3^a}{k_1^a + k_3^a} \right) \frac{\rho_{H_2O}}{F} \qquad (2.48)$$

where,

k_1^a = mass transfer factor of activity in core (m^3/sec)

k_3^a = mass transfer factor of activity in S/G (m^3/sec)

ρ_{H_2O} = coolant density (kg/m^3)

F = coolant flow rate (kg-H_2O/sec)

Release of activity occurs in the core and, therefore, the mass transfer factor of the activity in core, k_1^a , is

$$k_1^a = h_{rl}^a \, A_1$$

$$= \frac{1}{\frac{1}{h_{ds}^a \, A_1} + \frac{1}{h_1 \, A_1}} \qquad (2.74)$$

The activity deposits on the S/G, so that the mass transfer factor in the S/G, k_3^a, is

$$k_3^a = h_{dp}^a \, A_3$$

$$= \frac{1}{\frac{1}{h_3 \, A_3} + \frac{1}{h_{cr}^a \, A_3}} \qquad (2.75)$$

Therefore, the activity transport factor, β_a becomes

$$\beta_a = \left(\frac{1}{\frac{1}{h^a_{ds} A_1} + \frac{1}{h_1 A_1} + \frac{1}{h_3 A_3} + \frac{1}{h^a_{cr} A_3}} \right) \frac{\rho_{H_2O}}{F} \qquad (2.76)$$

It was assumed in the original vergion of CRUDSIM that the activity transport factor is always equal to the crud transport factor and both are represented by the empirically determined β. However, as derived above, both transport factors need not be the same, since their transport paths are different as follows.

Crud transport path : dissolution at the S/G surface -> mass transfer across the boundary layer in the S/G -> mass transfer across the boundary layer in the core -> crystal growth on the core surface.

Activity transport path : dissolution at the core surface -> mass transfer across the boundary layer in the core -> mass transfer across the boundary layer in the S/G -> crystal growth on the S/G surface.

When the dissolution and crystal growth coefficients are much larger than the mass transfer coefficients (that is, crud and activity transport are controlled by the mass transfer coefficients in the core and S/G), k_1 and k_3 become equal to k^a_1 and k^a_3, respectively, so that the crud transport factor, β_c, becomes equal to the activity transport factor β_a. However, as will be shown in Table 3.2, when only the mass transfer coefficients are considered, the estimated transport factor, β is

about 45 times larger than the empirically determined value. Therefore, the crystal growth and dissolution steps can not be neglected. Here arises the principal difficulty in the analytic calculation of the transport factor, because, as discussed in Section 2.3.2, both dissolution and crystal growth coefficients can be accurately determined only by experiments under realistic conditions, and not by calculation from basic principles.

From the above Eqs. (2.73) and (2.76), it can be also said that when the dissolution coefficient is equal to the crystal growth coefficient, the crud transport coefficient becomes equal to the activity transport coefficient. However, this equality has not yet been substantiated by experimental evidence.

On the other hand, if the crystal growth coefficient is much smaller than the dissolution and mass transfer coefficients (that is, the crystal growth is the rate controlling step of corrosion product and activity transport), and the crystal growth coefficient of the crud in the core is equal to that of the activity in the S/G, the crud transport factor, β_c becomes about a third of the activity transport factor, β_a , since the surface area, A_1 , of core fuel elements (where deposition of the crud occurs) is about a third of the S/G tubing surface area, A_3 (where deposition of the activity occurs). However, in this line of reasoning, the effect of the temperature difference between the core surface (~320 °C) and the S/G surface (~293 °C) is not considered ; this may be important in determining the crystal growth constant, k_{cr} , according to the following equation, as explained in Section 2.3.2 :

$$k_{cr} = k_0 \exp(-Q_{cr}/RT) \qquad (2.54)$$

where,

k_o = constant

Q_{cr} = the activation barrier energy of crystallization

R = gas constant

T = absolute temperature (^oK)

Therefore, the crystal growth coefficient of the activity in the S/G can be much smaller than that of the crud in the core due to its lower temperature, so that the activity transport factor may in fact be smaller than the crud transport factor. The effect of the difference between the crud and activity transport factors upon the crud and activity transport will be studied in Section 3.3.2.1.

2.3.5 Neutron Activation Factor

The neutron activation factor, α characterizes the production rate of the radioactive elements such as Co^{60} and Co^{58} in the core . To estimate the neutron activation factor α, it is necessary to know the neutron spectrum , $\phi(E)$ and the appropriate cross-sections, as a function of energy E, $\sigma(E)$.

A direct approach to determination of the neutron activation factor is measurement of the neutron activation by inserting the material of interest into the reactor. By this method, we can easily get the total reaction rate, $(\sigma\phi)$ which is the integral or the product of $\phi(E)$ and $\sigma(E)$ over all energies. This measurement technique can also be used to measure the neutron fluxes when the cross-section is known, or, conversely, to estimate a cross-section when the neutron flux is known.

The other parameter which is necessary to calculate the neutron activation factor is the atomic number density of the elements such as Co^{59} and Ni^{58} in the core crud, relative to that of the dominant element, Fe. These elements can be released from S/G tubing and pipes, and deposit on the core in variable proportion because the factors characterizing the dissolution and deposition of these elements are different. Hence the relative ratios of cobalt and nickel to iron in the core crud are not necessary equal to the alloy compositions of the S/G and the pipes. In practice, differences are measured in power plant core crud composition. Table 2.5 [P-3] shows the measured composition of each alloy and the core crud in a representative PWR. Based upon these values, the relative fraction of the each nuclide in the core crud can be calculated as follows.

Table 2.5 Composition and Weight Data for a Typical Westinghouse PWR [P-3]

	Composition (%)				Weight Data
	Fe	Ni	Cr	Co	(Fe+Ni+Cr)
Fuel Crud	68 ± 7	29 ± 6	3 ± 2	0.17 ± 0.17	Core Total = 12 kg
Circulating Metals	76 ± 7	19 ± 4	6 ± 6	0.2 ± 0.1	Concentration = 26 ± 11 ppb
in Coolant					
Make-up water	~86	~10	~3		Concentration = 100 ppb
Inconel 600					
Base metal	8	73	19	~0.05	
Fixed oxide	27 ± 6	30 ± 8	43 ± 7		Areal weight = 0.63 ± 0.12
Loose oxide	39 ± 9	40 ± 9	21 ± 5		(gm / m^2)
Total oxide	27 ± 5	33 ± 8	39 ± 9	0.61 ± 0.46	
304 S.S.					
Base metal	71	10	19	~0.07	
Fixed oxide	41 ± 7	21 ± 8	38 ± 5	0.62 ± 0.37	Areal weight = 8.8 ± 5.6
Loose oxide	55 ± 14	34 ± 13	11 ± 8	0.22 ± 0.13	(gm / m^2)
Total oxide	47 ± 8	23 ± 9	30 ± 6	0.54 ± 0.38	

$f_{Co^{59}} = 0.17/68 = 0.25 \times 10^{-2}$

$f_{Ni} = 29/68 = 0.426$

$f_{Ni^{58}} = 0.6788 \times 29/68 = 0.289$

where f_i is the weight ratio of element i to iron in the core crud.

Our immediate goal is to calculate the neutron activation factor, α, used in CRUDSIM, in units of [Ci/kg-Fe.day.% power], for the neutron spectrum in the MITR-II. The fluxes of both the thermal and fast neutrons, and the neutron cross-section for each activation reaction were obtained from West's measurements [B-13], as shown in Table 2.6.

(i) Co^{60} activation factor, α^{60}, (Ci/kg-Fe.day.% power)

The production rate of Co^{60} in the core is expressed by,

$$\alpha^{60}\, p\, I_1 = F^{60}\, N_{Co^{59}} (\sigma_a^{59}\, \phi) \qquad (2.77)$$

where,

F^{60} = conversion factor (Ci-sec/Co^{60} atom-day)

$N_{Co^{59}}$ = number of Co^{59} atoms per kg-Fe in the core crud.

Thus,

Table 2.6 Neutron Fluxes and Cross Sections in MITR-II [B-13]

Reaction	Core Average Neutron Flux $(n / cm^2 sec)$	Cross Section (energy spectrum averaged)
$Co^{59}(n, \gamma) Co^{60}$	$\bar{\phi}_{2200} = 2.6 \times 10^{13}$	$\bar{\sigma}_{2200} = 37$ b
$Ni^{58}(n, p) Co^{58}$	$\bar{\phi}_{E>1\ Mev} = 5.0 \times 10^{13}$	$\bar{\sigma}_{E>1\ Mev} = 100$ mb
$Fe^{54}(n, p) Mn^{54}$	$\bar{\phi}_{E>1.5\ Mev} = 2.5 \times 10^{13}$	$\bar{\sigma}_{E>1.5\ Mev} = 134$ mb
$Ni^{60}(n, p) Co^{60}$	$\bar{\phi}_{E>4\ Mev} = 4.6 \times 10^{12}$	$\bar{\sigma}_{E>4\ Mev} = 23.4$ mb

$$\bar{\sigma}_{E>E_i} = \frac{\int_0^{\infty} \phi_f(E)\, dE}{\int_{E_i}^{\infty} \phi_f(E)\, dE}\ \bar{\sigma}_f$$

$$\alpha^{60}\, p\, I_1 = \left(\frac{4.18 \times 10^{-9} \times 24 \times 3600}{3.7 \times 10^{10}}\right)\left(\frac{f_{Co^{59}}\, I_1 \times 1000 \times N_A}{59}\right)\left(\sigma_a^{59}\, \phi\right)$$

where,

$f_{Co^{59}}$ = weight ratio of Co^{59} to iron in the core crud.

From the above expression, the Co^{60} activation factor, α^{60} is found to be

$$\alpha^{60} = 9.963 \times 10^{-14}\ f_{Co^{59}}\ \frac{\left(\sigma_a^{59}\, \phi\right)}{p} \qquad (2.78)$$

Using the unit neutron absorption reaction rate, $\left(\sigma_a^{59}\, \phi\right)$ in the MITR-II from Table 2.6 and $f_{Co^{59}}$ from Table 2.5 (i.e., 0.25×10^{-2}), the Co^{60} activation factor, α^{60} becomes,

$$\alpha^{60} = 9.963 \times 10^{-14} \times 0.25 \times 10^{-2} \times \frac{9.62 \times 10^{14}}{100}$$

$$= 2.40 \times 10^{-3} \quad [\text{ Ci/kg-Fe.day.\% power }].$$

(ii) Co^{58} activation factor, α^{58} (Ci/kg-Fe.day.% power)

Similarly, the Co^{58} production rate is,

$$\alpha^{58}\, p\, I_1 = F^{58}\, N_{Ni^{58}}\, (\, \sigma_{np}^{58}\, \phi\,) \qquad (2.79)$$

That is,

$$\alpha^{58}\, p\, I_1 = \left(\frac{1.12 \times 10^{-7} \times 24 \times 3600}{3.7 \times 10^{10}}\right)\left(\frac{f_{Ni^{58}}\, I_1 \times 1000 \times N_A}{58}\right)\left(\sigma_{np}^{58}\,\phi\right)$$

where,

F^{58} = conversion factor (Ci-sec/Co^{58} atom-day)

$N_{Ni^{58}}$ = number of Ni^{58} atoms per kg-Fe in the core crud

$f_{Ni^{58}}$ = weight ratio of Ni^{58} (67.88 % of natural Ni) to iron in the core crud.

Therefore, the Co^{58} activation factor, α^{58} is,

$$\alpha^{58} = 2.727 \times 10^{-12}\, f_{Ni^{58}} \frac{\left(\sigma_{np}^{58}\,\phi\right)}{p} \qquad (2.80)$$

Using the unit neutron reaction rate, $(\sigma_{np}^{58}\phi)$ in the MITR-II from Table 2.6 and the $f_{Ni^{58}}$ from Table 2.5 (i.e., 0.289), the Co^{58} activation factor, α^{58} becomes,

$$\alpha^{58} = 2.727 \times 10^{-12} \times 0.289 \times \frac{5.0 \times 10^{12}}{100}$$

$$= 3.94 \times 10^{-2} \quad [\text{Ci/kg-Fe.day.\% power}].$$

In a typical 1000 MWe Westinghouse PWR, the neutron activation factors of Co^{60} and Co^{58} are quoted as being [B-9] :

$$\alpha^{60} = 2.145 \times 10^{-3}$$

$$\alpha^{58} = 7.38 \times 10^{-2}$$

Therefore, the activation factors in the MITR-II are within about a factor of 2 of those for a typical 1000 MWe PWR.

2.3.6 Corrosion Rate

The oxide film formed on both Inconel and stainless steel under PWR operating conditions has a duplex structure, as shown in Figure 2.6 for Inconel. The composition of the oxide film depends upon the nature of the base metal and the chemistry to which the metal is exposed, such as temperature, pH and concentrations of oxygen and hydrogen. The inner layer is composed of (Cr, Ni, $Fe)_3O_4$ and, in particular, Cr_2O_3 which forms a tight oxide film that protects the base metal from corrosion. The outer layer consists of relatively weakly bound and non-protective oxides : $(Fe, Ni)_2O_3$ or $(Fe,Ni)_3O_4$, depending upon the oxygen concentration in the coolant. [L-9] Therefore, the corrosion rate of the base metal is controlled by the passivity of the inner layer.

Several mechanisms have been proposed to describe the corrosion process.[F-3] Among them, the point defect model (PDM) has demonstrated good agreement with experimental results for the corrosion of both Inconel and stainless steel in aqueous environments [M-7] ; it predicts a logarithmic growth of oxide film with time. Under the logarithmic growth kinetics of the PDM, after a initial large corrosion rate during a pre-transition passivation period, the corrosion rate is inversely proportional to time.

During the corrosion process, oxygen is transported as an anion by diffusion across the passive oxide film to the base metal and forms stable oxides at the oxide film/base metal interface. Among Fe,Ni and Cr, the latter is the strongest oxide-forming element [G-1], and therefore, the oxygen in $(Fe,Ni)_2O_3$ may tend to move to neutral chromium in base metal to form the more stable

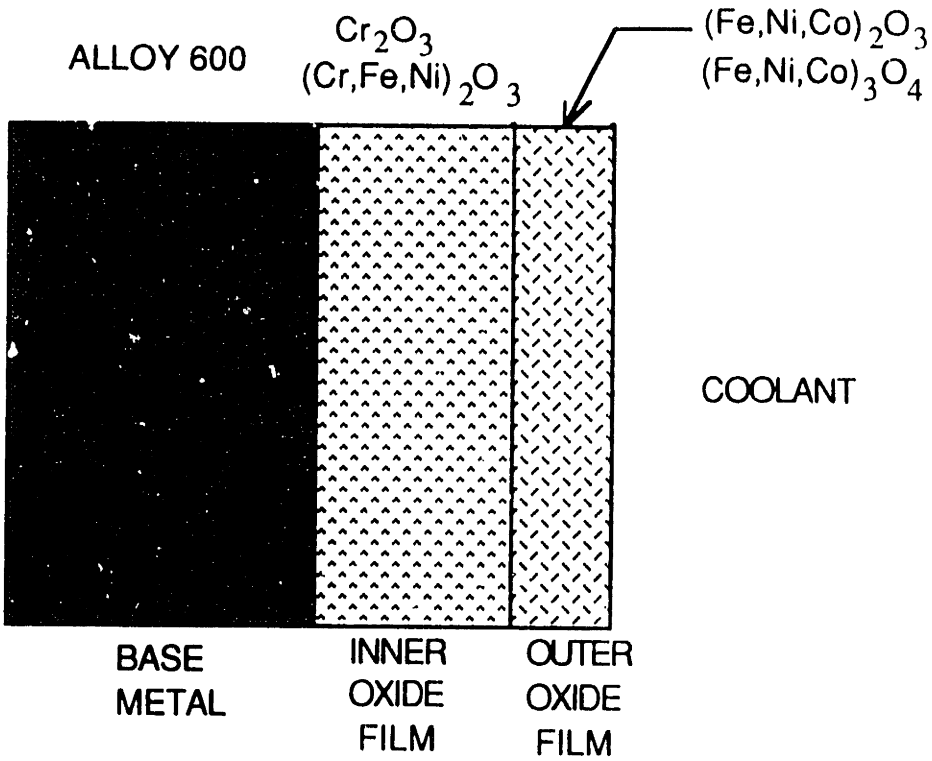

Figure 2.6 Configuration of Surface Oxide Film on S/G Inconel 600 Tubing

chromium oxide. Cations such as Fe and Ni, deprived of oxygen by the Cr in the inner layer are transported by diffusion, with the help of point defects, through the passive oxide film to the solution/oxide film interface and subsequently dissolve into the solution or are precipitated into porous oxides such as (Fe, $Ni)_3O_4$, depending upon the degree of saturation of Fe and Ni solubles in the solution. The thickness of the outer oxide layer depends upon the net dissolution rate of the Fe and Ni into the coolant (and, of course, the net effect of erosion/deposition of coolant-borne particulates).

Auger Electron Spectroscopy (AES) and X-ray Photoelectron Spectroscopy (XPS) analyses of the oxide films of both Inconel and stainless steel [L-9] [L-10] have shown that the chromium oxide is prominent in the inner layer, and that the Fe and Ni are dominant in the outer layer in comparison with the base metal composition. In the outer layer, there is also more oxygen, which is in transit from the coolant to the base metal. The driving force for the movement of charged ions of oxygen, Fe and Ni is considered to be the electrical potential gradient between the base metal and solution.

The magnitude of the diffusive mass transport of the Fe and Ni from the inner layer to the outer layer is designated as the "corrosion rate," CR, as used in the present modelling. It may depend on the oxygen level, pH and temperature of the coolant. Table 2.7 shows that the literature data on the corrosion rates (which is the mass depletion rate of base metal) of Inconel 600 and 304 stainless steel under PWR operating conditions exhibits large variations.

Table 2.7 Representative literature data on corrosion rates of Inconel 600 and 304 stainless steel under nominal PWR conditions

Data Set	Inconel 600 (mg/dm^2-month)	304 S.S. (mg/dm^2-month)	reference
1	5.25 ± 1	73.3 ± 46.7	P-3
2	~4.67	2	W-2
3	~1.1	-	B-9
4	0.5 ± 0.1	-	P-4

As will be discussed in Chapter 3, however, crud transport from S/G tubing to the core is independent of the corrosion rate, CR, and radio-nuclide transport is also insensitive to this parameter. Hence, for present purposes, it may not be particularly important to sort out these inconsistencies.

2.3.7 Solubility of Corrosion Products

The corrosion products formed on the surfaces of the S/G Inconel tubing and stainless steel under nominal PWR coolant chemistry - very low oxygen content (< 10 ppb) and high hydrogen partial pressure (~ 25 cc H_2/kg-H_2O) - are measured to be mainly nickel-ferrite ($Ni_xFe_{3-x}O_4$) or nickel-cobalt-ferrite ($Ni_xCo_yFe_{3-x-y}O_4$), with the x value (or x+y in the $Ni_xCo_yFe_{3-x-y}O_4$) ranging from 0.45 to 0.75. [K-2]

Based upon the composition ratio of nickel-ferrite, the solubility of the iron can be calculated by using chemical dissociation reactions of the nickel-ferrite. The dissolved iron consists of the four dominant ionic forms such as Fe^{++}, $Fe(OH)^-$, $Fe(OH)_2$, and $Fe(OH)_3^+$, and the solubility of the iron is the sum of the saturation (or equilibrium) concentrations of these ions. The saturation concentrations of these ions change differently with temperature and pH and so does the solubility of the iron. The chemical reactions and reaction constants of the nickel-ferrite, $Ni_xFe_{3-x}O_4$, and each of the iron ions are as follows.

(i) Fe^{++}

$$\frac{1}{(3-x)} Fe_{3-x}O_{4-x\,(c)} + \frac{1}{(3-x)} H_{2\,(g)} + 2\,H^+_{(aq)} \rightarrow Fe^{++}_{(aq)} + \frac{(4-x)}{(3-x)} H_2O$$

$$K_0 = \frac{[Fe^{++}]}{[P_{H_2}]^{1/(3-x)}\ [H^+]^2} \qquad (2.81)$$

(ii) $Fe(OH)^+$

$$\frac{1}{(3-x)} Fe_{3-x}O_{4-x\,(c)} + \frac{1}{(3-x)} H_{2\,(g)} + H^+_{(aq)} \rightarrow Fe(OH)^+_{(aq)} + \frac{1}{(3-x)} H_2O$$

$$K_1 = \frac{[Fe(OH)^+]}{[P_{H_2}]^{1/(3-x)}\ [H^+]} \qquad (2.82)$$

(iii) $Fe(OH)_2$

$$\frac{1}{(3-x)} Fe_{3-x}O_{4-x\,(c)} + \frac{1}{(3-x)} H_{2\,(g)} + \frac{(2-x)}{(3-x)} H_2O \rightarrow Fe(OH)_{2\,(aq)}$$

$$K_2 = \frac{Fe(OH)_2}{[P_{H2}]^{1/(3-x)}} \qquad (2.83)$$

(iv) $Fe(OH)_3^-$

$$\frac{1}{(3-x)} Fe_{3-x}O_{4-x\,(c)} + \frac{1}{(3-x)} H_{2\,(g)} + \frac{(5-2x)}{(3-x)} H_2O \rightarrow Fe(OH)^-_{3\,(aq)} + H^+_{(aq)}$$

$$K_3 = \frac{[Fe(OH)_3^-]\ [H^+]}{[P_{H2}]^{1/(3-x)}} \qquad (2.84)$$

Therefore, the solubility of the iron is

$$S = [Fe^{++}] + [Fe(OH)^+] + [Fe(OH)_2] + [Fe(OH)_3^-]$$

$$= [P_{H_2}]^{1/(3-x)} \left(K_0 [H^+]^2 + K_1 [H^+] + K_2 + K_3 \frac{1}{[H^+]} \right) \quad (2.85)$$

The dissociation constant, K_i of each reaction is a function of the free energy change of each reaction, ΔG_i .

$$K_i = EXP \left(\frac{-\Delta G_i}{RT} \right) \quad (2.86)$$

where,

$$\Delta G_i = \Delta H_i - \Delta S_i T \quad (2.87)$$

so,

$$\log_e K_i = - \frac{\Delta H_i}{RT} + \frac{\Delta S_i}{R} \quad (2.88)$$

The free energy change of the chemical reaction, ΔG_i varies with temperature and is difficult to measure, as are the reaction constants, K_i and the resulting solubility of the iron.

Lindsay [L-11] has calculated the solubility of the iron by fitting measurements of nickel-ferrite solubility. The model equation is,

$$S = 10^6 A P_{H2}^{1/(3-x)} \left(K_0 \frac{z^2}{\gamma_1^2} + K_1 z + \frac{K_2}{\gamma_0} + \frac{K_3}{\gamma_1^2 z} \right) \quad (2.89)$$

where,

S = iron solubility (μmols/kg)

A = stoichiometric factor for the solid = $(1-x)^{(1-x)/(3-x)}$

with x = the value of x for nickel-ferrite, or

x = the sum x+y for nickel-cobalt-ferrite

z = hydrogen ion concentration, given by $z = 10^{-pH}$

P_{H2} = hydrogen partial pressure (atm)

γ_1 = generic activity coefficient for univalent ions

γ_0 = activity coefficient for neutral species

The constants, K_i are expressed by,

$$\log_{10} K_0 = A_0 + \frac{B_0}{T} \qquad (2.90a)$$

$$\log_{10} K_1 = A_1 + \frac{B_1}{T} \qquad (2.90b)$$

$$\log_{10} K_2 = A_2 + \frac{B_2}{T} \qquad (2.90c)$$

$$\log_{10} K_3 = A_3 + \frac{B_3}{T} + \log_{10} K_w \qquad (2.90d)$$

where,

K_W = thermodynamic ion product for water

T = absolute temperature (^{o} K)

The parameters A_i and B_i, together with other thermodynamic properties, are determined by least square fitting of iron solubility measurements, and best-estimate values are shown in Table 2.8.

In the derivation of the above model, the following assumptions were used :

1. Dissolved iron species include only Fe^{++}, $Fe(OH)^+$, $Fe(OH)_2$, and $Fe(OH)_3^-$
2. No ferric iron species are in solution.

Table 2.8 Best Estimated Values of Constants in Eq. (2.90)

A0	-1.191
A1	-4.160
A2	-6.765
A3	6.309
B0	3400
B1	1543
B2	-31
B3	-5713

3. Conditions are neither so reducing nor so oxidizing that the molar ratio, in the solid, of trivalent iron to total divalent metal departs significantly from 2:1.
4. Transfer of one mole of iron from solid to solution involves 2/(3-x) moles of trivalent iron and (1-x)/(3-x) moles of divalent iron.
5. Generic (non-specific) activity coefficients, dependent only on ionic strength, apply.
6. The form of Eqs. (2.90a) to (2.90d) is justified by isocoulombic representation of solubility equilibria.

Figures 2.7, 2.8, 2.9 and 2.10 show the solubility variations of the iron ions such as Fe^{++}, $Fe(OH)^{+}$, $Fe(OH)_2$, and $Fe(OH)_3^{-}$ with temperature and pH at 300 °C. The solubility of the iron generally decreases with temperature. As shown in Figure 2.10, however, at high temperature and high pH, the solubility of the iron starts to increase due to the increase of the solubility of the $Fe(OH)_3^{-}$. As will be discussed later, this observation is the basis of the proposition that the operating pH of PWR primary coolant should be increased above pH 7 at 300 °C to decrease the corrosion product transport from S/G to core.

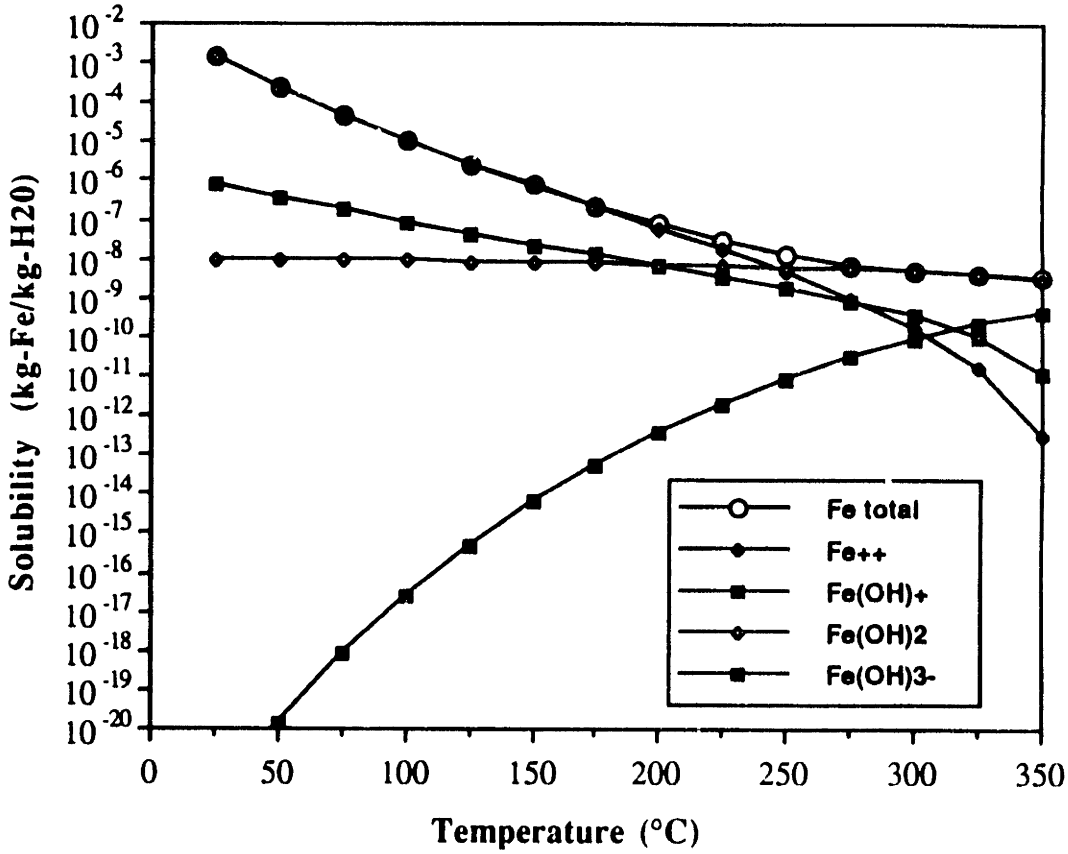

Figure 2.7 Fe Solubility versus Temperature at pH 6.5 at 300 °C with dissolved hydrogen concentration of 25 (cc-H_2/kg-H_2O)

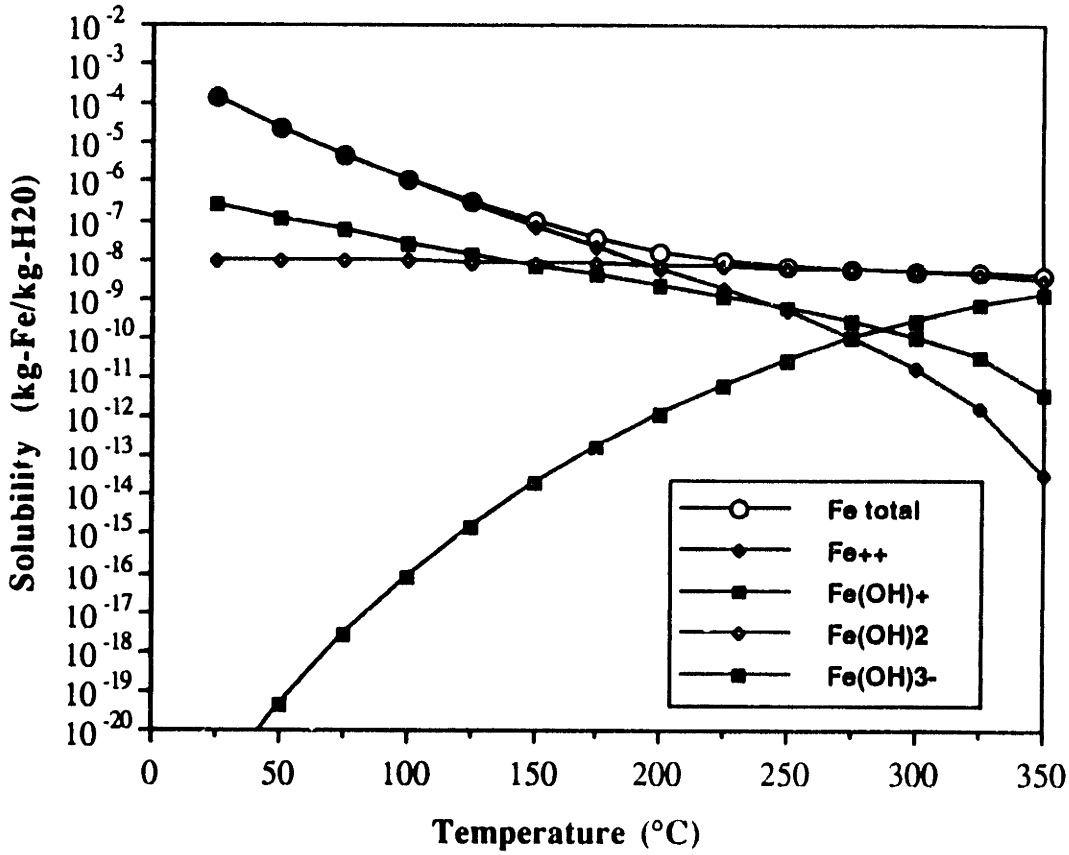

Figure 2.8 Fe Solubility versus Temperature at pH 7.0 at 300 °C with dissolved hydrogen concentration of 25 (cc-H_2/kg-H_2O)

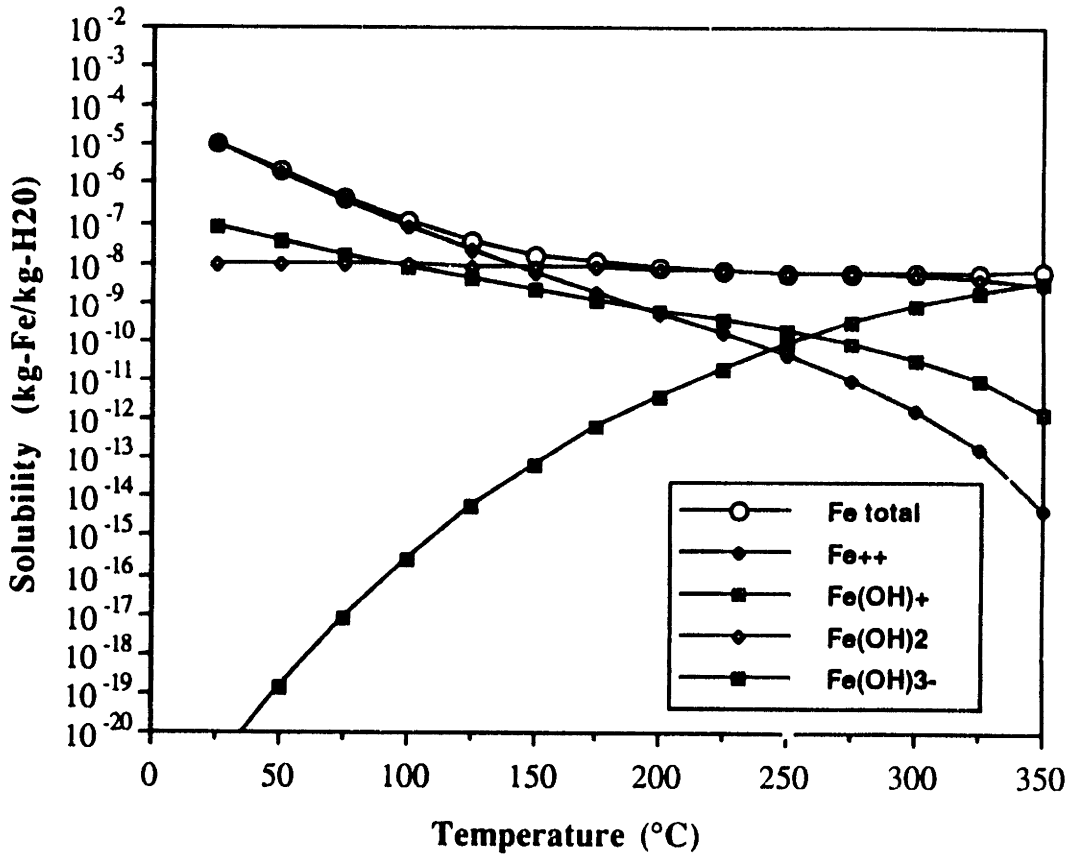

Figure 2.9 Fe Solubility versus Temperature at pH 7.5 at 300 °C with dissolved hydrogen concentration of 25 (cc-H_2/kg-H_2O)

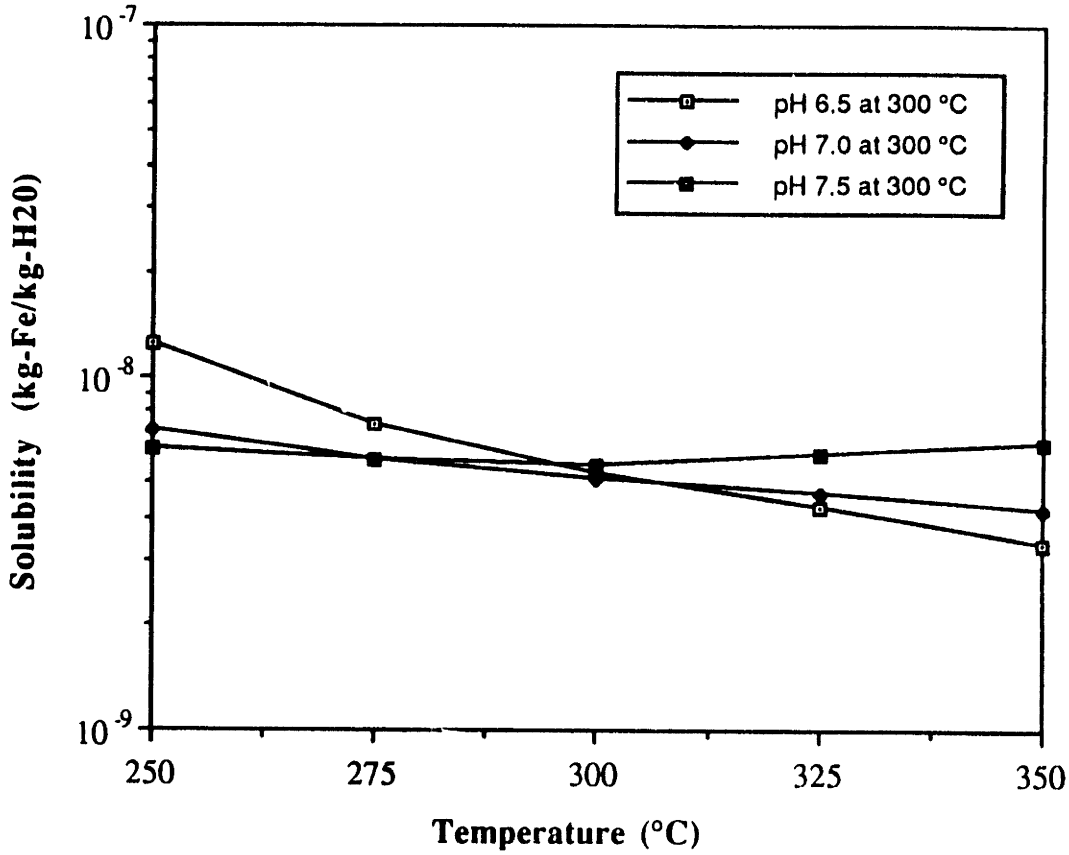

Figure 2.10 Fe solubility change with temperature and three different values of boric acid and lithium hydroxide concentration, each corresponding to a different value of pH at 300 °C with dissolved hydrogen concentration of 25 (cc-H_2/kg-H_2O)

2.4 Particulate Transport

2.4.1 Soluble versus particle transport

Dissolved species may precipitate as particles in super-saturated regions of the PWR primary loop. However,due to the difficulty in measuring particulates in hot and high pressure primary coolant, the amount and size distribution of such particles has not yet been fully confirmed. To sample and measure primary coolant, the use of long and small-diameter sampling tubing is necessary between the PWR primary system and measurement instruments. During sampling, coolant conditions (such as temperature, pressure and chemistry) may change, and hence the particle may dissolve, or it may deposit on the surface of the sampling tubing. These make it quite difficult to directly characterize the particles in the coolant. In particular, the solubility of corrosion products is very sensitive to temperature, so that a slight decrease in temperature may dissolve coolant-born particles.

In this section, some fundamental aspects of particle existence in the primary coolant will be studied by examining the relative behavior of particles and solubles in primary coolant. There are four possible fates for corrosion products (solubles and particles) in PWR primary coolant.

- Soluble species deposition on surfaces
- Solubles diffusion to particles in the coolant
- Particle deposition on surfaces
- Particle agglomeration in the coolant

By comparing the transfer rates for the above four ways of corrosion product behavior, we can judge, at least qualitatively, the relative importance of particle formation in the coolant. The relevant corrosion product transfer rates are as follows :

(i) Soluble deposition on wall

The solubles in a super-saturated region can deposit on a surface wall. The deposition of the solubles occurs by convective mass transfer and crystallization on the surface. The soluble deposition rate on the surface in the primary circuit (SW) can be obtained by

$$SW = \sum_i h^i_{d,\,sw}\, A_i \left(C^i_{s,\,bulk} - C^i_{s,\,surf.}\right) \qquad (2.91)$$

where,

$h^i_{d,\,sw}$ = soluble deposition coefficient on the surface in the i-th region (m/sec)

A_i = surface area in the i-th region (m^2)

$C^i_{s,\,bulk}$ = soluble concentration in bulk coolant in the i-th region (kg/m^3)

$C^i_{s,\,surf}$ = soluble concentration at the surface in the i-th region (kg/m^3)

i = regions where soluble species are super-saturated such as core, core outlet plenum, hot leg, and S/G inlet plenum.

The deposition coefficient of the solubles, $h^i_{d,sw}$, can be expressed as

$$h^i_{d,sw} = \frac{h^i_{mt,sw}\ h_{cr}}{h^i_{mt,sw} + h_{cr}} \qquad (2.92)$$

where,

$h^i_{mt,sw}$ = mass transfer coefficient of soluble species in the i-th region (m/sec)

h_{cr} = crystallization coefficient of soluble species (m/sec)

(ii) Soluble diffusion to particles in the coolant

The solubles in the super-saturated region can diffuse to the particles in the coolant and deposit on their surface. The soluble transfer rate is proportional to the particle concentration in the coolant, and more precisely, the total surface area of the particles. The soluble transfer rate to the particles (SP) can be expressed, as a function of the particle concentration and size, by

$$SP = \sum_i 4\ \pi\ r_p^2\ n_p\ h_{d,sp} \Delta C_i^p\ V_i \qquad (2.93)$$

where,

r_p = average radius of the particles (m)

n_p = number density of particles in the coolant (#/m^3)

$h_{d,sp}$ = soluble deposition coefficient on the particles (m/sec)

ΔC_i^p = soluble concentration difference between the super-saturated bulk region and the saturated particle surface in the i-th region (kg/m^3)

V_i = coolant volume of the i-th region (m^3)

i = regions where soluble species are super-saturated such as core, core outlet plenum, hot leg, and S/G inlet plenum.

The soluble deposition coefficient on the particle surface can be expressed by,

$$h_{d,\,sp} = \frac{h_{mt,sp}\ h_{cr}}{h_{mt,sp} + h_{cr}} \qquad (2.94)$$

where,

$h_{mt,sp}$ = mass transfer coefficient of solubles onto particles in the coolant (m/sec)

h_{cr} = crystallization coefficient of soluble species (m/sec)

The mass transfer coefficient of soluble species onto particles in the coolant is

$$h_{mt,sp} = \frac{D_s}{r_p} \qquad (2.95)$$

where,

D_s = diffusion coefficient of solubles (m^2/sec)

r_p = radius of particle (m)

(iii) Particle deposition on wall

A particle in the coolant can deposit on surfaces by convective mass transfer. Unlike soluble species deposition, particle deposition can occur everywhere in the primary circuit, independent of the soluble species saturation status in the coolant. The particle deposition rate on the surface (PW) can be expressed by

$$PW = \sum_i h^i_{mt,pw} A_i (C_{pt,bulk} - C_{pt,surf}) \qquad (2.96)$$

where,

$h^i_{mt,pw}$ = mass transfer coefficient of particles in the i-th region (m/sec)

A_i = surface area in the i-th region (m^2)

$C_{pt,bulk}$ = particle concentration in bulk coolant (kg/m^3)

$C_{pt,surf}$ = particle concentration at the surface (kg/m^3)

i = regions where particles can deposit, which includes all regions of the PWR primary loop.

In the deposition of a small particle ($r_p < 1\ \mu m$) on the wall, the sticking coefficient onto the wall is nearly 1 [B-12]. Therefore, the concentration of the particles on the wall, $C_{pt,surf}$ is almost zero.

(iv) Particle agglomeration in the coolant

The particles in the coolant may collide with each other, driven by Brownian thermal motion and agglomerate (i.e., stick together). The particle agglomeration rate (PA) can be expressed by [P-5]

$$PA = \sum_i 8 \pi D_p r_p n_p^2 \epsilon_a M_p V_i \qquad (2.97)$$

where,

D_p = diffusion coefficient of the particle (m^2/sec)

r_p = radius of the particle (m)

n_p = number density of the particles in the coolant ($\#/m^3$)

ϵ_a = probability that the particles stick together after a collision

M_p = mass of a particle (kg)

V_i = coolant volume in the i-th region (m^3)

i = regions where particle agglomeration can occur ; actually particles can agglomerate in all regions.

By comparing the ratios of the above four cases, we can get some insight into how coolant-borne particles behave. The values of the various parameters used in the calculations and further assumptions and approximations, are shown in Tables 2.9 and 2.10. In the calculation of soluble species deposition on both the wall and particles, two limiting cases are considered : mass transfer controlled and crystallization controlled, since, as discussed in Section 2.3.2, it is not yet clear which step is rate-controlling for soluble deposition. The ratios are as follows.

Table 2.9 Data used for typical 1000 MWe PWR Primary system

zone number (i)	region	coolant volume (m^3)	surface area (m^2)
1	core	22.8	5550
2	core outlet plenum hot leg S/G inlet plenum	49.38	~ 100
3	S/G tubing	78.72	20440
4	S/G outlet plenum cold leg RC pump core downcomer core lower plenum	132.72	~ 200
total		283.62	26290

coolant flow rate = 23.8 (m^3/sec)

total active coolant volume = 283.62 (m^3)

transit time per cycle = coolant volume / flow rate = 12 (sec)

Table 2.10 Data used in the calculations for particle/soluble behavior

- Coolant

$T = 300\ (^{o}C)$

$\rho_{H_2O} = 712.5\ (kg/m^3)$

- Soluble Species

$D_s = 1.1 \times 10^{-8}\ (m^2/sec)$

$r_s = 4.2 \times 10^{-9}\ (m)$ (obtained from the Einstein-Stokes relation and the diffusion coefficient)

$C_{s,\,bulk} = 5\ ppb = 3.6 \times 10^{-6}\ (kg\text{-}Fe/m^3)$

$(C_{s,\,bulk} - C_{s,\,surf.})_{core} \cong 0.1\ C_{s,\,bulk}$

$(C_{s,\,bulk} - C_{s,\,surf.})_{S/G} \cong 0.03\ C_{s,\,bulk}$

$\Delta C_i^p \cong 0\ 1\ C_{s,\,bulk}$

$h^1_{mt,sw} \cong h^3_{mt,sw} \cong 0.25 \times 10^{-2}\ (m/sec)$

$h^2_{mt,sw} \cong h^4_{mt,sw} \cong 0\ (m/sec)$

$h^i_{d,\,sw} \cong h^i_{mt,sw}$ and $h_{d,\,sp} \cong h_{mt,sp}$, when $h_{cr} >> h^i_{mt,sw}$ and $h^i_{mt,sp}$ (mass transfer controlled)

$h^i_{d,\,sw} \cong h_{cr}$ and $h_{d,\,sp} \cong h_{cr}$, when $h_{cr} << h^i_{mt,sw}$ and $h_{mt,sp}$ (crystal growth controlled), assuming $h_{cr} = 0.25 \times 10^{-4}\ (m/sec)\ \left(= \frac{1}{100} h^1_{mt,sw}\right)$

- Particles

$r_p = a_1\ r_s$

$C_p = a_2\ C_s$

$D_p = a_1^{-1}\ D_s$

$h_p^i = a_l^{-0.667} h_{sw}^i$ for all the i-th regions

$\rho_p = 3000\ (kg/m^3)$

$\epsilon_a = 1.0$

$C_{p,\,surf.}^i \cong 0$ for all the i-th regions

$n_p = C_p / M_p$

$M_p = \frac{4}{3} \pi r_p^3 \rho_p$

$$R^{mt}_{sp/sw} = \left(\frac{SP}{SW}\right)_{mt} = 11.68\ \frac{a_2}{a_1^2} \qquad (2.98)$$

$$R^{\alpha}_{sp/sw} = \left(\frac{SP}{SW}\right)_{\alpha} = 0.011\ \frac{a_2}{a_1} \qquad (2.99)$$

$$R_{pa/pw} = \frac{PF}{PW} = 19.5 \in_a a_1^{-2.33}\ a_2 \qquad (2.100)$$

$$R^{mt}_{pw/sp} = \left(\frac{PW}{SP}\right)_{mt} = 4.0\ a_1^{1.33} \qquad (2.101)$$

$$R^{\alpha}_{pw/sp} = \left(\frac{PW}{SP}\right)_{cr} = 4.2 \times 10^5\ a_1^{0.33} \qquad (2.102)$$

where,

a_1 = r_p/r_i (ratio of particle to ion radii)

a_2 = C_p/C_i (ratio of particle to ion concentrations)

subscript - mt = mass transfer controlled solubles deposition

subscript - cr = crystal growth controlled solubles deposition

Figures 2.11, 2.12 and 2.13 show how each ratio changes with particle radius at a constant concentration of particles. It is notable that, as the particle radius decreases, more solubles tend to diffuse to coolant-borne particles than to deposit on surfaces. Therefore, it may be assumed that small particles nucleate in the super-saturated region, grow until they reach a radius of about 0.01 μm by both soluble diffusion and particle agglomeration, and deposit on the surfaces still as a small particle before growing into larger ones, since a particle has a

Note :

PW = particle deposition rate on the surface wall

SP = soluble species deposition rate on the particles in the coolant

SW = soluble species deposition rate on the surface wall

PA = particle agglomeration rate in the coolant

(MT) = mass transfer controlled soluble species deposition

(CR) = crystal growth controlled soluble species deposition

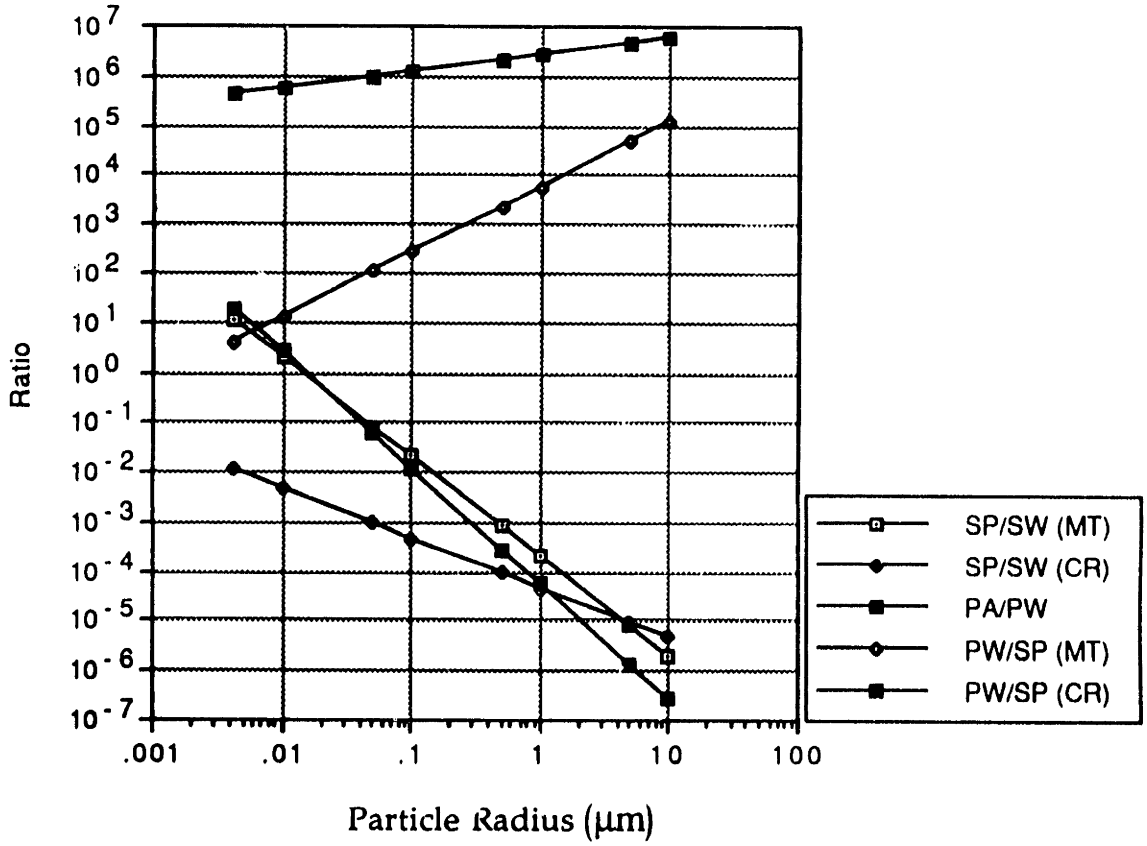

Figure 2.11 Relative Particle and Soluble Transfer Rates when $C_p/C_i = 1.0$

Note :

PW = particle deposition rate on the surface wall

SP = soluble species deposition rate on the particles in the coolant

SW = soluble species deposition rate on the surface wall

PA = particle agglomeration rate in the coolant

(MT) = mass transfer controlled soluble species deposition

(CR) = crystal growth controlled soluble species deposition

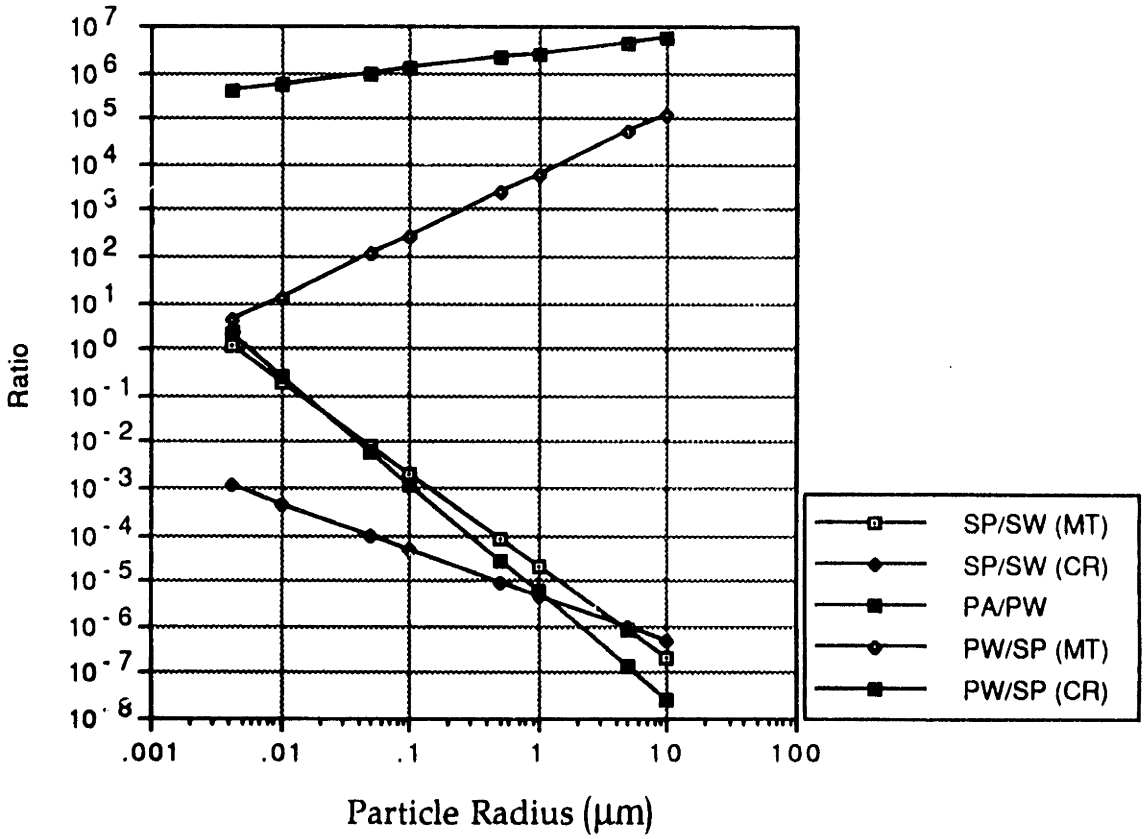

Figure 2.12 Relative Particle and Soluble Transfer Rates when $C_p/C_i = 0.1$

Note :

PW = particle deposition rate on the surface wall

SP = soluble species deposition rate on the particles in the coolant

SW = soluble species deposition rate on the surface wall

PA = particle agglomeration rate in the coolant

(MT) = mass transfer controlled soluble species deposition

(CR) = crystal growth controlled soluble species deposition

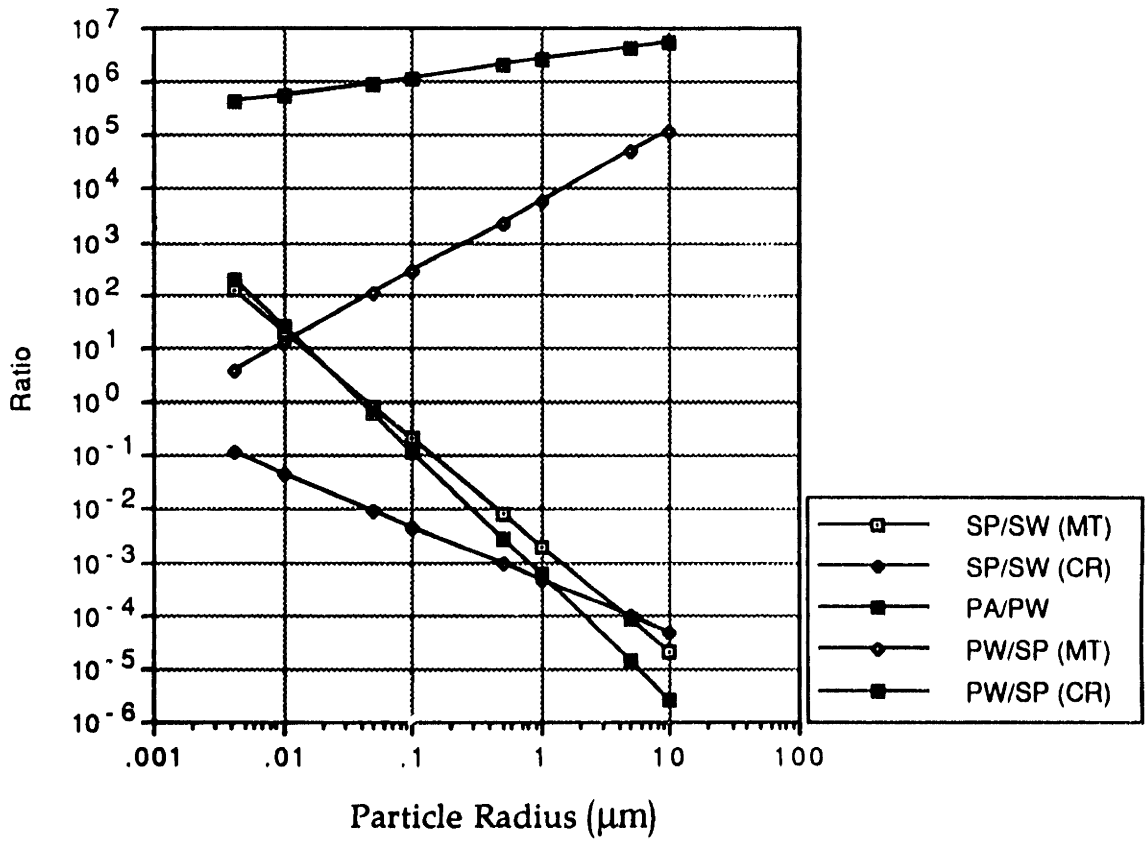

Figure 2.13 Relative Particle and Soluble Transfer Rates when $C_p/C_i = 10$

stronger tendency to deposit on a wall than to grow. However it must be noted that there is some uncertainty on how and at what rate particles nucleate in the super-saturated coolant, even though under saturated conditions, the soluble species collide with each other about 20,000 times per second due to thermal motion, so that there is some possibility for fast nucleation of particles under super-saturated conditions.

2.4.2 Corrosion Product Transport

Particulates are neglected in the modelling of corrosion product transport in Section 2.2.3, so that the release rate of the solubles in S/G tubing is equal to the deposition rate of the solubles on core fuel elements.

$$h_{dp} A_1 (S_2 - S_1) = h_{rl} A_3 (S_3 - S_2) \qquad (2.103)$$

or,

$$\frac{h_1 h_{cr}}{h_1 + h_{cr}} A_1 (S_2 - S_1) = \frac{h_3 h_{ds}}{h_3 + h_{ds}} A_3 (S_3 - S_2)$$

where,

S_i = average soluble species concentration in the i-th node (kg-Fe/m^3)

h_{dp} = deposition coefficient of solubles (m/sec)

h_{rl} = release coefficient of solubles (m/sec)

h_1 = mass transfer coefficient of solubles in the core (m/sec)

h_3 = mass transfer coefficient of solubles in the S/G (m/sec)

h_{cr} = crystallization coefficient of solubles (m/sec)

h_{ds} = dissolution coefficient of solubles (m/sec)

A_1 = surface area of core fuel elements (m^2)

A_3 = surface area of S/G tubing (m^2)

It is generally considered, as discussed in Section 2.3.2, that the crystal growth resistance is normally greater than the dissolution resistance, that is, $h_{cr} << h_{ds}$. In that case, two things can happen.

- Soluble species in the coolant change from saturated state (S_2) to super-saturated state (S_2') without particulate precipitation, so that the adjusted soluble release rate, h_{rl} (S_3 - S_2') becomes equal to the adjusted soluble deposition rate, h_{ds} (S_2' - S_1), which is the case modelled in Section 2.2.3.

- The particulates can precipitate in the coolant from super-saturated solubles, so that the particulate has an important role in corrosion product transport, as will be modelled in this section.

The corrosion product transport, including particulates, can be modelled by adding an additional node (a fourth node) for the particulate inventory in the coolant, as shown in Figure 2.14. In this case, the balance can be written as,

$$\text{soluble release rate (RS)} = k_3 (S_3 - S_2) \tag{2.104}$$

$$\text{soluble deposition rate (DS)} = k_1 (S_2 - S_1) \tag{2.105}$$

$$\text{particulate precipitation rate (PR)} = \text{RS} - \text{DS} = k_3 (S_3 - S_2) - k_1 (S_2 - S_1) \tag{2.106}$$

$$\text{particulate deposition rate in the i-th node } (DP_i) = f_{pi} \cdot PR \tag{2.107}$$

where,

f_{pi} = fractional deposition of particulate on the i-th node.

Therefore, the total corrosion product deposition rate (DR) in the core is the sum of soluble deposition (DS) and particulate deposition (DP_1), that is

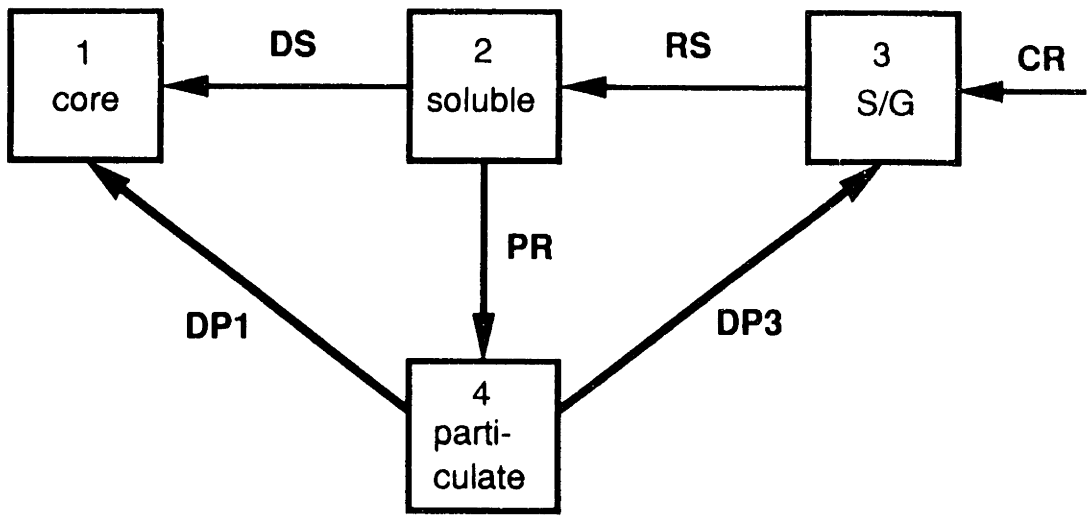

CR = corrosion rate in S/G

RS = crud release rate as soluble species in S/G

DS = crud deposition rate as soluble species in core

PR = crud precipitation rate in the coolant

DP1 = crud deposition rate as a particulate in core

DP3 = crud deposition rate as a particulate in S/G

Figure 2.14 Four Node Model - Crud Transport

$$DR = DS + D P_1 \tag{2.108}$$

Then, the crud balance equation for each node is as follows:

$$\frac{dI_1}{dt} = DS + D P_1 = DR \tag{2.109}$$

$$\frac{dI_2}{dt} = RS - DS - PR \tag{2.110}$$

$$\frac{dI_3}{dt} = CR - RS - D P_3 \tag{2.111}$$

$$\frac{dI_4}{dt} = PR - (DP_1 - D P_3) \tag{2.112}$$

And in the steady state, the soluble and particulate inventories of the coolant corrosion products are constant. Therefore,

$$\frac{dI_2}{dt} = \frac{dI_4}{dt} = 0$$

That is, the particulate precipitation rate is equal to the particulate deposition rate.

$$PR = k_3 (S_3 - S_2) - k_1 (S_2 - S_1) = D P_1 + D P_3 \tag{2.113}$$

Then, the crud deposition rate in the core is

$$DR = DS + D P_1$$
$$= k_1 (S_2 - S_1) + f_{p1} [k_3 (S_3 - S_2) - k_1 (S_2 - S_1)] \qquad (2.114)$$

And the fraction of particulate deposition in the core region is

$$f_{p1} = \frac{h_1^p A_1 (C_{pt,bulk} - C_{pt,surf})}{h_1^p A_1 (C_{pt,bulk} - C_{pt,surf}) + h_1^p A_1 (C_{pt,bulk} - C_{pt,surf})}$$

$$= \frac{h_1^p A_1}{h_1^p A_1 + h_3^p A_3} = \frac{k_1^p}{k_1^p + k_3^p} \qquad (2.115)$$

where,

$C_{pt,bulk}$ = particulate concentration in the coolant (kg/m^3)

$C_{pt,surf}$ = particulate concentration on the surface, which is nearly zero (kg/m^3)

h_i^p = particulate mass transfer coefficient in the i-th region (m/sec)

k_i^p = particulate mass transfer factor, which is the product of h_i^p and A_i (m^3/sec)

i = the i-th region (1 = core, 3 = S/G)

Similarly, the fraction of particulate deposition on S/G tubing is

$$f_{p3} = \frac{k_3^p}{k_1^p + k_3^p} \qquad (2.116)$$

Finally, the crud balance equations become

$$\frac{dI_1}{dt} = k_1 (S_2 - S_1) + f_{p1} [k_3 (S_3 - S_2) - k_1 (S_2 - S_1)]$$

$$= + \frac{k_3^p k_1}{k_1^p + k_3^p} (S_2 - S_1) + \frac{k_3 k_1^p}{k_1^p + k_3^p} (S_3 - S_2) \qquad (2.117)$$

$$\frac{dI_2}{dt} = 0 \qquad (2.118)$$

$$\frac{dI_3}{dt} = CR - k_1 (S_2 - S_1) + f_{p3} [k_3 (S_3 - S_2) - k_1 (S_2 - S_1)]$$

$$= CR - \frac{k_3^p k_1}{k_1^p + k_3^p} (S_2 - S_1) - \frac{k_3 k_1^p}{k_1^p + k_3^p} (S_3 - S_2) \qquad (2.119)$$

$$\frac{dI_4}{dt} = 0 \qquad (2.120)$$

It is to be noted that when the ionic iron inventory of the coolant is assumed constant with time, the particulate precipitation in the coolant is always equal to the total particulate deposition rate on plant surfaces, a relation which is also independent of the particulate size distribution in the coolant.

In summary, the crud transport equations become

$$\frac{dI_1}{dt} = \frac{k_3 k_1^p}{k_1^p + k_3^p} \left[S_3 - S_1 \frac{k_1 k_3^p}{k_3 k_1^p} + S_2 \left(\frac{k_1 k_3^p}{k_3 k_1^p} - 1 \right) \right] \qquad (2.121)$$

$$\frac{dI_3}{dt} = CR - \frac{k_3 k_1^p}{k_1^p + k_3^p}\left[S_3 - S_1 \frac{k_1 k_3^p}{k_3 k_1^p} + S_2\left(\frac{k_1 k_3^p}{k_3 k_1^p} - 1\right)\right] \qquad (2.122)$$

$$\frac{dI_2}{dt} = \frac{dI_4}{dt} = 0 \qquad (2.123)$$

Therefore, the dependence of the crud transport upon the solubility difference is unchanged even with the particulate precipitation in the coolant. The effect of the particulate precipitation on the absolute amount of the crud transport will be studied in Section 3.3.2.2.

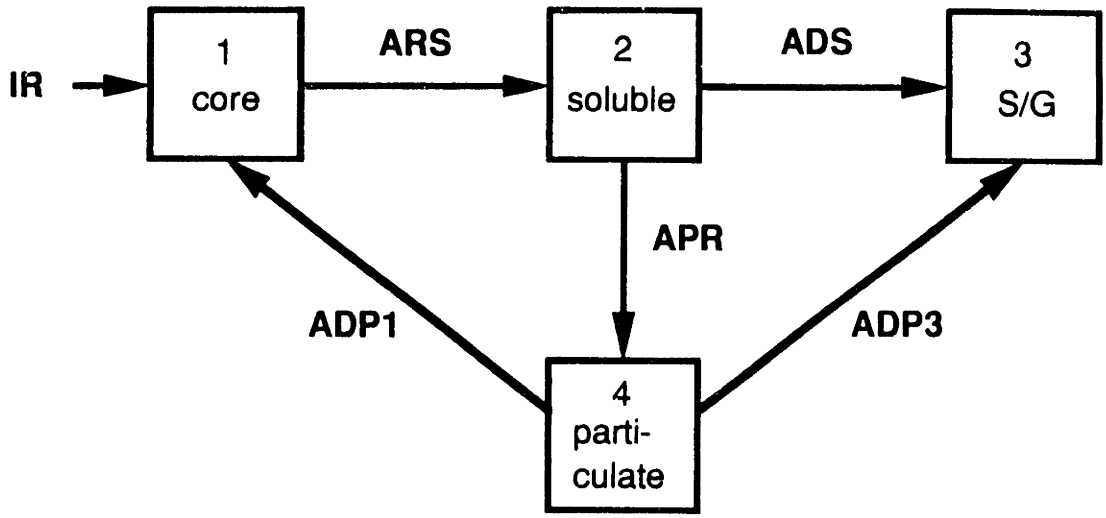

IR = activity production rate in core

ARS = activity release rate as soluble species in core

ADS = activity deposition rate as soluble species in S/G

APR = activity precipitation rate in the coolant

ADP1 = activity deposition rate as a particulate in core

ADP3 = activity deposition as a particulate in S/G

Figure 2.15 Four Node Model - Activity Transport

2.4.3 Activity Transport

Activity transport may also be affected by particulate precipitation. It can be assumed that when the solubles precipitate in the coolant, the same fraction of radioactive elements is also incorporated into the particulates along with the iron. As with crud transport, the activity transport can be modelled by adding an additional particulate node in the coolant, as shown in Figure 2.15. Then, we can write:

$$\text{Activity release rate as a soluble (ARS)} = k_1^a \left(\frac{A_1}{I_1} S_1 - \frac{A_2}{I_2} S_2 \right) \qquad (2.124)$$

$$\text{Activity deposition rate as a soluble (ADS)} = k_3^a \left(\frac{A_2}{I_2} S_2 - \frac{A_3}{I_3} S_3 \right) \qquad (2.125)$$

Activity precipitation rate as a particulate (APR) in the coolant

$$= \text{ARS} - \text{ADS} \qquad (2.126)$$

Activity deposition rate as a particulate in the i-th node (ADP_i)

$$= f_{pi}\,\text{APR} = \frac{k_i^p}{k_1^p + k_3^p}\,\text{APR} \qquad (2.127)$$

where,

k_1^a = activity transport factor in the core (m^3/sec)

k_3^a = activity transport factor in the S/G (m^3/sec)

Then, the activity balance equations become

$$\frac{dA_1}{dt} = -\lambda A_1 + IR - ARS + AD\,P_1$$

$$= -\lambda A_1 + \alpha P I_1 - k_1^a\left(\frac{A_1}{I_1}S_1 - \frac{A_2}{I_2}S_2\right) + \frac{k_1^p}{k_1^p + k_3^p}\left[k_1^a\left(\frac{A_1}{I_1}S_1 - \frac{A_2}{I_2}S_2\right)\right.$$

$$\left. - k_3^a\left(\frac{A_2}{I_2}S_2 - \frac{A_3}{I_3}S_3\right)\right] \qquad (2.128)$$

$$\frac{dA_2}{dt} = -\lambda A_2 + ARS - ADS - APR = 0 \qquad (2.129)$$

$$\frac{dA_3}{dt} = -\lambda A_3 + ADS + AD\,P_3$$

$$= -\lambda A_3 + k_3^a\left(\frac{A_2}{I_2}S_2 - \frac{A_3}{I_3}S_3\right) + \frac{k_3^p}{k_1^p + k_3^p}\left[k_1^a\left(\frac{A_1}{I_1}S_1 - \frac{A_2}{I_2}S_2\right)\right.$$

$$\left. - k_3^a\left(\frac{A_2}{I_2}S_2 - \frac{A_3}{I_3}S_3\right)\right] \qquad (2.130)$$

$$\frac{dA_4}{dt} = -\lambda A_4 + APR - AD\,P_1 - AD\,P_3 = 0 \qquad (2.131)$$

Next, the activity of the coolant in soluble form will be calculated. From Eq. (2.106), the fractional precipitation rate of the iron inventory in the coolant, P_2, is given by

$$P_2 = \frac{PR}{I_2} = \frac{k_3(S_3 - S_2) - k_1(S_2 - S_1)}{I_2} \qquad (2.132)$$

The amount of activity incorporated in particulates in the coolant, AP_2, is proportional to P_2 and given by:

$$AP_2 = P_2 A_2 \tag{2.133}$$

And AP_2 is also equal to APR, the difference between the ARS and ADS. So,

$$AP_2 = APR = ARS - ADS \tag{2.134}$$

That is,

$$\frac{A_2}{I_2}[k_3(S_3 - S_2) - k_1(S_2 - S_1)]$$

$$= k_1^a\left(\frac{A_1}{I_1} S_1 - \frac{A_2}{I_2} S_2\right) - k_3^a\left(\frac{A_2}{I_2} S_2 - \frac{A_3}{I_3} S_3\right)$$

So,

$$A_2 = \frac{I_2}{S_2}\left(\frac{k_1^a \frac{A_1}{I_1} S_1 + k_3^a \frac{A_3}{I_3} S_3}{k_1^a - k_1 - k_3^a + k_3 + k_3 \frac{S_3}{S_2} + k_1 \frac{S_1}{S_2}}\right) \tag{2.135}$$

The coolant activity in particulates, A_4, can be calculated by assuming that the ratios of activity to crud inventory in both the solubles and particulates in the coolant are the same, that is,

$$\frac{A_2}{I_2} = \frac{A_4}{I_4}$$

So,

$$A_4 = \frac{I_4}{I_2} A_2 \tag{2.136}$$

In summary, the activity transport equations with particulate precipitation are

$$\frac{dA_1}{dt} = -\lambda A_1 + \alpha P I_1 - \frac{k_1^a k_3^p}{k_1^p + k_3^p}\left[\frac{A_1}{I_1} S_1 - \frac{A_3}{I_3} S_3 \frac{k_3^a k_1^p}{k_1^a k_3^p} + \frac{A_2}{I_2} S_2 \left(\frac{k_3^a k_1^p}{k_1^a k_3^p} - 1\right)\right] \tag{2.137}$$

$$\frac{dA_3}{dt} = -\lambda A_3 + \frac{k_1^a k_3^p}{k_1^p + k_3^p}\left[\frac{A_1}{I_1} S_1 - \frac{A_3}{I_3} S_3 \frac{k_3^a k_1^p}{k_1^a k_3^p} + \frac{A_2}{I_2} S_2 \left(\frac{k_3^a k_1^p}{k_1^a k_3^p} - 1\right)\right] \tag{2.138}$$

$$\frac{dA_2}{dt} = \frac{dA_4}{dt} = 0 \tag{2.139}$$

and

$$A_2 \frac{I_2}{S_2} = \frac{k_1^a \frac{A_1}{I_1} S_1 + k_3^a \frac{A_3}{I_3} S_3}{k_1^a - k_1 - k_3^a + k_3 + k_3 \frac{S_3}{S_2} + k_1 \frac{S_1}{S_2}} \qquad (2.140)$$

Therefore, the dependence of activity transport upon the solubility difference is also unchanged with particulate precipitation in the coolant. The effect of the particulate precipitation on the activity transport will be studied in Section 3.3.2.2.

2.5 Other Considerations

2.5.1 Thermal Diffusion

A general expression for the mass current from the Boltzmann transport equation, based on a hard sphere model, which is similar to the governing equation of neutron diffusion, is as follows [D-3] [M-8]

$$J = -k_1 \frac{\partial (CV)}{\partial x} \tag{2.141}$$

where

C = concentration (kg/cm^3)

V = drift velocity (cm/sec)

k_1 = constant (cm)

J = mass current ($kg/cm^2 \cdot sec$)

and $k_1 V$ is defined to be the diffusion coefficient, that is,

$$D = k_1 V \quad (cm^2/sec) \tag{2.142}$$

Then, Eq. (2.141) becomes

$$J = -k_1 \left(C \frac{\partial V}{\partial x} + V \frac{\partial C}{\partial x} \right)$$

$$= - k_1 V \left(\frac{\partial C}{\partial x} + \frac{C}{V} \frac{\partial V}{\partial x} \right)$$

$$= - DC \left(\frac{1}{C} \frac{\partial C}{\partial x} + \frac{1}{V} \frac{\partial V}{\partial T} \frac{\partial T}{\partial x} \right)$$

so that

$$J = - DC \left(\frac{1}{C} \frac{\partial C}{\partial x} + S \frac{\partial T}{\partial x} \right) \qquad (2.143)$$

where

$$S = \frac{1}{V} \frac{\partial V}{\partial T} \quad , \qquad (2.144)$$

which is defined as the Soret coefficient in thermal diffusion analyses.

The diffusion coefficient of the electrolyte is also given by the Nernst-Einstein relation: Eq.(2.65)

$$D = \frac{RT}{F^2} \left(\frac{1}{n^+} + \frac{1}{n^-} \right) t_+^o \, t_-^o \, \Lambda^o = k_2 \, T \, \Lambda^0 \qquad (2.145)$$

where,

- D = diffusion coefficient of the electrolyte (cm^2 / sec)
- R = the gas constant (8.314 J/mole ^oK)
- T = absolute temperature (^oK)
- F = Faraday's constant (96,500 c/g-equiv.)
- $n^{+,-}$ = the valence of the ions involved
- $t^o_{+,-}$ = the transference number of the ions
- Λ^o = the limiting conductance of the electrolyte.

In Eq. (2.142), k_1 is a function of density, and can be expressed by, (as usually done in the case of neutron diffusion):

$$k_1 = \frac{1}{3\Sigma} = \frac{1}{3N\sigma} \quad \alpha \quad \frac{1}{\rho\sigma} \tag{2.146}$$

The last equivalence is valid because the atomic number density, N, is proportional to the density ρ. Therefore, the diffusion coefficient becomes

$$D = K_1 V = k' \frac{V}{\rho} \tag{2.147}$$

That is, the diffusion coefficient is proportional to drift velocity, V, and inversely proportional to the density of the medium. From Eqs. (2.145) and (2.147),

$$k' \frac{V}{\rho} = k_2 T \Lambda^\circ \tag{2.148}$$

Hence, the drift velocity becomes

$$V = \frac{k_2}{k'} (\rho \Lambda^\circ T) = k_3 (\rho \Lambda^\circ T) \tag{2.149}$$

Then, the Soret coefficient in Eq. (2.144) can be expressed by

$$S = \frac{1}{V} \frac{\partial V}{\partial T} = \frac{\partial (\ln V)}{\partial T} = \frac{1}{\rho} \frac{\partial \rho}{\partial T} + \frac{1}{T} + \frac{1}{\Lambda^\circ} \frac{\partial \Lambda^\circ}{\partial T}$$

or

$$S = \frac{\partial (\ln \rho \, \Lambda^{o} T)}{\partial T} \qquad (2.150)$$

Based on the above relation, Soret coefficients can be calculated using conductivity data. The derivative in Eq.(2.150) can be computed from the discrete data points as follows:

$$S = \frac{\ln (\rho \Lambda^{o} T)_{at\, T_1} - \ln (\rho \Lambda^{o} T)_{at\, T_2}}{T_1 - T_2} \qquad (2.151)$$

If one invokes the Walden product relation, namely that $\Lambda_o(T)\,\mu(T)$ is constant, then Eq. (2.150) becomes

$$S = \frac{\partial \left(\ln \frac{\rho T}{\mu}\right)}{\partial T} \equiv \frac{\partial \left(\ln \frac{T}{\nu}\right)}{\partial T} \qquad (2.152)$$

where,

ν = kinematic viscosity of water ($\equiv \frac{\mu}{\rho}$)

Note that Eq. (2.152) depends upon only on solvent properties. This result can also be arrived at by an alternative approach. Eqs. (2.144) and (2.147) combine to give

$$S = \frac{\partial (\ln D \, \rho)}{\partial T} \qquad (2.153)$$

Since the Stokes-Einstein relation predicts $D \sim \frac{T}{\mu}$; substitution into Eq. (2.153) yields Eq. (2.152). Hence, we also expect this relation to be valid for small non-ionic particulates. (Thus, we speculate that thermophoresis may also decrease as temperature increase, although we have not considered this phenomenon in detail.)

Figure 2.16 gives the Soret coefficient for a representative ionic salt NaCl, as a function of temperature, computed using Eq. (2.151). Also shown is the curve predicted by Eq. (2.152). The results show that the Soret coefficient steadily decreases with temperature. The Soret coefficient of the electrolyte near 300 ^{o}C (PWR primary coolant temperature) is very small (~ 10^{-3} $^{o}C^{-1}$), even though at room temperature it is about 2×10^{-2} $^{o}C^{-1}$. Assuming the same functional behavior for all diffusing species, one has for corrosion product deposition on the core, from Eq.(2.143) using representative parameter data :

$$J_1 = - DC \left(\frac{1}{C} \frac{\Delta C}{\Delta x} + S \frac{\Delta T}{\Delta x} \right) = - \frac{DC}{\Delta x} \left(\frac{\Delta C}{C} + S \, \Delta T \right)$$

$$\cong - \frac{DC}{\Delta x} (0.14 - 0.02)$$

$$\cong - \frac{DC}{\Delta x} (0.14)$$

That is, since $\left| \frac{\Delta C}{C} \right| >> S \, \Delta T$ near 300 ^{o}C, the Soret diffusion effect on mass transfer is negligible at the operating temperature of PWR coolant.

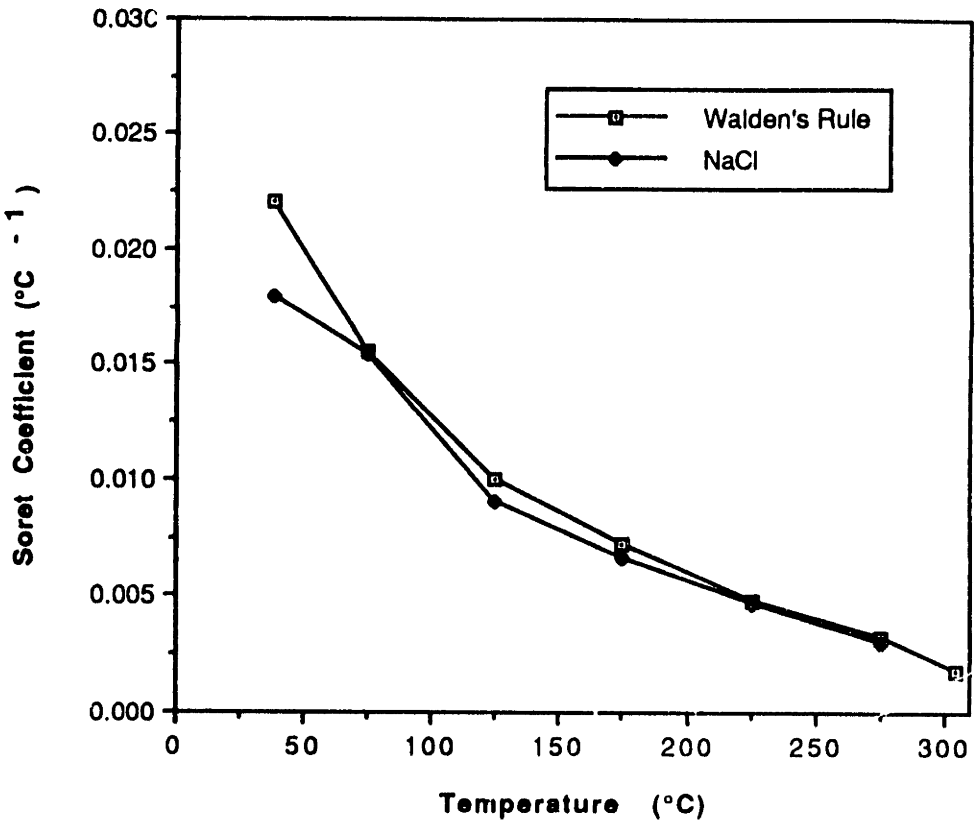

Figure 2.16 Calculated Soret Coefficients of NaCl Electrolyte and those from Walden's Rule

In view of this finding, it is considered that the thermal diffusion effect on mass transfer across flow boundary layers is not significant. It must be noted, however, that the theory just outlined is based upon a "hard sphere" diffusion model. Thus, there is still room for a more refined treatment of this issue.

2.5.2 Recoil Release of Radio-activated Elements

Nuclei which react with fast neutrons are recoiled with appreciable energy. Thus, there is a possibility that radio-activated nuclides in the core crud will be directly released into the coolant, following reactions such as

Ni^{58} (n,p) Co^{58} $\quad E_n > 1$ Mev

Fe^{54} (n,p) Mn^{54} $\quad E_n > 1.5$ Mev

For the reaction of Co^{59} (n,γ) Co^{60} , the possibility of direct recoil release of radio-activated Co^{60} is negligible due to the much smaller recoil energy induced by thermal neutron absorption.

The range of the recoiled nuclide is a function of the nuclide's recoil energy and the density of the medium into which the nuclide is recoiled. For low energy heavy ions in a matrix of similar atomic mass, the range of the ion is fairly well approximated by [M-9]

$$R \approx 3.5 \times 10^{-7} (E/\rho) \qquad (2.154)$$

where,

R = range (cm)

E = the ion energy (kev)

ρ = the density of the medium (gm/cm^3)

The energy of the recoiled nuclide can be calculated in the inelastic collision by considering energy and momentum conservation. Since the neutron energy spectrum in the reactor is not discrete but continuous, the average range of the recoiled nuclide, $R_{avg.}$ can be expressed by,

$$R_{avg.} = \frac{\int R(E).\sigma(E).\phi(E)\, dE}{\int \sigma(E).\phi(E)\, dE} \qquad (2.155)$$

where,

R(E) = the average range of the recoiled nuclide for the incident neutron energy, E (cm)

$\sigma(E)$ = cross-section of the reaction with a neutron of energy E (cm^2)

$\phi(E)\, dE$ = neutron flux with energy between E and E+dE (n/cm^2 sec)

Since it is not easy to determine the distribution functions, R(E), $\sigma(E)$ and $\phi(E)$ for each medium, each nuclear reaction and each reactor type, it is more straightforward to try to measure the range of the recoiled nuclide by inserting the specimens of interest into the reactor itself. Measurements are available of the range of Co^{58} for a fission neutron spectrum [Z-1]. For the Ni^{58} (n,p) Co^{58} reaction with fission energy spectrum neutrons, the spectrum averaged cross section ($\overline{\sigma_f}$) was measured to be 89 mb, and the average projected range of the recoiled Co^{58} nuclides in Ni foil, $\overline{R_p}$ was 38.5 nm, or 0.034 (mg/cm^2)

From the range of the recoiled nuclide, we can calculate the probability that it will be directly released into the coolant. Since the incident neutrons are almost isotropic inside the reactor, the direction of the recoiled nuclides is also isotropic. The probability of recoil release from the core crud can be calculated as follows. As shown in Figure 2.17 , the probability that an isotropically recoiled nuclide at x will be released into the coolant, p(x), is equal to the probability that the nuclide is recoiled into a solid angle less than θ, that is,

$$p(x) = \int_{\Omega \le \theta} d\Omega \frac{1}{4\pi}$$

$$= \frac{1}{4\pi} \int_0^{2\pi} d\phi \int_0^{\theta} \sin\theta \, d\theta$$

$$= \frac{1}{2}(1-\cos\theta)$$

$$= \frac{1}{2}\left(1 - \frac{(R_p - x)}{R_p}\right)$$

$$= \frac{x}{2R_p} \qquad (2.156)$$

Therefore, the average escape probability for the recoiled nuclide having the projected range, R_p, can be calculated. At first, when the crud thickness (t_d) is greater than the projected range (R_p), that is, $t_d > R_p$, the average recoil release probability ($p_{avg.}$) is

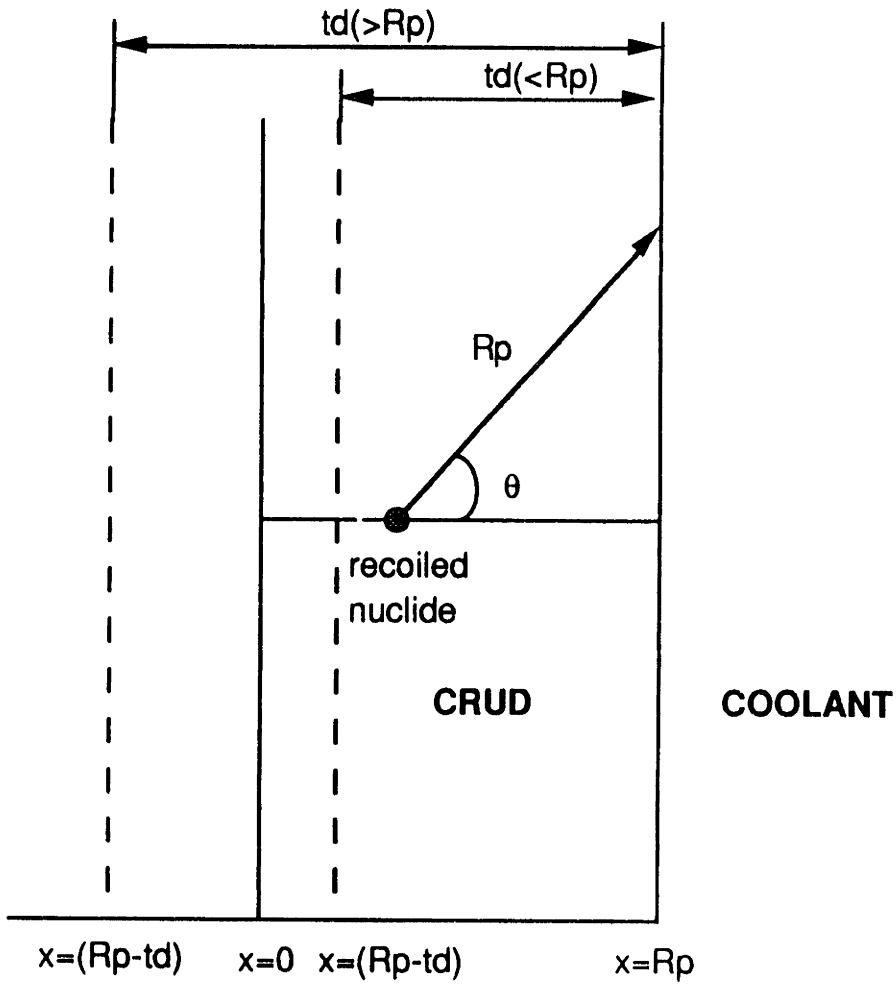

Figure 2.17 Geometry for Calculating the Direct Recoil Release of Nuclei

$$p_{avg.} = \frac{1}{t_d}\int_0^{R_p} p(x)\,dx$$

$$= \frac{1}{t_d}\int_0^{R_p} \frac{x}{2R_p}\,dx$$

$$= \frac{R_p}{4t_d} \qquad (2.157)$$

And when $t_d < R_p$, the average recoil release probability in the core crud, $p_{avg.}$ is

$$p_{avg.} = \frac{1}{t_d}\int_{R_p-t_d}^{R_p} p(x)\,dx$$

$$= \frac{1}{t_d}\int_{R_p-t_d}^{R_p} \frac{x}{2R_p}\,dx$$

$$= \frac{1}{2} - \frac{t_d}{4R_p} \qquad (2.158)$$

In the above, the lower integration limit was changed from x=0 to $x = R_p - t_d$, since the material in the region $0 < x < R_p - t_d$ is not crud, but Zircaloy, when t_d is less than the range, R_p.

In summary, the average probability of direct recoil release of an activated nuclide from a core crud film by an isotropic neutron source is,

(i) $t_d > R_p$

$$p_{avg.} = \frac{R_p}{4t_d} \qquad (2.159)$$

(ii) $t_d < R_p$

$$p_{avg.} = \frac{1}{2} - \frac{t_d}{4R_p} \qquad (2.160)$$

where,

R_p = projected recoil range (cm, or mg/cm^2)

t_d = core crud thickness (cm, or mg/cm^2)

Figure 2.18 shows the direct recoil release probability of Co^{58} versus the crud thickness. We can see that at an initial value of zero crud, the recoil release probability is at its maximum, 50 %, and after about a month, corresponding to a core crud thickness of 0.01 mg/cm^2, it is still 43 %.

Another possible route to recoil release of radioactive nuclides is by scattering reactions with neutrons, or primary and secondary knock-on atoms. This mechanism can be considered as indirect recoil release of the radioactive nuclide, since this phenomenon applies for all crud elements, including both the radioactive and non-radioactive elements. Since cladding nuclei in a LWR experience roughly one displacement per atom (dpa) per effective full power year, this mechanism is worthy of consideration.

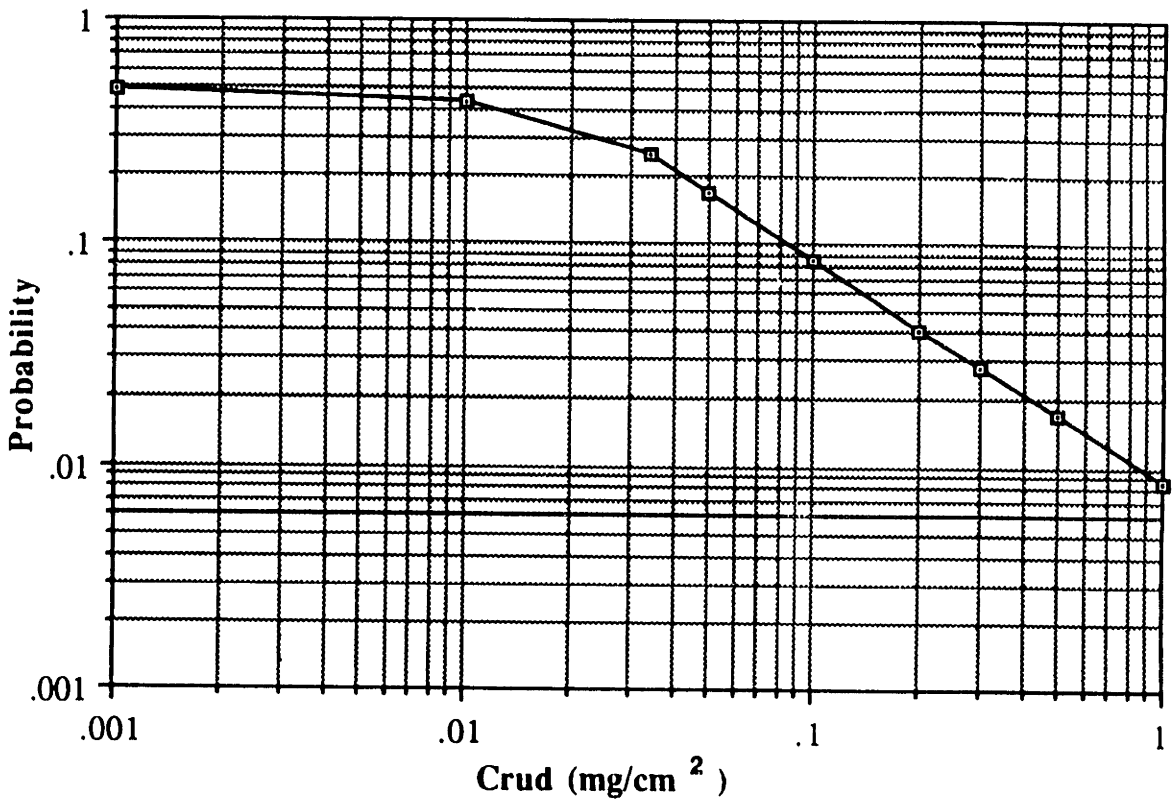

Figure 2.18 Probability of direct recoil release of Co^{58} produced by the (n,p) reaction of Ni^{58}, as a function of crud thickness

Sputtering of metals by fast neutron-induced primary and secondary knock-ons has been measured in reactors. [B-14] The sputtering yield Y_n (atoms/neutron) of metal by the fast neutron ($E_n > 0.1$ Mev) is about 10^{-5}. Hence the sputtering yield of crud is approximately

$$Y_{total} = \phi_{ft}\, Y_n \frac{A(Fe)}{N_A} 10^5 \left(\frac{mg/dm^2}{g/cm^2}\right) \times 2.6 \times 10^5 \left(\frac{sec}{montth}\right) \qquad (2.161)$$

$$= 1.2 \times 10^{-3} \ (mg/dm^2\ month)$$

where,

ϕ_{ft} = fast neutron flux (~ 5×10^{13} $n/cm^2.sec$)

Y_n = sputtering yield (10^{-5} atoms/neutron)

A(Fe) = atomic number (55.8 gm/atomic mole)

N_A = Avogadro's number (6.023×10^{23} atoms/mole)

Then, the release rate of radioactive Co^{58} nuclei in the crud is the product of the fraction of Co^{58} in the crud ($f_{Co}58$) and the total sputtering yield (Y_{total}), that is, $f_{Co}58 . Y_{total}$, which is negligible compared with the direct recoil release of Co^{58}. Since the crud in the core can reach about 1 mg/dm^2 after one month, only about 0.12 % of the crud is removed by indirect recoil release ; the same value applies to its contained Co^{58} and Co^{60}.

The direct recoil release of the radioactivity can be modeled as follows. Let r_r, the probability ($p_{avg.}$) that Co^{58} produced by (n,p) reaction of Ni^{58} (or Co^{60} by (n,γ) reaction of Co^{59}) is directly recoiled into the coolant. Then Eqs. (2.32), (2.33), and (2.34) for Co^{58} (or Co^{60}) are changed as follows.

$$\frac{dA_1}{dt} = -\lambda A_1 - k_1^a \left[\frac{A_1}{I_1} S_1 - \frac{A_2}{I_2} S_2\right] + [1 - r_r] \alpha p I_1 \qquad (2.162)$$

$$\frac{dA_2}{dt} = -\lambda A_2 + k_1^a \left[\frac{A_1}{I_1} S_1 - \frac{A_2}{I_2} S_2\right] + r_r \alpha p I_1 - k_3^a \left[\frac{A_2}{I_2} S_2 - \frac{A_3}{I_3} S_3\right] \qquad (2.163)$$

$$\frac{dA_3}{dt} = -\lambda A_3 + k_3^a \left[\frac{A_2}{I_2} S_2 - \frac{A_3}{I_3} S_3\right] \qquad (2.164)$$

Assume $\frac{dA_2}{dt} = 0$, and neglect the decay in the coolant, λA_2. Then,

$$0 = k_1^a \left[\frac{A_1}{I_1} S_1 - \frac{A_2}{I_2} S_2\right] + r_r \alpha p I_1 - k_3^a \left[\frac{A_2}{I_2} S_2 - \frac{A_3}{I_3} S_3\right]$$

$$\frac{A_2}{I_2} S_2 = \frac{1}{k_1^a + k_3^a} \left[k_1^a \frac{A_1}{I_1} S_1 + k_3^a \frac{A_3}{I_3} S_3 + r_r \alpha p I_1\right] \qquad (2.165)$$

Insertion of Eq. (2.165) into Eqs. (2.162) and (2.164) gives,

$$\frac{dA_1}{dt} = -\lambda A_1 - \frac{k_1^a k_3^a}{k_1^a + k_3^a}\left[\frac{A_1}{I_1} S_1 - \frac{A_3}{I_3} S_3\right] + \alpha p I_1 \left[1 - r_r \frac{k_3^a}{k_1^a + k_3^a}\right] \tag{2.166}$$

$$\frac{dA_3}{dt} = -\lambda A_3 + \frac{k_1^a k_3^a}{k_1^a + k_3^a}\left[\frac{A_1}{I_1} S_1 - \frac{A_3}{I_3} S_3\right] + r_r \frac{k_3^a}{k_1^a + k_3^a} \alpha p I_1 \tag{2.167}$$

Using the above revised set of equations, the Co^{58} activity may be estimated as a function of the assumed fraction of direct recoil release, r_r. If there is some amount of Co^{58} directly recoiled, the activity ratio of Co^{58} in the core to that in the S/G will differ from the activity ratio of Co^{60} in the core to that in the S/G , so that this comparison can be used to determine whether direct recoil release is an important mechanism. As the direct recoil release probability increases, the ratio of Co^{58}/Co^{60} will decrease in the core and increase in the S/G. Sensitivity analysis of the recoil release of Co^{58} will be discussed in Section 3.3.2.4.

2.5.3 Refuelling of the Core

Refuelling of the core is usually done annually in a typical PWR. The oldest one-third of the total inventory of fuel assemblies in the core is replaced by new fuel. Therefore, some fraction of the crud inventory in the core, f, is removed by the refuelling. The fraction, f, can be approximated as follows:

$f \cong \frac{1}{2}$ if the crud in the core builds up linearly as a function of time

$f \cong \frac{1}{3}$ if the crud inventory saturates rapidly

Of the above two assumptions, it is more reasonable to assume a linear buildup of the core crud inventory, especially when the crud transport is driven by the solubility difference around the coolant circuit. Hence, in the steady state, the crud inventory in the core should be reduced by half in the CRUDSIM program whenever there is refuelling . However, the first and second refuellings after the first startup of the plant remove only one-third and two-fifths, respectively, of the total core crud inventory, because the removed fuel assemblies were in the core for only one and two years, respectively.

2.5.4 Purification Effect

There is a purification of the coolant through the chemical and volume control system (CVCS) in a PWR. The fraction of purification flow is about 0.02% of total coolant flow. Since a quite effective ion exchange resin filter bed is used, the efficiency of purifying the bypassed coolant is very high (over 90%). The purification effect can be modeled as described below.

When purification of the coolant is included, Eqs. (2.25) and (2.33) become:

$$\frac{dI_2}{dt} = k_3 (S_3 - S_3) - k_1 (S_2 - S_1) - f_p S_2 \qquad (2.168)$$

$$\frac{dA_2}{dt} = - \lambda A_2 + k_1^a \left(\frac{A_1}{I_1} S_1 - \frac{A_2}{I_2} S_2\right) - k_3^a \left(\frac{A_2}{I_2} S_2 - \frac{A_3}{I_3} S_3\right)$$

$$- f_p \frac{A_2}{I_2} S_2 \qquad (2.169)$$

And,

$$\frac{dI_p}{dt} = f_p S_2 \qquad (2.170)$$

$$\frac{dA_p}{dt} = - \lambda A_p + f_p \frac{A_2}{I_2} S_2 \qquad (2.171)$$

where,

f_p = bypassed purification flow rate (m^3/sec)

I_p = crud inventory of the purification system

A_p = activity of the purification system.

Then, when $\frac{dI_2}{dt}$ and $\frac{dA_2}{dt}$ are assumed to be zero, Eqs. (2.35) and (2.36) are changed to

$$S_2 = \frac{k_1}{k_1 + k_3 + f_p} S_1 + \frac{k_3}{k_1 + k_3 + f_p} S_3 \tag{2.172}$$

$$\frac{A_2}{I_2} S_2 = \frac{k_1^a}{k_1^a + k_3^a + f_p} \frac{A_1}{I_1} S_1 + \frac{k_3^a}{k_1^a + k_3^a + f_p} \frac{A_3}{I_3} S_3 \tag{2.173}$$

Insert Eq. (2.172) into Eqs. (2.24) and (2.26), to obtain :

$$\frac{dI_1}{dt} = \frac{k_1 k_3}{k_1 + k_3 + f_p}\left[S_3 - S_1\left(1 + \frac{f_p}{k_3}\right)\right] \tag{2.174}$$

$$\frac{dI_3}{dt} = CR - \frac{k_1 k_3}{k_1 + k_3 + f_p}\left[S_3\left(1 + \frac{f_p}{k_1}\right) - S_1\right] \tag{2.175}$$

$$\frac{dI_p}{dt} = f_p\left(\frac{k_1}{k_1 + k_3 + f_p} S_1 + \frac{k_3}{k_1 + k_3 + f_p} S_3\right) \tag{2.176}$$

Insertion of Eq. (2.173) into Eqs. (2.32) and (2.34) gives

$$\frac{dA_1}{dt} = -\lambda A_1 + \alpha P I_1 - \frac{k_1^a k_3^a}{k_1^a + k_3^a + f_p}\left[\left(1 + \frac{f_p}{k_3^a}\right)\frac{A_1}{I_1} S_1 - \frac{A_3}{I_3} S_3\right] \tag{2.177}$$

$$\frac{dA_3}{dt} = -\lambda A_3 + \frac{k_1^a k_3^a}{k_1^a + k_3^a + f_p}\left[\frac{A_1}{I_1} S_1 - \frac{A_3}{I_3} S_3\left(1 + \frac{f_p}{k_1^a}\right)\right] \tag{2.178}$$

$$\frac{dA_p}{dt} = -\lambda A_p + f_p\left[\frac{k_1^a}{(k_1^a + k_3^a + f_p)} \frac{A_1}{I_1} S_1 + \frac{k_3^a}{(k_1^a + k_3^a + f_p)} \frac{A_3}{I_3} S_3\right] \tag{2.179}$$

It is obvious that Eqs. (2.174) through (2.179) are different from Eqs. (2.37) through (2.40), where the purification effect is neglected. However, since the bypassed purification flow rate is so small (0.02% of total coolant flow), the effect of purification on activity transport is not significant to the net crud and activity transport: a conclusion supported later herein when numerical studies show that $f_p << k_1$ or k_3 .

2.5.5 Erosion of Surface Oxide Film

Corrosion products on the outer side of the surface oxide film in a PWR primary loop can be detached from the oxide surface film by the shear force caused by the flowing coolant. It is generally considered that the erosion of corrosion products is proportional to the shear force exerted by the coolant flow, and that the erosion rate can be expressed as [K-3] [T-3],

$$J_{er} = k_{er} \frac{\tau^n}{\psi} W \tag{2.180}$$

where,

k_{er} = erosion constant

τ = shear stress

ψ = deposit strength

W = mass of deposits susceptible to erosion

n = the power to which erosion depends upon shear stress

The erosion constant depends upon the physical and chemical conditions at the interface between the coolant and the corrosion product deposit, such as the presence of impurities and heat flux. The deposit strength depends upon the nature of the deposit and its interaction with the surface. The erosion constant and deposit strength can only be determined through experiments under specific physical and chemical conditions.

The relationship between the shear stress and flow velocity under turbulent flow is,

$$\tau = \frac{1}{8} \frac{\mu^{0.2} \rho^{0.8} V^{1.8}}{D_e^{0.2}} \qquad (2.181)$$

where,

μ = viscosity of the fluid (N.sec/m^2)

ρ = density of the fluid (kg/m^3)

V = velocity of the flow (m/sec)

D_e = hydraulic diameter of flow channel (m)

That is, the shear stress is proportional to the flow velocity to a power on the order of 1.8 under turbulent flow. Then, the erosion rate, J_{er} , is proportional to the flow velocity to the order of $\underline{1.8\ n}$. Several experiments have shown a dependence of erosion rate on flow velocity ranging between 1.1 and 1.9. [B-15] Furthermore, the value of n, which defines how the erosion rate depends upon the shear stress, is normally considered 1.0.

Cleaver and Yates [C-5] [C-6] have proposed that the turbulent bursts which occur randomly, both spatially and temporally, on surfaces under turbulent flow conditions cause the erosion of surface deposits, instead of the viscous shear stress. In other words, when the hydrodynamic lifting force on the deposit by the turbulent burst is larger than the adhesion force of the deposits, detachment of the deposits occurs. However, the expression for the erosion rate by this mechanism [E-1] has a similar form to Eq.(2.180), namely

$$J_{er} = C \frac{\tau \beta}{\mu \psi} \qquad (2.182)$$

where,

C = constant

τ = shear stress

β = the fraction of the surface covered by bursts at any instant

ψ = deposit strength

μ = absolute viscosity of the liquid

The corrosion products deposited around the PWR primary coolant loop are considered to be mainly nickel-ferrite. Measurements are not yet available for the erosion constant and deposit strength of corrosion products under PWR operating conditions. In experiments by Lister [L-1] of corrosion product release under PWR operating conditions, an increase in velocity by a factor of 3 had no significant effect on the release rates, even though by Eq. (2.181), the erosion release should have increased by about 7 times. Therefore, it is generally believed that under PWR operating conditions (which are relatively much cleaner than conventional heat exchanger systems), erosion by the flow shear stress has an insignificant role on corrosion product transport.

2.6 Summary and Conclusions

In Section 2.2, the CRUDSIM type corrosion product transport equations are derived analytically, based on the assumption that the solubility change of the crud as a function of temperature is the dominant driving force for corrosion product transport in a PWR coolant loop.

Section 2.3 shows how the parameters used in the modelling can be calculated. Some emphasis is placed on determination of the diffusion coefficients of the soluble species, since reliable data is not available at high temperatures.

In Section 2.4, the possibility of particulate precipitation in the coolant is studied and its effects on corrosion product transport is derived. The analysis shows that very small particulates may precipitate in the coolant, but the solubility difference between the S/G surface, bulk coolant and the core surface is still the driving force for corrosion product transport.

In Section 2.5. some other mechanisms which may affect corrosion product transport are studied, and it is found that the effects of coolant purification and thermal diffusion may not be significant.

Chapter 3. CRUDSIM/MIT Results and Model Evaluation

3.1 Introduction

Modeling of corrosion product transport mechanisms has been addressed in Chapter 2, and the formulations have been transformed into simple forms of the governing equations. Appendix A documents the FORTRAN program, CRUDSIM/MIT, which employs all the models and variables explained in Chapter 2. The CRUDSIM/MIT program can be used to predict the transport of corrosion products and radioactivity in PWR primary coolant, and, of principal present interest, in the MIT in-pile loop simulation : the PWR Coolant Chemistry Loop (PCCL).

In this Chapter, the CRUDSIM/MIT code will be evaluated by comparing its predictions for the MIT PCCL with measured results. The MIT PCCL is a small scale loop operated under constant coolant chemistry in the MIT reactor to closely simulate the primary circuit of a typical PWR power plant. [W-3] [D-1] [S-2]

In Section 3.2, the MIT PCCL will be compared with a typical PWR in terms of the operating coolant conditions and mass transfer characteristics of the system.

As pointed out in Chapter 2, there is considerable uncertainty in the quantative prediction of several transport mechanisms and parameters. Therefore, in Section 3.3, a sensitivity analysis for these mechanisms and

parameters will be carried out to establish the relative importance in the net transport of corrosion products and radioactivity, and the key mechanisms and parameters will be identified. Also, analytic solutions of the CRUDSIM equations under constant coolant chemistry conditions will be derived to provide insight into transport phenomena.

And finally, in Section 3.4, the models employed in CRUDSIM/MIT will be evaluated by comparison with the MIT PCCL measurements available to date.

3.2 Comparison of a Typical PWR and the MIT PCCL

3.2.1 Operating Conditions

The PWR coolant chemistry loop (PCCL) is operated in the M.I.T. reactor (MITR) to simulate a typical PWR primary coolant circuit in terms of coolant temperature, coolant flow conditions, heat transfer coefficient and heat flux, surface area ratio of metals of construction, and neutron flux. The main near term objective of PCCL runs is to find the optimum coolant chemistry conditions which minimize radioactivity deposition in the S/G.

Figure 3.1 shows the schematic of the MIT PWR coolant chemistry loop (PCCL). A comparison of the characteristics and operating conditions of the PCCL and a typical Westinghouse designed 1000 MWth PWR power plant are given in Table 3.1.

The history of a representative PCCL run can be divided into three steps, that is, pre-filming, pre-conditioning, and irradiation in the MITR.

At first, the Inconel tubing and S.S plena (for all loops to be tested subsequently) are pre-filmed under static wet conditions for 1000 hrs (41.67 days) under the following conditions :

Li	-	1.41 ppm
Boron	-	600 ppm
pH (300 °C)	-	7.0

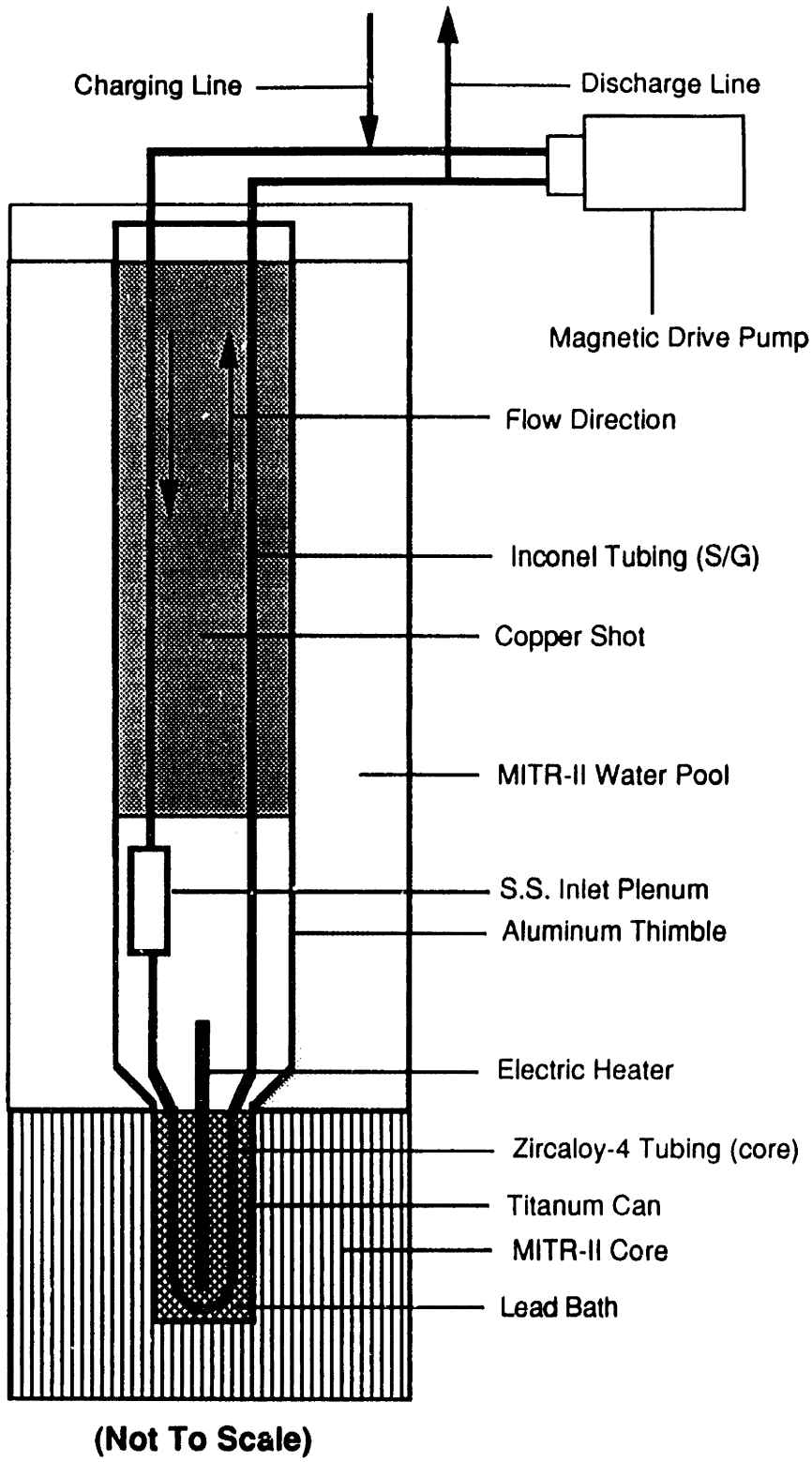

Figure 3.1 Schematic of MIT PWR Coolant Chemistry Loop (PCCL)

Table 3.1 Comparison of Transport Related Parameters for a Representative PWR and the MIT PCCL

	CORE		S/G	
	PWR	PCCL	PWR	PCCL
Coolant Inlet Temperature (^{o}C)	285	273.9	285	273.9
Coolant Outlet Temperature (^{o}C)	320	315.6	320	315.6
Avg. Coolant Temperature (^{o}C)	302.5	294.8	302.5	294.8
Avg. Coolant Density (gm/cm^3)	0.707	0.723	0.707	0.723
Avg. Coolant Viscosity ($N.S/m^2$) ($\times 10^{-6}$)	90.48	92.78	90.48	92.78
Coolant Flow Rate (kg-H_2O/sec)	1.70×10^4	0.0684	1.70×10^4	0.0684
Hydraulic Diameter (cm)	1.19	0.652	2.1	0.6159
Flow Area (m^2)	4.75	3.34×10^{-5}	4.67	2.98×10^{-5}
Total Surface Area (m^2)	7000	0.041	19148	0.1952
Heat Transfer Area (m^2)	5550	0.026	19138	0.097
Thermal Power (Mwth)	3411	15.04×10^{-3}	3411	$15.04 \times^{-3}$
Avg. Heat Flux (kw/m^2)	614.6	578.5	178.23	155.1
Heat Transfer Coefficient ($kw/m^2\ ^{o}C$)	34.9	24.9	31.4	27.9
Temperature Difference in Boundary Layer, $\Delta\overline{T}_{B\text{-}L}$ (^{o}C)	17.6	23.23	- 5.68	- 5.57

T_{hot}	-	288 °C (550 °F)
T_{cold}	-	288 °C (550 °F)
H_2	-	25 cc-H_2/kg-H_2O
O_2	-	less than 10 ppb

and an almost zero coolant flow rate.

Zircaloy tubing is excluded from the pre-filming step. After the pre-filming, the loop components are kept dry, filled with N_2 gas, until pre-conditioning.

The pre-conditioning of each loop, individually lasts 30 days. Recirculating coolant conditions are the same as for the pre-filming run as regards coolant temperature, flow rate and hydrogen and oxygen level, but different in chemical conditions such as boron and lithium concentrations, and consequently at different pH. The pH values of the pre-conditioning runs differ from run to run, and are the same as the subsequent in-pile run. After pre-conditioning, the loop is kept in cold, wet storage under reference chemistry conditions.

Then the loop, pre-filmed and pre-conditioned, is finally inserted in the MITR and operated for about 30 days under constant loop conditions with about 20 days of full reactor power irradiation. The chemistry conditions scheduled for pre-conditioning and in-pile operation are :

(i) pH - 7.0 at 300 °C - Reference chemistry

Boron - 800 ppm

Li	-	1.84 ppm
H_2	-	25 cc-H_2/kg-H_2O

(ii) pH - 6.5 at 300 °C

Boron	-	800 ppm
Li	-	0.56 ppm
H_2	-	25 cc-H_2/kg-H_2O

(iii) pH - 7.5 at 300 °C

Boron	-	800 ppm
Li	-	6.26 ppm
H_2	-	25 cc-H_2/kg-H_2O

(iv) pH - 7.0 at 300 °C

Boron	-	0 ppm
Li	-	0.28 ppm
H_2	-	25 cc-H_2/kg-H_2O

At the time of preparation of this thesis writeup, two runs of category (i) under reference chemistry conditions had been completed.

3.2.2 Mass Transfer Characteristics

Table 3.2 compares the mass transfer parameters of the PCCL and a typical Westinghouse designed PWR. The mass transfer coefficients of the PCCL in the core and S/G are about 35 % and 21 % less than those of the PWR, respectively.

Table 3.2 Comparison of Mass Transfer Parameters of a Representative PWR and the MIT PCCL

Variable	CORE		S/G	
	PWR	PCCL	PWR	PCCL
Flow Velocity (m/sec)	5.1	2.83	5.2	3.18
Re	4.7×10^5	1.4×10^5	8.5×10^5	1.5×10^5
Sc	11.9	11.9	11.9	11.9
Sh†	2846	1028	4707	1080
h (cm/sec)	0.26	0.17	0.24	0.19
beta (MT)††	0.45	0.38	0.45	0.38

† Berger-Hau mass transfer correlation used (see Section 2.3.1)

†† beta (MT) - the theoretical value of the CRUDSIM transport factor, β , which is calculated considering only mass transfer, neglecting resistance in the dissolution and crystallization steps.

D_{Fe}++(300 ^{o}C) = 1.08×10^{-4} (cm^2/sec)

The surface area ratio of S/G to core is 3.45 in the PWR and 3.75 in the MIT PCCL. The product of area and mass transfer coefficient controls total mass transfer rate. The crud and activity transport factors used in CRUDSIM/MIT, which act to control the overall transport of corrosion products and radioactivity can be analytically calculated using the following relations.

$$\beta_c = \left(\frac{k_1 k_3}{k_1 + k_3}\right)\left(\frac{\rho_{H_2O}}{F}\right) \tag{2.47}$$

$$\beta_a = \left(\frac{k_1^a k_3^a}{k_1^a + k_3^a}\right)\left(\frac{\rho_{H_2O}}{F}\right) \tag{2.48}$$

When only the mass transfer is considered in calculation of the transport factors, neglecting the steps of dissolution and crystal growth of corrosion products, the crud transport factor, β_c is equal to the activity transport factor, β_a, which is the case for the original CRUDSIM code. The calculated β-value for the PCCL is about 16 % less than that of the PWR, as shown in Table 3.2. Therefore, it can be said that the PCCL is a good simulation of an actual PWR on the basis of matching β . If deemed desirable, even closer agreement could be achieved by adjusting the loop design and operating parameters slightly. However, it should be noted that the empirically determined value of β in a PWR power plant (the value which best reproduces plant crud buildup data in CRUDSIM) is about 0.01, which is about 45 times less than that calculated considering only diffusion limited mass transfer coefficients. This fact strongly indicates that the dissolution and crystal growth steps are not negligible but may be the actual controlling steps in the transport of corrosion products and radioactivity. This

conclusion is supported by reference [S-3], which also concludes that the controlling step for corrosion product transport is not the mass transfer across the flow boundary layer, but the crystal growth on the depositing surface. However, we expect that the coefficients of crystal growth and dissolution in the PCCL are similar to those in a PWR, since in both cases, the same materials are used and the environment (temperature and coolant chemistry) are similar.

3.3 CRUDSIM/MIT Calculation Results

3.3.1 Analytic solutions under constant chemistry conditions

3.3.1.1 Short time behavior

The corrosion product and radioactivity balance equations of the 2 node model are as follows. (see Section 2.2.4)

$$\frac{dI_3}{dt} = R - \beta_c F (S_3 - S_1) \tag{3.1}$$

$$\frac{dI_1}{dt} = \beta_c F (S_3 - S_1) \tag{3.2}$$

$$\frac{dA_3}{dt} = - \lambda A_3 + \beta_a F (\frac{A_1}{I_1} S_1 - \frac{A_3}{I_3} S_3) \tag{3.3}$$

$$\frac{dA_1}{dt} = - \lambda A_1 - \beta_a F (\frac{A_1}{I_1} S_1 - \frac{A_3}{I_3} S_3) + \alpha P I_1 \tag{3.4}$$

Short time behavior depends strongly on initial conditions. We consider here two of the more realistic initial conditions : clean core and dirty S/G, and dirty core and dirty S/G.

First, Eqs. (3.1) through (3.4) are expanded as linear polynomials to analyze the short time behavior.

Let $k_1 = \beta_c F (S_3 - S_1)$ (3.5)

$k_2 = R - \beta_c F (S_3 - S_1)$ (3.6)

Integration of Eq.s (3.1) and (3.2) gives,

$I_3 (t) = I_{30} + k_2 t$ (3.7)

$I_1 (t) = I_{10} + k_1 t$ (3.8)

Over the short time period considered, let

$A_3 (t) = a_1 t + a_2 t^2 + a_3 t^3 + \cdots$ (3.9)

$A_1 (t) = b_1 t + b_2 t^2 + b_3 t^3 + \cdots$ (3.10)

Insertion of Eq.s (3.7) through (3.10) into Eq.s (3.3) and (3.4) gives,

$$\frac{d}{dt}(a_1 t + a_2 t^2 + a_3 t^3) = -\lambda (a_1 t + a_2 t^2 + a_3 t^3)$$

$$+ \beta_a F\left(\frac{(b_1 t + b_2 t^2 + b_3 t^3) S_1}{I_{10} + k_1 t} - \frac{(a_1 t + a_2 t^2 + a_3 t^3) S_3}{I_{30} + k_2 t}\right) \quad (3.11)$$

$$\frac{d}{dt}(b_1 t + b_2 t^2 + b_3 t^3) = -\lambda (b_1 t + b_2 t^2 + b_3 t^3)$$

$$- \beta_a F\left(\frac{(b_1 t + b_2 t^2 + b_3 t^3) S_1}{I_{10} + k_1 t} - \frac{(a_1 t + a_2 t^2 + a_3 t^3) S_3}{I_{30} + k_2 t}\right)$$

$$+ \alpha P (I_{10} + k_1 t) \qquad (3.12)$$

(i) Clean core and Dirty S/G

$I_1 (0) = 0$ (no crud on core at start of irradiation)

$I_3 (0) = I_{30}$ (initial S/G crud inventory)

where,

$$\frac{(R - \beta_c F (S_3 - S_1)) t}{I_{30}} << 1 ,$$

which means that the cold zone inventory does not change significantly in the time span of interest.

And $A_3 (0) = A_1 (0) = 0$

Equation (3.11) becomes

$$a_1 + 2 a_2 t + 3 a_3 t^2 = -\lambda (a_1 t + a_2 t^2)$$

$$+ \beta_a F \left(\frac{(b_1 + b_2 t + b_3 t^2) S_1}{k_1} - \frac{\left(1 - \frac{k_2 t}{I_{30}}\right)(a_1 t + a_2 t^2 + a_3 t^3) S_3}{I_{30}} \right)$$

$$= \frac{\beta_a F b_1 S_1}{k_1} + t \left(-\lambda a_1 + \frac{\beta_a F b_2 S_1}{k_1} - \frac{\beta_a F a_1 S_3}{I_{30}} \right)$$

$$+ t^2 \left(-\lambda a_2 + \frac{\beta_a F b_3 S_1}{k_1} - \frac{\beta_a F S_3}{I_{30}} \left(a_2 - \frac{k_2 a_1}{I_{30}} \right) \right)$$

Therefore, the coefficients are related by

$$a_1 = \frac{\beta_a F S_1 b_1}{k_1}$$

$$2 a_2 = - a_1 \left(\lambda + \frac{\beta_a F S_3}{I_{30}} \right) + \frac{\beta_a F b_2 S_1}{k_1}$$

$$3 a_3 = \frac{\beta_a F k_2 a_1 S_3}{I_{30}^2} - a_2 \left(\lambda + \frac{\beta_a F S_3}{I_{30}} \right) + \frac{\beta_a F b_3 S_1}{k_1}$$

Similarly Eq. (3.12) becomes,

$$b_1 + 2 b_2 t + 3 b_3 t^2 = -\lambda (b_1 t + b_2 t^2)$$

$$- \beta_a F \left(\frac{S_1}{k_1} (b_1 + b_2 t + b_3 t^2) - \frac{S_3}{I_{30}} \left(a_1 t + \left(a_2 - \frac{k_2 a_1}{I_{30}} \right) t^2 \right) \right)$$

$$+ \alpha P k_1 t$$

$$= - \frac{\beta_a F b_1 S_1}{k_1} + t \left(-\lambda b_1 - \frac{\beta_a F b_2 S_1}{k_1} + \frac{\beta_a F a_1 S_3}{I_{30}} + \alpha P k_1 \right)$$

$$+ t^2 \left(-\lambda b_2 - \frac{\beta_a F b_3 S_1}{k_1} + \frac{\beta_a F S_3}{I_{30}} \left(a_2 - \frac{a_1 k_2}{I_{30}} \right) \right)$$

Hence,

$$b_1 = -\frac{\beta_a F S_1 b_1}{k_1}$$

$$2 b_2 = -\lambda b_1 - \frac{\beta_a F b_2 S_1}{k_1} + \frac{\beta_a F a_1 S_3}{I_{30}} + \alpha P k_1$$

$$3 b_3 = -\lambda b_2 - \frac{\beta_a F b_3 S_1}{k_1} + \frac{\beta_a F S_3}{I_{30}}\left(a_2 - \frac{a_1 k_2}{I_{30}}\right)$$

so that,

$$a_1 = 0$$

$$b_1 = 0$$

$$a_2 = \frac{\alpha P \beta_a F S_1}{2\left(2 + \frac{\beta_a F S_1}{\beta_c k_1}\right)} = \frac{\alpha P \beta_a F S_1}{2\left(2 + \frac{\beta_a S_1}{\beta_c (S_3 - S_1)}\right)}$$

$$b_2 = \frac{\alpha P k_1}{2 + \frac{\beta_a F S_1}{k_1}} \quad \frac{\alpha P \beta_c F (S_3 - S_1)}{2 + \frac{\beta_a S_1}{\beta_c (S_3 - S_1)}} \qquad (3.13)$$

Therefore, the activity changes with time are

$$A_3 (t) = \frac{\alpha P \beta_a F S_1}{2\left(2 + \frac{\beta_a S_1}{\beta_c (S_3 - S_1)}\right)} t^2 + \ldots \qquad (3.14)$$

$$A_1(t) = \frac{\alpha P \beta_c F (S_3 - S_1)}{2 + \frac{\beta_a S_1}{\beta_c (S_3 - S_1)}} t^2 + \cdots \qquad (3.15)$$

Equations (3.14) and (3.15) show that the activities in both core and S/G have second order dependence on time, and since $S_1/(S_3-S_1)$ is usually larger than 2, the activity in the S/G is proportional to the solubility difference between the S/G and the core surfaces, (S_3-S_1).

(ii) Dirty core and Dirty S/G

$I_1(0) = I_{10}$ (initial core crud inventory)

$I_3(0) = I_{30}$ (initial S/G crud inventory)

where,

$$\frac{(R - \beta_c F (S_3 - S_1))\, t}{I_{30}} << 1 \quad \text{and} \quad \frac{(R - \beta_c F (S_3 - S_1))\, t}{I_{10}} << 1 ,$$

which means that both the cold and hot inventories do not change significantly in the time span of interest.

And $A_3(0) = A_1(0) = 0$.

Equation (3.11) becomes,

$$a_1 + 2\,a_2\,t + 3\,a_3\,t^2 = -\lambda\,(a_1\,t + a_2\,t^2)$$

$$+ \beta_a\,F\left(\frac{S_1}{I_{10}}\left(1 - \frac{k_1\,t}{I_{10}}\right)(b_1\,t + b_2\,t^2) - \frac{S_3}{I_{30}}\left(1 - \frac{k_2\,t}{I_{30}}\right)(a_1\,t + a_2\,t^2)\right)$$

$$= t\left(-\lambda\,a_1 + \beta_a\,F\left(\frac{b_1\,S_1}{I_{10}} - \frac{a_1\,S_3}{I_{30}}\right)\right)$$

$$+ t^2\left(-\lambda\,a_2 + \beta_a\,F\left(\frac{b_2\,S_1}{I_{10}} - \frac{b_1\,k_1\,S_1}{I_{10}^2} - \frac{a_2\,S_3}{I_{30}} + \frac{a_1\,k_2\,S_3}{I_{30}^2}\right)\right)$$

Thus,

$$a_1 = 0$$

$$2\,a_2 = \frac{\beta_a\,F\,S_1\,b_1}{I_{10}}$$

$$3\,a_3 = -\lambda\,a_2 + \beta_a\,F\left(\frac{S_1}{I_{10}}\left(b_2 - \frac{b_1\,k_1}{I_{10}}\right) - \frac{S_3}{I_{30}}\left(a_2 - \frac{a_1\,k_2}{I_{30}}\right)\right)$$

Equation (3.12) becomes

$$b_1 + 2\,b_2\,t + 3\,b_3\,t^2 = -\lambda\,(b_1\,t + b_2\,t^2)$$

$$- \beta_a\,F\left(\frac{S_1}{I_{10}}\left(1 - \frac{k_1\,t}{I_{10}}\right)(b_1\,t + b_2\,t^2) - \frac{S_3}{I_{30}}\left(1 - \frac{k_2\,t}{I_{30}}\right)(a_1\,t + a_2\,t^2)\right)$$

$$+ \alpha\,P\,I_{10} + \alpha\,P\,k_1\,t$$

$$= \alpha\,P\,I_{10} + t\left(-\lambda\,b_1 - \beta_a\,F\left(\frac{b_1\,S_1}{I_{10}} - \frac{a_1\,S_3}{I_{30}}\right) + \alpha\,P\,k_1\right)$$

$$+ t^2 \left(- \lambda\, b_2 - \beta_a\, F \left(\frac{S_1}{I_{10}} \left(b_2 - \frac{k_1\, b_1}{I_{10}} \right) - \frac{S_3}{I_{30}} \left(a_2 - \frac{k_2\, a_1}{I_{30}} \right) \right) \right)$$

and therefore

$$b_1 = \alpha\, P\, I_{10}$$

$$2\, b_2 = - \lambda\, b_1 - \frac{\beta_a\, F\, S_1\, b_1}{I_{10}} + \alpha\, P\, k_1$$

$$3\, b_3 = -\lambda\, b_2 - \beta_a\, F \left(\frac{S_1}{I_{10}} \left(b_2 - \frac{b_1\, k_1}{I_{10}} \right) - \frac{S_3}{I_{30}} \left(a_2 - \frac{a_1\, k_2}{I_{30}} \right) \right)$$

so that,

$$a_1 = 0$$

$$b_1 = \alpha\, P\, I_{10}$$

$$a_2 = \frac{1}{2} \alpha\, P\, \beta_a\, F\, S_1$$

$$b_2 = \frac{\alpha\, P}{2} \left(k_1 - \lambda\, I_{10} - \beta_a\, F\, S_1 \right) \qquad (3.16)$$

Therefore, the activity changes with time are

$$A_3(t) = \frac{\alpha P \beta_a F S_1}{2} t^2 + \cdots \qquad (3.17)$$

$$A_1(t) = \alpha P I_{10}\, t + \frac{\alpha P}{2}\left[\beta_c F\left\{S_3 - \left(1 + \frac{\beta_a}{\beta_c}\right)S_1\right\} - \lambda I_{10}\right] t^2 + \cdots \qquad (3.18)$$

The S/G activity is still proportional to the time to the second power. However, the core activity is now linearly proportional to time. It is also noted that the S/G activity is proportional not to (S_3-S_1) but to S_1 for the initial short time period considered. As will be shown in Section 3.3.2.5, the S/G activity with non zero initial core crud inventory is larger at high pH than at low pH for a short initial period whose duration depends upon the amount of initial core crud.

Hence it is not advisable to start an experiment with a heavily crudded core - a key guideline used in planning the M.I.T. loop pre-filming and pre-conditioning runs, which were run at very low flow rate ; and, in addition, the Zircaloy tube was excluded from the prefilming run.

3.3.1.2 Asymptotic long term behavior

After many years of PWR operation, the activities of the S/G and core surfaces converge to steady state values, due in part to the fact that the crud inventory in the core does not increase indefinitely because of the crud removal by periodic refuelling, and due to radioactive decay.

Thus, it can be assumed that crud inventories in the core and S/G are constant : I_1^∞ and I_3^∞, respectively. Then, the activity change with time can be determined as follows.

Equation (3.3) becomes

$$\frac{dA_3}{dt} = -\lambda A_3 + \beta_a F \left(\frac{A_1}{I_1^\infty} S_1 - \frac{A_3}{I_3^\infty} S_3 \right)$$

$$= -\left(\lambda + \beta_a F \frac{S_3}{I_3^\infty} \right) A_3 + \beta_a F \frac{S_1}{I_1^\infty} A_1 \qquad (3.19)$$

and Eq.(3.4) becomes

$$\frac{dA_1}{dt} = -\lambda A_1 - \beta_a F \left(\frac{A_1}{I_1^\infty} S_1 - \frac{A_3}{I_3^\infty} S_3 \right) + \alpha P I_1^\infty \qquad (3.20)$$

Add Eq.(3.19) to Eq.(3.20), and let

$$A_t = A_1 + A_3$$

$$\frac{dA_t}{dt} = -\lambda A_t + \alpha P I_1^\infty$$

$$A_t = \frac{\alpha P I_1^\infty}{\lambda} \left(1 - e^{-\lambda t} \right)$$

Therefore,

$$A_1(t) = A_t - A_3$$

$$= \frac{\alpha P I_1^{\infty}}{\lambda}\left(1 - e^{-\lambda t}\right) - A_3 \qquad (3.21)$$

Insert Eq.(3.21) into Eq.(3.19).

$$\frac{dA_3}{dt} = -\left(\lambda + b_c\right) A_3 + b_h \left(\frac{\alpha P I_1^{\infty}}{\lambda}\left(1 - e^{-\lambda t}\right) - A_3\right)$$

$$\frac{dA_3}{dt} + \left(\lambda + b_c + b_h\right) A_3 = \frac{b_h \alpha P I_1^{\infty}}{\lambda}\left(1 - e^{-\lambda t}\right)$$

where,

$$b_c = \beta_a F \frac{S_3}{I_3^{\infty}}$$

$$b_h = \beta_a F \frac{S_1}{I_1^{\infty}}$$

Let $\lambda_t = \lambda + b_c + b_h$

Then

$$\frac{dA_3}{dt} + \lambda_t A_3 = \frac{b_h \alpha P I_1^{\infty}}{\lambda}\left(1 - e^{-\lambda t}\right)$$

So, $A_3(t)$ is,

$$A_3(t) = e^{-\lambda_t t} \int_0^t \frac{b_h \alpha P I_1^{\infty}}{\lambda} \left(1 - e^{-\lambda t'}\right) e^{\lambda_t t'} dt$$

$$= \frac{b_h \alpha P I_1^{\infty}}{\lambda} e^{-\lambda_t t} \left[\frac{1}{\lambda_t} e^{\lambda_t t} - \frac{1}{\lambda_t - \lambda} e^{(\lambda_t - \lambda) t}\right]_0^t$$

$$A_3(t) = \frac{\alpha P \beta_a F S_1}{\lambda} \left[\frac{1}{\lambda + b_c + b_h} - \frac{e^{-\lambda t}}{b_c + b_h} + \frac{\lambda e^{-(\lambda + b_c + b_h) t}}{(\lambda + b_c + b_h)(b_c + b_h)}\right] \quad (3.22)$$

where,

$$b_c = \beta_a F \frac{S_3}{I_3^{\infty}}$$

$$b_h = \beta_a F \frac{S_1}{I_1^{\infty}}$$

From Eqs. (3.21) and (3.22), the core activity is

$$A_1(t) = \frac{\alpha P}{\lambda} \left[I_1^{\infty} - \frac{\beta_a F S_1}{\lambda + b_c + b_h} - \left(I_1^{\infty} - \frac{\beta_a F S_1}{b_c + b_h}\right) e^{-\lambda t} - \frac{\beta_a F S_1 \lambda e^{-(\lambda + b_c + b_h) t}}{(b_c + b_h)(\lambda + b_c + b_h)}\right] \quad (3.23)$$

where,

$$b_c = \beta_a F \frac{S_3}{I_3^\infty}$$

$$b_h = \beta_a F \frac{S_1}{I_1^\infty}$$

It is noted in Eq.(3.22) that the saturation time of Co^{58} and Co^{60} activities directly depends upon their half lives. After about 1 year, Co^{58} is well on the way to convergence, while (under the conditions analyzed here) Co^{60} requires about 20 years to saturate comparably. Thus, the asymptotic S/G activity becomes

$$A_3^\infty = \frac{\alpha P \beta_a F S_1}{\lambda \left[\lambda + \beta_a F \left(\frac{S_3}{I_3^\infty} + \frac{S_1}{I_1^\infty}\right)\right]} \qquad (3.24)$$

And the asymptotic core activity becomes

$$A_1^\infty = \frac{\alpha P}{\lambda} I_1^\infty - A_3^\infty = \frac{\alpha P}{\lambda}\left[I_1^\infty - \frac{\beta_c F S_1}{\lambda + \beta_a F \left(\frac{S_3}{I_3^\infty} + \frac{S_1}{I_1^\infty}\right)}\right] \qquad (3.25)$$

Asymptotic activities in both the S/G and core show a dependence on the average core crud inventory, which can be calculated by the relation :

$$I_1^\infty = \frac{1}{2} T \beta_c F (S_3 - S_1) \qquad (3.26)$$

where T is the time during which a given batch of fuel elements stays in core.

Equation (3.26) shows the solubility difference dependence of the average core crud inventory. Therefore, by reducing the solubility difference one can decrease I_1^∞ and consequently the asymptotic activities in both S/G and core.

From Eqs. (3.14) and (3.24), we can see that there is a relation between the short time and the asymptotic long term activity in the S/G and the core for the case of zero initial core crud inventory. The ratio of the short time to the asymptotic long term activity in the S/G is

$$\frac{A_3(t)}{A_3^\infty} = \frac{\lambda t^2}{2}\left[\frac{\lambda + \beta_a F\left(\frac{S_1}{I_1^\infty} + \frac{S_3}{I_3^\infty}\right)}{2 + \frac{\beta_a S_1}{\beta_c (S_3 - S_1)}}\right] \qquad (3.27)$$

And, the ratio of the short time to the asymptotic long term activity in the core is

$$\frac{A_1(t)}{A_1^\infty} = \frac{\lambda t^2 \beta_c F (S_3 - S_1)}{\left[I_1^\infty - \frac{\beta_a F S_1}{\lambda + \beta_a F\left(\frac{S_3}{I_3^\infty} + \frac{S_1}{I_1^\infty}\right)}\right]\left[2 + \frac{\beta_a S_1}{\beta_c (S_3 - S_1)}\right]} \qquad (3.28)$$

For representative parameter values, additional approximations can be made, eg :

$$\left(\frac{\beta_a}{\beta_c}\right) \approx 1\,,\ \frac{S_3 - S_1}{S_1} << 1,\ I_3^\infty >> \left(\frac{S_3}{S_1}\right) I_1^\infty$$

in which case Eq. (3.27) reduces to

$$\frac{A_3(t)}{A_3^{\infty}} \cong \frac{\lambda_1 t^2}{T} \qquad (3.27a)$$

Equation (3.27a) shows that short and long run results depend (to first order) only on fixed physical constants. This result depends of course on whether the above approximations prove valid for situations of actual interest - an issue requiring experimental confirmation. A similar limiting case analysis for Eq. (3.28) gives an even simpler limiting approximation,

$$\frac{A_1(t)}{A_1^{\infty}} \cong \left(\frac{2t}{T}\right)^2 \qquad (3.28a)$$

Using typical parameter values for a representative PWR operating at pH 7, the ratio of the activity at 30 days to the asymptotic activity gives,

S/G

From Eq. (3.27), $\frac{A_3(30\ \text{day})}{A_3^{\infty}} = 0.012$ for Co^{51}

$= 3.05 \times 10^{-4}$ for Co^{60}

From Eq. (3.27a), $\frac{A_3(30\ \text{day})}{A_3^{\infty}} = 0.021$ for Co^{51}

$= 3.61 \times 10^{-4}$ for Co^{60}

Core

From Eq. (3.28), $\frac{A_1(30\ day)}{A_1^{\infty}} = 0.0056$ for Co^{58}

$= 0.0037$ for Co^{60}

From Eq. (3.28a), $\frac{A_1(30\ day)}{A_1^{\infty}} = 0.0044$ for Co^{58} and Co^{60}

The above analytically estimated ratios are supported by numerical results calculated using CRUDSIM/MIT, which gives for an actual PWR,

S/G

$\frac{A_3(30\ day)}{A_3^{\infty}} = 0.013$ for Co^{58}

$= 4.23 \times 10^{-4}$ for Co^{60}

Core

$\frac{A_1(30\ day)}{A_1^{\infty}} = 0.0050$ for Co^{58}

$= 0.0026$ for Co^{60}

The difference between the analytical predictions and CRUDSIM/MIT calculations is due to the refuelling of core fuel assemblies, and a small contribution comes from the approximations used in the analytic short time prediction. Annual removal of fuel assemblies reduces the activity inventory of a PWR primary circuit by approximately the amount of the above differences.

The above relations, Eqs. (3.27) and (3.28), show that the asymptotic long term behavior of activities in the S/G and core is directly proportional to the short time activities in the S/G and core. Therefore, short term operations (30 days) can be used to deduce the asymptotic long term behavior of activities in the S/G and core.

3.3.2 Sensitivity Analyses of Parameters

3.3.2.1 Transport Factor, β

The transport factor, β controls the transport rate of corrosion products and radioactivity, as shown in Eqs. (2.5) through (2.8). As explained in Section 2.3.4, in the transport of corrosion products and radioactivity, four steps are involved. ; dissolution at the S/G surface (core surface in radioactivity transport), mass transfer in the S/G, mass transfer in the core and crystal growth on the core surface (S/G surface in radioactivity transport).

In the original CRUDSIM code, the empirical parameter, β accounts for all of these steps. The value of 0.01, which was empirically determined by matching PWR operational data, is normally used for β , which combines the effect of both the crud transport factor and the activity transport factor. Figures 3.2 and 3.3 show the trends for the crud inventory in the core and the Co^{58} activity in the S/G with time for different β values ; the behavior of Co^{60} activity is identical for the short time spans considered. It is obvious from Eqs. (2.5) through (2.8) and demonstrated in these figures that as β increases, the transport rate of the corrosion products and radioactivity increases. A factor of 2 increase in β increases the S/G activity by a factor of about 2.

However, as discussed in Section 2.3.4, the activity transport factor, β_a is not necessarily equal to the crud transport factor, β_c, since their transport paths are different. PWR operational data actually shows that the activity transport factor may be somewhat smaller than the crud transport factor. [B-9] Therefore,

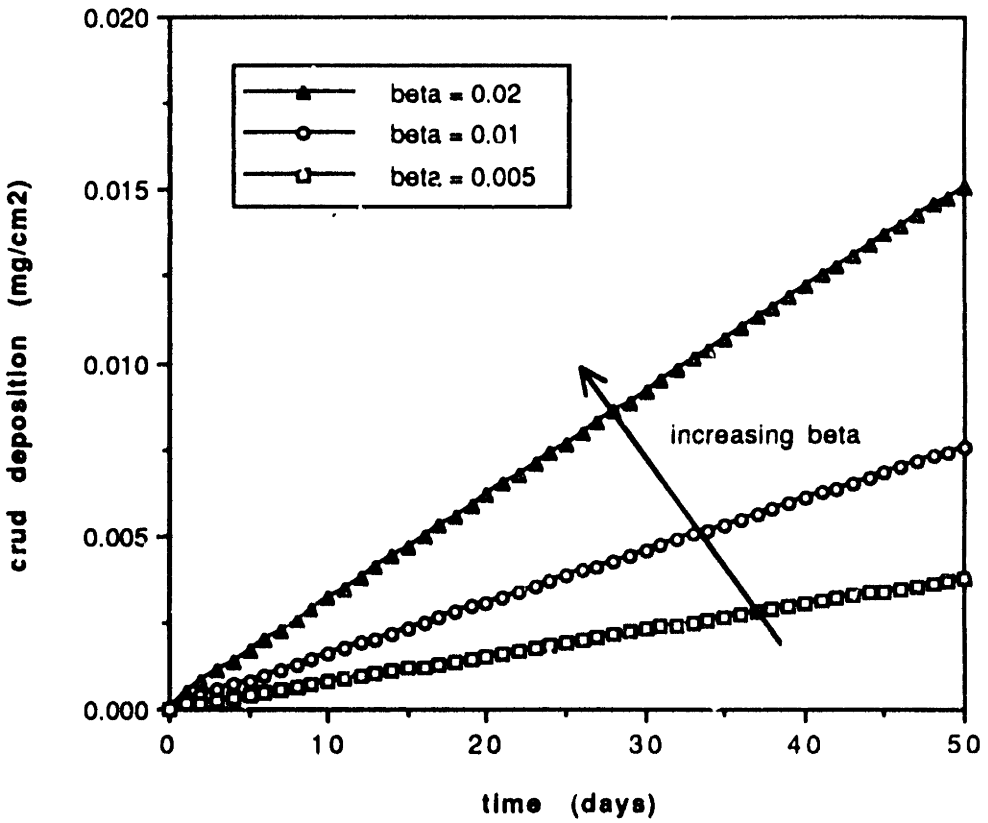

Figure 3.2 Core crud deposition as a function of CRUDSIM transport factor, beta

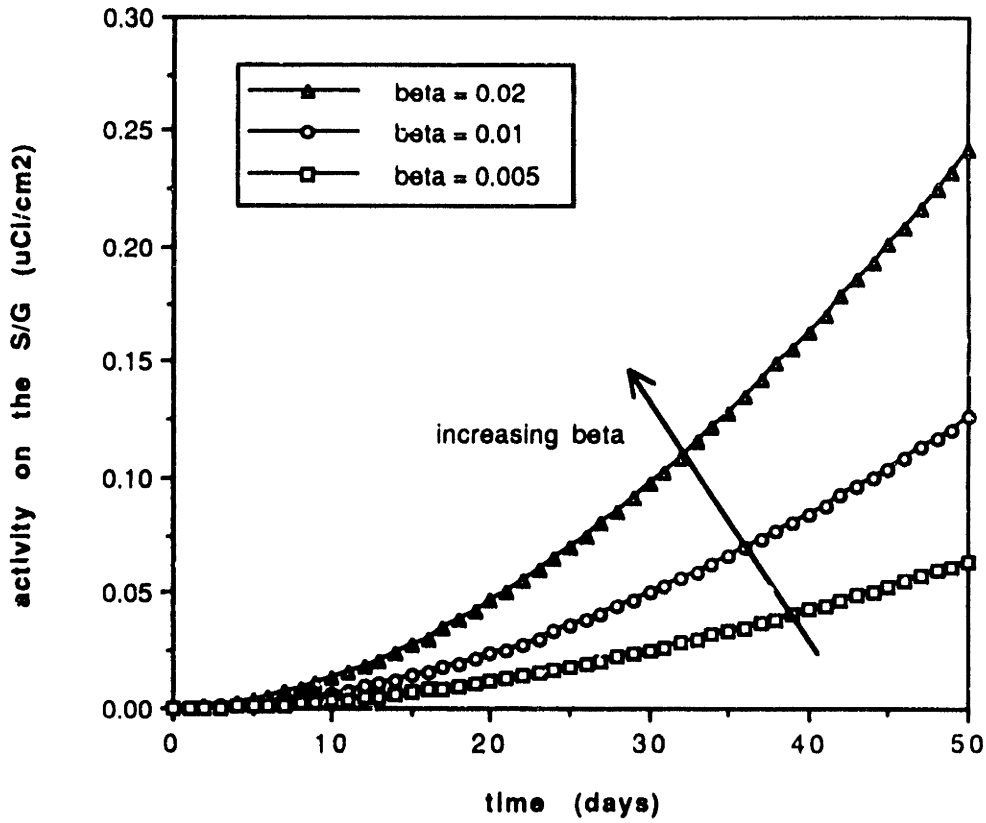

Figure 3.3 Co^{58} activity buildup in S/G as a function of CRUDSIM transport factor, beta

we will examine how the crud and activity transport are changed when different values are used for the crud and activity transport factors. As the activity transport factor, β_a increases, more activity is transported from the core to the S/G. Figures 3.4 and 3.5 show that the change in activity transport factor does not alter the trends of the activities in the core and S/G, but changes their relative magnitudes. That is, as shown in Figure 3.6, as the activity transport factor, β_a, decreases, the ratio of S/G to core activity decreases.

3.3.2.2 Particulate Precipitation

As derived in Section 2.4, particulate precipitation in the coolant does not change the dependence of the crud and activity transport upon the solubility differences between the S/G surface, bulk coolant and core surface. However, particulate precipitation in the coolant can change the absolute amount of the crud and activity transport, since the particulates in the coolant can deposit on both core and S/G surfaces, regardless of the solubility difference between S/G and core. For example, when all the crud released from the S/G is assumed to precipitate in the coolant, the net crud transport from the S/G to the core can be decreased by about a factor of 4, since about three quarters of the particulates in the coolant can redeposit back on the S/G surface, considering that the surface area ratio of S/G to core is about 3 and mass transfer coefficients in both regions are similar.

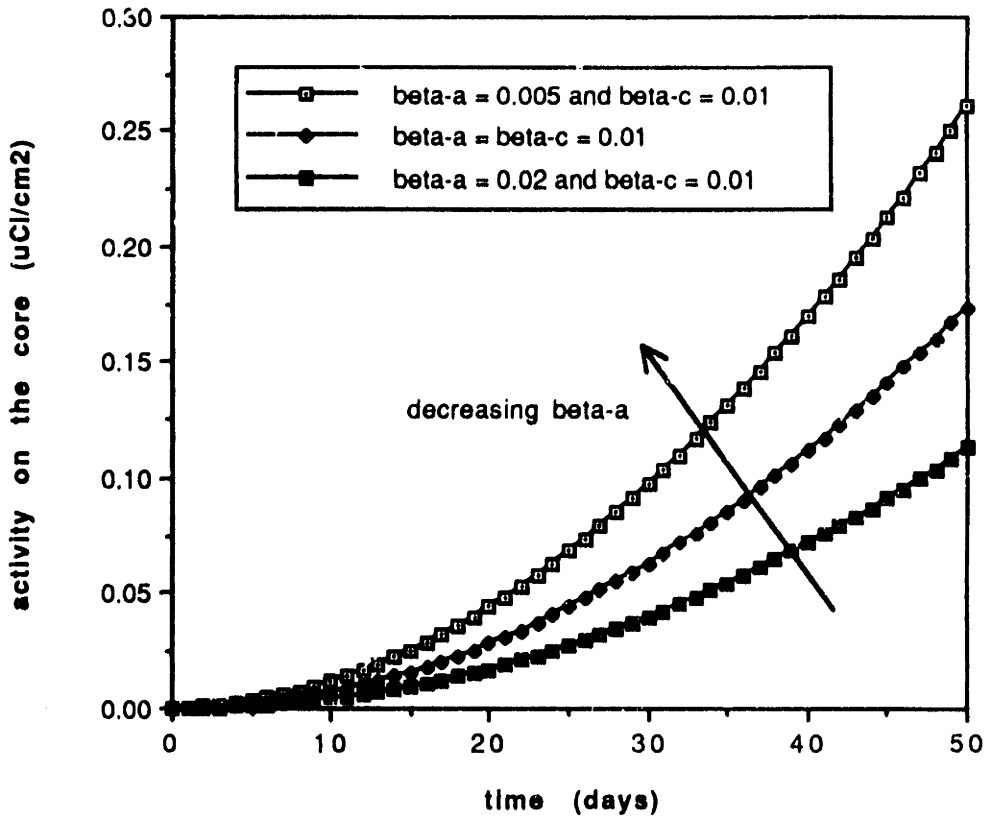

Figure 3.4 Co^{58} activity buildup in the core as a function of activity transport factor (beta-a)

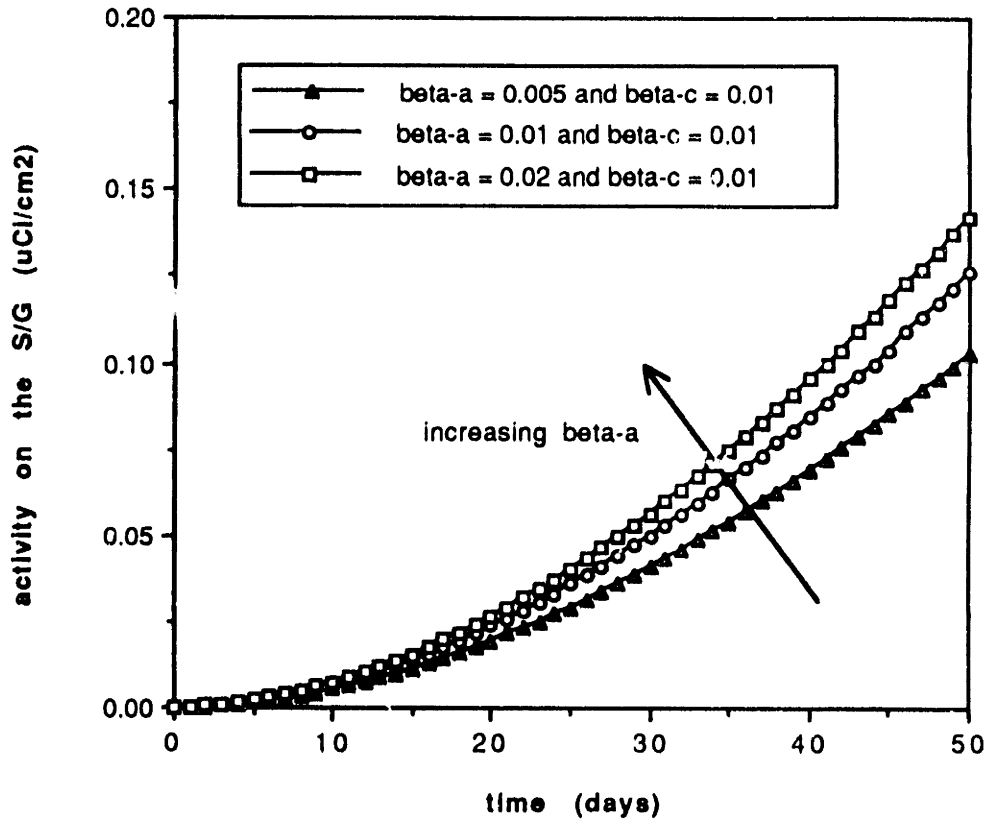

Figure 3.5 Co^{58} activity buildup in the S/G as a function of activity transport factor (beta-a)

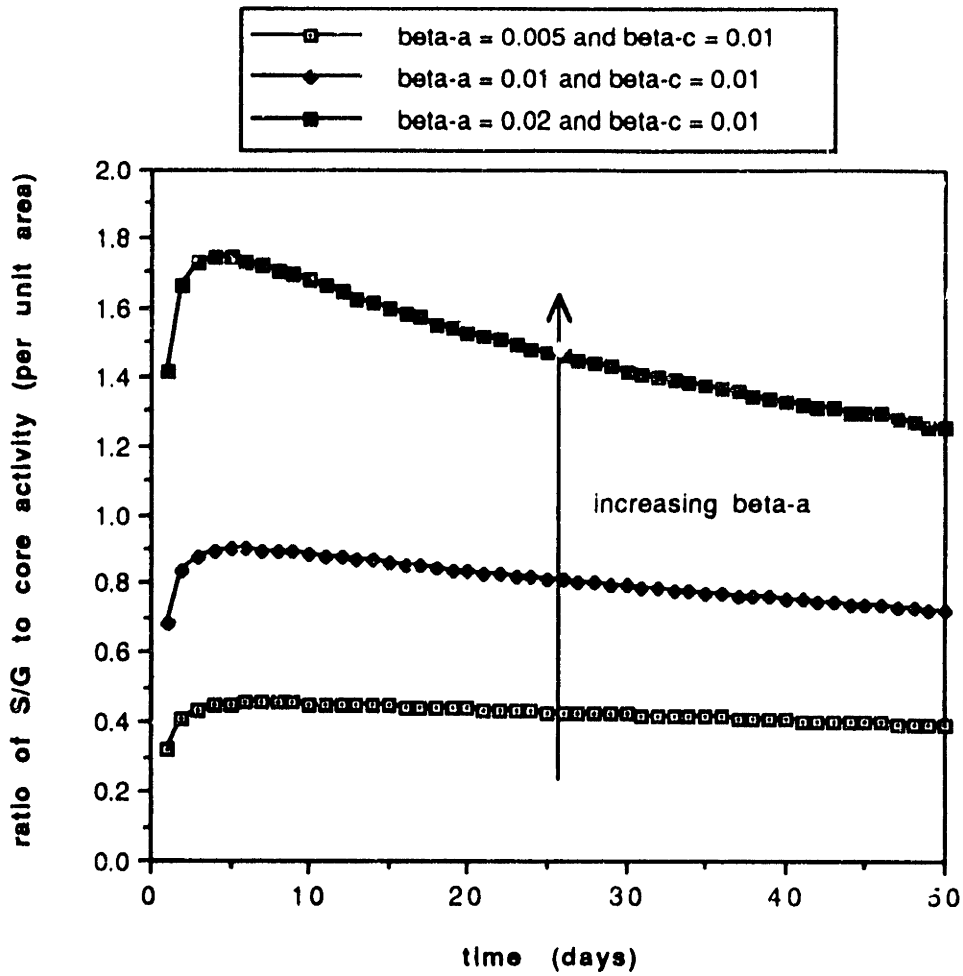

Figure 3.6 Activity ratio of Co^{58} in the S/G to that in the core as a function of activity transport factor (beta-a)

The crud and activity transport equations with particulate precipitation have been implemented (as an option) in CRUDSIM/MIT , and the effect of the particulate precipitation analyzed. Figures 3.7 and 3.8 show the core crud and S/G activity change when the crystal growth resistance on the surface approaches infinity, that is, there is 100 % particulate precipitation of the soluble crud in the coolant, in comparison with the value of 0 % particulate precipitation in the coolant assumed in the original CRUDSIM. The results show a decrease of about 76 % in core crud and a 68 % decrease in Co^{58} S/G activity at 50 days. These decreases are more or less equivalent to the decreases of the same magnitudes in the crud and activity transport factors.

3.3.2.3 Coolant pH, Temperature and Hydrogen Pressure

The CRUDSIM equations show that the crud transport rate is proportional to the solubility difference of corrosion products between the S/G tubing surface and the core fuel element surface. The solubility difference originates from its dependence upon the temperature and pH of the coolant, as shown in Eq. (2.89). Therefore, crud and activity transport also depends on the coolant temperature and pH.

Figure 3.9 shows the predicted Co^{58} activity change in the S/G section of the PCCL with time at different pH values. The activity at low pH is larger than that at high pH, since the solubility difference between S/G tubing and core fuel element surfaces at low pH is larger than that at high pH, and at pH values above

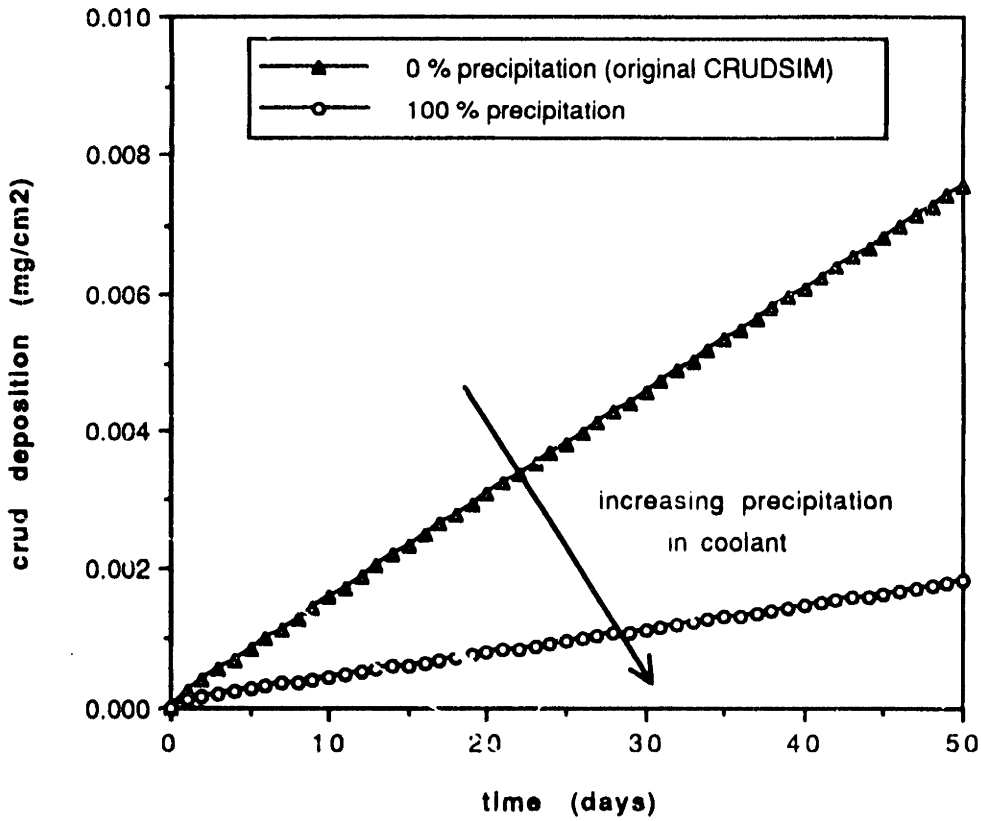

Figure 3.7 Core crud buildup as a function of particulate precipitation in the coolant

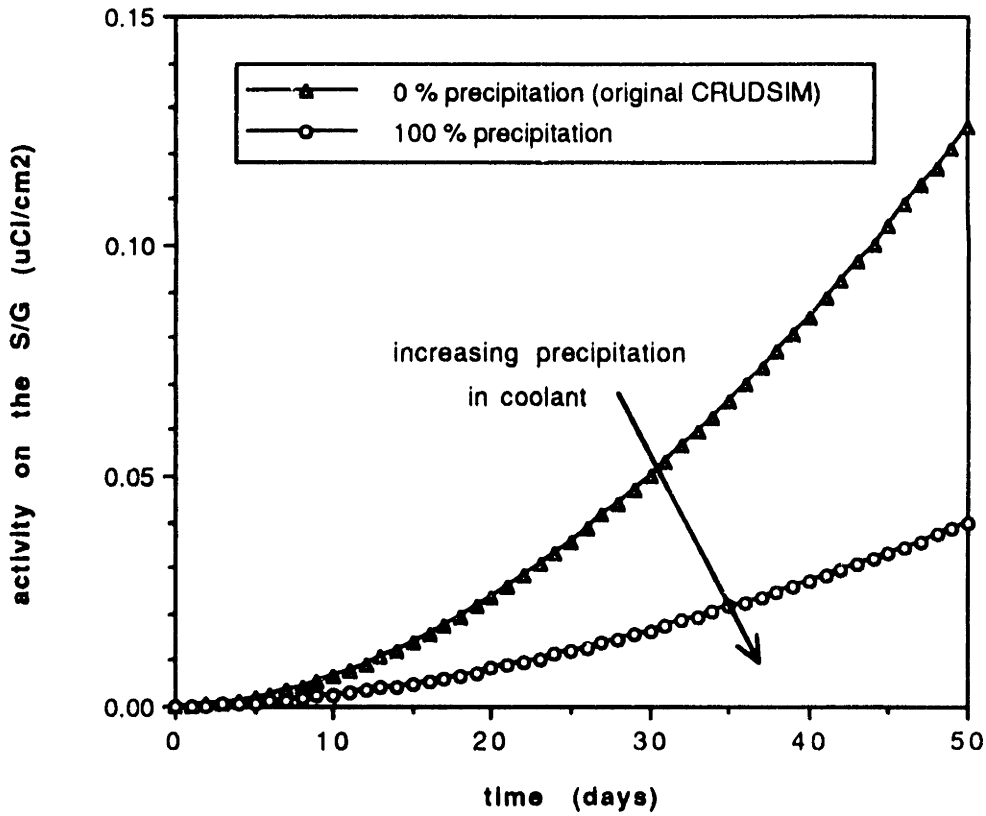

Figure 3.8 Co^{58} activity buildup in the S/G as a function of particulate precipitation in the coolant

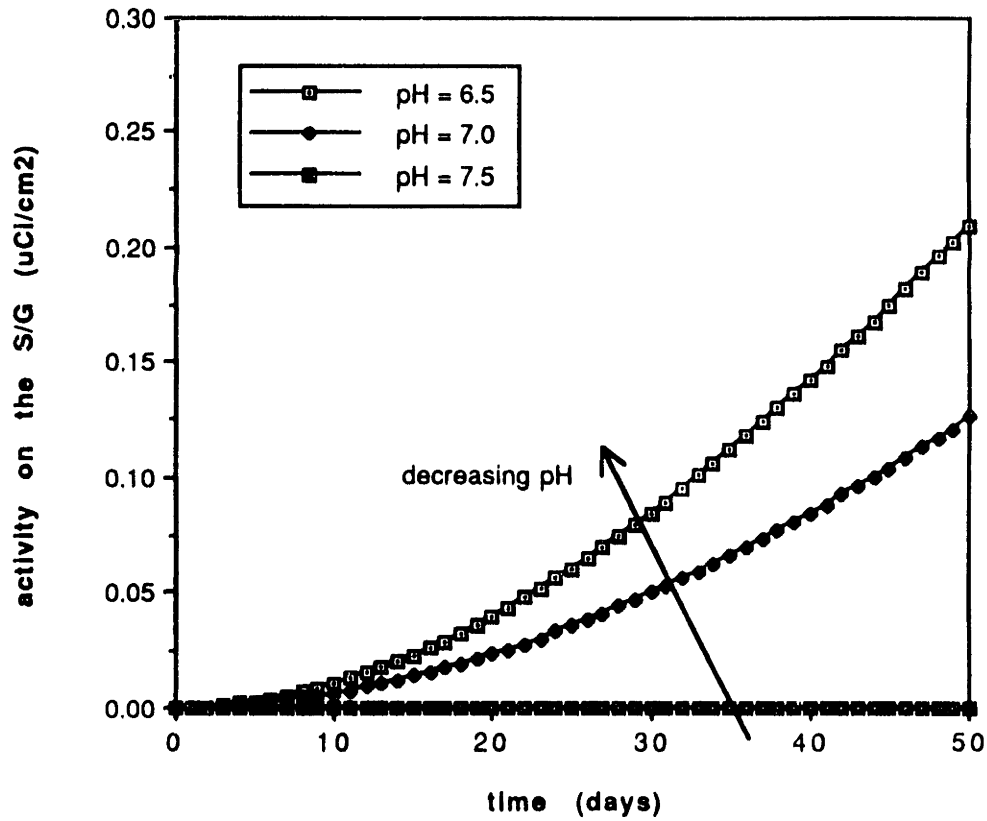

Figure 3.9 Co^{58} activity buiidup in the S/G as a function of pH

7.5, the solubility at the core fuel surface becomes larger than that at the S/G tubing surface, so that no crud is transported from the S/G to the core by the solubility difference mechanism, and subsequently the activities on the core and the S/G are virtually zero - at least theoretically. Therefore, following this line of reasoning it is desirable to maintain the coolant pH at or above 7.5. Figure 3.10 shows the relative activity of Co^{58} in the S/G for operation at different pH levels in the PCCL. It shows that the activity difference between pH 6.5 and pH 7.0 is about a factor of 1.7, and that at pH 7.5 the activity is almost zero.

The solubility is also a function of temperature. Figure 2.10 shows that at high pH, solubility can increase at high temperature. Therefore, the solubility difference between the S/G tubing surface and the core surface also depends on the average coolant temperature, even when the temperature difference between surfaces is the same. Figure 3.11 shows how the S/G activity changes as a function of average coolant temperature at pH 7. A sufficiently high coolant temperature can decrease the crud transport from the S/G to the core.

Solubility of the corrosion products is proportional to the hydrogen pressure to the one-third power, as shown in Eq. (2.89) This implies that as the hydrogen pressure decreases, the solubility decreases. In the extreme limit, the solubility becomes zero at zero hydrogen pressure, so that according to this relation, no soluble crud would be present in the coolant.

However, the limiting case is not relevant to PWR primary coolant. In the calculation of the solubility in Section 2.3.6, it was assumed that the coolant is in a reducing condition, that is, there is no free oxygen available and only free

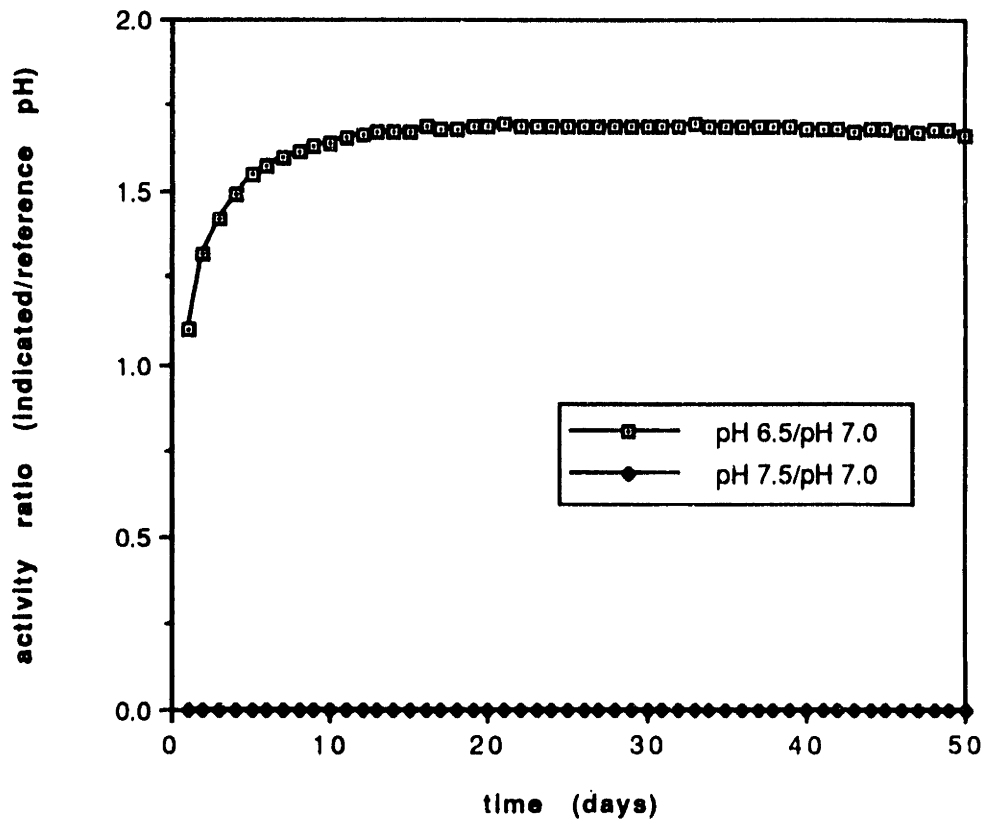

Figure 3.10 Ratio of Co^{58} activity in the S/G at indicated pH to that at reference pH 7

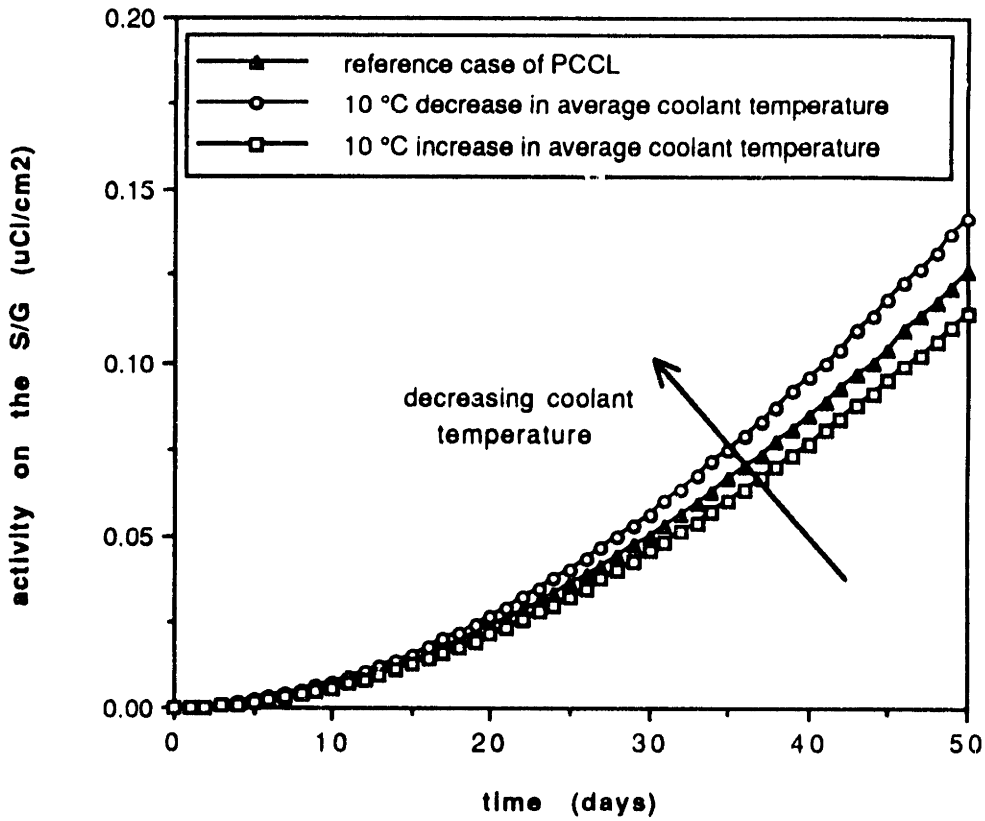

Figure 3.11 Co^{58} activity buildup in the S/G at pH 7 as a function of average coolant temperature

hydrogen is present. In reality, if there is no hydrogen in PWR primary coolant, free oxygen produced in the core by radiolysis of water accumulates, so that the coolant is no longer under reducing conditions, and therefore, Eq. (2.89) for the solubility is no longer valid. If there is a considerable amount of free oxygen available in the coolant, the corrosion rate of the metals in the PWR primary circuit increases rapidly, and so does the solubility of the corrosion products. Therefore, free oxygen in the coolant can increase the corrosion product transport significantly. [S-1] Apart from that, other deleterous processes such as stress corrosion cracking are enhanced. Hence, operation in an oxidizing region is strictly to be avoided.

These facts suggest that there is a preferred hydrogen concentration : large enough to suppress free oxygen in the coolant, but small enough to decrease the solubility. The hydrogen concentration under normal PWR operating conditions ranges from 20 (cc-H_2/kg-H_2O) to 35 (cc-H_2/kg-H_2O). CANDU reactors, however, operate at much lower values : 3 - 10 (cc-H_2/kg-H_2O). Figure 3.12 shows that under reducing conditions, lower hydrogen concentrations give lower activity in the S/G, since the solubility decreases with hydrogen concentration. Activity reduction by a factor of two appears achievable.

3.3.2.4 Direct Recoil Release of Co^{58}

Radioactive Co^{58} nuclei produced by the (n,p) reaction of Ni^{58} can, in theory, have a large probability of direct recoil release into the coolant during

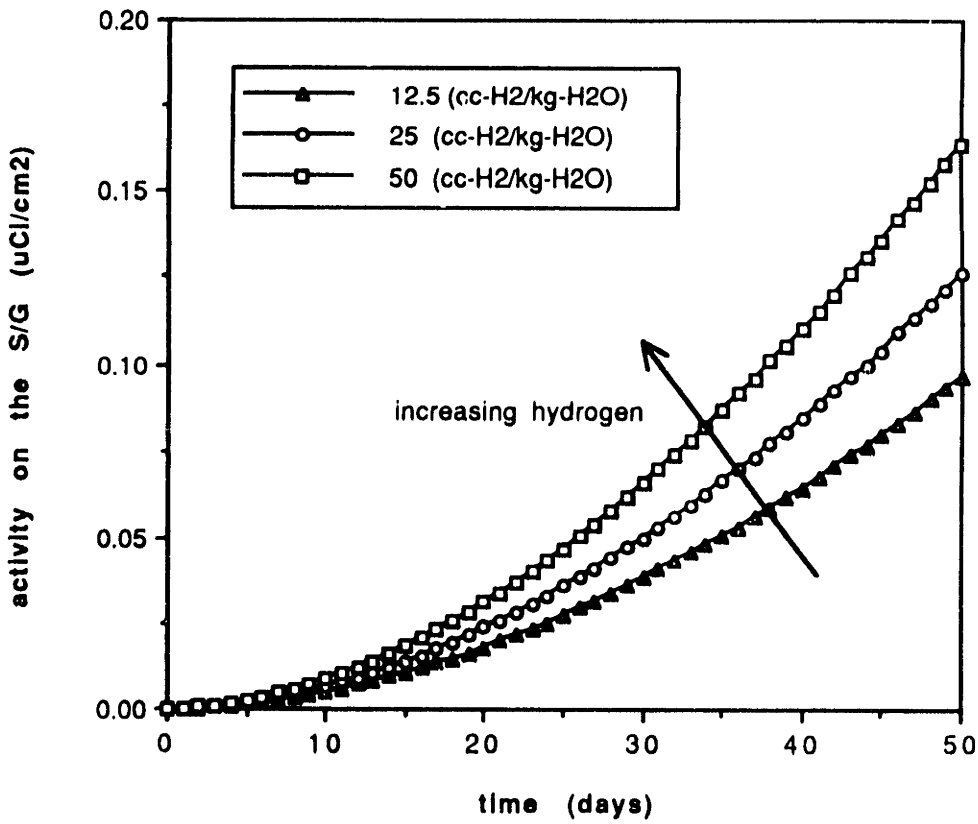

Figure 3.12 Co^{58} activity buildup in the S/G as a function of hydrogen concentration

initial stages of operation (when crud layers are very thin), as explained in Section 2.5.2. The Co^{58} can be directly recoil released at a yield of approximately 50 %. Figure 3.13 shows that the recoil release of Co^{58} does not change the trend of S/G activity with time (t^2 dependence). However, the presence of this effect can be checked by comparing the activity ratios of Co^{58} to Co^{60} (which has little chance of direct recoil release due to its predominant production by thermal neutron capture.) in the core, coolant and S/G.

Figures 3.14, 3.15 and 3.16 show the activity ratio of Co^{58} to Co^{60} in the core, coolant and S/G as a function of the probability of direct recoil release of Co^{58}. They show that when direct recoil release of Co^{58} is predominant, the ratio of Co^{58} to Co^{60} in the S/G will be larger than the corresponding ratio in the core. However, as derived in Section 2.3.4, the ratio of Co^{58} to Co^{60} also depends on the composition of the core crud (eg. Ni^{58} and Co^{59}). Therefore, without accurate data on the core crud composition, it is difficult to tell the extent of Co^{58} direct recoil release from the ratio of Co^{58} to Co^{60} in core, coolant and S/G.

However, the ratio of the (Co^{58}/Co^{60}) ratio in the S/G to the (Co^{58}/Co^{60}) ratio in the core will eliminate the effect of core crud composition and so directly indicate the significance of Co^{58} direct recoil release. Figure 3.17 shows the ratio of the (Co^{58}/Co^{60}) ratio in the S/G to the (Co^{58}/Co^{60}) ratio in the core, and how it can identify the relative extent of Co^{58} recoil release without accurate information on the core crud composition. The long term effect of the direct recoil release of Co^{58} on S/G activity is shown in Figure 3.18, including the effect of annual fuel assembly refuelling. Direct recoil release of 25 % of the Co^{58} increase the asymptotic S/G Co^{58} activity by 21 %.

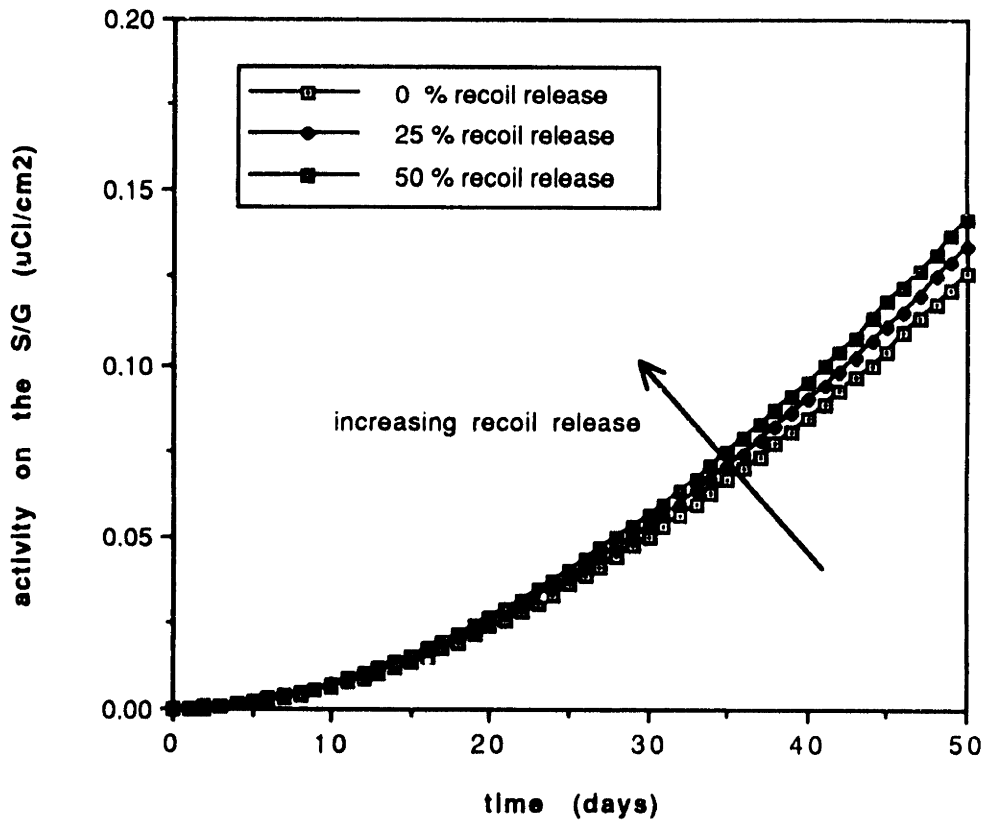

Figure 3.13 Co^{58} activity buildup in the S/G as a function of recoil release of Co^{58}

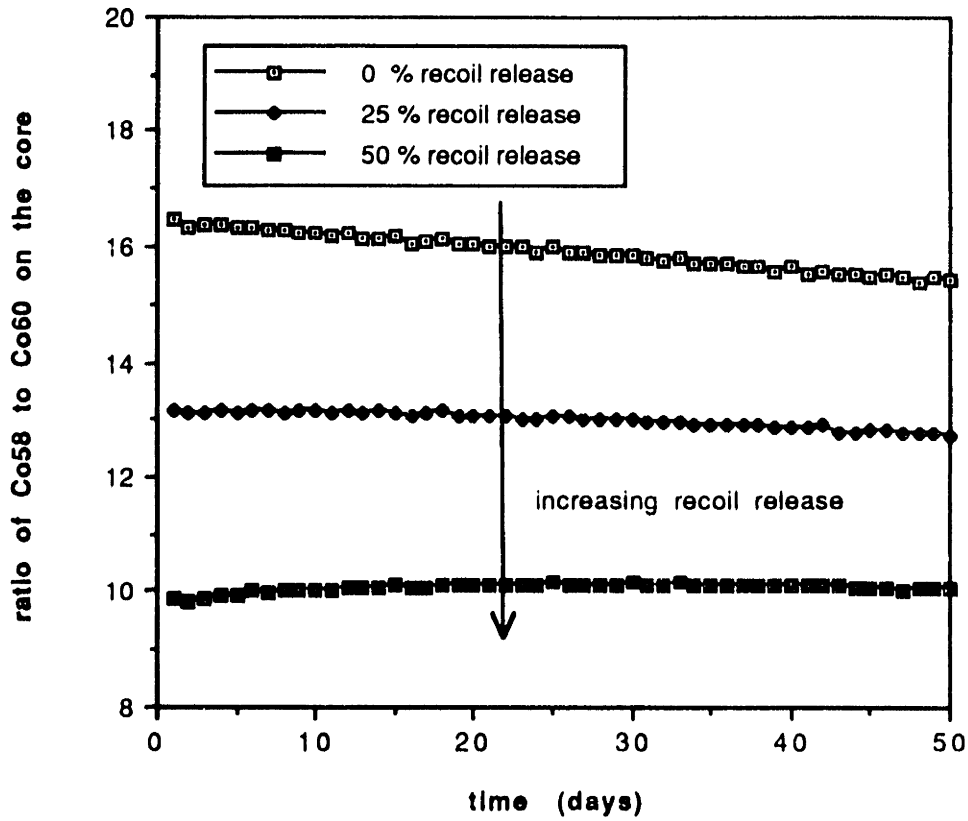

Figure 3.14 Activity ratio of Co^{58} to Co^{60} in the core as a function of recoil release of Co^{58}

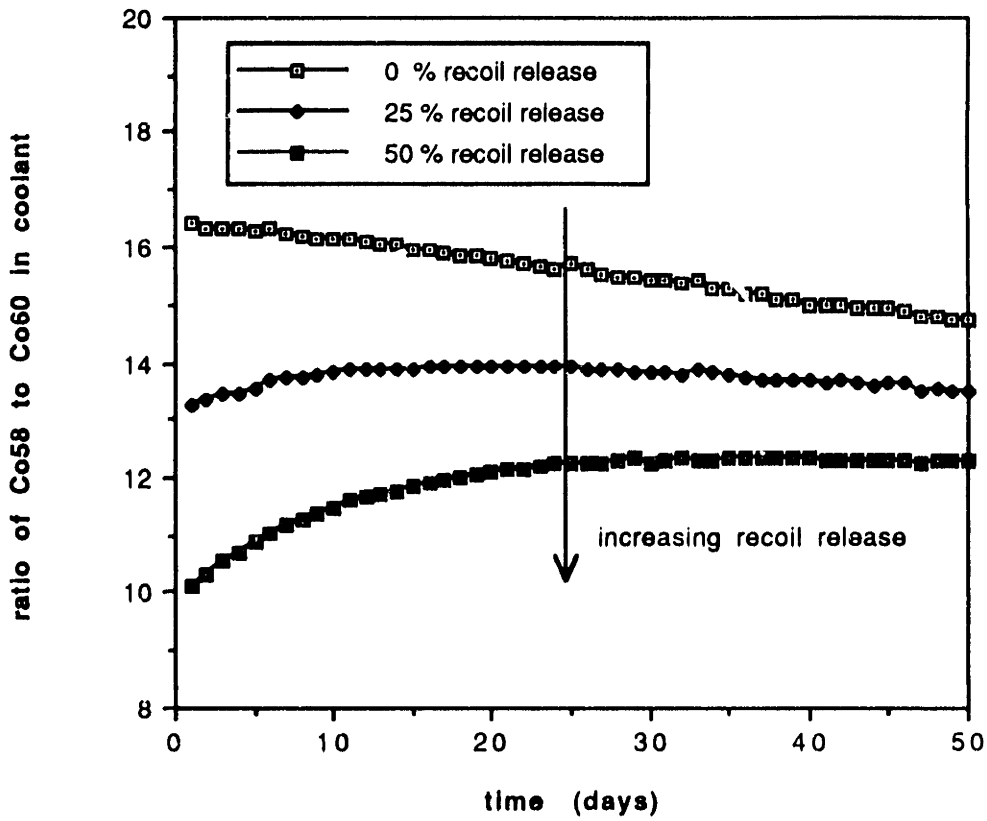

Figure 3.15 Activity ratio of Co^{58} to Co^{60} in the coolant as a function of recoil release of Co^{58}

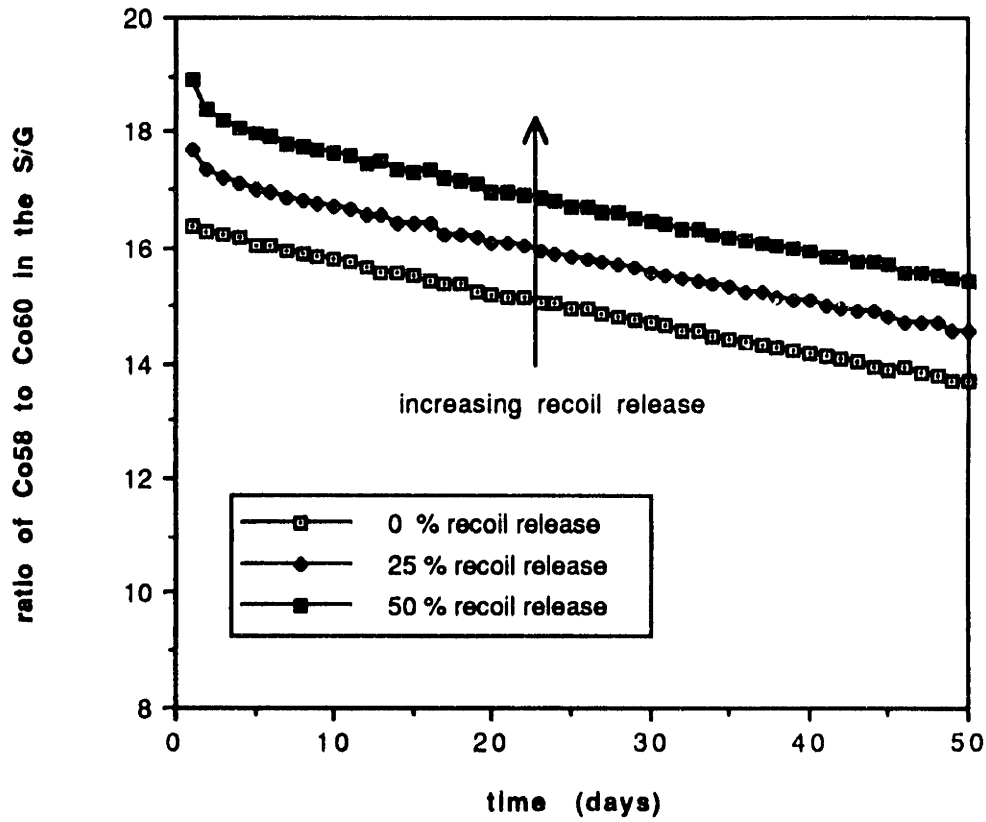

Figure 3.16 Activity ratio of Co^{58} to Co^{60} in the S/G as a function of recoil release of Co^{58}

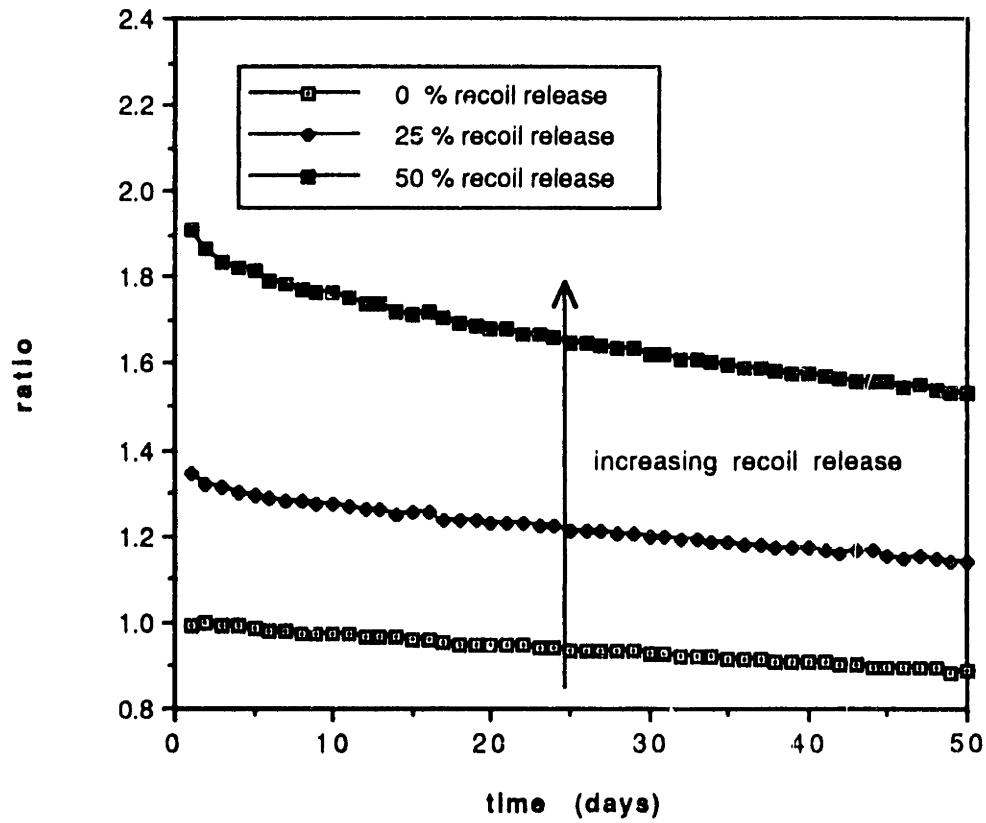

Figure 3.17 Ratio of (Co^{58}/Co^{60}) in the S/G to (Co^{58}/Co^{60}) in the core as a function of recoil release of Co^{58}

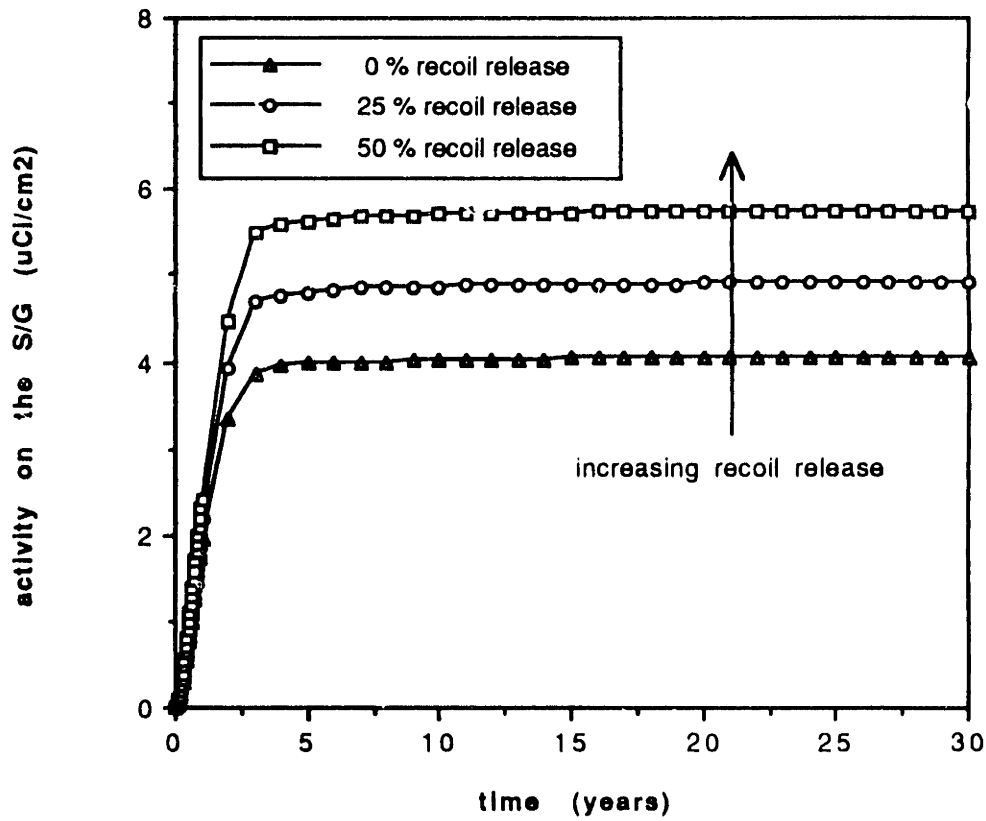

Figure 3.18 Co^{58} activity buildup in the S/G in the long term as a function of recoil release of Co^{58}

3.3.2.5 Initial Crud Inventory and Corrosion Rate

The initial crud inventory in the S/G and core can affect the activity trends in these regions. Figure 3.19 shows the S/G activity as a function of the initial crud inventory in the S/G. It shows that the activity is very insensitive to the initial inventory in the S/G.

However, as shown in Figures 3.20 and 3.21, the activities in the core and S/G are significantly affected by the initial crud inventory in the core. With zero initial inventory, the activities in the core and S/G are proportional to time to the second power. However, if there is a non-zero initial inventory, the activities in the core and S/G have a linear dependency on time, as derived in Section 3.3.1.

The pH dependency of S/G activity as a function of time is also changed. As shown in Figure 3.22, the activity in the S/G at high pH is larger than at low pH until a certain amout of time has elapsed, which depends on the initial core crud inventory, since the activity transport from the core to the S/G is larger at high pH than at lower pH due to the change in solubility difference (that is, the solubility difference between the core surface and the S/G surface). In this case, the early activity trend in the S/G is controlled not by the net crud transport from the S/G to the core, but by the activity transport from the core to the S/G, since initially there is a sufficient crud inventory in the core to outweigh the immediate effects of pH. But, in the long run, as shown in Figure 3.23, the activity in the S/G at low pH becomes larger than that at high pH, the time interval depending upon the amount of the initial crud inventory in the core.

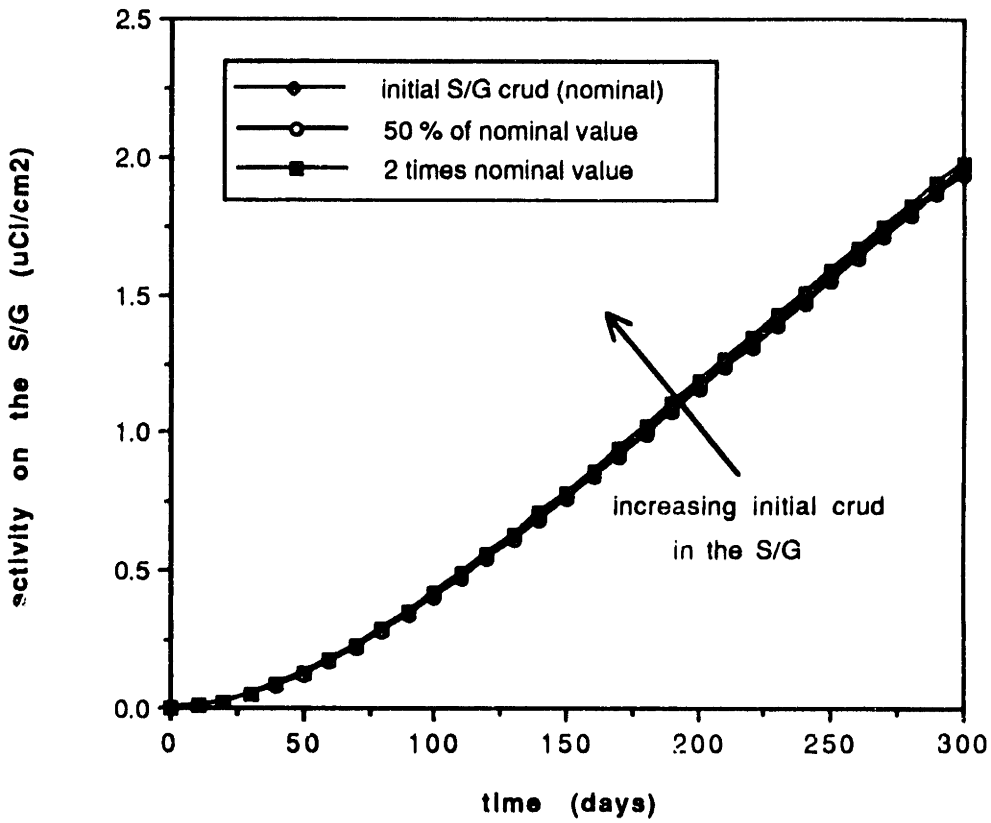

Figure 3.19 Co^{58} activity buildup in the S/G as a function of initial crud inventory in the S/G

- Key to legend

3070 core 58 - Co^{58} activity in core when 30 day pre-conditioning at pH 7.0 at full coolant flowis followed by operation of the PCCL at pH 7.0.

6070 core 58 - Co^{58} activity in core when 60 day pre-conditioning at pH 7.0 at full coolant flowis followed by operation of the PCCL at pH 7.0.

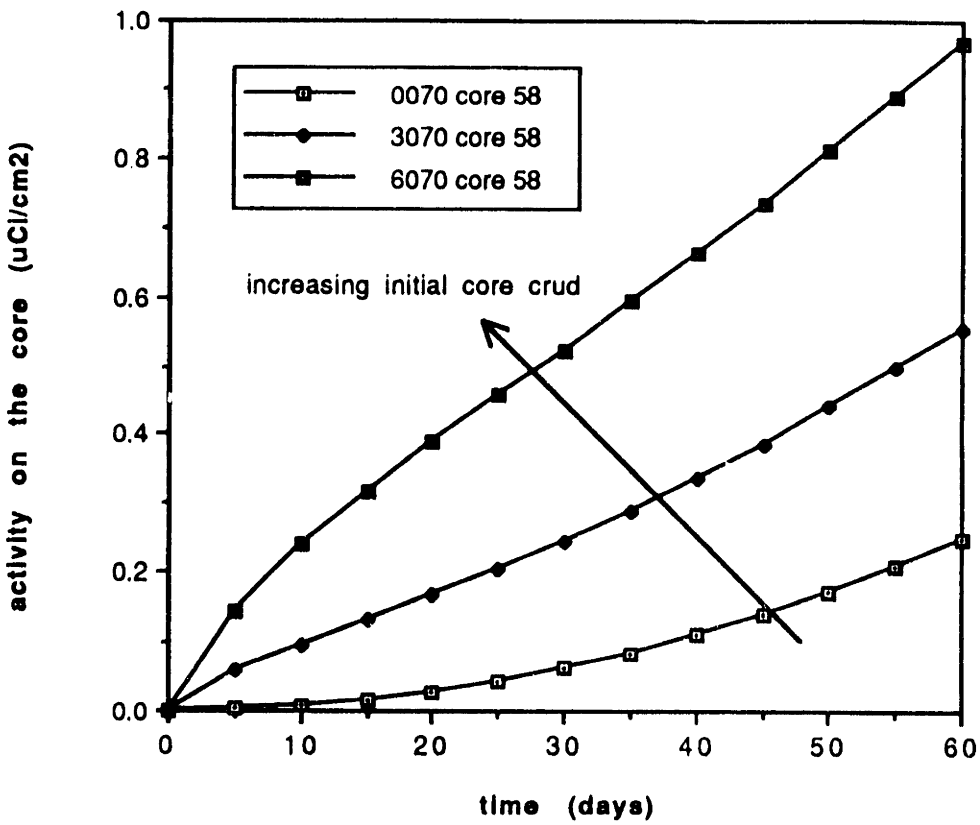

Figure 3.20 Co^{58} activity buildup in the core as a function of initial core crud inventory

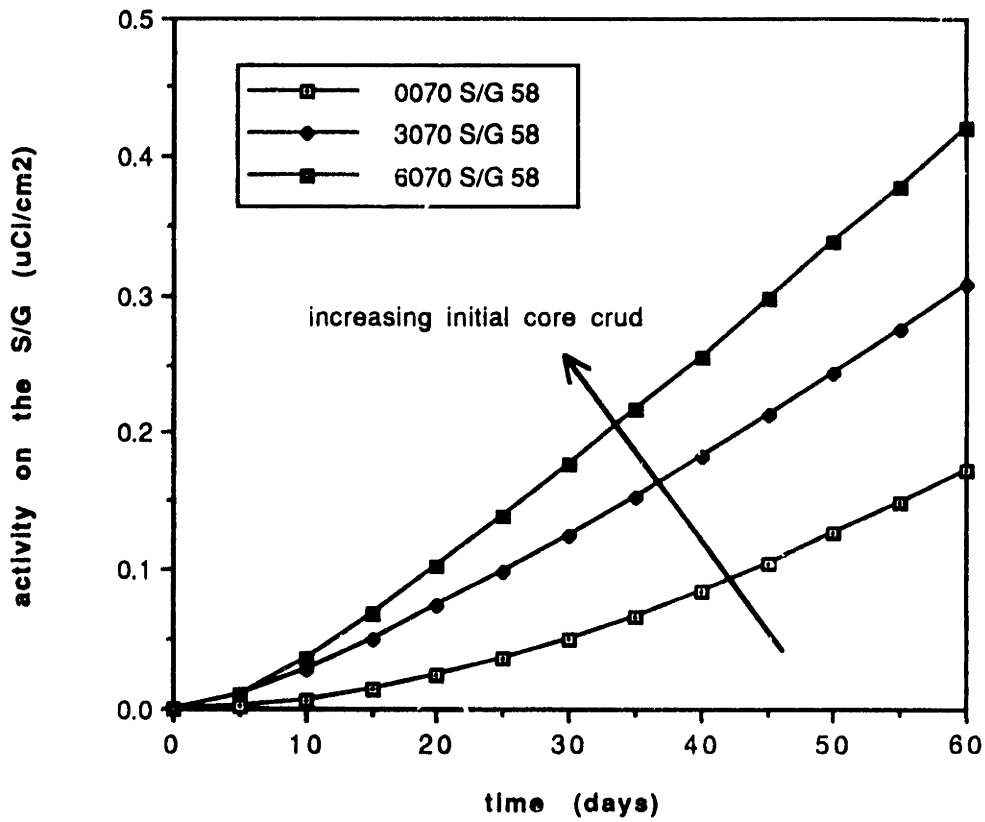

Figure 3.21 Co^{58} activity buildup in the S/G as a function of initial core crud inventory

- Key to legend

6065 S/G 58 - Co^{58} activity in S/G when 60 day pre-conditioning at pH 7.0 at full coolant flow is followed by operation of the PCCL at pH 6.5

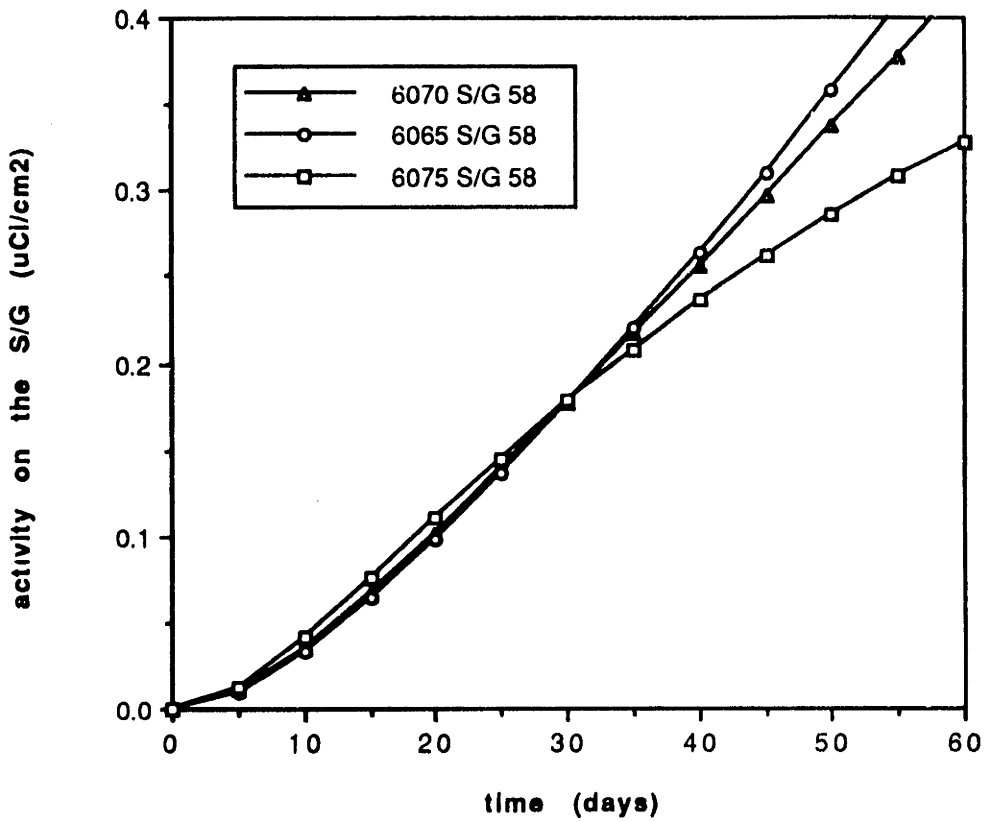

Figure 3.22 Co^{58} activity buildup in the S/G as a function of pH with initial core crud equivalent to 60 day pre-conditioning

- Key to legend

30 75/70 S/G 58 - ratio of Co^{58} activity in S/G of the PCCL at pH 7.5 operation to that at pH 7.0 operation after 30 day pre-conditioning at pH 7.0 at full coolant flow

60 65/70 S/G 58 - ratio of Co^{58} activity in S/G of the PCCL at pH 6.5 operation to that at pH 7.0 operation after 60 day pre-conditioning at pH 7.0 at full coolant flow

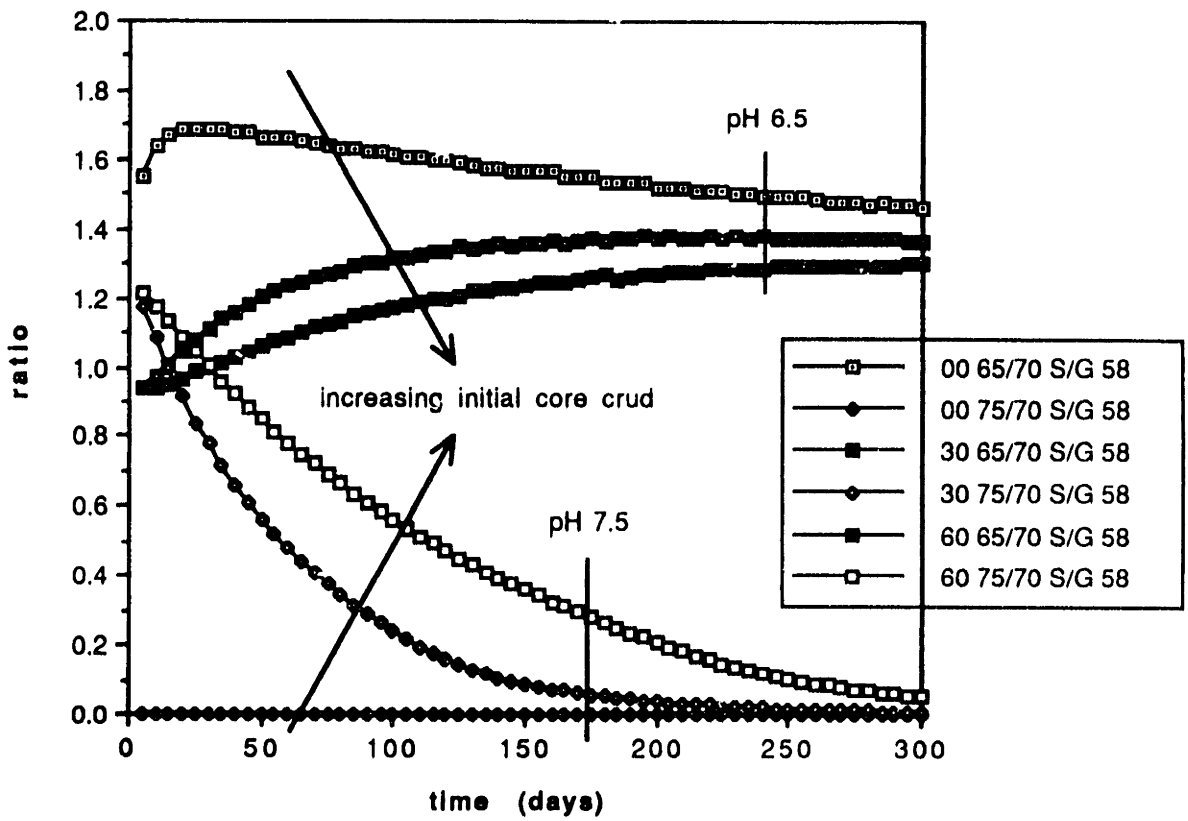

Figure 3.23 Activity ratios (indicated to reference case) of Co^{58} in the S/G as a function of initial core crud inventory and pH

At pH 7.5, the crud transport from the S/G to the core is zero, and the crud in the core is actually transported to the S/G due to the negative solubility difference between the S/G surface and the core surface. Then, as shown in Figure 3.24, if there is enough initial crud inventory in the core, the activity in the S/G at pH 7.5 increases initially and, some time later, begins to decrease since the initial crud in the core is leached out to the S/G and no crud is supplied to the core due to the negative solubility difference.

Next examined is the effect of the corrosion rate of S/G tubing on the activity trend in the S/G. Figure 3.25 shows that the corrosion rate of the S/G has little influence upon activities in the core and S/G. This is an obvious result predictable from Eq. (3.2), which indicates that the crud transport rate from the S/G to the core is independent of the corrosion rate of the S/G. Equations (3.3) and (3.4) suggests that activity transport from the core to the S/G can be slightly affected by the amount of the S/G crud inventory, which depends on the corrosion rate of the S/G. However, its effect is negligible, considering the much larger impact of other variables.

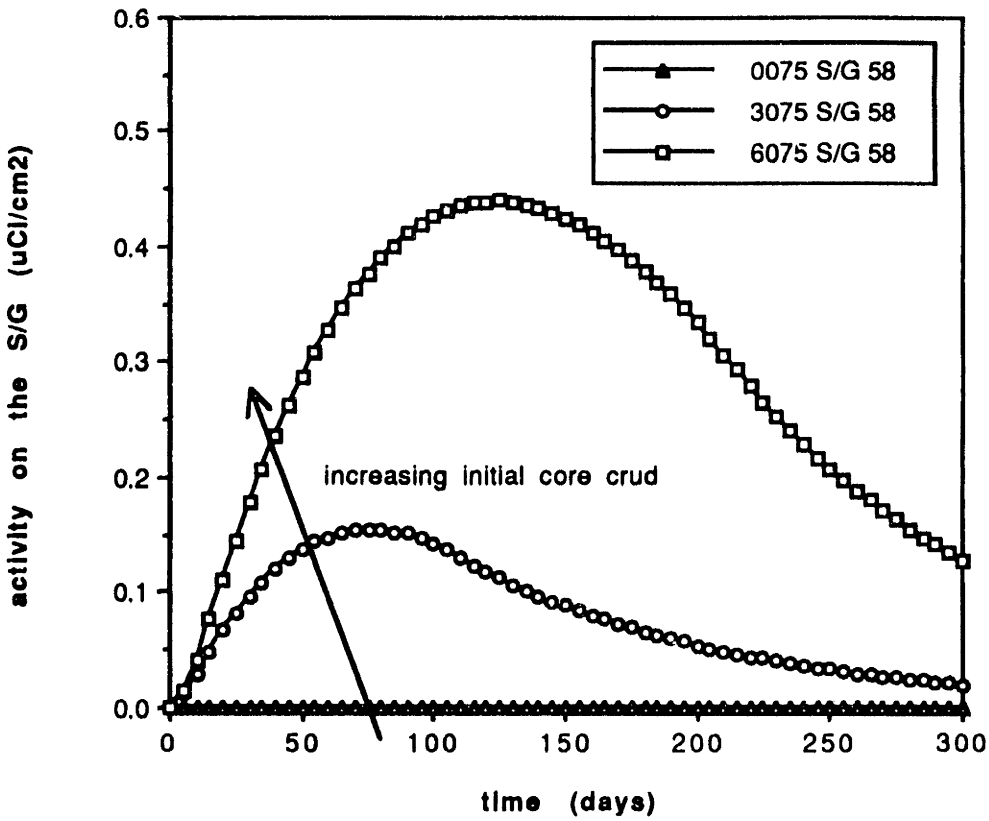

Figure 3.24 Co^{58} activity buildup in the S/G at pH 7.5 as a function of initial core crud inventory

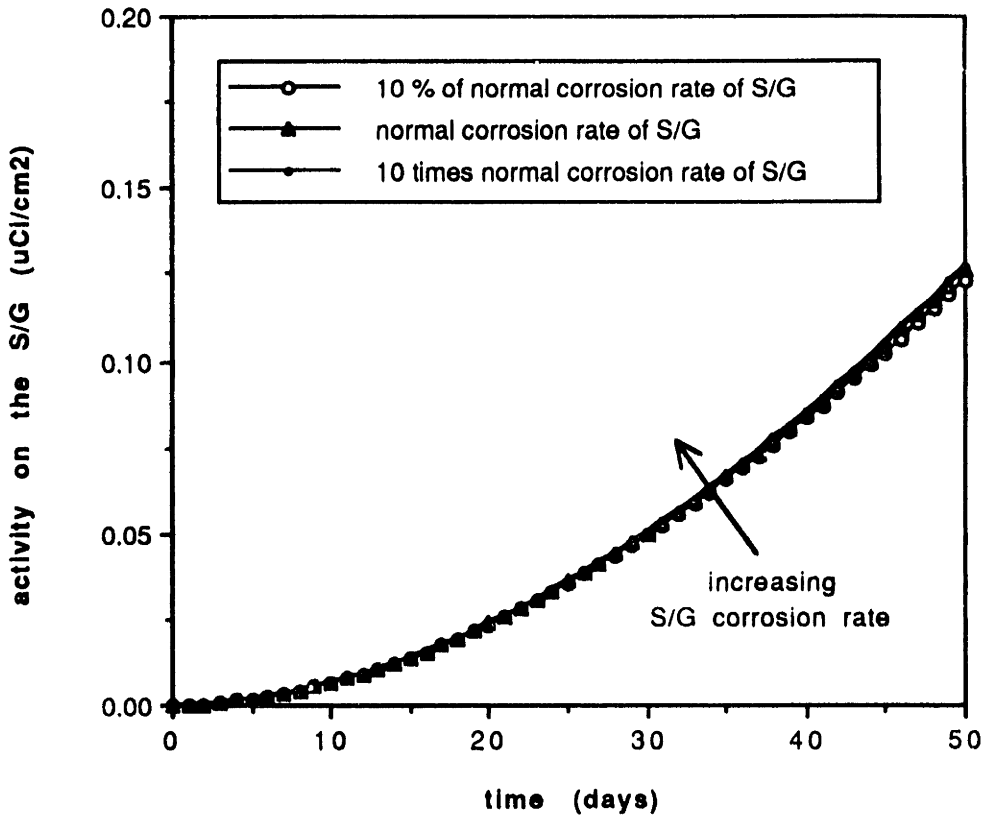

Figure 3.25 Co^{58} activity buildup in the S/G as a function of the S/G corrosion rate

3.4 Comparision of CRUDSIM/MIT Prediction with PCCL Results

3.4.1 Possible Tests of CRUDSIM/MIT Model

The measurements to be obtained before, during and after each PCCL run include :

(i) Initial crud inventory in core and S/G - the amount of Fe, Ni, Cr and Co.

(ii) Activities in the S/G - Co^{58}, Co^{60} and other elements

(iii) Activities in the core - Co^{58}, Co^{60} and other elements

(iv) Crud deposited in core - the amount of Fe, Ni, Cr and Co.

(v) Activities and crud on both deposition monitor filter in discharge line during a run and in the ion exchanger after a run. - Co^{58}, Co^{60} and other elements for activity, and Fe, Ni, Cr and Co for crud.

The data called for above can be used to evaluate and benchmark the CRUDSIM/MIT model as follows :

(i) The crud inventory in the core for different pH chemistries will test the solubility difference driven crud transport model.

(ii) Activities in the core and S/G for different pH chemistries will test the activity transport aspects of the solubility difference driven transport model.

(iii) Activity ratios of Co^{58} and Co^{60} in the core, S/G and particularly the deposition monitor will shed light on the relative importance of the direct recoil release of Co^{58} in the core.

(iv) Crud composition in the core will give the corrosion release and deposition tendency of each metalic element - Fe, Ni, Cr and Co. It will also test the validity of the assumption that Fe and Co are released and deposit in fixed ratio.

(v) The deposition monitor and ion exchanger will trace the activity changes in the coolant as a function of time and thereby help infer the relative magnitude of the characteristic time constants governing transport processes.

As noted earlier, only two reference runs (pH = 7) have been completed to date, and not all post mortem data is in hand. Nevertheless, some useful and interesting comparisons can be made (next section). A more comprehensive tabulation of data will be documented in a forthcoming Ph. D thesis by Sanchez [S-2]. Hence during the coming year, more comprehensive comparisons can be made.

3.4.2 PCCL Results and CRUDSIM/MIT Predictions

The first reference run of the PCCL at pH 7 has been completed and partial results are available to date. Run No. 1 was operated for 4 full reactor power days followed by 3 zero reactor power days each week (so called, 4 by 3 run) due to MIT reactor shut-down over weekends. It lasted a total of 42 days at temperature and loop heat flux and 22 full reactor power days. During the zero reactor power stages, the electric heater was still on so that the PCCL thermal conditions were maintained essentially the same (with only 16.7 °C decrease in average coolant temperature over weekends caused by the absence of irradiation heating). During run No. 1, the PCCL was shut down several times due to unexpected transients. Two loss of pumping power incidents occurred due to power line transients in the local utility grid and an overly sensitive pump power supply. Following these transients, crud bursts were observed. The activity in the deposition monitor filter, which directly indicates the coolant activity, increased to about 20 times its normal value. The cause of the crud burst is considered to be the sharp temperature drop of the coolant following system shut-down, and the resulting large increase of the solubility of the corrosion products, so that activity deposited on metal surfaces is dissolved into the coolant. Table 3.3 summarizes the measurements available to date on PCCL Run No. 1.

Using the available data from PCCL Run No. 1, crud and activity transport factors and the extent of recoil release of Co^{58} can be evaluated. Figure 3.26 shows the predicted Co^{58} activity buildup in the S/G as a function of the crud and activity transport factors (here assumed to be the same). The measured value of Co^{58} activity in the S/G in Run No. 1 is 0.013 ($\mu Ci/cm^2$), which implies a

Table 3.3 Preliminary Results of PCCL Run No. 1

		Run No. 1†
Duration (days)		42
Full power days		22
S/G (Inconel)	Co^{58}	13 ± 1.3 (nCi/cm^2) or 12.6 ± 1.3 (μCi)
	Co^{60}	2.4 ± 0.24 (nCi/cm^2) or 2.33 ± 0.23 (μCi)
	(Co^{58}/Co^{60})	5.4 ± 1.2
Core†† (Zircaloy)	Co^{58}	~78 (nCi/cm^2) or ~20.3 (μCi)
	Co^{60}	not available
	(Co^{58}/Co^{60})	not available
Filters†††	Co^{58}	0.48 ± 0.05 (μCi)
	Co^{60}	0.096 ± 0.01 (μCi)
	(Co^{58}/Co^{60})	5.0 ± 1.1
Ion Exchanger	Co^{58}	23 (μCi) ± 2.3
	Co^{60}	1.1 ± 0.11 (μCi)
	(Co^{58}/Co^{60})	21 ± 4.7

† Run No. 1 is a reference run at pH =7.0 at 300 °C, achieved by a combination of H_3BO_3 at 800 ppm B and LiOH at 1.84 ppm Li, and the activities in the pump, discharge line and out-of-core connecting lines are not available.

†† Note : based only on one upper segment of in-core Zircaloy and not corrected for nickel or cobalt content of base metal

††† Filters - combined results of sequential filters (sintered S. S. having pore size of 10 μm)

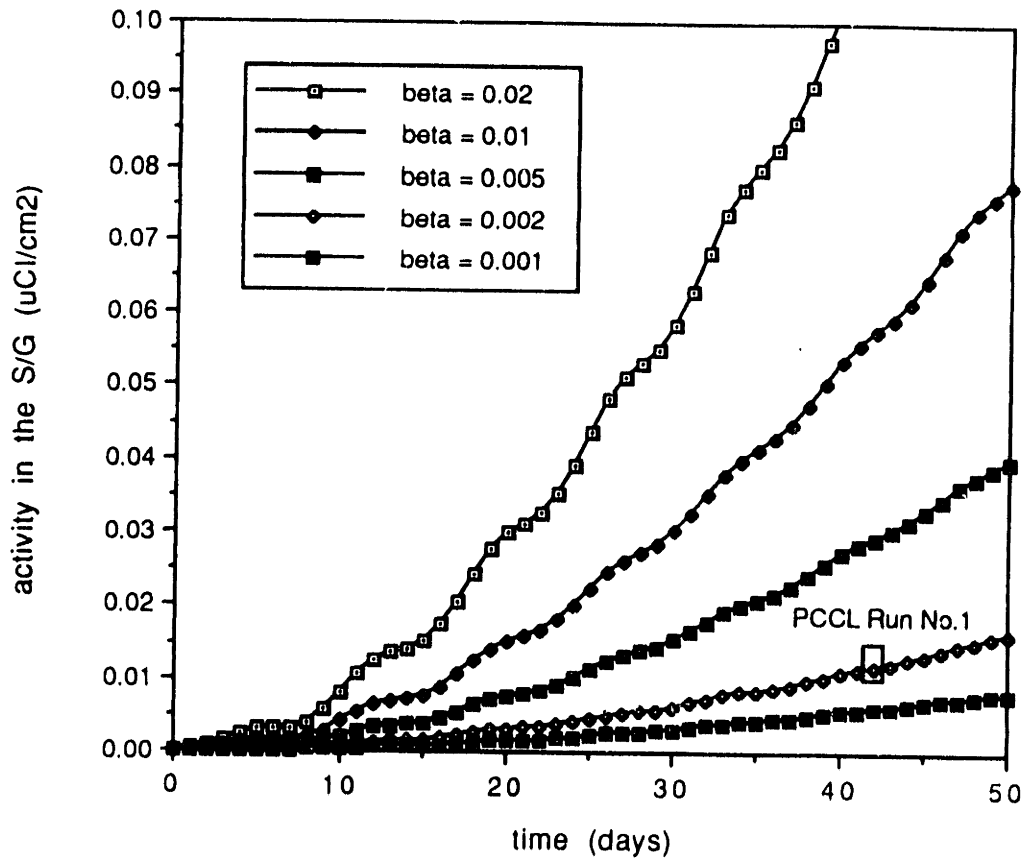

Figure 3.26 Co^{58} activity buildup in the S/G as a function of CRUDSIM transport factor (beta-c = beta-a)

value of $\beta < 0.005$. However, as discussed in Section 2.3.4, the activity transport factor (β_a) is not necessary equal to the crud transport factor (β_c). The relationship between the crud and activity transport factors can be derived by comparing the ratio of Co^{58} (or Co^{60}) in the core to that in the S/G, as shown in Figure 3.27 (the ratio of Co^{60} is very close to that of Co^{58}). Note that this analysis is based upon diffusion (not recoil) release for the Co^{58}. The experimental data indicates a value of 0.17 for this ratio for Co^{58}. From the preceding, a consistent set of crud and activity transport factors for the PCCL, evaluated by trial and error, are as follows.

$$\beta_c \approx 0.005$$
$$\beta_a \approx 0.001$$

Use of these values as (the only) empirical input, CRUDSIM/MIT successfully replicates the measured core and S/G activities for PCCL Run No. 1, as shown in Figure 3.28.

The significance of direct recoil release of Co^{58} can also be checked using PCCL Run No. 1 results, by comparing the ratio of (Co^{58}/Co^{60}) in the core to that in the S/G as a function of the probability of direct recoil release of Co^{58}, as discussed in Section 3.3.2.4. When direct recoil release of Co^{58} is predominant, the ratio of Co^{58} to Co^{60} in the S/G will be larger than the corresponding ratio in the core. Figure 3.29 shows the ratio of (Co^{58}/Co^{60}) in the S/G to that in the core as a function of the probability of direct recoil release of Co^{58}. Calculations in Section 2.5.2 shows that more than 40 % of the Co^{58} can be directly recoil released into the coolant, which indicates that the ratio of (Co^{58}/Co^{60}) in the S/G to that

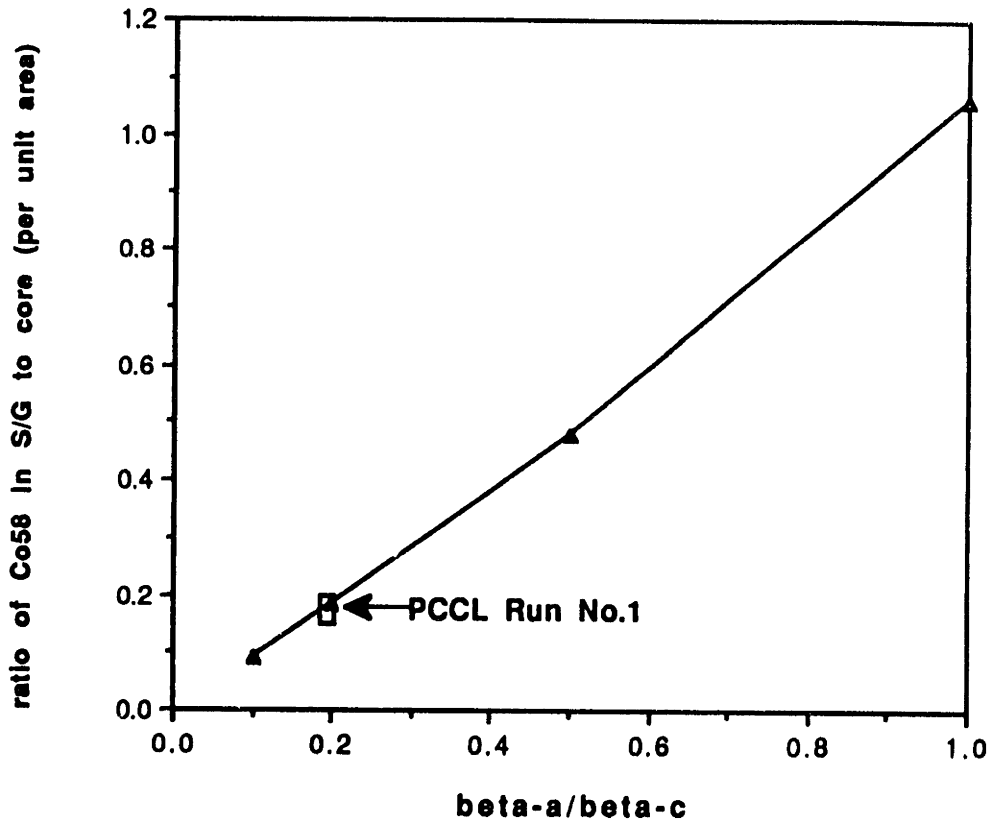

Figure 3.27 Ratio of Co^{58} activity in the S/G to that in the core (per unit area) versus ratio of the activity transport factor to the crud transport factor (beta-c = 0.005)

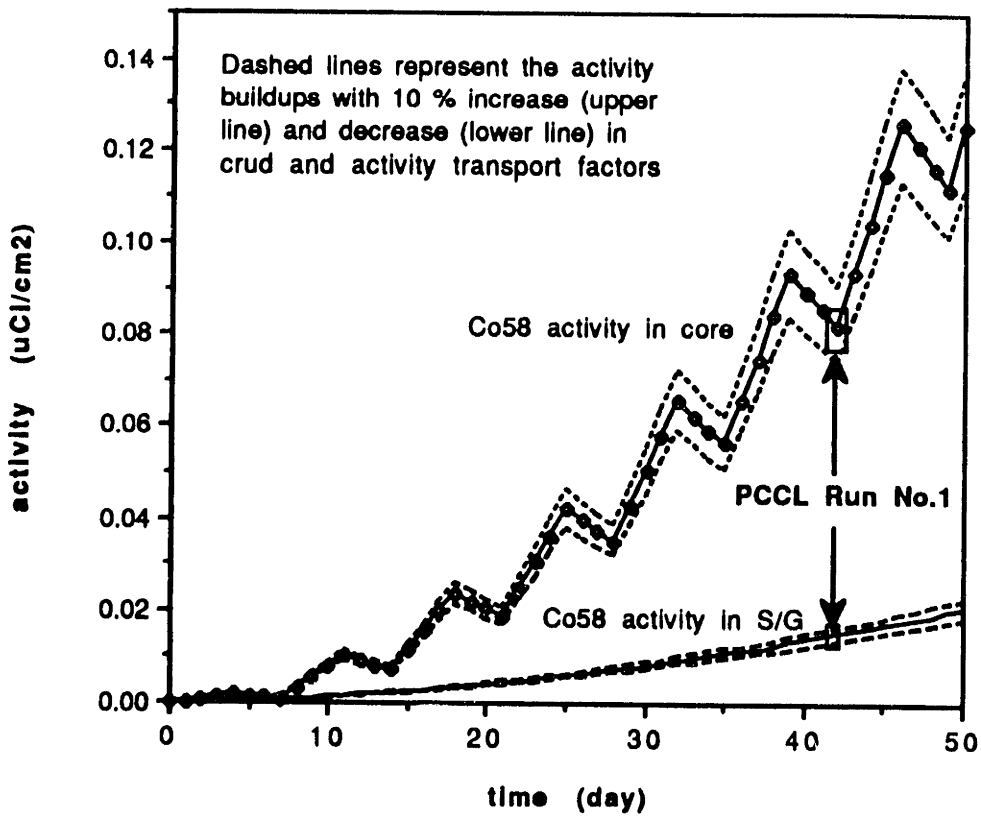

Figure 3.28 Comparison of computed and measured S/G Co^{58} activities for PCCL Run No. 1 (beta-c = 0.005, beta-a = 0.001)

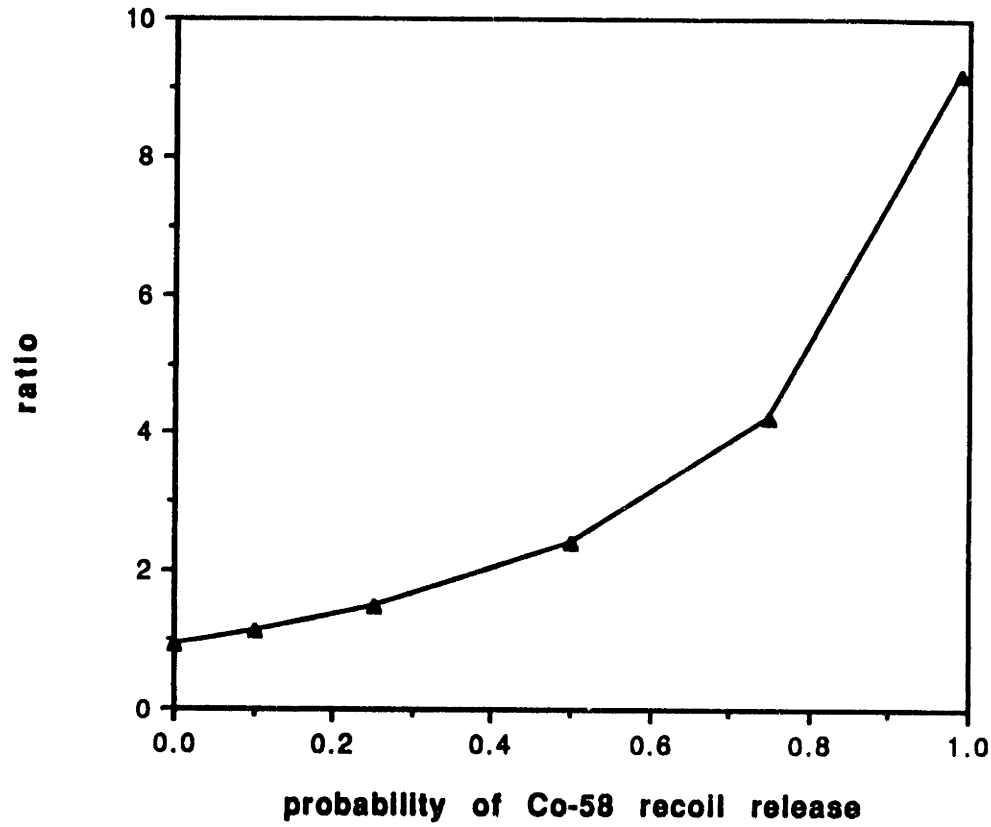

Figure 3.29 Ratio of (Co^{58}/Co^{60}) in the S/G to that in the core as a function of the probability of direct recoil release of Co^{58} at 42 days of PCCL Run No.1 (beta-c = 0.005 and beta-a = 0.001)

in the core should be more than 2.0 for PCCL Run No.1. However, since Co^{60} activity in the core for PCCL Run No.1 is not available, the ratio can not be estimated at present.

As mentioned before, only S/G and core activities of PCCL Run No. 1 are available at present. As more data are obtained, we can further test the CRUDSIM/MIT model, as discussed in Section 3.4.1, and deduce the crud and activity transport factors which can not be estimated analytically now, since the crystallization and dissolution coefficients are not available.

3.5 Summary and Conclusions

In Section 3.2, the MIT PCCL was compared with a typical PWR in terms of its operating conditions and mass transfer characteristics. It shows that the MIT PCCL should be a good simulation of a PWR for crud and activity transport studies.

In Section 3.3, the CRUDSIM/MIT equations were analytically solved for both short time and asymptotic long term behaviors, and the dependence of the activities in the core and S/G upon time, coolant pH and initial crud inventory was identified. It was shown that short runs should be a valid prediction of long term behavior. Sensitivity analyses of the important parameters were carried out using CRUDSIM/MIT for the MIT PCCL, and the critical parameters for crud and activity transport were identified : primarily the transport parameter, β and the initial core crud inventory.

In Section 3.4, best-estimate results for the MIT PCCL predicted by CRUDSIM/MIT were compared with measurements, and the transport parameter, β was adjusted to match the measured results. The comparison shows that the model employed in CRUDSIM/MIT is capable of describing the MIT PCCL satisfactorily, and, by inference, the primary system of a PWR power plant.

Chapter 4 Summary, Conclusions and Recommendations

4.1 Summary and Conclusions

4.4.1 Introduction

Radioactivity on out-of-core surfaces in PWR primary coolant systems is a major source of radiation exposure to plant maintenance personnel. Its buildup is caused by the movement of corrosion products throughout the PWR primary circuit. The efforts to control the transport of the corrosion products (crud) and activity can be divided into two categories. : coolant chemistry and materials. The latter includes the selection of materials free of detrimental elements such as Co^{59} which captures neutrons to form Co^{60} (the main source of long lasting radioactivity), the development of more corrosion resistant materials under PWR operating conditions, and the pre-treatment of materials, such as electropolishing and pre-oxidation to form protective passive films. The former strategy, which is of primary interest here, involves the control of coolant pH and redox potential by the addition of chemicals such as lithium hydroxide and hydrogen.

Modeling and numerical estimation of crud and activity transport is essential to any systematic approach to the control of deposited radioactivity. Several computer codes have been developed to calculate the crud and activity transport in a PWR primary circuit such as CORA [K-1], PACTOLE [B-5] and CRUDSIM [B-9]. However, considerable uncertainty still exists in the understanding of crud and activity transport mechanisms, even though these

codes have been continuously updated and sometimes drastically changed, as more data accumulates from actual plant operation and experimental loops. Because of its conceptual simplicity and successful application to the explanation of plant activity trends, we have concentrated in the work reported here on the CRUDSIM model, focusing on a systematic derivation of its constituent equations from basic principles and reconciliation of the resulting formulation with the apparently different structure of the more conventional modeling used in PACTOLE and CORA.

In addition to the intrinsic interest in the phenomenon of corrosion product and activity transport, the installation of in-pile loops in the MIT research reactor to carry out definitive experiments on the effect of coolant chemistry provided a compelling practical motivation : the need to plan and interpret these experiments.

4.1.2 Modeling Aspects

Table 4.1 lists a variety of mechanisms for crud and activity transport. The following aspects characterize the current consensus of the experts in this field, as interpreted by the present author :

(1) Coolant chemistry has a strong effect on the crud and activity transport, and there may exist an optimum coolant chemistry condition - pH, in particular, through its effect on transition metal solubility - which gives minimum activity buildup on out-of-core surfaces.

(2) The soluble species of the corrosion products are the dominant form in the crud and activity transport. (a basic assumption of CRUDSIM code)

(3) The particulate form of crud in the coolant can also contribute to crud and activity transport. However, the extent of its existence in the coolant and its contribution to net crud and activity transport are not fully confirmed due in part to considerable technical difficulties in its measurement in hot primary coolant.

(4) Among the many possible mechanisms in Table 4.1, several are probably minor net contributors to crud and activity transport, in particular :
- erosion of surface oxide films under PWR operating flow conditions
- some irradiation effects such as magnetic/electrostatic field effects and direct photoreduction
- sedimentation of particles in low velocity regions
- electrophoresis

The CRUDSIM code is formulated to model the effect of coolant chemistry, especially pH, on crud and activity transport. However, key aspects are empirical in nature. Hence, the principal initial objective of the present work was to start from basic phenomena for crud and activity transport and to derive a transport model which can be reconciled, term by term with the original CRUDSIM equations.

The PWR primary circuit can be divided into three principal sections. : core, coolant and S/G. The driving force for crud transport in the PWR primary coolant comes from coolant temperature changes and the resulting changes in corrosion product solubility. As the coolant temperature changes around the

Table 4.1 Potential Corrosion Product Transport Mechanisms in a PWR Primary Circuit

Core and S/G surfaces	Boundary Layer in Core and S/G	Bulk Coolant
Dissolution of metal ions† into coolant Erosion of surface metal oxide to release particulates†† Deposition of ions and particulates on surfaces by crystal growth, adsorption and ion exchange And in core only : Recoil release of ionic nuclei Removal by refuelling Other radiation effects ; .Magnetic/electrostatic field effects .Direct photoreduction	Conventional mass transfer of ions and particulates Thermal diffusion ; .Soret effect of ions .Thermophoresis of particulates Electrophoresis	Convection of ions and particulates Precipitation and dissolution of particulates Removal by purification in CVCS Sedimentation in low velocity regions

† ions - all types of soluble species in the coolant such as divalent ions and hydrated oxide ions.

†† particulates - charged or neutral particles, i.e., colloids or nickel ferrite crystals

PWR primary circuit, the saturation status of the corrosion products in the coolant also changes, as shown in Figure 4.1. In the core, where the coolant temperature increases, the soluble species exist in a super-saturated state, so that there is a driving force for the soluble species to deposit on the core surface, or precipitate as particulates. On the other hand, in the S/G, as the coolant temperature decreases, the soluble species become under-saturated, so that there is a driving force for the corrosion products on the S/G surfaces and the particulates in the coolant to dissolve into the coolant to restore a saturation concentration of corrosion products in the coolant. Figure 4.2 shows in schematic fashion the sequence of crud movement in a PWR primary circuit.

Crud transport as soluble species can be modelled as shown in Figure 4.3. In the PWR primary circuit, the path for crud transport from the S/G to the core is

dissolution at the S/G tubing surface
mass transfer across the boundary layer in the S/G
mass transfer across the boundary layer in the core
crystallization on the core fuel surface

Recirculation of the highly turbulent coolant through the PWR primary circuit transfers the corrosion products from the S/G to the core without any significant intervening resistance. On the other hand, the activity produced in the core is transported from the core to the S/G, driven by its concentration gradients, and its path is

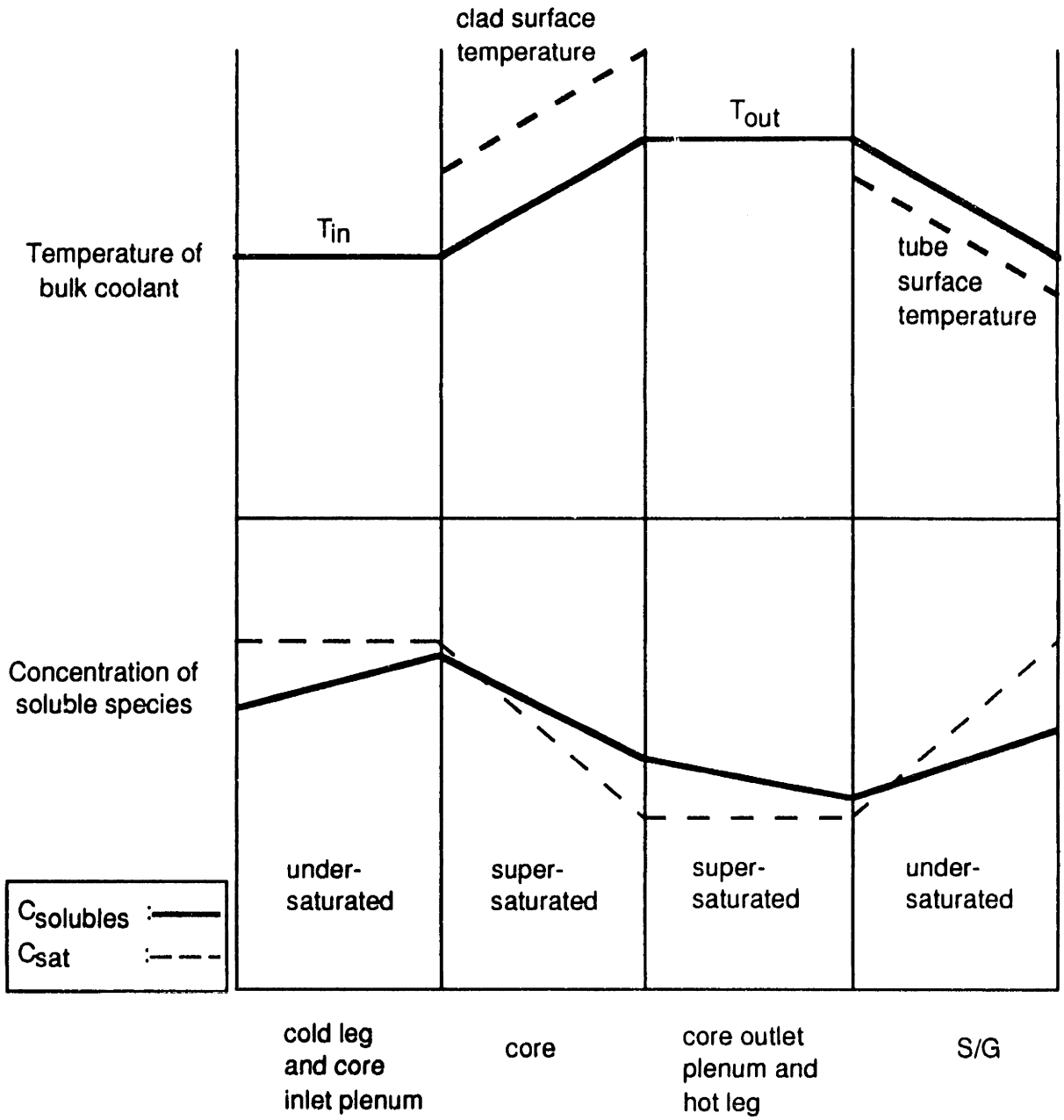

Figure 4.1 Profile of coolant temperature and soluble species concentration in PWR primary circuit.

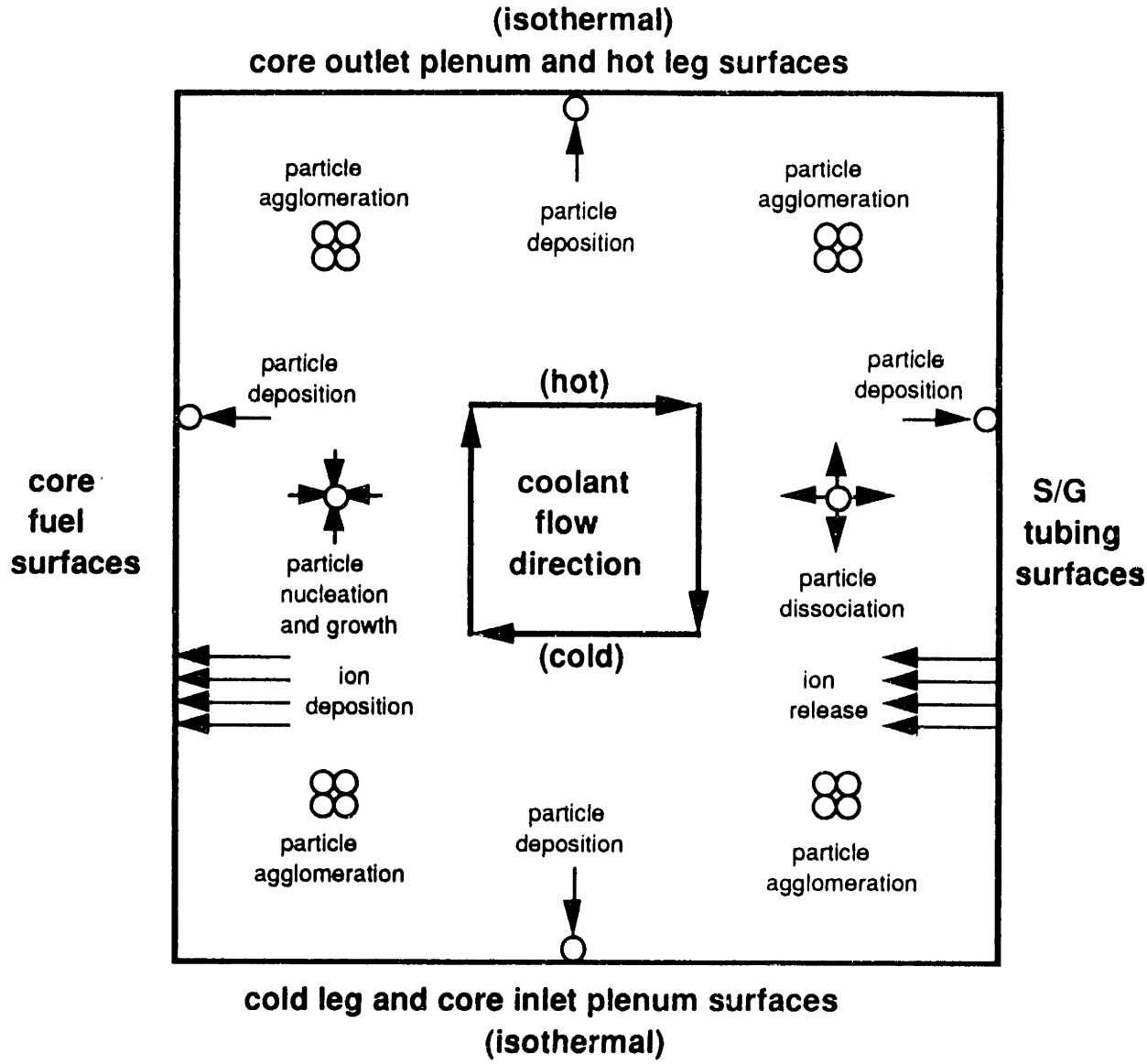

Figure 4.2 Movement of Corrosion Products in a PWR Primary Circuit

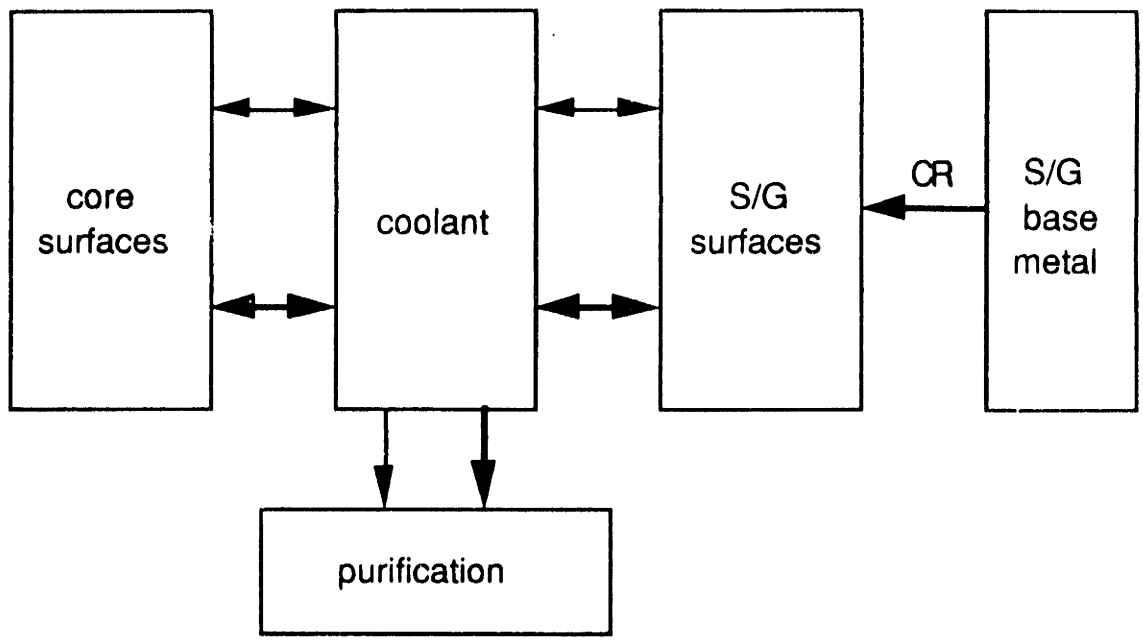

Figure 4.3 Diagram of a PWR Primary Circuit used in Modeling

dissolution at the core fuel surface

mass transfer across the boundary layer in the core

mass transfer across the boundary layer in the S/G

crystallization on the S/G surface

Since the bulk primary coolant is a resistance-free path for crud and activity transport, it can be removed from the mathematical formulation, assuming that the crud and activity inventories in the coolant quickly reach quasi- steady-state values. The balance equations of crud and activity transport as soluble species can be shown to be, after considerable preliminaries (required to show how extended surfaces can be collapsed to single nodes in a consistent manner, with all lumped variables properly averaged) :

$$\frac{dI_1}{dt} = \frac{k_1 k_3}{k_1 + k_3} (S_3 - S_1) \tag{4.1}$$

$$\frac{dI_3}{dt} = CR - \frac{k_1 k_3}{k_1 + k_3} (S_3 - S_1) \tag{4.2}$$

$$\frac{dA_1}{dt} = - \lambda A_1 + \alpha P I_1 - \frac{k_1^a k_3^a}{k_1^a + k_3^a} \left(\frac{A_1}{I_1} S_1 - \frac{A_3}{I_3} S_3 \right) \tag{4.3}$$

$$\frac{dA_3}{dt} = - \lambda A_3 + \frac{k_1^a k_3^a}{k_1^a + k_3^a} \left(\frac{A_1}{I_1} S_1 - \frac{A_3}{I_3} S_3 \right) \tag{4.4}$$

where,

I_1 = crud inventory in the core (kg)

I_3 = crud inventory in the S/G (kg)

A_1 = activity inventory in the core (Ci)

A_3 = activity inventory in the S/G (Ci)

S_1 = average solubility of crud at the core surface (kg/m^3)

S_3 = average solubility of crud at the S/G surface (kg/m^3)

CR = corrosion rate of S/G tubing (kg)

k_1 = mass transfer factor of crud in the core (m^3/sec)

k_3 = mass transfer factor of crud in the S/G (m^3/sec)

k_1^a = mass transfer factor of activity in the core (m^3/sec)

k_3^a = mass transfer factor of activity in the S/G (m^3/sec)

λ = decay constant (sec^{-1})

α = neutron activation factor (Ci/kg-Fe. % power. sec)

P = percent of full power (% power)

The above equations are quite similar to the following CRUDSIM equations.

$$\frac{dI_h}{dt} = \beta F (S_c - S_h) \qquad (4.5)$$

$$\frac{dI_c}{dt} = R - \beta F (S_c - S_h) \qquad (4.6)$$

$$\frac{dA_h}{dt} = - \lambda A_h - \beta F (\frac{A_h}{I_h} S_h - \frac{A_c}{I_c} S_c) + \alpha P I_h \qquad (4.7)$$

$$\frac{dA_c}{dt} = - \lambda A_c + \beta F (\frac{A_h}{I_h} S_h - \frac{A_c}{I_c} S_c) \qquad (4.8)$$

where,

I_h = iron inventory in the hot tank (kg-Fe)

I_c = iron inventory in the cold tank (kg-Fe)

A_h = activity inventory in the hot tank, such as Co^{58} and Co^{60} (Ci)

A_c = activity inventory in the cold tank, such as Co^{58} and Co^{60} (Ci)

S_h = iron solubility in the hot tank (kg-Fe/kg-H_2O)

S_c = iron solubility in the cold tank (kg-Fe/kg-H_2O)

R = iron input into the cold tank (kg-Fe/sec)

λ = decay constant (sec^{-1})

α = neutron activation factor (Ci/kg-Fe. % power. sec)

P = percent of full power (% power)

β = empirical transport factor for the crud and activity

F = coolant flow rate (kg-H_2O/sec)

Since the most important corrosion product for which reliable solubility data is available is iron, only iron is considered in the crud transport model of CRUDSIM. Nickel and cobalt are postulated to follow the iron in fixed proportions.

Thus, the first major conclusion of the present work is that there is a one-to-one correspondence of derived and original variables as follows :

$I_h = I_1$

$I_c = I_3$

$A_h = A_1$

$A_c = A_3$

$$S_h = \frac{S_1}{\rho_{H_2O}}$$

$$S_c = \frac{S_3}{\rho_{H_2O}}$$

The density of coolant appears in these latter relations because S_h in CRUDSIM is in [kg-Fe/kg-H_2O] and S_1 is in [kg-Fe/m^3] and, in addition, we find that

$$\beta_c = \left(\frac{k_1\, k_3}{k_1 + k_3}\right)\frac{\rho_{H_2O}}{F}$$: defined as the crud transport factor

$$\beta_a = \left(\frac{k_1^a\, k_3^a}{k_1^a + k_3^a}\right)\frac{\rho_{H_2O}}{F}$$: defined as the activity transport factor

The differences between the CRUDSIM model and the above derived model are now clarified, and can be summarized as follows :

- In the present formulation, the crud transport from the S/G to the core is proportional to the solubility difference of corrosion products between the S/G and core surfaces, (S_3 - S_1). In the CRUDSIM model, the crud transport is proportional to the solubility difference between the cold and hot "tanks", (S_c - S_h), at temperatures which are those of the core inlet and outlet, respectively. However, these driving forces can be shown to be inextricably linked by basic heat and mass transfer considerations.

- The crud and activity transport factors which are considered to be equal in CRUDSIM (and input as an empirical transport factor) are not necessarily equal, since the mass flow sequences differ . Some PWR plant data indicates that the activity transport factor may be smaller than the crud transport factor.

Establishment of the above correspondence opens the way to analytic determination of parameters which are empirically specified in CRUDSIM. It also shows that CRUDSIM may be considered to be a compatible alternative formulation of the models used in CORA and PACTOLE.

However, since the kinetics of dissolution and crystallization are not yet fully understood, these coefficients can not be estimated from basic principles, and it is not possible at present to analytically estimate crud and activity transport factors. Calculations show that when only fluid boundary layer mass transfer resistance is considered, neglecting the dissolution and crystallization steps, the crud and activity transport factors are overestimated by a factor of about 45. This result strongly indicates that mass transfer across the boundary layers is not the only, or controlling step in crud and activity transport, and that the crystallization and dissolution steps are not negligible. At present, one can only infer the required magnitude of these coefficients from experimental results, such as those which will become available from operation of the PCCL at MIT.

Other mechanisms for crud and activity transport were also studied and the results can be summarized as follows :

- The effect of thermal diffusion on the mass transfer across the core and S/G boundary layer, where large temperature gradients exist due to the high heat flux at the core and S/G surfaces, may not be significant, since the computed Soret coefficient of the soluble species becomes insignificant at the high temperature of the PWR primary coolant (~300° C).
- The probability of direct recoil release of Co^{58} can be theoretically calculated using an experimentally measured recoil range for Co^{58}. The probability approaches, at maximum, 50 % for initial operation at zero crud thickness and decreases as the crud thickness increases.
- Purification by the CVCS system has a negligible effect on the net crud and activity transport due to the small flow rates involved.
- Simplified theoretical calculations show that particulates may precipitate in the bulk coolant and agglomerate to form very small particles (less than 0.01 μm radius), and then deposit on the core and S/G surfaces before growing into larger particles, due to the much stronger tendency of particulates to deposit on the surfaces than to grow.
- Particulate precipitation from the super-saturated soluble species in the coolant does not change the solubility difference dependence of the crud transport from the S/G to the core. It only decreases the amount of net crud transport from the S/G to the core due to re-deposition of the particulates on the S/G by, at maximum, the fractional core surface area in a PWR primary circuit, ie, approximately 1/4.

The balance equations derived above, Eqs. (4.1) through (4.4), can be solved analytically for both short time periods and the asymptotic long term. This exercise reveals that :

- S/G activity builds up as a second order function of time for the initial short time period.
- There is a well defined relationship between the short time and asymptotic long term activities. Therefore, short run activity measurements using loops such as the PCCL can be used to predict the long term effect of differences in coolant chemistry.
- The asymptotic activity in the S/G depends upon the asymptotic core crud inventory, which is proportional to the solubility difference between the S/G and core surfaces. The saturation time for the activity of a given radionuclide depends upon its half life and the refuelling interval for core fuel assemblies.

4.1.3 Parametric Studies

The model derived as described above was transformed into a computer program, called CRUDSIM/MIT. A sensitivity analysis of the model's parameters using the code shows that

- The crud and activity transport factors, β_c and β_a, control the relative magitude of the crud and activity transport.
- Crud transport from the S/G to the core is proportional to the solubility difference of the corrosion products between fluid at the S/G and core surfaces. The solubility of the corrosion products depends upon the coolant pH, temperature and dissolved hydrogen concentration. Coolant

chemistry conditions such as high pH, high temperature and small hydrogen concentrations give smaller solubility differences between the S/G and core surfaces, and hence less crud transport from the S/G to the core, and less activity buildup in the S/G.

- The corrosion rate of the S/G tubing, and initial crud inventory in the S/G has little effect on the crud and activity transport in this model. On the other hand, the initial crud inventory in the core has a strong effect on activity transport, a point which will be discussed further later.

Even though a smaller hydrogen pressure gives a smaller solubility difference, a certain minimum hydrogen concentration is necessary to suppress accumulation of free oxygen produced by radiolysis of water. Therefore, there may exist an optimum hydrogen pressure, small enough to reduce crud solubility and large enough to scavenge free oxygen. CANDU reactors, for example, are operated with hydrogen concentration in their primary coolant a factor of three lower than in typical PWRs.

4.1.4 Relation to PCCL Experiments

The MIT PWR Coolant Chemistry Loop (PCCL) is operated in the MIT reactor to simulate the PWR primary circuit in terms of coolant temperature and flow conditions, heat and mass transfer characteristics, heat flux, neutron flux and surface area ratios of materials of construction. Its schematic is shown in Figure 4.4, and the comparison of its operating characteristics with a

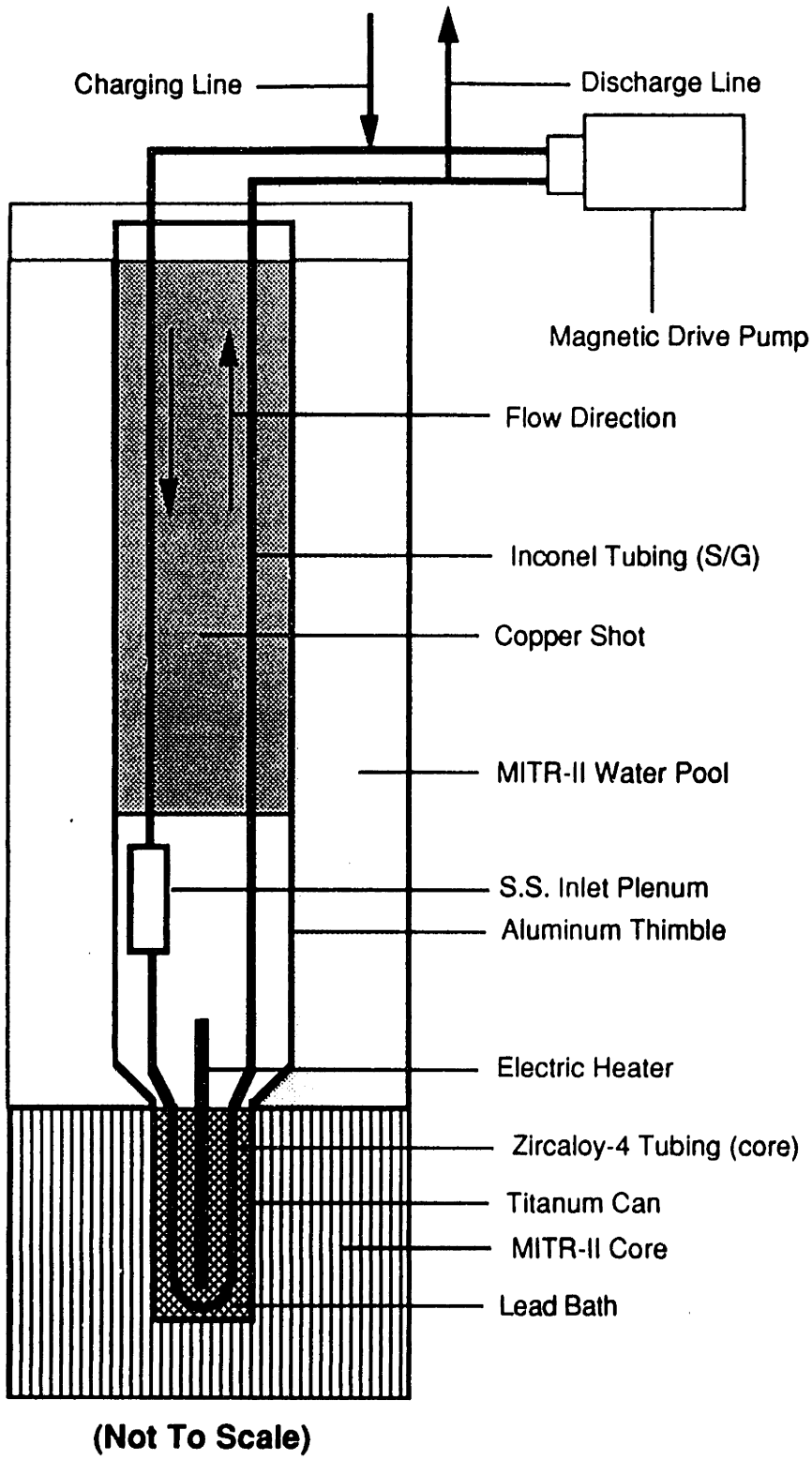

Figure 4.4 Schematic of MIT PWR Coolant Chemistry Loop (PCCL)

representative PWR is shown in Table 4.2. So far, only data on the first reference run ($pH_{300\ °C}$ = 7) is available for comparison with CRUDSIM/MIT predictions.

The measured value of S/G Co^{58} activity at 42 days is 0.013 ($\mu Ci/cm^2$), which implies a value of $\beta < 0.005$, based upon the preceding sensitivity analysis (here it is assumed that the crud and activity transport factors are equal). However, as previously noted, the activity transport factor (β_a) is not necessary equal to the crud transport factor (β_c). The relationship between the crud and activity transport factors can be derived by comparing the ratio of Co^{58} in the core to that in the S/G, as shown in Figure 4.5. The experimental data indicates a value of ~ 0.17 for this ratio. From the preceding, a consistent set of crud and activity transport factors for the PCCL, evaluated by trial and error, are as follows.

$$\beta_c \approx 0.005$$
$$\beta_a \approx 0.001$$

Use of these values as (the only) empirical input, CRUDSIM/MIT successfully replicates the measured core and S/G activities for PCCL Run No. 1, as shown in Figure 4.6. The MIT PCCL is also scheduled to operate at different pH values (6.5, 7.0 and 7.5 at 300 °C) to find an optimum pH, which gives minimum activity buildup in the S/G. CRUDSIM/MIT predicts, as shown in Figure 4.7, that :

- Co^{58} activity buildup in the S/G at pH 6.5 is about 1.7 times higher (at 30 days) than at pH 7.0.
- At pH 7.5 at 300 °C, the activity buildup in the S/G can be significantly reduced. Theoretically, zero activity is deposited in the S/G, since at pH

Table 4.2 Comparison of Operating Characteristics of MIT PCCL with a representative PWR

	CORE		S/G	
	PWR	PCCL	PWR	PCCL
Coolant Inlet Temperature (^oC)	285	273.9	285	273.9
Coolant Outlet Temperature (^oC)	320	315.6	320	315.6
Coolant Flow Rate (kg-H_2O/sec)	$1.70x10^4$	0.0684	$1.70x10^4$	0.0684
Hydraulic Diameter (cm)	1.19	0.652	2.1	0.6159
Flow Area (m^2)	4.75	$3.34x10^{-5}$	4.67	$2.98x10^{-5}$
Heat Transfer Area (m^2)	5550	0.026	19138	0.097
Thermal Power (Mwth)	3411	$15.04x10^{-3}$	3411	$15.04x^{-3}$
Avg. Heat Flux (kw/m^2)	614.6	578.5	178.23	155.1
Temperature Difference in Boundary Layer, $\Delta\overline{T}_{B-L}$ (^oC)	17.6	23.23	- 5.68	- 5.57
Flow Velocity (m/sec)	5.1	2.83	5.2	3.18
Re	$4.7x10^5$	$1.4x10^5$	$8.5x10^5$	$1.5x10^5$
Sc	11.9	11.9	11.9	11.9
Sh	2846	1028	4707	1080
Mass transfer coefficient (cm/sec)	0.26	0.17	0.24	0.19
beta (MT)†	0.45	0.38	0.45	0.38

† beta (MT) - the theoretical value of the CRUDSIM transport factor, β, which is calculated considering only mass transfer, neglecting resistance in the dissolution and crystallization steps.

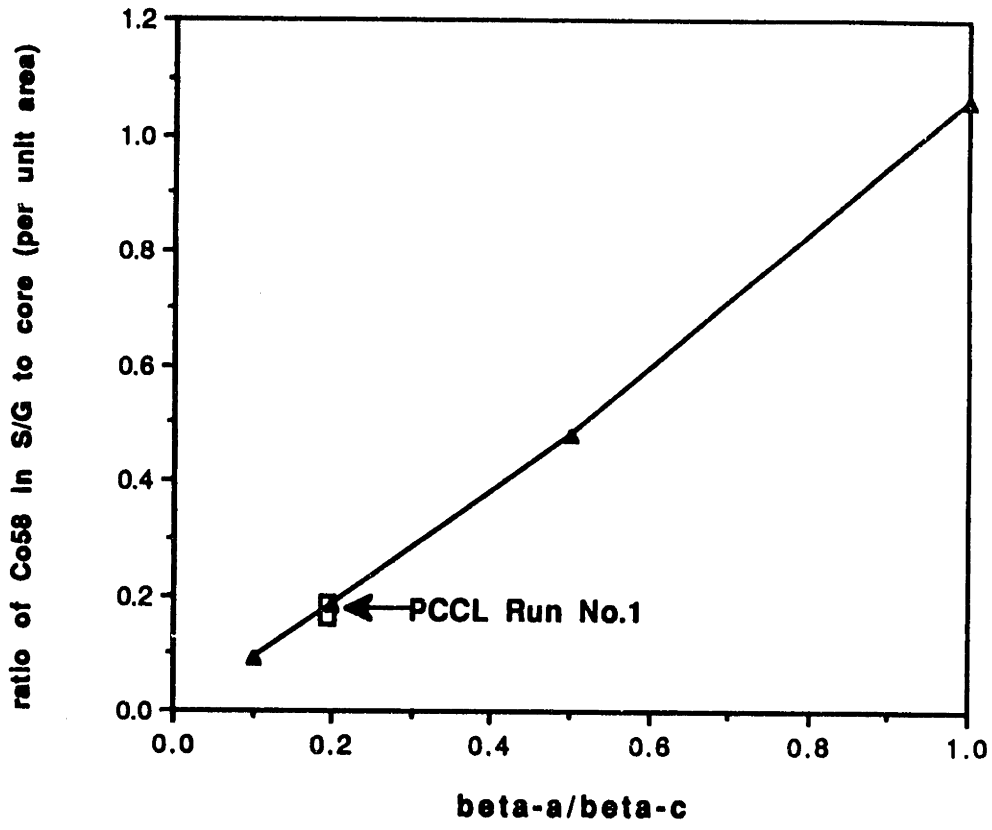

Figure 4.5 Ratio of Co^{58} activity in the S/G to that in the core (per unit area) versus ratio of the activity transport factor to the crud transport factor (beta-c = 0.005)

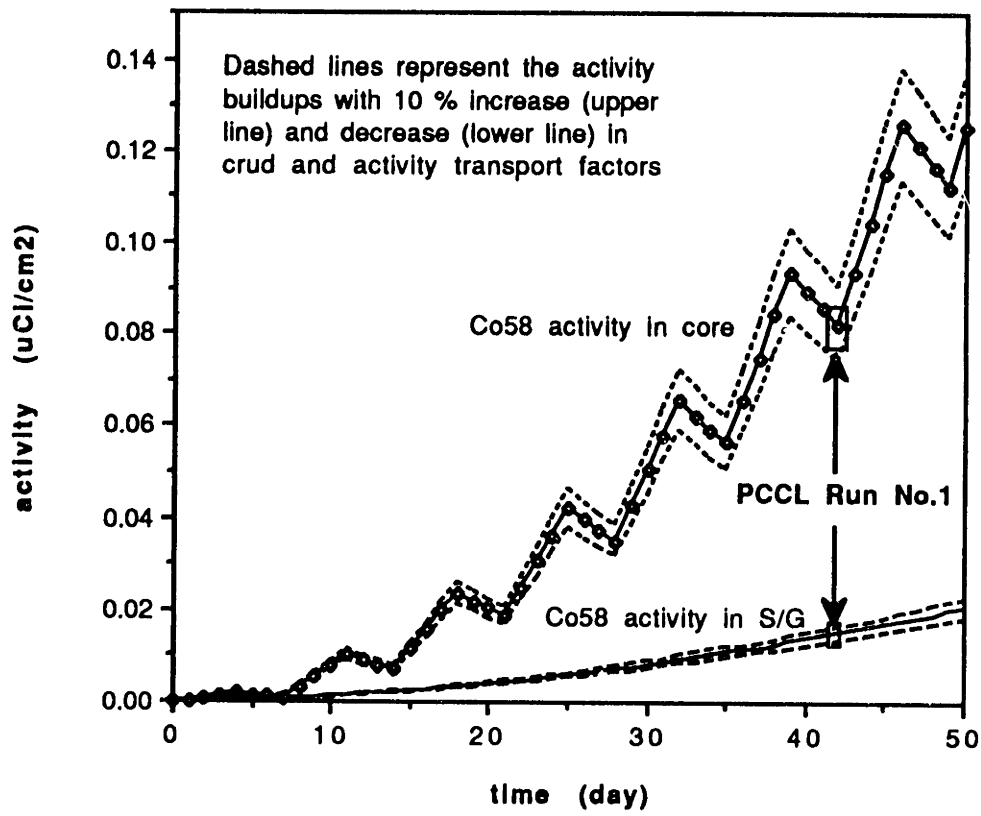

Figure 4.6 Comparison of computed and measured S/G Co^{58} activities for PCCL Run No. 1 (beta-c = 0.005, beta-a = 0.001)

- Key to legend

30 75/70 S/G 58 - ratio of Co^{58} activity in S/G of the PCCL at pH 7.5 operation to that at pH 7.0 operation, after 30 day pre-conditioning at pH 7.0 and full coolant flow rate

60 65/70 S/G 58 - ratio of Co^{58} activity in S/G of the PCCL at pH 6.5 operation to that at pH 7.0 operation, after 60 day pre-conditioning at pH 7.0 and full coolant flow rate

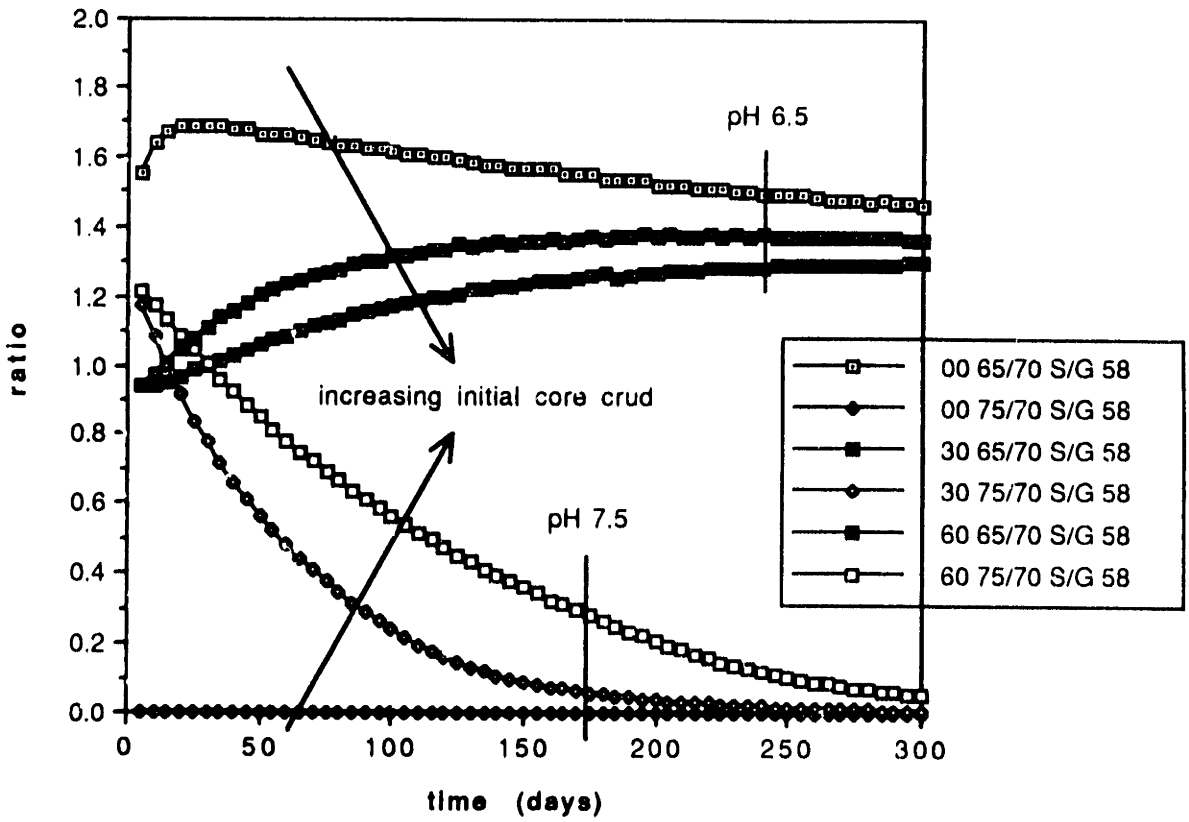

Figure 4.7 Activity ratios (indicated to reference case) of Co^{58} in the S/G as a function of initial core crud inventory and pH

7.5, no crud is transported from the S/G to the core due to the negative solubility difference between fluid at the S/G and core surfaces, that is, (S_3 - S_1) is negative.

- The relatively short 30 day run results can be used to predict asymptotic long term behavior, since the activity ratios for different pHs change little beyond 30 days for PCCL runs which start with zero initial crud inventory in the core.

Here, it should be emphasized that if there exists initially substantial crud on core fuel surfaces, the activity in the S/G actually increases rapidly at pH values above 7.5 for an initial period ; however, eventually the S/G activity decreases since no more crud is supplied to the core from the S/G at high pH due to the negative solubility difference between the S/G and the core surfaces. Figure 4.7 shows the trend of Co^{58} S/G activity (as a ratio to a $pH_{300\,°C}$ = 7 reference run) for different pH values as a function of initial core crud inventory. This observation shows the importance of starting short PCCL runs with low (almost zero) initial crud inventories on the in-core Zircaloy tubing if the results of a 30 day short run are to be considered indicative of asymptotic long term behavior. Based upon the above finding, the Zircaloy tubing for the PCCL was excluded from the initial 30 day prefilming run and the subsequent 30 day preconditioning was carried out at low (almost zero) flow to minimize crud transport from the Inconel to the Zircaloy.

The importance of direct recoil release of Co^{58} can be checked by comparing the ratio of (Co^{58}/Co^{60}) in the S/G to that in the core as a function of the probability of direct recoil release of Co^{58}. When direct recoil release of Co^{58}

is predominant, the ratio of Co^{58} to Co^{60} in the S/G will be larger than the corresponding ratio in the core. Calculation shows that more than 40 % of Co^{58} may be directly recoil released into the coolant for PCCL Run No.1. However, since Co^{60} activity in the core for PCCL Run No.1 is not at present available, this estimate can not be compared with PCCL Run No.1 results.

In conclusion, the more significant conclusions are,

- The above derived model supports the empirical CRUDSIM model.
- The results of 30 day PCCL runs starting with zero initial crud inventory in the core can be used as a measure of asymptotic long term behavior.
- Mass transfer across boundary layers in the S/G and core is not the sole controlling step in crud and activity transport, since one over-estimates crud and activity transport factors by about a factor of 45 , if the added resistances of the dissolution and crystallization steps are neglected.
- Crud and activity transport factors can not be calculated analytically, since quantitative models for prediction of the dissolution and crystallization coefficients are not presently available. However, the results of loop tests, such as those planned for the PCCL can be used to estimate the crud and activity transport factors.
- Operation of PWR primary coolant at high pH (>7.5) which gives a negative solubility difference between the S/G and the core is desirable to minimize the S/G activity buildup.

4.2 Recommendations for Future Work

In the course of the present work, a number of areas deserving further attention have been identified, as follows :

- Quantification of the resistance of the dissolution and crystallization steps for soluble corrosion products will make it possible to calculate the crud and activity transport factors, β_c and β_a , and obviate the current need for empirical estimation of these parameters. This would enable CRUDSIM/MIT computations to be made using only basic principles and chemical data.

- More accurate calculation of the role of particulate precipitation kinetics in the bulk coolant will help to understand the role of particulates in the coolant, particularly when compared with measured soluble vs. particulate concentrations in the PCCL. We have shown in the present work that the CRUDSIM/MIT formulation can accomodate an intermediate step of particle formation prior to deposition.

- Based upon separately reported comparisons between CRUDSIM/MIT and PACTOLE code calculations [B-1], the effect of corrosion products and impurities such as Co^{59} , introduced into the primary coolant from the CVCS needs to be investigated further, and if confirmed to be significant, some means for incorporation of this phenomenon in CRUDSIM/MIT should be implemented - for example, by superposition of an additional contribution to the crud transport to the core.

- Finally, more and a greater variety of comparisons between CRUDSIM/MIT and PCCL data are essential.

REFERENCES

(B-1) Proceedings of International Conference on Water Chem. of Nucl. React. Sys., Bournemouth, BNES, London, 1978.

(B-2) Proc. of 2nd Int. Conf. on Water Chem. of Nucl. React. Sys., Bournemouth, 2BNES, London, 1980

(B-3) Proc. of 3rd Int. Conf. on Water Chem. of Nucl. React. Sys., Bournemouth, 3BNES, London, 1984

(B-4) Proc. of 4th Int. Conf. on Water Chem. of Nucl. React. Sys., Bournemouth, 4BNES, London, 1986

(B-5) P. Beslu, et al, "A computer code PACTOLE to predict activation of corrosion products in PWRs", Proceedings of International Conference on Water Chem. of Nucl. React. Sys., Bournemouth, BNES, London, 1978.

(B-6) P. Beslu, "Mechanisms and driving forces in corrosion product transport and build-up : PACTOLE code", IAEA Specialist Meeting, San Miniato, Italy, October, 1981.

(B-7) P. Beslu and A. Lalet, "Computer prediction in radiation exposure reduction", JAIF Int. Conf. on Water Chem. in Nucl. Power Plants, Japan, 1988.

(B-8) P. Borys, C. B. Lee, M. J. Driscoll and R. Sanchez, "Parametric studies of the MIT PWR coolant chemistry loop using the PACTOLE code", MITNRL-034, 1989.

(B-9) C. A. Bergmann and W. T. Lindsay, et al, "The role of coolant chemistry in PWR radiation field buildup", EPRI NP-4247, 1985.

(B-10) F. P. Berger and K. Hau, "Mass transfer in turbulent pipe flow measured by the electrochemical method", Int. J. Heat Mass Transfer, Vol. 20, pp. 1185-1194, 1977.

(B-11) S. K. Beal, "Particulate fouling of heat exchangers", Int. Conf. on Fouling in Heat Transfer Equipment, Troy, New York, 1979.

(B-12) S. K. Beal, "Particle deposition in turbulent flow", Nucl. Sci. and Eng., 40, pp. 1-11, 1970.

(B-13) S. E. Best, "Characterization of the MIT research reactor for fusion reactor related studies", M. S. Thesis, Nucl. Eng. Dept., MIT, 1979.

(B-14) R. Behrisch, "Sputtering of Solids with Neutrons", Sputtering by Particle Bombardment II, Topics in Applied Physics, V52, Springer Verlag, 1983.

(B-15) S. K. Beal, "Correlation for the sticking probability and erosion of particles", J. Aerosol Science, Vol. 9, pp. 455-461, 1978.

(C-1) P. Cohen, Water Coolant Technology of Power Reactors, Gordon and Breach Science Publisher, 1969.

(C-2) G. C. W. Comley, "The significance of corrosion products in water reactor coolant circuits", Progress in Nuclear Energy, Vol. 16, No. 1, pp. 41-72, 1985.

(C-3) J. W. Cleaver and B. Yates, "A sub-layer model for the deposition of particles from a turbulent flow", Chem. Eng. Sci., Vol. 30, pp. 983-992, 1975.

(C-4) M.R. Christoffersen, "The kinetics of crystal growth and dissolution of calcium monohydrogen phosphate dihydrate", J. Crystal Growth, 87, pp.51-61, 1988.

(C-5) J. W. Cleaver and B. Yates, "Mechanism of detachment of colloidal particles from a flat substrate in a turbulent flow", J. Coll. Interf. Sci., 44, pp. 464-474, 1973.

(C-6) J. W. Cleaver and B. Yates, "The effect of re-entrainment on particle deposition", Chem. Eng. Sci., Vol. 31, pp. 147-151, 1976.

(D-1) M. J. Driscoll, O. K. Harling, G. E. Kohse, and R. G. Ballinger, "The MIT in-pile loops for coolant chemistry and corrosion studies", Proc. of JAIF Int. Conf. on Water Chem. in Nuclear Power Plants, Tokyo, Japan, April, 19-22, 1988.

(D-2) J. A. Dean, Lange's Handbook of Chemistry, McGraw-Hill Book Company, New York, 1985.

(D-3) J. J. Duderstadt, Transport Theory, Wiley-Interscience Publication, 1979.

(E-1) N. Epstein, "Fouling : technical aspects", presented at the 1st Int. conf. on the fouling of heat exchangers, Troy, New York, 1979.

(F-1) S. K. Friedlander and H. F. Johnstone, Ind. Eng. Chem., 49, 1151, 1957.

(F-2) J. D. Frantz and W. L. Marshall, "Electrical conductances and ionization constants of salt...", Amer. J. Sci., Vol. 284, pp. 651-667, June, 1984.

(F-3) M. G. Fontana, Corrosion Engineering, McGraw-Hill Book Company, New York, 1986.

(G-1) A. Glassner, "The thermochemical properties of the oxides, fluorides, and chlorides to 2500 ^{o}K", ANL-5750, USAEC, Washington, 1957.

(H-1) J. P. Holman, Heat Transfer, McGraw-Hill Book Company, New York, 1986.

(H-2) C. I. Hussain, et al, "Diffusion controlled deposition of particulate matter from flowing slurries", Heat Transfer, Vol. 5, pp. 2573, 1986.

(H-3) J. Hubbard and L. Onsager, " Dielectric dispersion and dielectric friction in electrolyte solutions. I", J. Chem. Phys., 67, 4850, 1977.

(H-4) J. Hubbard, "Dielectric dispersion and dielectric friction in electrolyte solution. II", J. Chem. Phys., 68, 1649, 1978.

(H-5) A. L. Hines and R. N. Maddox, Mass transfer : fundamentals and application, Englewood Cliffs, New Jersey, 1985.

(J-1) Proc. of JAIF Int. Conf. on Water Chem. in Nuclear Power Plants, Tokyo, Japan, April, 1988.

(J-2) S.J. Jancic and P.A.M. Grootscholten, "Industrial Crystallization", D. Reidel Publishing Company, Boston, 1984.

(K-1) S. Kang and J. Sejvar, "The CORA-II model of PWR corrosion product transport", EPRI NP-4246, 1985.

(K-2) R. H. Kunig and Y. L. Sandler, "The solubility of simulated PWR primary circuit corrosion products", EPRI NP-4248, 1986.

(K-3) D. Q. Kern and R. E. Seaton, "A theoretical analysis of thermal surface fouling", Brit. Chem. Eng., Vol. 4, No. 5, pp. 258-262, 1959.

(L-1) D. H. Lister, et. al., "Corrosion product release in LWRs", EPRI Report NP-3888, 1985.

(L-2) I. Lambert, et al, "Corrosion product solubility in PWR primary coolant", Proc. of 4th Int. Conf. on Water Chem., Bournemouth, 4BNES, London, 1986

(L-3) D.H. Lister, "Mass transfer in the contamination of isothermal steel surfaces", Nuclear Science and Eng., 61, 107-118, 1976.

(L-4) D.H. Lister, et. al., "The mechanism and kinetics of corrosion product release from stainless steel in lithiated high temperature water", Corrosion Science, Vol. 27, No. 2, pp. 113-140, 1987.

(L-5) W.T. Lindsay, "Estimation of diffusion coefficients for electrolytes in water to 300 ^{o}C", Power Industry Research, 1, 173-200, 1981.

(L-6) T. S. Light and S.L. Licht, "Conductivity and resistivity of water from the melting to critical points", Analytical Chemistry, Vol.59, No.19, 2327-2330, Oct. 1987.

(L-7) T. S. Light, "Temperature dependence and measurement of resistivity of pure water", Analytical Chemistry, Vol.56, No.7, 1138-1142, June, 1984.

(L-8) H. Latrous et al, "Self-diffusion coefficients and structure of trivalent transplutonium ion ^{249}Bk in aqueous solution", Trans. Am. Nucl. Soc., Suppl. 3, Vol. 56, pp. 66-67, 1988.

(L-9) J. B. Lumsden, "The nature of corrosion films in simulated LWR water", EPRI NP-4061M, 1985.

(L-10) J. B. Lumsden, "Oxide film compositions and morphology on alloy 600 tubes from steam generators", EPRI NP-5712, 1988.

(L-11) W. T. Lindsay, Jr., "Correlation of iron solubility from nickel ferrites", Westinghouse R&D Center, R&D Report 88-8S21-WBPED-R1, 1988.

(M-1) M. Metge, et al, "Cobalt sources in PWR primary systems - PACTOLE prediction", Proc. of 4th Int. Conf. on Water Chem., Bournemouth, 4BNES, London, 1986

(M-2) A. M. Morillon, "Modelling of radionuclide transport in a simulated PWR environment", S. M. Thesis, Nucl. Eng. Dept. MIT, 1987.

(M-3) T. Mizushina, "The electrochemical method in transport phenomena", Adv. Heat Transfer, 7, 87, 1971.

(M-4) W.L. Marshall, "Electrical conductance of liquid and super-critical water ... ", J. Chem. and Eng. Data , Vol.32, No.2, 221-226, 1987.

(M-5) W.L. Marshall, "Reduced state relationship for limiting electrical conductances of aqueous ions over wide ranges of temperature and pressure", J. Chem. Phys., 87, 3639-3643, 1987.

(M-6) L. Meites, CRC Handbook Series in Inorganic Electrochemistry, CRC Press, Boca Raton Fla., 1980.

(M-7) D. D. Macdonald, et al, "The growth and breakdown of passive films on metal surfaces", EPRI NP-4069M, 1985.

(M-8) V. G. Molinari and L. Pollachini, "Slow neutron distribution in a temperature gradient", Nucl. Sci. Eng. 91, pp. 458, 1985.

(M-9) J. W. Mayer, et al, "Ion Implantation in Semiconductors", Academic Press, New York, 1970.

(N-1) R. H. Notter and C. A. Sleicher, "The eddy diffusivity in the turbulent boundary layer near a wall", Chem. Eng. Sci., 26, pp. 161-171, 1971.

(N-2) J. Nyvlt, "The kinetics of industrial crystallization", Elsevier, New York, 1985.

(N-3) M. Nakahara and K. Ibuki, "Is the Walden product useful", J. Phys. Chem., 90, 3026-3030, 1986.

(O-1) E. H. Oelkers and H. C. Helgeson, "Calculation of the thermodynamic and transport properties of aqueous species at high pressures and temperature", Geochim. et Cosmoch. Acta, Vol. 52, pp. 63-85, 1988.

(P-1) Joao De Deus R. S. Pinheiro, "Fouling of heat transfer surfaces", Heat Exchanger Sourcebook, edited by J. W. Palen, Hemisphere Publishing Corporation, 1986.

(P-2) B. S. Petukhov, "Heat transfer and friction in turbulent pipe flow with variable physical properties", Adv. Heat Transfer, 6, 504, 1970.

(P-3) M. Polley and M. Pick, "Iron, nickel and chromium mass balances in Westinghouse PWR primary circuits", Proceedings of International Conference on Water Chem. of Nucl. React. Sys., Bournemouth, 4 BNES, London, 1986.

(P-4) M. E. Pick, "The nature of PWR stainless steel and Inconel oxides in relation to decontamination in permanganate based (NP and AP) processes", Water Chemistry of Nuclear Reactor Systems-3, BNES, London, England, 1983.

(P-5) R. F. Probstein, Physicochemical Hydrodynamics, Butterworth, Boston, 1989.

(Q-1) A. S. Quist and W. L. Marshall, "Assignment of limiting equivalent conductances for single ions to 400 °C", The J. of Phys. Chem., 69, 2984, 1965.

(R-1) D. E. Rosner, Transport Processes in Chemically Reacting Flow Systems, Butterworths, Boston, 1986.

(R-2) R. A. Robinson, Electrolyte Solutions, Butterworth, 1970.

(S-1) A. Strasser, et. al., "Corrosion product buildup on LWR fuel rods", EPRI NP-3789, 1985.

(S-2) R. Sanchez, "Use of a pressurized in-pile loop to reduce dose rates by improving PWR coolant chemistry", Ph. D. Thesis, Dept. of Nucl. Eng., MIT, 1989.

(S-3) T. Swan, "Review of the United Kingdom PWR primary-circuit-chemistry program-Progress Report No.1", EPRI NP-6368, 1989.

(T-1) T. Moore, "Robots join the nuclear work force", EPRI Journal, Nov., 1984.

(T-2) C.Y. Tai and C.H. Lin, "Crystal growth kinetics of the two step model", J. Crystal Growth, 82, pp.377-384, 1987.

(T-3) J. Taborek, "Fouling-the major unresolved problem in heat transfer", Chem. Eng. Prog., Vol. 68, No. 2, pp. 59-67, No. 7, pp. 69-78, 1972.

(W-1) C. Wood, "Recent developments in LWR radiation field control", Progress in Nuclear Energy, Vol. 19, No. 3, pp. 241-266, 1987.

(W-2) Westinghouse Design PWR Technology Manual, NRC Technical Training Manual.

(W-3) J. H. Wicks, "Design, construction and testing of an in-pile loop for PWR simulation", S. M. Thesis, Dept. of Nucl. Eng., MIT, 1987.

(Z-1) J. F. Ziegler, "Stopping and Range of Ions in Solids", Pergamon, New York,1985.

Nomenclature

Roman Alphabet

A_c	activity in cold tank (S/G and coolant) (Ci)
A_h	activity in hot tank (core) (Ci)
A_i	activity in the i-th node (Ci)
A_p	activity in the purification system (Ci)
a_1	ratio of particle to ion radii
a_2	ratio of particle to ion concentration
ADP_1	activity deposition rate as a particle in core (Ci/sec)
ADP_3	activity deposition rate as a particle in S/G (Ci/sec)
ADS	activity deposition rate as a soluble in S/G (Ci/sec)
APR	activity precipitation rate in the coolant (Ci/sec)
ARS	activity release rate as a soluble in core (Ci/sec)
ASD	activity deposition rate as a soluble in S/G (Ci/sec)
ASR	activity release rate as a soluble in core (Ci/sec)
c	concentration of the electrolyte (molality)
C_{bulk}	soluble species concentration in bulk coolant (kg/m^3)
C_i	soluble species concentration at the interface (kg/m^3)
$C_i(x)$	soluble species concentration at position, x, in the i-th node (kg/m^3)
C_p	particle concentration in the coolant (kg/m^3) , or specific heat capacity of the fluid (J/kg.°C)
C_{sat}	saturation concentration (kg/m^3)
$C^i_{pt,bulk}$	particle concentration in bulk coolant of the i-th region (kg/m^3)
$C^i_{pt,surf}$	particle concentration at the surface of the i-th region (kg/m^3)
$C^i_{s,bulk}$	soluble concentration in bulk coolant in the i-th region (kg/m^3)
$C^i_{s,surf}$	soluble concentration at the surface in the i-th region (kg/m^3)
ΔC^p_i	soluble concentration difference between the supersaturated bulk coolant and the saturated particle surface in the i-th region (kg/m^3)
CR	corrosion rate of S/G tubing (kg/sec)
D_{ab}	diffusion coefficient of the species ab (m^2/sec)
D_e	hydraulic diameter of the fluid channel (m)
D_p	diffusion coefficient of particles (m^2/sec)
D_s	diffusion coefficient of soluble species (m^2/sec)
DP_i	particle deposition rate in the i-th node (kg/sec)
E	ion energy (kev)

F	coolant flow rate (kg/day) , or Faraday's constant (96500 c/g-equiv.)
f_i	weight ratio of element i to iron in the core crud
f_p	bypassed purification flow rate (m^3/sec)
f_{pi}	fractional deposition of particulates on the i-th node
h_1	mass transfer coefficient of soluble crud in core (m/sec)
h_2	mass transfer coefficient of soluble crud in S/G (m/sec)
h_{cr}	crystallization coefficent of soluble species (m/sec)
h^a_{cr}	crystallization coefficent of activity (m/sec)
h_{dp}	deposition coefficient of soluble species (m/sec)
h^a_{dp}	deposition coefficient of activity (m/sec)
h_{ds}	dissolution coefficient of soluble species (m/sec)
h^a_{ds}	dissolution coefficient of activity (m/sec)
h_{mt}	mass transfer coefficient (m/sec)
h_{rl}	release coefficient of soluble species (m/sec)
h^a_{rl}	release coefficient of activity (m/sec)
H^1_{in}	inlet of core fuel element flow channel
H^1_{out}	outlet of core fuel element flow channel
H^3_{in}	inlet of S/G tubing flow channel
H^3_{out}	outlet of S/G tubing flow channel
$h_{d,sp}$	soluble deposition coefficient on the particles (m/sec)
$h^i_{d,sw}$	soluble deposition coefficient on the surface in the i-th region (m/sec)
$h^i_{mt,pw}$	mass transfer coefficient of particles in the i-th region (m/sec)
$h_{mt,sp}$	mass transfer coefficient of soluble species onto particles in the coolant (m/sec)
$h^i_{mt,sw}$	mass transfer coefficient of soluble species in the i-th region (m/sec)
I_c	iron inventory in cold tank (S/G and coolant) (kg-Fe)
I_h	iron inventory in hot tank (core) (kg-Fe)
I_i	corrosion product inventory in the i-th node (kg-Fe)
I_p	corrosion product inventory of the purification system (kg-Fe)
IR	activity production rate in core (Ci/sec)
J_{cr}	crystallization rate (kg/m^2.sec)
J_{dp}	deposition rate (kg/m^2.sec)
J_{ds}	dissolution rate (kg/m^2.sec)
J_{er}	erosion rate (kg/m^2.sec)

J_{mt} mass transfer rate ($kg/m^2.sec$)

J_{rl} release rate ($kg/m^2.sec$)

k thermal conductivity of the fluid ($w/m^2.°K$)

k_{cr} crystallization constant $\left[\frac{kg/m^2.sec}{(kg/m^3)^n}\right]$

k_{ds} dissolution constant $\left[\frac{kg/m^2.sec}{(kg/m^3)^n}\right]$

k_{er} erosion constant

K_i chemical reaction constant

K_w thermodynamic ion product for water

k_o constant

k_1 mass transfer factor of soluble species between core fuel element surface and bulk coolant (m^3/sec)

k_1^a mass transfer factor of activity between core fuel element surface and bulk coolant (m^3/sec)

k_3 mass transfer factor of soluble species between S/G tubing surface and bulk coolant (m^3/sec)

k_3^a mass transfer factor of activity between S/G tubing surface and bulk coolant (m^3/sec)

L_1 length of core fuel element channel (m)

L_3 length of S/G tubing channel (m)

M_p mass of a particle (kg)

n order of a reaction

N_A Avogadro's number

n_p particle number density in the coolant ($\#/m^3$)

$n^{+,-}$ valence of the positive or negative ion

Nu Nusselt number

P core percent power (%)

PF particle flocculation rate (kg/sec)

P_{H_2} hydrogen partial pressure (atm)

P_{w1} wetted perimeter of the core fuel element (m)

P_{w3} wetted perimeter of S/G tubing (m)

Pr Prandtl number

PR particle precipitation rate (kg/sec)

PW particle deposition rate on the surface (kg/sec)

Q_{cr} activation barrier energy of crystallization

Q_{ds} activation barrier energy of dissolution

R gas constant (8.314 J/mole °K), or

	iron addition rate into cold tank (S/G and coolant) (kg-Fe/day)
R(E)	average range of the recoiled nuclide for the incident neutron energy, E (cm)
r_p	radius of a particle (m)
r_s	radius of a soluble species (m)
R_p	projected recoil range (cm, or mg/cm^2)
Re	Reynolds number
S	Soret coefficient (°C^{-1})
S_c	iron solubility in cold tank (S/G and coolant) (kg-Fe/kg H_2O)
S_h	iron solubility in hot tank (core) (kg-Fe/kg H_2O)
S_i	iron solubility in the i-th node (kg.Fe/m^3)
S_i	average soluble saturation concentration in the i-th node (kg/m^3)
$S_i(x)$	soluble saturation concentration at position x in the i-th node (kg/m^3)
Sc	Schmidt number
SD	deposition rate of soluble species onto core fuel surface (kg/sec)
Sh	Sherwood number
SP	mass transfer rate of soluble species to the particles (kg/sec)
SR	soluble species release rate from S/G tubing (kg/sec)
SW	deposition rate of soluble species on the surface of the PWR primary circuit (kg/sec)
T	absolute temperature (°K)
T_{avg}	average bulk coolant temperature (°C)
t_d	core crud thickness (cm, or mg/cm^2)
T_i	temperature in the i-th node (°C)
$T_i(x)$	temperature at the position, x, in the i-th node (°C)
T_{in}	coolant inlet temperature (°C)
T_{out}	coolant outlet temperature (°C)
$t^{\oplus}_{\ominus}$	transference number of positive or negative ion
ΔT_1	temperature difference between core surface and bulk coolant (°C)
ΔT_3	temperature difference between S/G surface and bulk coolant (°C)
V	velocity of the fluid (m/sec)
V	drift velocity (m/sec)
V_i	coolant volume of the i-th region (m^3)
W	mass of deposits susceptible to erosion (kg)
Y_n	sputtering yield of metal by fast neutrons (atoms/neutron)
z	hydrogen ion concentration (10^{-pH})
$\|Z_A^+\|$	absolute value of the charge of A^+ ion

Greek Alphabet

α	neutron activation factor (Ci/kg-Fe. % power.day)
α_i	neutron activation factor in the i-th node (Ci/kg-Fe. % power.day)
β	fraction of the surface covered by flow burst at any instant, or transport factor
γ_0	generic activity coefficient for neutral species
γ_1	generic activity coefficient for univalent ions
λ	radioactive decay constant (day^{-1})
$\lambda^o_{+,-}$	limiting positive or negative ion conductance ($cm^2/\Omega.equiv.$)
Λ^o_{ab}	limiting electrolyte conductance ($cm^2/\Omega.equiv.$)
ϵ_f	probability that the particles stick together after a collision
ρ	density of the fluid (kg/m^3)
ρ_{H_2O}	coolant density (kg/m^3)
ρ_p	particle density (kg/m^3)
μ	viscosity of the fluid ($N.S/m^2$)
ψ	deposit strength
τ	shear stress
σ^i_a	neutron absorption cross section of element i (cm^2)
σ^i_{np}	(n,p) reaction cross section of element i (cm^2)
Σ	macroscopic cross section (cm^{-1})
ϕ	neutron flux ($n/cm^2.sec$)
ϕ_{ft}	fast neutron flux ($n/cm^2.sec$)

Subscripts

node

1	core fuel element surfaces
2	bulk coolant
3	S/G tubing surfaces
4	particles in bulk coolant

region

1	core fuel element flow channel
2	core outlet plenum, hot leg and S/G inlet plenum
3	S/G tubing flow channel
4	S/G outlet plenum, cold leg and core inlet plenum

Appendix A. CRUDSIM/MIT Code Listing and Sample Input and Output

The appendix consists of

(i) A listing of the CRUDSIM/MIT program.

(ii) Sample input data for the MIT PCCL.

(iii) Sample output for the MIT PCCL.

CRUDSIM/MIT is written in the FORTRAN language and can be compiled and run on an IBM-PC. The sequence in which input data are prepared is given in Table A.1, and a description of the input variables is shown in Table A.2. The following is a brief summary of the procedure to run the CRUDSIM/MIT program on an IBM compatible, Compaq computer (eg. the unit in Rm NW 12-234). The file name of the CRUDSIM/MIT program stored on the hard disc in the Compaq computer is **CRUDMIT.FOR**.

(1) prepare input data file, eg. CRUDMIT.DAT

(2) compile and link source program, CRUDMIT.FOR, using MSFORT 41 compiler

type Fl CRUDMIT.FOR [return]

(3) run the program, CRUDMIT.FOR

type CRUDMIT [return]

The screen will show " enter input file name ---> " , then

type CRUDMIT.DAT [return]

Table A.1 Configuration of Input Data

DAYS, IN, NTMA, NTS, BETAC, BETAA

BORON, ALIT, CH2, FLOW, ONOFF, P1, TIN, TOUT, DTBL1, DTBL3, FPUR, DEN, VIS

IH, IC, AH1, AH2, AC1, AC2, AD1, AD2

IREF, IPAR

INPRIN

DE1, DE3, AR1, AR3, AF1, AF3

DSOL, DPAR

ALPH1, ALPH2, LAMD1, LAMD2

RR58, RR60

HCRYSC, HCRYSA, HDISSC, HDISSA

CR

(If more than one operation cycle is to be run, provide the next two lines of input per operation cycle : calculation parameters and plant operation condition. If a negative value of the variable, DAYS, is provided, the program stops running)

DAYS, IN, NTMA, NTS, BETAC, BETAA

BORON, ALIT, CH2, FLOW, ONOFF, P1, TIN, TOUT, DTBL1, DTBL3, FPUR,DEN,VIS

Table A.2 Description of Input Variables

No.	Variable	Type	Description
1	DAYS	real	duration of operation (day)
2	IN	real	time step size of numerical calculation (day) : 0.1 (recommended)
3	NTMA	integer	number of time steps per printing output
4	NTS	integer	number of meshes in numerical integration of solubility by temperature (normally 1 < nts < 50) : 10 (recommended)
5	BETAC	real	crud transport factor in CRUDSIM/MIT
6	BETAA	real	activity transport factor in CRUDSIM/MIT
7	BORON	real	concentration of boron (ppm)
8	ALIT	real	concentration of LiOH (ppm)
9	CH2	real	hydrogen concentration (cc/kg-H_2O)
10	FLOW	real	coolant flow rate (kg.H_2O/day)
11	ONOFF	integer	coolant flow, on or off (1 or 0)
12	P1	real	% power for calculation of neutron activation
13	TIN	real	core inlet temperature (°C)
14	TOUT	real	core outlet temperature (°C)
15	DTBL1	real	temperature difference across the boundary layer in the core (°C)
16	DTBL3	real	temperature difference across the boundary layer in the S/G (°C)
17	FPUR	real	bypass flow rate of purification system (kg.H_2O/day)
18	DEN	real	average density of the coolant (kg/m^3)
19	VIS	real	average viscosity of the coolant (n.sec/m^2)
20	IH	real	initial crud inventory in the core (kg-Fe)
21	IC	real	initial crud inventory in the S/G (kg-Fe)
22	AH1	real	initial cobalt-60 activity in the core (Ci)
23	AH2	real	initial cobalt-58 activity in the core (Ci)
24	AC1	real	initial cobalt-60 activity in the S/G (Ci)
25	AC2	real	initial cobalt-58 activity in the S/G (Ci)
26	AD1	real	initial cobalt-60 activity in the purification system (Ci)
27	AD2	real	initial cobalt-58 activity in the purification system (Ci)
28	IREF	integer	refuelling of fuel assemblies, on or off (1 or 0)

29	IPAR	integer	particulate precipitation in the coolant, on or off (1 or 0)
30	INPRIN	integer	printing of input data and detailed output, on or off (1 or 0)
31	DE1	real	hydraulic diameter of core fuel channel (m)
32	DE3	real	hydraulic diameter of S/G tube (m)
33	AR1	real	total surface area of the core (m^2)
34	AR3	real	total surface area of the S/G (m^2)
35	AF1	real	coolant flow area in the core (m^2)
36	AF3	real	coolant flow area in the S/G (m^2)
37	DSOL	real	diffusion coefficient of soluble species (m^2/sec)
38	DPAR	real	diffusion coefficient of particulates (m^2/sec)
39	ALPH1	real	cobalt-60 production rate in the core (Co-60 Ci/kg-Fe.day.%power)
40	ALPH2	real	cobalt-58 production rate in the core (Co-58 Ci/kg-Fe.day.%power)
41	LAMD1	real	decay constant of cobalt-60 (day^{-1})
42	LAMD2	real	decay constant of cobalt-58 (day^{-1})
43	RR58	real	fractional direct recoil release of cobalt-58 produced by (n,p)
44	RR60	real	fractional direct recoil release of cobalt-60 produced by (n,r)
45	HCRYSC	real	crystal growth coefficient of corrosion products in the core (m/sec)
46	HCRYSA	real	crystal growth coefficient of activity in the S/G (m/sec)
47	HDISSC	real	dissolution coefficient of corrosion products in the S/G (m/sec)
48	HDISSA	real	dissolution coefficient of activity in the core (m/sec)
49	CR	real	corrosion rate of the S/G (kg/day)

The screen will show " enter output file name ---> " , then

type CRUDMIT.OUT [return]

The user can specify any input and output file names. If the input file specified by the user does not exist, or there already exists an output file having the same name as the one specified by the user, the screen will ask again. Then, re-enter the input or output file name.

(4) print output file

type print CRUDMIT.OUT [return]

A floppy disc containing the FORTRAN source code, and its compiled and linked version has been filed with the Nuclear Engineering Department Computer Library in NW 12-234. Table A.3 is a printout of a sample input file for the MIT PCCL Reference Run No. 2, and Table A.4 is a printout of its output. Table A.5 is a listing of the CRUDSIM/MIT program.

Table A.3 Input Data File for Sample Problem

```
50.,0.1,10,10,0.01,0.005
800.,1.84,25.0,5914.,1,100.,273.9,315.6,23.23 ,-5.57,4.617,723.,9.278e-5
1.e-10,0.250e-4,0.,0.,0.,0.,0.,0.
1,0
1
0.652e-2,0.6159e-2,0.026,0.097,3.34e-5,2.98e-5
1.08e-8,6.9e-10
2.400e-3,3.94e-2,3.6e-4,9.78e-3
0.0 ,0.0
1.e6,1.e6,1.e6, 1.e6
3.55e-7
-1,-1,-1,-1,-1,-1
```

Table A.4

Listing of Output File for Sample Problem

(1) Calculation parameter

```
days  =   .50000E+02 day
in    =   .10000E+00 day
ntma  =         10
nts   =         10
betac =   .10000E-01
betaa =   .50000E-02
```

(2) Plant operating conditions

```
boron =   .80000E+03 ppm
alit  =   .18400E+01 ppm
ch2   =   .25000E+02 cc/kg-H2O
flow  =   .59140E+04 kg-H2O/day
onoff =         1
pl    =   .10000E+03 % power
tin   =   .27390E+03 oC
tout  =   .31560E+03 oC
dtbl1 =   .23230E+02 oC
dtbl3 =  -.55700E+01 oC
fpur  =   .46170E+01 kg-H2O/day
den   =   .72300E+03 kg/m3
vis   =   .92780E-04 n.sec/m2
```

(3) Initial conditions

```
ih    =   .10000E-09 kg-Fe
ic    =   .25000E-04 kg-Fe
ah1   =   .00000E+00 Ci
ah2   =   .00000E+00 Ci
ac1   =   .00000E+00 Ci
ac2   =   .00000E+00 Ci
ad1   =   .00000E+00 Ci
ad2   =   .00000E+00 Ci
```

(4) Options

```
iref  =         1
ipar  =         0
```

(5) Output print option

```
inprin =        1
```

(6) Plant geometry

```
de1   =   .65200E-02 m
de3   =   .61590E-02 m
ar1   =   .26000E-01 m2
ar3   =   .97000E-01 m2
af1   =   .33400E-04 m2
af3   =   .29800E-04 m2
```

(7) Diffusion coefficient

```
dsol  =   .10800E-07 m2/sec
```

dpar = .69000E-09 m2/sec

(8) Radioactivity parameter

alph1 = .24000E-02 Co-60 Ci/kg-Fe.day.%power
alph2 = .39400E-01 Co-58 Ci/kg-Fe.day.%power
lamd1 = .36000E-03 day-1
lamd2 = .97800E-02 day-1

(9) Recoil release

rr58 = .00000E+00
rr60 = .00000E+00

(10) Crystal growth and dissolution

hcrysc = .10000E+07 m/sec
hcrysa = .10000E+07 m/sec
hdissc = .10000E+07 m/sec
hdissa = .10000E+07 m/sec

(11) Other parameters

cr = .35500E-06 kg/day

Mass transfer parameter calculation

VARIABLE	CORE	S/G
Vel (m/sec)	.28345E+01	.31770E+01
Re	.14402E+06	.15248E+06
Sc-sol	.11882E+02	same
Sc-par	.18598E+03	same
Sh-sol	.10281E+04	.10798E+04
Sh-par	.25716E+04	.27010E+04
h-sol (m/sec)	.17029E-02	.18934E-02
h-par (m/sec)	.27215E-03	.30260E-03
k-sol (m3/sec)	.44276E-04	.18366E-03
ak-sol (m3/sec)	.44276E-04	.18366E-03
k-par (m3/sec)	.70759E-05	.29352E-04
fksol	.19424E+00	.80576E+00
afks	.19424E+00	.80576E+00
fkpar	.19424E+00	.80576E+00
beta-sol(m3/sec)	.35676E-04	same
beta-act(m3/sec)	.35676E-04	same
beta-par(m3/sec)	.57015E-05	same
betac	.37683E+00	same
betaa	.37683E+00	same

TIME (day)	S/G CRUD (mg/cm2)	CORE CRUD (mg/cm2)	Co60 S/G (uCi/cm2)	Co58 S/G (uCi/cm2)	Co60 Core (uCi/cm2)	Co58 Core (uCi/cm2)	Co60 Cool (uCi/cm3)	Co58 Cool (uCi/cm3)
.0	.258E-01	.385E-06	.000E+00	.000E+00	.000E+00	.000E+00	.000E+00	.000E+00
1.0	.261E-01	.243E-03	.531E-05	.868E-04	.166E-04	.272E-03	.464E-07	.760E-06
2.0	.264E-01	.393E-03	.180E-04	.293E-03	.438E-04	.716E-03	.769E-07	.126E-05
3.0	.268E-01	.543E-03	.369E-04	.597E-03	.838E-04	.137E-02	.108E-06	.176E-05
4.0	.271E-01	.692E-03	.619E-04	.998E-03	.137E-03	.223E-02	.140E-06	.228E-05
5.0	.274E-01	.842E-03	.930E-04	.149E-02	.203E-03	.330E-02	.172E-06	.280E-05
6.0	.277E-01	.991E-03	.130E-03	.208E-02	.282E-03	.458E-02	.206E-06	.334E-05
7.0	.281E-01	.114E-02	.174E-03	.277E-02	.374E-03	.607E-02	.240E-06	.388E-05
8.0	.284E-01	.129E-02	.223E-03	.354E-02	.479E-03	.777E-02	.274E-06	.444E-05
9.0	.287E-01	.144E-02	.278E-03	.440E-02	.598E-03	.968E-02	.309E-06	.500E-05
10.0	.290E-01	.159E-02	.340E-03	.535E-02	.730E-03	.118E-01	.345E-06	.556E-05
11.0	.294E-01	.174E-02	.407E-03	.639E-02	.875E-03	.141E-01	.381E-06	.614E-05
12.0	.297E-01	.189E-02	.481E-03	.751E-02	.103E-02	.167E-01	.418E-06	.672E-05
13.0	.300E-01	.204E-02	.560E-03	.871E-02	.121E-02	.194E-01	.456E-06	.730E-05
14.0	.303E-01	.219E-02	.646E-03	.100E-01	.139E-02	.223E-01	.494E-06	.789E-05
15.0	.307E-01	.234E-02	.737E-03	.114E-01	.159E-02	.255E-01	.532E-06	.849E-05
16.0	.310E-01	.249E-02	.835E-03	.128E-01	.180E-02	.289E-01	.571E-06	.909E-05
17.0	.313E-01	.264E-02	.938E-03	.144E-01	.203E-02	.324E-01	.611E-06	.970E-05
18.0	.316E-01	.279E-02	.105E-02	.160E-01	.227E-02	.362E-01	.650E-06	.103E-04
19.0	.320E-01	.294E-02	.116E-02	.177E-01	.252E-02	.402E-01	.691E-06	.109E-04
20.0	.323E-01	.309E-02	.128E-02	.194E-01	.279E-02	.443E-01	.731E-06	.115E-04
21.0	.326E-01	.324E-02	.141E-02	.213E-01	.307E-02	.487E-01	.773E-06	.122E-04
22.0	.329E-01	.339E-02	.154E-02	.232E-01	.336E-02	.533E-01	.814E-06	.128E-04
23.0	.333E-01	.353E-02	.168E-02	.251E-01	.367E-02	.581E-01	.856E-06	.134E-04
24.0	.336E-01	.368E-02	.183E-02	.272E-01	.399E-02	.631E-01	.898E-06	.141E-04
25.0	.339E-01	.383E-02	.198E-02	.293E-01	.432E-02	.683E-01	.941E-06	.147E-04
26.0	.342E-01	.398E-02	.213E-02	.315E-01	.467E-02	.737E-01	.984E-06	.153E-04
27.0	.346E-01	.413E-02	.230E-02	.338E-01	.503E-02	.792E-01	.103E-05	.160E-04
28.0	.349E-01	.428E-02	.246E-02	.361E-01	.541E-02	.850E-01	.107E-05	.166E-04
29.0	.352E-01	.443E-02	.264E-02	.385E-01	.580E-02	.910E-01	.111E-05	.172E-04
30.0	.355E-01	.458E-02	.282E-02	.410E-01	.620E-02	.972E-01	.116E-05	.179E-04
31.0	.359E-01	.473E-02	.300E-02	.435E-01	.662E-02	.104E+00	.120E-05	.185E-04
32.0	.362E-01	.488E-02	.320E-02	.461E-01	.705E-02	.110E+00	.125E-05	.192E-04
33.0	.365E-01	.503E-02	.339E-02	.487E-01	.749E-02	.117E+00	.129E-05	.198E-04
34.0	.369E-01	.518E-02	.360E-02	.515E-01	.795E-02	.124E+00	.134E-05	.205E-04
35.0	.372E-01	.533E-02	.380E-02	.542E-01	.843E-02	.131E+00	.138E-05	.211E-04
36.0	.375E-01	.548E-02	.402E-02	.571E-01	.891E-02	.138E+00	.143E-05	.218E-04
37.0	.378E-01	.563E-02	.424E-02	.600E-01	.941E-02	.146E+00	.148E-05	.224E-04
38.0	.382E-01	.578E-02	.447E-02	.629E-01	.993E-02	.154E+00	.152E-05	.231E-04
39.0	.385E-01	.593E-02	.470E-02	.659E-01	.105E-01	.162E+00	.157E-05	.237E-04
40.0	.388E-01	.608E-02	.493E-02	.690E-01	.110E-01	.170E+00	.162E-05	.244E-04
41.0	.391E-01	.623E-02	.518E-02	.721E-01	.116E-01	.178E+00	.166E-05	.250E-04
42.0	.395E-01	.638E-02	.543E-02	.753E-01	.121E-01	.186E+00	.171E-05	.257E-04
43.0	.398E-01	.653E-02	.568E-02	.785E-01	.127E-01	.195E+00	.176E-05	.263E-04
44.0	.401E-01	.668E-02	.594E-02	.818E-01	.133E-01	.204E+00	.181E-05	.270E-04
45.0	.404E-01	.683E-02	.621E-02	.851E-01	.139E-01	.213E+00	.185E-05	.276E-04
46.0	.408E-01	.698E-02	.648E-02	.885E-01	.145E-01	.222E+00	.190E-05	.283E-04
47.0	.411E-01	.713E-02	.676E-02	.920E-01	.152E-01	.232E+00	.195E-05	.289E-04
48.0	.414E-01	.728E-02	.704E-02	.955E-01	.158E-01	.241E+00	.200E-05	.296E-04
49.0	.417E-01	.742E-02	.733E-02	.990E-01	.165E-01	.251E+00	.205E-05	.302E-04
50.0	.421E-01	.757E-02	.762E-02	.103E+00	.172E-01	.261E+00	.210E-05	.309E-04

Boron - 800.00 (ppm)
Lithium - 1.84 (ppm)
pH(300 oC) - 7.0004

T(coolant inlet) - 273.90 (oC)
pH(coolant inlet) - 6.7706
S(coolant inlet) - .5887E-08 (kg-Fe/kg-H2O)

T(coolant outlet) - 315.60 (oC)
pH(coolant outlet) - 7.1967
S(coolant outlet) - .4806E-08 (kg-Fe/kg-H2O)
S(coolant average) - .5284E-08 (kg-Fe/kg-H2O)

T(core inlet surface) - 297.13 (oC)
T(core outlet surface) - 338.83 (oC)
S(core surface average) - .4778E-08 (kg-Fe/kg-H2O)

T(S/G outlet surface) - 268.33 (oC)
T(S/G inlet surface) - 310.03 (oC)
S(S/G surface average) - .5436E-08 (kg-Fe/kg-H2O)

Table A.5

Listing of CRUDSIM/MIT Program

```
      program crudmit
      implicit real (a-z)
      REAL*8 TIME,IN
      integer dur,j1,onoff,nx,ix,ntime,ntma
      integer m,n,index
      integer j,i,nrf,imm,nnrf
      integer iref,ipur,irec,ibet,ipar,inprin
      integer nts
      dimension rf(51)
      common /www/ w
      common /bbb/a2,b2,c2,d3,q,s1,s
      common /ccc/a,b,k1,k2,k3,k4,k6,p,t,t1,x0,x1,x2,x3,x4,y,z
      common /ddd/d1,d2,i,j
      common /eee/alit,boron,dt,dw,e1,e2,lgkw,m,mw,n,nw,r9,t2,t3
      common /fff/ch2,h,k10,k11,k12,k13,L3,ph2,s11,s10,x
      common /bet/ den,del,de3,vel1,vel3,vis,dsol,dpar,ar1,ar3,betsla,
     1             flow,af1,af3,betslc,betpar,betac,betaa,ksol1,ksol3,
     2             kpar1,kpar3,fksol1,fksol3,fkpar1,fkpar3,hcrysc,
     3             hcrysa,hdissc,hdissa,aksol1,aksol3,afks1,afks3,
     4             inprin
      common /cfeoh/sfe,sfeoh,sfeoh2,sfeoh3
      COMMON /NELAN/ LAMCAT,LAMLI,LAMH,LAMAN,LAMOH,LAMB1,LAMB2,LAMB3,
     1          LAMB4,LAMZERO,DIEL,LALFA,LBETA,KAPCOEF
      COMMON /NETAW/ ETAW,ETA,IS,Q4,GAM,Q6,Q5,LIOH,YXK,ETAM,ETA0,
     1          DWR,AYE,JAY,TW,TR
      character*24 crudin,crudout,actout
c
c
c     ccccccccccccccc ccccccccccccccccccccc
c     c  Input and output files selection  c
c     ccccccccccccccccccccccccccccccccccccc
c
c
   88 write(*,1000)
      read(*,1010)crudin
      open(4,file=crudin,status='old',err=8888)
   99 write(*,1002)
      read(*,1010)actout
      open(6,file=actout,status='new',err=9999)
 1002 format('   enter output file name ---------> ')
 1000 format('   enter input file name ---------> ')
 1010 format(a16)
      index = 0
      go to 4444
 8888 print 8000
 8000 format('  no file by that name   ')
      go to 88
 9999 print 9000
 9000 format('  this file name may has been saved before ',/,
     1  '  try again')
      go to 99
c
c
c     ccccccccccccccccccccccccccccc
c     c    INPUT DATA READING      c
c     ccccccccccccccccccccccccccccc
c
c     (1)  Calculation parameter
c
c       DAYS - duration of operation (day)
```

```
c       IN - time step size of numerical calculation (day) : 0.1 (recommended)
c       NTMA - number of time step per printing output
c       NTS - number of meshes in numerical integration of solubility
c             by temperature (normally 1 < nts < 50) : 10 (recommended)
c       BETAC- crud transport factor in CRUDSIM/MIT
c       BETAA- activity transport factor in CRUDSIM/MIT
c
c
 4444 READ (4,*) DAYS,IN,NTMA,NTS,BETAC,BETAA
c
      if (days.lt.0) go to 3021
c     (2) Plant operating condition
c
c       BORON - concentration of boron (ppm)
c       ALIT - concentration of LiOH (ppm)
c       CH2 - hydrogen content (cc/kg-H2O)
c       FLOW - coolant flow rate (kg.H2O/day)
c       ONOFF - coolant flow on or off (1 or 0)
c       P1 - % power for calculation of neutron activation
c       TIN - core inlet temperature (oC)
c       TOUT - core outlet temperature at full power (oC)
c       DTBL1 - temperature differences across boundary layer in core (oC)
c       DTBL3 - temperature difference across boundary layer in S/G (oC)
c       FPUR - bypass flow rate of purification system (kg.H2O/day)
c       DEN - density of average coolant (kg/m3)
c       VIS - viscosity of average coolant (n.sec/m2)
c
      READ (4,*)BORON,ALIT,CH2,FLOW,ONOFF,P1,TIN,TOUT,DTBL1,DTBL3,
     1          FPUR,DEN,VIS
c
c     (3)  Initial conditions
c
c       IH - initial crud inventory in core (kg-Fe)
c       IC - initial crud inventory in S/G (kg-Fe)
c       AH1 - initial cobalt-60 activity in core (Ci)
c       AH2 - initial cobalt-58 activity in core (Ci)
c       AC1 - initial cobalt-60 activity in S/G (Ci)
c       AC2 - initial cobalt-58 activity in S/G (Ci)
c       AD1 - initial cobalt-60 activity in purification system (Ci)
c       AD2 - initial cobalt-58 activity in purification system (Ci)
c
c   Index control
c
      index = index +1
c
      if(index.ge.2) go to 2289
c
      READ (4,*) IH,IC,AH1,AH2,AC1,AC2,AD1,AD2
c
c     (4)  Option
c
c       IREF = refuelling of fuel assemblies, on or off (1 or 0)
c       IPAR = particulate precipitation in coolant, on or off (1 or 0)
c
      READ(4,*) IREF,IPAR
c
c     (5) Output print option
c
c       INPRIN = print of input data and detailed output, on or off (1 or 0)
c
```

```
      READ (4,*) INPRIN
c
c     (6) Plant geometry
c
c       DE1 - hydraulic diameter of core fuel channel (m)
c       DE3 - hydraulic diameter of S/G tube (m)
c       AR1 - surface area of core (m2)
c       AR3 - surface area of S/G (m2)
C       AF1 - coolant flow area in core (m2)
C       AF3 - coolant flow area in S/G (m2)
c
      READ (4,*)DE1,DE3,AR1,AR3,AF1,AF3
c
c     (7)  Diffusion coefficients
c
c       DSOL - diffusion coefficient of soluble (m2/sec)
c       DPAR - diffusion coefficient of particulate (m2/sec)
c
      READ (4,*) DSOL,DPAR
c
c     (8)  Radioactivity parameters
c
c       ALPH1 - cobalt-60 production rate in core (Co-60 Ci/kg-Fe.day.%power)
c       ALPH2 - cobalt-58 production rate in core (Co-58 Ci/kg-Fe.day.%power)
c       LAMD1 - decay constant of cobalt-60 (day-1)
c       LAMD2 - decay constant of cobalt-58 (day-1)
c
      READ (4,*) ALPH1,ALPH2,LAMD1,LAMD2
c
c     (9)  Recoil release
c
c       RR58 - fractional recoil release of cobalt-58 produced by (n,p)
c       RR60 - fractional recoil release of cobalt-60 produced by (n,p)
c
      READ (4,*) RR58,RR60
c
c     (10)  Crystal growth and dissolution
c
c      HCRYSC - crystal growth coefficient of corrosion product in core (m/sec)
c      HCRYSA - crystal growth coefficient of activity in S/G (m/sec)
c      HDISSC - dissolution coefficient of corrosion product in S/G (m/sec)
c      HDISSA - dissolution coefficient of activity in core (m/sec)
c
      READ (4,*) HCRYSC,HCRYSA,HDISSC,HDISSA
c
c     (11)  Other parameters
c
c       CR - corrosion rate of S/G (kg/day)
c
      READ (4,*) CR
c
c     ccccccccccccccccccccccccccc
c     c  First  Initialization  c
c     ccccccccccccccccccccccccccc
c
      time=0.
      day=0.
      saw1 = 0.
      saw2 = 0.
c
```

```
c     ccccccccccccccccccccccccccccccccccccccccccccccccccccc
c     c   PRINTING OF INPUT DATA IF INPRIN IS NOT ZERO    c
c     ccccccccccccccccccccccccccccccccccccccccccccccccccccc
c
c     if (inprin.eq.0) go to 5444
      go to 9413
c
 2289 if (inprin.eq.0) go to 3019
 9413 write(6,3601) days,in,ntma,nts,betac,betaa
 3601 format(4x,'(1) Calculation parameter',//,
     1       4x,'days  = ',e12.5,' day',/,
     2       4x,'in    = ',e12.5,' day',/,
     3       4x,'ntma  = ',i10,/,
     3       4x,'nts   = ',i10,/,
             4x,'betac = ',e12.5,/,
     4       4x,'betaa = ',e12.5,/)
      write (6,3602) boron,alit,ch2,flow,onoff,p1,tin,tout,dtbl1,
     1               dtbl3,fpur,den,vis
 3602 format(4x,'(2) Plant operating conditions',//,
     1       4x,'boron = ',e12.5,' ppm',/,
     2       4x,'alit  = ',e12.5,' ppm',/,
     3       4x,'ch2   = ',e12.5,' cc/kg-H2O',/,
     6       4x,'flow  = ',e12.5,' kg-H2O/day',/,
     1       4x,'onoff = ',i10,/,
     1       4x,'p1    = ',e12.5,' % power',/,
     4       4x,'tin   = ',e12.5,' oC       ',/,
     5       4x,'tout  = ',e12.5,' oC       ',/,
     5       4x,'dtbl1 = ',e12.5,' oC       ',/,
     5       4x,'dtbl3 = ',e12.5,' oC       ',/,
     1       4x,'fpur  = ',e12.5,' kg-H2O/day',/,
     7       4x,'den   = ',e12.5,' kg/m3    ',/,
     8       4x,'vis   = ',e12.5,' n.sec/m2  ',//)
c
c   Index control
c
      if(index.ge.2) go to 3018
c
      write(6,3603)ih,ic,ah1,ah2,ac1,ac2,ad1,ad2
 3603 format(4x,'(3) Initial conditions',//,
     1       4x,'ih    = ',e12.5,' kg-Fe',/,
     2       4x,'ic    = ',e12.5,' kg-Fe',/,
     3       4x,'ah1   = ',e12.5,' Ci',/,
     4       4x,'ah2   = ',e12.5,' Ci',/,
     5       4x,'ac1   = ',e12.5,' Ci',/,
     6       4x,'ac2   = ',e12.5,' Ci',/,
     7       4x,'ad1   = ',e12.5,' Ci',/,
     8       4x,'ad2   = ',e12.5,' Ci',/)
      write(6,3604)iref,ipar
 3604 format(4x,'(4) Options',//,
     1       4x,'iref  = ',i10,/,
     5       4x,'ipar  = ',i10,//)
      write(6,3605)inprin
 3605 format(4x,'(5) Output print option',//,
     1       4x,'inprin =',i10,/)
      write(6,3606)del,de3,ar1,ar3,af1,af3
 3606 format(4x,'(6) Plant geometry',//,
     1       4x,'del   = ',e12.5,' m     ',/,
     2       4x,'de3   = ',e12.5,' m     ',/,
     3       4x,'ar1   = ',e12.5,' m2    ',/,
     4       4x,'ar3   = ',e12.5,' m2    ',/,
```

```
     5       4x,'af1   = ',e12.5,' m2    ',/,
     6       4x,'af3   = ',e12.5,' m2    ',//)
      write(6,3607)dsol,dpar
 3607 format(4x,'(7) Diffusion coefficient',//,
     1       4x,'dsol  = ',e12.5,' m2/sec  ',/,
     2       4x,'dpar  = ',e12.5,' m2/sec  ',/)
      write(6,3608)alph1,alph2,lamd1,lamd2
 3608 format(4x,'(8) Radioactivity parameter',//,
     1      4x,'alph1 = ',e12.5,' Co-60 Ci/kg-Fe.day.%power',/,
     2      4x,'alph2 = ',e12.5,' Co-58 Ci/kg-Fe.day.%power',/,
     3      4x,'lamd1 = ',e12.5,' day-1',/,
     4      4x,'lamd2 = ',e12.5,' day-1',//)
      write(6,3609)rr58,rr60
 3609 format(4x,'(9) Recoil release',//,
     1       4x,'rr58  = ',e12.5,/,
     2       4x,'rr60  = ',e12.5,//)
      write(6,3611) hcrysc, hcrysa,hdissc,hdissa
 3611 format(4x,'(10) Crystal growth and dissolution',//,
     1       4x,'hcrysc = ',e12.5,' m/sec',/,
     1       4x,'hcrysa = ',e12.5,' m/sec',/,
     2       4x,'hdissc = ',e12.5,' m/sec',/,
     2       4x,'hdissa = ',e12.5,' m/sec',/)
      write(6,3610) cr
 3610 format(4x,'(11) Other parameters',//,
     1       4x,'cr    = ',e12.5,' kg/day',/)
c
c
c     ccccccccccccccccccccccccccc
c     c  SECOND INITIALIZATION   c
c     ccccccccccccccccccccccccccc
c
c
c   -  THREE BATCH CORE
c
c   A is new fuel assembly
c   B is one year old fuel assembly
c   C is two year old fuel assembly
c
c
 5444 FA=1./3.
      FB=1./3.
      FC=1./3.
      nrf=50
      j1=1
      iha=ih*fa
      ihb=ih*fb
      ihc=ih*fc
      ah1a=ah1*fa
      ah1b=ah1*fb
      ah1c=ah1*fc
      ah2a=ah2*fa
      ah2b=ah2*fb
      ah2c=ah2*fc
      nx=0
      ntime=0
c
c
c
      ais21=0.
      ais22=0.
```

```
c
c
      betinc=betac
      betina=betaa
      fksol1=0.22
      fksol3=0.78
c
      call cbeta
      betac=betinc
      betaa=betina
c
c
      xxc=ksol1*kpar3/(ksol3*kpar1)
      xxa=aksol3*kpar1/(aksol1*kpar3)
c
      if(ipar.eq.0) xxc=1.0
      if(ipar.eq.0) xxa=1.0
c
c  specific value calculation
c
c  sic and sih in (mg/cm2)
c
      sic = ic/ar3*100.
      sih = ih/ar1*100.
c
c  sac1, sac2, sah1 and sah2 in (uci/cm2)
c
      sac1 = ac1/ar3*100.
      sac2 = ac2/ar3*100.
      sah1 = ah1/ar1*100.
      sah2 = ah2/ar1*100.
c
c
c   automatic refuelling time setting
c
      rf(1)=300.
      do 2290 imm=2,50
      rf(imm)=rf(imm-1)+300.
 2290 continue
c
c
c
 3018 write(6,6770)
 6770 format(1x,' TIME  ',1x,'S/G CRUD ',1x,'CORE CRUD',1x,'Co60 S/G '
     1 ,1x,'Co58 S/G ',1x,'Co60 Core',1x,'Co58 Core',1x,'Co60 Cool'
     2 ,1x,'Co58 Cool',/
     1 ,1x,' (day) ',1x,'(mg/cm2) ',1x,'(mg/cm2) ',1x,'(uCi/cm2)'
     1 ,1x,'(uCi/cm2)',1x,'(uCi/cm2)',1x,'(uCi/cm2)',1x,'(uCi/cm3)'
     2 ,1x,'(uCi/cm3)',/)
      write(6,6771) time,sic,sih,sac1,sac2,sah1,sah2,saw1,saw2
 3019 r=onoff*cr
      f=onoff*flow
c
c
      dur=days/in+1
c
c     t9=tin+.01*(tout-tin)*p1
c
      T9=TOUT
      if(onoff.eq.0) go to 2060
```

```
c
c
c   Solubility calculation at coolant inlet and outlet temperatures
c
c
      t3=t9
      call num1
      sout1=s11*.055847
      phh=p
      t3=tin
      call num1
      sin1=s11*.055847
      phc=p
c
c   Average solubility calculation
c
      tin1 = tin + dtbl1
      tout1= tout + dtbl1
      call intsol(tin1,tout1,nts,shavg)
      tin3 = tin + dtbl3
      tout3 = tout + dtbl3
      call intsol(tin3,tout3,nts,scavg)
c
c
      call intsol(tin,tout,nts,swavg)

c
c   average solubility used
c
      sc=scavg
      sh=shavg
c
c
c
c
 2060 bfsc=betac*f*sc*in
      bfsh=betac*f*sh*in
c     if(ic.lt.bfsc)ic=bfsc
c     if(ih.lt.bfsh)ih=bfsh
c
c
c   Calculation do loop
c
c
      do 2190 j1=1,dur
c
      DIHA=F*FA*((sc-sh*xxc)-swavg*(1.-xxc))*BETAC*IN
      DIHB=F*FB*((sc-sh*xxc)-swavg*(1.-xxc))*BETAC*IN
      DIHC=F*FC*((sc-sh*xxc)-swavg*(1.-xxc))*BETAC*IN
      DIC=-(DIHA+DIHB+DIHC)+R*IN
      rapi6=r*60*alph1*p1*in*afks3
      DAC1A=-F*FA*BETAA*((SC*AC1/IC*xxa-SH*AH1A/IHA)-ais21*(xxa-1.))*IN
     1      +rapi6*iha
      DAC1b=-F*FA*BETAA*((SC*AC1/IC*xxa-SH*AH1b/IHb)-ais21*(xxa-1.))*IN
     1      +rapi6*ihb
      DAC1c=-F*FA*BETAA*((SC*AC1/IC*xxa-SH*AH1c/IHc)-ais21*(xxa-1.))*IN
     1      +rapi6*ihc
c
c     DAC1B=-F*FB*BETAA*(SC*AC1/IC-SH*AH1B/IHB)*IN+rapi6*ihb
c     DAC1C=-F*FC*BETAA*(SC*AC1/IC-SH*AH1C/IHC)*IN+rapi6*ihc
```

```
c
      DAC1=DAC1A+DAC1B+DAC1C-LAMD1*IN*AC1
      rapi5=rr58*alph2*p1*in*afks3
c
c
c     DAC2A=-F*FA*BETAA*(SC*AC2/IC-SH*AH2A/IHA)*IN+rapi5*iha
c     DAC2B=-F*FB*BETAA*(SC*AC2/IC-SH*AH2B/IHB)*IN+rapi5*ihb
c     DAC2C=-F*FC*BETAA*(SC*AC2/IC-SH*AH2C/IHC)*IN+rapi5*ihc
c
c
      DAC2A=-F*FA*BETAA*((SC*AC2/IC*xxa-SH*AH2A/IHA)-ais22*(xxa-1.))*IN
     1      +rapi5*iha
      DAC2b=-F*FA*BETAA*((SC*AC2/IC*xxa-SH*AH2b/IHb)-ais22*(xxa-1.))*IN
     1      +rapi5*ihb
      DAC2c=-F*FA*BETAA*((SC*AC2/IC*xxa-SH*AH2c/IHc)-ais22*(xxa-1.))*IN
     1      +rapi5*ihc
c
      DAC2=DAC2A+DAC2B+DAC2C-LAMD2*IN*AC2
      DAH1A=ALPH1*P1*IHA*IN-DAC1A-LAMD1*IN*AH1A
      DAH1B=ALPH1*P1*IHB*IN-DAC1B-LAMD1*IN*AH1B
      DAH1C=ALPH1*P1*IHC*IN-DAC1C-LAMD1*IN*AH1C
      DAH1=DAH1A+DAH1B+DAH1C
      DAH2A=ALPH2*P1*IHA*IN-DAC2A-LAMD2*IN*AH2A
      DAH2B=ALPH2*P1*IHB*IN-DAC2B-LAMD2*IN*AH2B
      DAH2C=ALPH2*P1*IHC*IN-DAC2C-LAMD2*IN*AH2C
      DAH2=DAH2A+DAH2B+DAH2C
c
c  purification effect
c
      dad1=fpur*in*(fksol1*ah1*sh/ih+fksol3*ac1*sc/ic) -lamd1*in*ad1
      dad2=fpur*in*(fksol1*ah2*sh/ih+fksol3*ac2*sc/ic) -lamd2*in*ad2
c
      IHA=IHA+DIHA
      IHB=IHB+DIHB
      IHC=IHC+DIHC
      IH=IHA+IHB+IHC
      IC=IC+DIC
      AC1=AC1+DAC1
      AC2=AC2+DAC2
      AH1A=AH1A+DAH1A
      AH1B=AH1B+DAH1B
      AH1C=AH1C+DAH1C
      AH2A=AH2A+DAH2A
      AH2B=AH2B+DAH2B
      AH2C=AH2C+DAH2C
      AH1=AH1A+AH1B+AH1C
      AH2=AH2A+AH2B+AH2C
c
c
      ais21=(aksol1*ah1*sh/ih+aksol3*ac1*sc/ic)/(aksol1-aksol3+
     1      ksol3*(sc/swavg+1.)+ksol1*(sh/swavg-1.))
      ais22=(aksol1*ah2*sh/ih+aksol3*ac2*sc/ic)/(aksol1-aksol3+
     1      ksol3*(sc/swavg+1.)+ksol1*(sh/swavg-1.))
c
c  purification activity
c
      ad1=ad1+dad1
      ad2=ad2+dad2

c
```

```
c  Activity check
c
c
      if(iha.lt.(bfsh*fa)) ah1a=ah1a-alph1*p1*(iha-diha)*in
      if(ihb.lt.(bfsh*fb)) ah1b=ah1b-alph1*p1*(ihb-dihb)*in
      if(ihc.lt.(bfsh*fc)) ah1c=ah1c-alph1*p1*(ihc-dihc)*in
      ah1=ah1a+ah1b+ah1c
      if(iha.lt.(bfsh*fa)) ah2a=ah2a-alph2*p1*(iha-diha)*in
      if(ihb.lt.(bfsh*fb)) ah2b=ah2b-alph2*p1*(ihb-dihb)*in
      if(ihc.lt.(bfsh*fc)) ah2c=ah2c-alph2*p1*(ihc-dihc)*in
      ah2=ah2a+ah2b+ah2c
      if(ic.lt.bfsc) ic=bfsc
      if(iha.lt.(bfsh*fa)) iha=bfsh*fa
      if(ihb.lt.(bfsh*fb)) ihb=bfsh*fb
      if(ihc.lt.(bfsh*fc)) ihc=bfsh*fc
      if(ac1.lt.0.) ac1=0.
      if(ac2.lt.0.) ac2=0.
      if(ah1a.lt.0.) ah1a=0.
      if(ah1b.lt.0.) ah1b=0.
      if(ah1c.lt.0.) ah1c=0.
      ah1=ah1a+ah1b+ah1c
      if(ah2a.lt.0.) ah2a=0.
      if(ah2b.lt.0.) ah2b=0.
      if(ah2c.lt.0.) ah2c=0.
      ah2=ah2a+ah2b+ah2c
c
c
c  Refuelling time check
c
c
      if(iref.eq.0) go to 2291
c
      nnrf=nrf
      if(nrf.eq.0)nnrf=1
      if(nrf.eq.0) go to 2291
      do 2292 imm=1,nnrf
      if(abs(time-rf(imm)).gt.1.e-5) go to 2292
c
c   Refuelling
c
      ihc=ihb
      ihb=iha
      iha=bfsh*fa
      ih=iha+ihb+ihc
      ah1c=ah1b
      ah1b=ah1a
      ah1a=0.
      ah1=ah1a+ah1b+ah1c
      ah2c=ah2b
      ah2b=ah2a
      ah2a=0.
      ah2=ah2a+ah2b+ah2c
 2292 continue
c
 2291 time=time+in
      ntime=ntime+1
c
c     ccccccccccccccccccccccccccccc
c     c specific value calculation  c
c     ccccccccccccccccccccccccccccc
```

```
c
c  sic and sih in (mg/cm2)
c
      sic = ic/ar3*100.
      sih = ih/ar1*100.
c
c  sac1, sac2, sah1 and sah2 in (uCi/cm2)
c
      sac1 = ac1/ar3*100.
      sac2 = ac2/ar3*100.
      sah1 = ah1/ar1*100.
      sah2 = ah2/ar1*100.
c
c  coolant activity calculation
c
c  saw1 and saw2 in (uCi/cc)
c
      if(ipar.ne.0) go to 9091
c
      saw1 = den*(fksol1*ah1*sh/ih+fksol3*ac1*sc/ic)
      saw2 = den*(fksol1*ah2*sh/ih+fksol3*ac2*sc/ic)
      go to 9092
c
c
 9091 saw1 = den*ais21
      saw2 = den*ais22
c
c
 9092 if(ntime.lt.ntma) go to 2190
 6777 write(6,6771)time,sic,sih,sac1,sac2,sah1,sah2,saw1,saw2
 6771 format(1x,f6.1,1x,8e10.3)
      ntime=0
c
c
c   print of test values
c
c     aish1=ah1*sh/ih
c     aish2=ah2*sh/ih
c     aisc1=ac1*sc/ic
c     aisc2=ac2*sc/ic
c     write(6,8013) xxc,xxa,ais21,ais22,aish1,aish2,aisc1,aisc2
c8013 format(//,4x,'xxc,xxa     =',2e12.4,
c    1        /,4x,'ais21,ais22 =',2e12.4,
c    2        /,4x,'aish1,aish2 =',2e12.4,
c    3        /,4x,'aisc1,aisc2 =',2e12.4,/)
c
c
 2190 continue
c
c
      if(inprin.eq.0) go to 7270
c
c
c   Printing of boron and lithium concentration and pH (300 oC)
c
      t3=300.
      call num1
      ph300 = p
      write(6,7271) boron, alit, ph300
 7271 format(////,4x,'Boron   = ',f8.2,' (ppm)',
```

```
     1          /,4x,'Lithium = ',f8.2,' (ppm)',
     1          /,4x,'pH(300 oC) = ',f8.4,/)
c
c  Printing of temperature ,pH and solubility
c
      write(6,3011) tin,phc,sinl,tout,phh,soutl,swavg
 3011 format(//,4x,'T(coolant inlet)     =',f8.2,4x,'(oC)',
     1     /,4x,'pH(coolant inlet)    =',f8.4,
     1     /,4x,'S(coolant inlet)     =',e12.4,2x,'(kg-Fe/kg-H2O)',
     1    //,4x,'T(coolant outlet)    =',f8.2,4x,'(oC)',
     1     /,4x,'pH(coolant outlet)   =',f8.4,
     1     /,4x,'S(coolant outlet)    =',e12.4,2x,'(kg-Fe/kg-H2O)',
     1     /,4x,'S(coolant average)   =',e12.4,2x,'(kg-Fe/kg-H2O)',
     1    /)
c
c  Printing of core and S/G surface temperatures and those average
c  solubilities
c
      write(6,6601)tin1,tout1,shavg,tin3,tout3,scavg
 6601 format(//,4x,'T(core inlet surface)    =',f8.2,4x,'(oC)',
     1     /,4x,'T(core outlet surface)   =',f8.2,4x,'(oC)',
     1     /,4x,'S(core surface average) =',e12.4,2x,'(kg-Fe/kg-H2O)',
     1    //,4x,'T(S/G  outlet surface)   =',f8.2,4x,'(oC)',
     1     /,4x,'T(S/G  inlet surface)    =',f8.2,4x,'(oC)',
     1     /,4x,'S(S/G  surface average) =',e12.4,2x,'(kg-Fe/kg-H2O)',
     1    //////)
c
c
c
 7270 day=day+days
      nx=nx+1
c
c
      go to 4444
c
 3021 stop
      end


      subroutine cbeta
      implicit real (a-z)
      common /bet/ den,de1,de3,vel1,vel3,vis,dsol,dpar,ar1,ar3,betsla,
     1             flow,af1,af3,betslc,betpar,betac,betaa,ksol1,ksol3,
     2             kpar1,kpar3,fksol1,fksol3,fkpar1,fkpar3,hcrysc,
     3             hcrysa,hdissc,hdissa,aksol1,aksol3,afks1,afks3,
     4             inprin
c
c     ccccccccccccccccccccccccccc
c     c    beta calculation      c
c     ccccccccccccccccccccccccccc
c
c   re1 = Reynolds number in core
c   re3 = Reynolds number in S/G
c   scsol = Schmit number of soluble
c   scpar = Schmit number of particulate
c   shsol1 = Sherwood number of soluble in core
c   shsol3 = Sherwood number of soluble in S/G
c   shpar1 = Sherwood number of particulate in core
c   shpar3 = Sherwood number of particulate in S/G
c   hsol1 = mass transfer coefficient of soluble in core (m/sec)
```

```
c    hsol3 = mass transfer coefficient of soluble in S/G (m/sec)
c    hpar1 = mass transfer coefficient of particulate in core (m/sec)
c    hpar3 = mass transfer coefficient of particulate in S/G (m/sec)
c    ksol1 = mass transfer factor of soluble in core (m3/sec)
c    ksol3 = mass transfer factor of soluble in S/G (m3/sec)
c    aksol1= mass transfer factor of activity in core (m3/sec)
c    aksol3= mass transfer factor of activity in S/G (m3/sec)
c    kpar1 = mass transfer factor of particulate in core (m3/sec)
c    kpar3 = mass transfer factor of particulate in S/G (m3/sec)
c    betslc = beta value of soluble
c    betsla = beta value of activity
c    betpar = beta value of particulate
c    betac  = crud transport factor in CRUDSIM
c    betaa  = activity transport factor in CRUDSIM
c
c
      vel1 = flow/(3600.*24.*den*af1)
      vel3 = flow/(3600.*24.*den*af3)
      re1=den*de1*vel1/vis
      re3=den*de3*vel3/vis
      scsol=vis/den/dsol
      scpar=vis/den/dpar
c
c
c     ccccccccccccccccccccccccccccc
c     c Dittus-Boelter correlation  c
c     ccccccccccccccccccccccccccccc
c
c     shsol1=0.023*re1**0.8*scsol**(1./3.)
c     shsol3=0.023*re3**0.8*scsol**(1./3.)
c     shpar1=0.023*re1**0.8*scpar**(1./3.)
c     shpar3=0.023*re3**0.8*scpar**(1./3.)
c
c
c     ccccccccccccccccccccccccccc
c     c Burger-Hau correlation  c
c     ccccccccccccccccccccccccccc
c
      shsol1=0.0165*re1**0.86*scsol**(1./3.)
      shsol3=0.0165*re3**0.86*scsol**(1./3.)
      shpar1=0.0165*re1**0.86*scpar**(1./3.)
      shpar3=0.0165*re3**0.86*scpar**(1./3.)
c
c
      hsol1 = dsol*shsol1/de1
      hsol3 = dsol*shsol3/de3
      hpar1 = dpar*shpar1/de1
      hpar3 = dpar*shpar3/de3
      ksol1 = hsol1*ar1*hcrysc/(hcrysc + hsol1)
      ksol3 = hsol3*ar3*hdissc/(hdissc + hsol3)
      aksol1 = hsol1*ar1*hdissa/(hdissa + hsol1)
      aksol3 = hsol3*ar3*hcrysa/(hcrysa + hsol3)
      kpar1 = hpar1*ar1
      kpar3 = hpar3*ar3
      fksol1=ksol1/(ksol1+ksol3)
      fksol3=ksol3/(ksol1+ksol3)
      afks1 = aksol1/(aksol1 + aksol3)
      afks3 = aksol3/(aksol1 + aksol3)
      fkpar1=kpar1/(kpar1+kpar3)
      fkpar3=kpar3/(kpar1+kpar3)
```

```
c
c
c     betslc = ksol1*ksol3/(ksol1+ksol3)
c     betsla = aksol1*aksol3/(aksol1+aksol3)
c
      betslc = ksol3*kpar1/(kpar1+kpar3)
      betsla = aksol1*kpar3/(kpar1+kpar3)
c
c
      betpar = kpar1*kpar3/(kpar1+kpar3)
      betac  = betslc/flow*den*3600.*24.
      betaa  = betsla/flow*den*3600.*24.
c
c  Printing of mass transfer parameters
c
      if(inprin.eq.0) return
      write(6,3601)vel1,vel3,re1,re3,scsol,scpar,shsol1,shsol3,shpar1,
     1 shpar3,hsol1,hsol3,hpar1,hpar3,ksol1,ksol3,aksol1,aksol3,kpar1,
     1 kpar3,fksol1,fksol3,afks1,afks3,fkpar1,fkpar3,betslc,betsla,
     1 betpar,betac,betaa
 3601 format(//////,4x,' Mass transfer parameter calculation ',/,
     1            4x,'-----------------------------------',//,
     2       4x,'VARIABLE     ',8x,'CORE',12x,' S/G  ',//,
     1       4x,'Vel   (m/sec)   ',e12.5,4x,e12.5,/,
     3       4x,'Re              ',e12.5,4x,e12.5,/,
     4       4x,'Sc-sol          ',e12.5,4x,'      same     ',/,
     5       4x,'Sc-par          ',e12.5,4x,'      same     ',/,
     6       4x,'Sh-sol          ',e12.5,4x,e12.5,/,
     7       4x,'Sh-par          ',e12.5,4x,e12.5,/,
     8       4x,'h-sol (m/sec)   ',e12.5,4x,e12.5,/,
     9       4x,'h-par (m/sec)   ',e12.5,4x,e12.5,/,
     1       4x,'k-sol (m3/sec)  ',e12.5,4x,e12.5,/,
     1       4x,'ak-sol (m3/sec) ',e12.5,4x,e12.5,/,
     1       4x,'k-par (m3/sec)  ',e12.5,4x,e12.5,/,
     1       4x,'fksol           ',e12.5,4x,e12.5,/,
     1       4x,'afks            ',e12.5,4x,e12.5,/,
     1       4x,'fkpar           ',e12.5,4x,e12.5,/,
     2       4x,'beta-sol(m3/sec)',e12.5,4x,'      same',/,
     2       4x,'beta-act(m3/sec)',e12.5,4x,'      same',/,
     3       4x,'beta-par(m3/sec)',e12.5,4x,'      same',/,
     4       4x,'betac           ',e12.5,4x,'      same',/,
     4       4x,'betaa           ',e12.5,4x,'      same',//////)
c
c
      return
      end


      subroutine intsol(ts1,ts2,nts,savg)
      implicit real (a-z)
      integer iss,jss,nts,ints
      dimension tx(50), ss(50)
      common /www/ w
      common /bbb/a2,b2,c2,d3,q,s1,s
      common /ccc/a,b,k1,k2,k3,k4,k6,p,t,t2,x0,x1,x2,x3,x4,y,z
      common /ddd/d1,d2,i,j
      common /eee/alit,boron,dt,dw,e1,e2,lgkw,m,mw,n,nw,r9,t2,t3
      common /fff/ch2,h,k10,k11,k12,k13,L3,ph2,s11,s10,x
      common /bet/ den,del,de3,vel1,vel3,vis,dsol,dpar,ar1,ar3,betsla,
     1             flow,af1,af3,betslc,betpar,betac,betaa,ksol1,ksol3,
```

```
     2              kpar1,kpar3,fksol1,fksol3,fkpar1,fkpar3,hcrysc,
     3              hcrysa,hdissc,hdissa,aksol1,aksol3,afks1,afks3,
     4              inprin
      common /cfeoh/sfe,sfeoh,sfeoh2,sfeoh3
      COMMON /NELAM/ LAMCAT,LAMLI,LAMH,LAMAN,LAMOH,LAMB1,LAMB2,LAMB3,
     1          LAMB4,LAMZERO,DIEL,LALFA,LBETA,KAPCOEF
      COMMON /NETAW/ ETAW,ETA,IS,Q4,GAM,Q6,Q5,LIOH,YXK,ETAM,ETA0,
     1          DWR,AYE,JAY,TW,TR
c
c
c    This subroutine calculate the average iron solubility(Savg) between
c    temperatures ts1 and ts2 by dividing the temperature range, NTS times.
c
c
c
      ints=nts
      if(abs(ts1-ts2).lt.1.e-4) nts=1
c
      rnts = float(nts)
c     write(6,1060) rnts,nts
c1060 format(//,4x,'rnts, nts = ',f10.2, 2x,i6,//)
c
      dts=(ts2-ts1)/rnts
      tx(1)=ts1+0.5*dts
      if(nts.eq.1) go to 2010
c
      do 1000 iss=2,nts
      tx(iss)=tx(iss-1)+dts
c
c     write(6,1240)iss,tx(iss)
c1240 format(/,4x,'iss, t =',i6,2x,e12.4)
c
 1000 continue
c
 2010 sum=0.
c
      do 2000 iss=1,nts
      t3=tx(iss)
      call num1
      ss(iss)=s11*0.055847
      sum=sum+ss(iss)
c
c     write(6,1062)iss,t3,ss(iss)
c1062 format(4x,'iss, temp, sol =',i4,2x,e12.4,2x,e12.4)
c
 2000 continue
c
      savg=sum/rnts
      nts=ints
      return
      end


      subroutine num1
      implicit real (a-z)
      integer m,n
      integer j,i
      common /www/ w
      common /bbb/a2,b2,c2,d3,q,s1,s
      common /ccc/a,b,k1,k2,k3,k4,k6,p,t,t1,x0,x1,x2,x3,x4,y,z
```

```
      common /ddd/d1,d2,i,j
      common /eee/a1,b1,dt,dw,e1,e2,lgkw,m,mw,n,nw,r9,t2,t3
      common /fff/ch2,h,k10,k11,k12,k13,L3,ph2,s11,s10,x
      common /cfeoh/ sfe,sfeoh,sfeoh2,sfeoh3
c     nickel ferrite solubility correlation,x~.5
c     one constrained parameter,min log squared deviation
c     h2 press exponent = 1/(3-x)
c
c
      x=.5
      call num2
      z=10.**(-p)
      k10=10.**(-1.191+3400./t2)
      k11=10.**(-4.160+1543./t2)
      k12=10.**(-6.765-31./t2)
      l3=lgkw+6.309-5713./t2
      k13=10.**l3
      h=-90100.+5.83e+07/t2
      ph2=8.038e-07*ch2*h
c
      ppp=ph2**(1./(3.-x))*0.055847
      sfe=ppp*k10*z**2.
      sfeoh=ppp*k11*z
      sfeoh2=ppp*k12
      sfeoh3=ppp*k13/z
c
      s10=k10*z**2.+k11*z+k12+k13/z
      s11=s10*ph2**(1./(3.-x))
      return
      end


      subroutine num2
      implicit real (a-z)
      integer m,n
      integer j,i
      common /www/ w
      common /bbb/a2,b2,c2,d3,q,s1,s
      common /ccc/a,b,k1,k2,k3,k4,k6,p,t,t1,x0,x1,x2,x3,x4,y,z
      common /ddd/d1,d2,i,j
      common /eee/a1,b1,dt,dw,e1,e2,lgkw,m,mw,n,nw,r9,t2,t3
      COMMON /NETAW/ ETAW,ETA,IS,Q4,GAM,Q6,Q5,LIOH,YXK,ETAM,ETA0,
     1          DWR,AYE,JAY,TW,TR
c
c
c               THIS PROGRAM CALCULATES THE AT-TEMPERATURE pH OF
c               MIXTURES OF LITHIUM HYDROXIDE AND BORIC ACID USING
c               ORNL DATA FOR BORIC ACID IONIZATION, WATER IONIZATION
c               CORRELATION OF MARSHALL AND FRANCK, AND "GENERIC"
c               ACTIVITY COEFFICIENTS FOR HIGH TEMPERATURE WATER.
c                 ** INCOMPLETE IONIZATION OF LiOH IS CONSIDERED. **
c               VALID RESULTS SHOULD BE OBTAINED AT TEMPERATURES
c               UP TO 350 C, IONIC STRENGTHS UP TO AT LEAST 1 MOLAL
c               FOR TEMPERATURES OVER 100 C. USABLE AT ROOM TEMP.
c               FOR LOW IONIC STRENGTHS TYPICAL OF PRIMARY COOLANT.
c
c               INPUT DATA ARE ENTERED ON LINES 1200-1299, AS FOLLOWS:
c
c               1200 DATA PPM Li, PPM B, TEMP (DEG. C), etc.
c
```

```
C               EXECUTION IS SLOW BECAUSE OF NESTED SEARCH ROUTINES
C               FOR SOLVING THE SETS OF NON-LINEAR EQUATIONS.
C               NEVERTHELESS, THE CORRECT ANSWER IS EVENTUALLY
C               REACHED. INTERMEDIATE VALUES OF pH ARE PRINTED TO
C               SCREEN TO ALLOW MONITORING OF PROGRESS TOWARD
C               SOLUTION OF THE EQUATIONS. THIS PROGRAM IS NOT
C               RECOMMENDED FOR PRINTING EXTENSIVE TABLES.
C
C
C
      t2=t3+273.15
      alg=alog(10.)
      k1=10.**(1573.21/t2+28.6059+.012078*t2-(13.2258*alog(t2)/alg))
      k2=10.**(2756.1/t2-18.7322-.00033*t2+(5.835*alog(t2)/alg))
      k3=10.**(3339.5/t2-7.85-.00033*t2+(1.497*alog(t2)/alg))
      k4=10.**(12820./t2-134.33-.00033*t2+(42.10501*alog(t2)/alg))
      dt=374.11-t3
      mw=3.1975-.3151548*dt**(1./3.)-1.203374e-3*dt+7.489081e-13*dt**4
      nw=1.+.1342489*dt**(1./3.)-3.946263e-3*dt
      dw=nw/mw
      r9=(13.957-1262.2/t2+856410./t2**2)*alog(dw)/alg
      lgkw=-4.098-3245.2/t2+223620./t2**2-3.9847e+07/t2**3+r9
      k6=10**lgkw
      LGK5Q=12.53106-3839.082/T2+1222431/T2**2
      LGK5=LGK5Q+LGKW
      K5=10.**LGK5
      CALL DIELECT
      CALL WATER
      ETAW=ETA
      CALL CONDUCT
      CALL FACTOR
      a=a1/6940.
      b=b1/10811.
      IS=A+.0000001
 5126 CALL ACTIVIT
      Q4=K4/GAM**2
      Q6=K6/GAM**2
      Q5=K5/GAM**2
      P=1.
      m=0
      n=0
      e1=1.
      e2=-1.
      IF(B.GT.1.E-9) CALL NUM3
C     call num3
      call num4
      go to 5480
 5450 if(abs(e1).lt..0001) go to 6150
      if(abs(t).lt.1e-15) go to 6150
      tt1=t*t1
      if(tt1.lt.0) go to 5590
 5480 if(m.eq.0) go to 5530
 5490 p=p+e1
      IF(B.GT.1.E-9) CALL NUM3
C     call num3
      call num5
      go to 5450
 5530 n=0
      m=1
      e2=-e1/2.
```

```
      go to 5490
 5560 if(abs(e1).lt..0001) go to 6150
      if(abs(t).lt.1e-15) go to 6150
      tt1=t*t1
      if(tt1.lt.0) go to 5480
 5590 if(n.eq.0) go to 5640
 5600 p=p+e2
      IF(B.GT.1.E-9) CALL NUM3
C     call num3
      call num5
      go to 5560
 5640 m=0
      n=1
      e1=-e2/2.
      go to 5600
C6150 return
 6150 IS1=IS
      IS=(Y+X1+X2+X3+4.*X4+Z+Q6/Y)/2.
      AISI=(IS-IS1)/IS1
      IF(ABS(AISI).LT.9.999999E-4) GO TO 5111
      GO TO 5126
 5111 CALL ROBINS
      RETURN
      end


      subroutine num3
      implicit real (a-z)
      integer i,j
      common /www/ w
      common /bbb/a2,b2,c2,d3,q,s1,s
      common /ccc/a,b,k1,k2,k3,k4,k6,p,t,t1,x0,x1,x2,x3,x4,y,z
      common /ddd/d1,d2,i,j
      COMMON /NETAW/ ETAW,ETA,IS,Q4,GAM,Q6,Q5,LIOH,YXK,ETAM,ETA0,
     1          DWR,AYE,JAY,TW,TR
c
c
      w=1.
      d1=-1.
      d2=1.
      i=0
      j=0
C     y=k6/(10.**(-p))
      y=Q6/(10.**(-p))
      a2=1.+y*k1
      b2=2.*y*k2*b
      c2=3.*y*k3*b**2
C     d3=4.*y**2*K4*b**3
      d3=4.*y**2*Q4*b**3
      call num6
      go to 5790
 5760 if(abs(d1).lt.9.999999e-06) go to 5970
      if(abs(s).lt.1e-10) go to 5970
      ss1=s*s1
      if(ss1.le.0) go to 5890
 5790 if(j.eq.0) go to 5840
 5800 alg=alog(10.)
      q=alog(w)/alg
      q=q+d1
      call num7
```

```
      go to 5760
 5840 i=0
      j=1
      d2=-d1/2.
      go to 5800
 5860 if(abs(d1).lt.9.999999e-06) go to 5970
      if(abs(s).lt.1e-10) go to 5970
      ssl=s*sl
      if(ssl.lt.0) go to 5790
 5890 if(i.eq.0) go to 5940
 5900 alg=alog(10.)
      q=alog(w)/alg
      q=q+d2
      call num7
      go to 5860
 5940 j=0
      i=1
      d1=-d2/2.
      go to 5900
 5970 return
      end


      subroutine num4
      implicit real (a-z)
      common /www/ w
      common /ccc/a,b,k1,k2,k3,k4,k6,p,t,t1,x0,x1,x2,x3,x4,y,z
      COMMON /NETAW/ ETAW,ETA,IS,Q4,GAM,Q6,Q5,LIOH,YXK,ETAM,ETA0,
     1          DWR,AYE,JAY,TW,TR
c     print p
c     y=k6/10.**(-p)
      y=Q6/10.**(-p)
c     z=a
      z=a/(1.+Y/Q5)
      LIOH=Z*Y/Q5
      x0=w*b
      x1=y*x0*k1
      x2=y*x0**2*k2
      x3=k3*y*x0**3
c     yxk=y*x0**2*k4**.5
      yxk=y*x0**2*Q4**.5
      if(yxk.lt.1e-15) go to 6120
c     x4=k4*y**2*x0**4
      x4=Q4*y**2*x0**4
      go to 6130
 6120 x4=0.
C6130 t=y+x1+x2+x3+2.*x4-z-k6/y
 6130 t=y+x1+x2+x3+2.*x4-z-Q6/y
      return
      end


      subroutine num5
      implicit real (a-z)
      common /www/ w
      common /ccc/a,b,k1,k2,k3,k4,k6,p,t,t1,x0,x1,x2,x3,x4,y,z
      COMMON /NETAW/ ETAW,ETA,IS,Q4,GAM,Q6,Q5,LIOH,YXK,ETAM,ETA0,
     1          DWR,AYE,JAY,TW,TR
      t1=t
c     print p
```

```
C     y=k6/10.**(-p)
      y=Q6/10.**(-p)
C     z=a
      Z=A/(1.+Y/Q5)
      LIOH=Z*Y/Q5
      x0=w*b
      x1=y*x0*k1
      x2=y*x0**2*k2
      x3=k3*y*x0**3
C     yxk=y*x0**2*k4**.5
      yxk=y*x0**2*Q4**.5
      if(yxk.lt.1e-15) go to 6120
C     x4=k4*y**2*x0**4
      x4=Q4*y**2*x0**4
      go to 6130
 6120 x4=0.
C6130 t=y+x1+x2+x3+2.*x4-z-k6/y
 6130 t=y+x1+x2+x3+2.*x4-z-Q6/y
      return
      end


      subroutine num6
      implicit real (a-z)
      common /www/ w
      common /bbb/a2,b2,c2,d3,q,s1,s
      s=a2*w+b2*w**2+c2*w**3+d3*w**4-1.
      return
      end


      subroutine num7
      implicit real (a-z)
      common /www/ w
      common /bbb/a2,b2,c2,d3,q,s1,s
      s1=s
      w=10.**q
      s=a2*w+b2*w**2+c2*w**3+d3*w**4-1.
      return
      end


      SUBROUTINE ROBINS
      implicit real (a-z)
      common /ccc/a,b,k1,k2,k3,k4,k6,p,t,t1,x0,x1,x2,x3,x4,y,z
      common /eee/a1,b1,dt,dw,e1,e2,lgkw,m,mw,n,nw,r9,t2,t3
      COMMON /NELAM/ LAMCAT,LAMLI,LAMH,LAMAN,LAMOH,LAMB1,LAMB2,LAMB3,
     1          LAMB4,LAMZERO,DIEL,LALFA,LBETA,KAPCOEF
      COMMON /NETAW/ ETAW,ETA,IS,Q4,GAM,Q6,Q5,LIOH,YXK,ETAM,ETA0,
     1          DWR,AYE,JAY,TW,TR
C        This subroutine handles calculation of electrical conductivity
C        of electrolyte mixtures that include Li, H, OH and four
C        borate ions (monomer and three polyions). Equivalent
C        conductance is calculated from Robinson and Stokes eq. 7.36,
C        p.144. Although this equation is accurate only at concentrations
C        up to ionic strength 0.1 (molal), an attempt is made to improve
C        accuracy at higher concentrations by correction according to
C        the relative viscosity of the solution mixture.
      SIGEQCATM=Z+Q6/Y
      SIGEQANM=Y+X1+X2+X3+2.*X4
```

```
      LAMCAT=(LAMLI*Z+LAMH*Q6/Y)/SIGEQCATM
      LAMAN=(LAMOH*Y+LAMB1*X1+LAMB2*X2+LAMB3*X3+2.*LAMB4*X4)/SIGEQANM
      LAMZERO=LAMCAT+LAMAN
      LLFACT=LALFA*LAMZERO+LBETA
      RSFACT=1.+KAPCOEF*(IS*DW)**.5
      CALL  POTTER
      EQCOND=(LAMZERO-(LLFACT/RSFACT)*(IS*DW)**.5)*ETAW/ETAM
      SPCOND=1000.*EQCOND*(SIGEQCATM+SIGEQANM)*DW/2.
C
C   Equivalent conductance = 'EQCOND ' in mho-cm2/equiv.
C   Specific conductivity = 'SPCOND ' in micromhos/cm
C
      RETURN
      END


      SUBROUTINE ACTIVIT
      implicit real (a-z)
      common /eee/a1,b1,dt,dw,e1,e2,lgkw,m,mw,n,nw,r9,t2,t3
      COMMON /NETAW/ ETAW,ETA,IS,Q4,GAM,Q6,Q5,LIOH,YXK,ETAM,ETA0,
     1          DWR,AYE,JAY,TW,TR
C
C                THIS SUBROUTINE CALCULATES GENERIC ACTIVITY
C                COEFFICIENTS FOR UNIVALENT ELECTROLYTES
C                100 TO 350 DEG. C, SAT. PRESSURE
C
C                T3 is DEGREES CENTIGRADE
C                IS is MOLAL IONIC STRENGTH
C
      QM=2.95869-.321502*(T3/100.)-.17233*(T3/100.)**2
C
C                QM is MEISSNER'S q FITTED TO NaCl AT THE
C                SOLUBILITY LIMIT, 100 TO 350 DEG. C
C
      AP=.484582+.158173*(T3/100.)-.214065*(T3/100.)**2
      AP=AP+.256199*(T3/100.)**3-.105332*(T3/100.)**4
     1     +.0157603*(T3/100.)**5
C
C                AP is PITZER-SILVESTER LIMITING SLOPE FOR
C                LOG GAMMA AT SATURATION PRESSURE
C
      BM=.75-6.500001E-02*QM
      CM=1.+5.500001E-02*QM*EXP(-.023*IS**3)
C
C                BM AND CM ARE PARAMETERS IN MEISSNER EQS.
C
      GAMDH=10.**(-AP*IS**.5/(1.+CM*IS**.5))
C
C                GAMDH is MEISSNER VERSION OF DEBYE-HUCKEL
C                EXPRESSION
C
      GAM=GAMDH*(1.+BM*(1.+.1*IS)**QM-BM)
C
C                GAM is MOLAL ACTIVITY COEFFICIENT FOR A
C                1-1 SALT OR FOR A SINGLE UNIVALENT ION
C
      RETURN
      END
```

```
      SUBROUTINE DIELECT
      implicit real (a-z)
      common /eee/a1,b1,dt,dw,e1,e2,lgkw,m,mw,n,nw,r9,t2,t3
      COMMON /NELAM/ LAMCAT,LAMLI,LAMH,LAMAN,LAMOH,LAMB1,LAMB2,LAMB3,
     1          LAMB4,LAMZERO,DIEL,LALFA,LBETA,KAPCOEF
C         This subroutine calculates the dielectric constant of
C         water and steam from the Uematsu and Franck correlation
C         (IAPS 1977 Release) for temperatures 0 to 550 C at
C         densities 0 to 1.15 g/cc, corresponding to pressures
C          0 to 500 MPa (0 to 5000 atm). However, results in
C         immediate vicinity of critical point should be used
C         with caution. Inputs are density g/cc, temperature deg.K.
C
      TD=T2/298.15
      DIE1=7.62571
      DIE2=244.03
      DIE3=-140.569
      DIE4=27.7841
      DIE5=-96.28049
      DIE6=41.7909
      DIE7=-10.2099
      DIE8=-45.2059
      DIE9=84.63949
      DIE10=-35.8644
      DIEL=1.+DW*DIE1/TD+DW**2*(DIE2/TD+DIE3+DIE4*TD)
      DIEL=DIEL+DW**3*(DIE5/TD+DIE6*TD+DIE7*TD**2)
      DIEL=DIEL+DW**4*(DIE8/TD**2+DIE9/TD+DIE10)
      RETURN
      END


      SUBROUTINE CONDUCT
      implicit real (a-z)
      common /eee/a1,b1,dt,dw,e1,e2,lgkw,m,mw,n,nw,r9,t2,t3
      COMMON /NELAM/ LAMCAT,LAMLI,LAMH,LAMAN,LAMOH,LAMB1,LAMB2,LAMB3,
     1          LAMB4,LAMZERO,DIEL,LALFA,LBETA,KAPCOEF
      COMMON /NETAW/ ETAW,ETA,IS,Q4,GAM,Q6,Q5,LIOH,YXK,ETAM,ETA0,
     1          DWR,AYE,JAY,TW,TR
C         This subroutine calculates limiting ionic conductances for
C         lithium, hydrogen, hydroxyl and four borate ions, from zero
C         to 350 C, from the Walden products of these ions represented
C         as a function of temperature. Inputs are temperature T3 (deg C)
C         and T2 (deg K), viscosity of pure water ETAW (cp). Output limiting
C         conductances are LAMLI, LAMH, LAMOH, LAMB1, LAMB2, LAMB3 and
C         LAMB4, respectively.
C
      LAMLI=(32.96253+.1542925*T3-7.298788E-04*T3**2
     1      +1.281526E-06*T3**3)/ETAW
      LAMH=(10.**(.7425291+.9297435*(1000./T2)-.1954584*(1000./T2)**2
     1      +2.199885E-02*(1000./T2)**3))/ETAW
      LAMOH=(10.**(1.224781+.3830048*(1000./T2)-1.869787E-03*(1000.
     1      /T2)**2-6.565726E-03*(1000./T2)**3))/ETAW
      LAMB1=31.33/ETAW
      LAMB2=16.32/ETAW
      LAMB3=13.62/ETAW
      LAMB4=27.24/ETAW
      RETURN
      END
```

```
      SUBROUTINE FACTOR
      implicit real (a-z)
      common /eee/a1,b1,dt,dw,e1,e2,lgkw,m,mw,n,nw,r9,t2,t3
      COMMON /NELAM/ LAMCAT,LAMLI,LAMH,LAMAN,LAMOH,LAMB1,LAMB2,LAMB3,
     1         LAMB4,LAMZERO,DIEL,LALFA,LBETA,KAPCOEF
      COMMON /NETAW/ ETAW,ETA,IS,Q4,GAM,Q6,Q5,LIOH,YXK,ETAM,ETA0,
     1         DWR,AYE,JAY,TW,TR
C        This subroutine calculates temperature dependent factors that
C        are used in computation of the change of electrolytic conductance
C        with concentration. Needed inputs are temperatures T3 deg C,
C        T2 deg K, dielectric constant of pure water DIEL, and
C        viscosity of pure water ETAW.
      LALFA=820394./(DIEL*T2)**1.5
      LBETA=82.5/(.01*ETAW*(DIEL*T2)**.5)
      KAPCOEF=216.21/(DIEL*T2)**.5
      RETURN
      END


      SUBROUTINE WATER
      implicit real (a-z)
      common /eee/a1,b1,dt,dw,e1,e2,lgkw,m,mw,n,nw,r9,t2,t3
      COMMON /NETAW/ ETAW,ETA,IS,Q4,GAM,Q6,Q5,LIOH,YXK,ETAM,ETA0,
     1         DWR,AYE,JAY,TW,TR
C        This subroutine calculates the viscosity of water and
C        steam from the Watson, Basu and Sengers equation
C        (9th ICPS, 1979). Values are accurate between 0 and
C        800 C and pressures 0.1 to 100 MPa, except in the
C        critical region between 372 and 379.5 C, density between
C        0.24 and 0.41 g/cc. Inputs are T2 (temperature K) and
C        DW (density g/cc). Output is ETA (viscosity, centipoises).
C
      TR=T2/647.27
      AYE=(1./TR)-1.
      DWR=DW/.317763
      JAY=DWR-1.
      VIS0=.0181583
      VIS1=.0177624
      VIS2=.0105287
      VIS3=-.0036744
      ETA0=(TR**.5)/(VIS0+VIS1*TR**(-1.)+VIS2*TR**(-2.)+VIS3*TR**(-3.))
      VIS00=.5132047
      VIS10=.3205656
      VIS40=-.7782567
      VIS50=.1885447
      VIS01=.2151778
      VIS11=.7317883
      VIS21=1.241044
      VIS31=1.476783
      VIS02=-.2818107
      VIS12=-1.070786
      VIS22=-1.263184
      VIS03=.1778064
      VIS13=.460504
      VIS23=.2340379
      VIS33=-.4924179
      VIS04=-.0417661
      VIS34=.1600435
      VIS15=-1.578386E-02
      VIS36=-3.629481E-03
```

```
      TERM0=VIS00+VIS01*JAY+VIS02*JAY**2+VIS03*JAY**3+VIS04*JAY**4
      TERM1=VIS10+VIS11*JAY+VIS12*JAY**2+VIS13*JAY**3+VIS15*JAY**5
      TERM2=VIS21*JAY+VIS22*JAY**2+VIS23*JAY**3
      TERM3=VIS31*JAY+VIS33*JAY**3+VIS34*JAY**4+VIS36*JAY**6
      ETA=ETA0*EXP(DWR*(TERM0+TERM1*AYE+TERM2*AYE**2+TERM3*AYE**3
     1    +VIS40*AYE**4+VIS50*AYE**5))
      ETA=ETA/1000.
      RETURN
      END


      SUBROUTINE WATER2
      implicit real (a-z)
      COMMON /NETAW/ ETAW,ETA,IS,Q4,GAM,Q6,Q5,LIOH,YXK,ETAM,ETA0,
     1         DWR,AYE,JAY,TW,TR
C        This subroutine calculates the viscosity of water and
C        steam from the Watson, Basu and Sengers equation
C        (9th ICPS, 1979). Values are accurate between 0 and
C        800 C and pressures 0.1 to 100 MPa, except in the
C        critical region between 372 and 379.5 C, density between
C        0.24 and 0.41 g/cc. Inputs are T2 (temperature K) and
C        DW (density g/cc). Output is ETA (viscosity, centipoises).
C
C     TR=T2/647.27
C     AYE=(1./TR)-1.
C     DWR=DW/.317763
C     JAY=DWR-1.
      VIS0=.0181583
      VIS1=.0177624
      VIS2=.0105287
      VIS3=-.0036744
      ETA0=(TR**.5)/(VIS0+VIS1*TR**(-1.)+VIS2*TR**(-2.)+VIS3*TR**(-3.))
      VIS00=.5132047
      VIS10=.3205656
      VIS40=-.7782567
      VIS50=.1885447
      VIS01=.2151778
      VIS11=.7317883
      VIS21=1.241044
      VIS31=1.476783
      VIS02=-.2818107
      VIS12=-1.070786
      VIS22=-1.263184
      VIS03=.1778064
      VIS13=.460504
      VIS23=.2340379
      VIS33=-.4924179
      VIS04=-.0417661
      VIS34=.1600435
      VIS15=-1.578386E-02
      VIS36=-3.629481E-03
      TERM0=VIS00+VIS01*JAY+VIS02*JAY**2+VIS03*JAY**3+VIS04*JAY**4
      TERM1=VIS10+VIS11*JAY+VIS12*JAY**2+VIS13*JAY**3+VIS15*JAY**5
      TERM2=VIS21*JAY+VIS22*JAY**2+VIS23*JAY**3
      TERM3=VIS31*JAY+VIS33*JAY**3+VIS34*JAY**4+VIS36*JAY**6
      ETA=ETA0*EXP(DWR*(TERM0+TERM1*AYE+TERM2*AYE**2+TERM3*AYE**3
     1    +VIS40*AYE**4+VIS50*AYE**5))
      ETA=ETA/1000.
      RETURN
      END
```

```
      SUBROUTINE POTTER
      implicit real (a-z)
      common /eee/a1,b1,dt,dw,e1,e2,lgkw,m,mw,n,nw,r9,t2,t3
      COMMON /NETAW/ ETAW,ETA,IS,Q4,GAM,Q6,Q5,LIOH,YXK,ETAM,ETA0,
     1          DWR,AYE,JAY,TW,TR
c        This subroutine estimates the viscosity of concentrated
c        electrolyte mixtures by use of the Potter correlation for
c        viscosity of NaCl (Trans. Geothermal Resources Council, Vol 2,
c        p. 543 (1978)) as an approximation at equal ionic strength.
c        Inputs are temperature T3 deg. C, ionic strength IS (molal).
c        Approximate useful range 25 to 350 C, ionic strength 0 to 4
c        on molal scale.
c
      REL1=.001599
      REL2=-.562893
      REL3=.0393889
      REL4=-.120946
      REL5=.014211
      REL6=-8.7747E-04
      TW=REL1*IS+REL2*IS**2+REL3*IS**3+T3*(1.+REL4*IS+REL5*IS**2
     1   +REL6*IS**3)
      DTW=374.11-TW
      MWW=3.1975-.3151548*DTW**(1./3.)-1.203374E-03*DTW
     1    +7.489081E-13*DTW**4
      NWW=1.+.1342489*DTW**(1./3.)-3.946263E-03*DTW
      DWW=NWW/MWW
      TR=(TW+273.15)/647.27
      AYE=(1./TR)-1.
      DWR=DWW/.317763
      JAY=DWR-1.
      CALL WATER2
      ETAM=ETA
      RETURN
      END
```